University of Alberta

Multiloop Calculations in Perturbative Quantum Field Theory

by

Ian Richard Blokland ©

A thesis submitted to the Faculty of Graduate Studies and Research in partial fulfillment of the requirements for the degree of Doctor of Philosophy

Department of Physics

Edmonton, Alberta
Fall 2004

Canada

Table of Contents

TABLE OF CONTENTS

List of Tables

List of Figures

Chapter 1

Introduction

For thousands of years, mankind has endeavored to understand the fundamental nature of matter. Over time, a succession of paradigms has emerged, and within the last one-hundred years, an exceptional model — the Standard Model — has been developed. The quantitative predictions of the Standard Model have been verified by experiment to such a high degree of precision that one might, in all modesty, claim that it is the most successful physical theory ever created. This thesis deals with high-precision theoretical predictions of the Standard Model and the techniques that can be used to obtain them. In this chapter, we set the stage by outlining the background and motivation for the work to follow.

1.1 Quantum Field Theory

The Standard Model describes three of the four fundamental forces of nature — the strong, weak, and electromagnetic — by means of quantum field theory. Quantum field theory arises from the merger of quantum mechanics with special relativity; a definitive introduction to quantum field theory is provided in the wonderful book by Peskin and Schroeder [1]. For our immediate purposes, there is one feature of quantum field theory that requires special emphasis.

Insofar that a particular physical theory is defined by its particle content and symmetries in a Lagrangian, physical observables for the quantum field theory can be expressed in a formal way via functional path integrals. Unfortunately, for all but a handful of artificial exceptions, exact results cannot be obtained, and thus, certain approximations are needed to render the calculations tractable. The most common approximation arises in perturbative quantum field theory, wherein an exact prediction of the theory can be mapped onto an asymptotic series in a small parameter. This small parameter is related to the strength of the

interaction between particles and the various terms of the series can be visualized as sets of Feynman diagrams with different numbers of interaction vertices. Feynman rules, which can be obtained from the Lagrangian of the theory, provide a recipe for translating the features of these diagrams into mathematical expressions which are then used to calculate the approximate predictions of the theory.

1.2   The Standard Model

The Standard Model is able to make quantitative predictions about thousands of physical processes in particle physics in terms of only 19 free parameters. These 19 parameters are listed in Table 1.1. An excellent introductory reference

Description	Free Parameters	Related Parameters
Lepton masses	m_e, m_μ, m_τ	Yukawa
Quark masses	$m_u, m_d, m_s, m_c, m_b, m_t$	couplings
CKM matrix	$\theta_{12}, \theta_{13}, \theta_{23}, \delta$	A, λ, ρ, η or V_{ij}
Coupling constants	g, g_w, g_s	$\sin \theta_w$
Higgs doublet	m_H, m_W	λ_H, v
Strong CP	θ_{CP}	

Table 1.1: The 19 free parameters of the Standard Model.

for the Standard Model is the book by Griffiths [2]. Our starting point will be the Feynman rules for the Standard Model, as per the conventions of Cheng and Li [3]. For brevity, we shall restrict ourselves to the Feynman rules that are used in this thesis.

The first set of Feynman rules, shown in Table 1.2, concerns the external lines in a diagram. Here, $u(p)$ and $\bar{u}(p)$ are four-component Dirac spinors and p denotes the four-momentum carried by the particle.

The second set of Feynman rules, shown in Table 1.3, deals with interaction vertices. In the quark-quark-W boson vertex, i and j are quark flavor labels and V_{ij} is a CKM matrix element. For the three-gluon vertex, the four-momenta k_1, k_2, and k_3 are all taken to be flowing into the vertex. For the gluon-ghost vertex, keep in mind that a closed ghost loop requires an additional factor of (-1) due to its fermionic statistics.
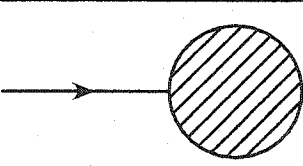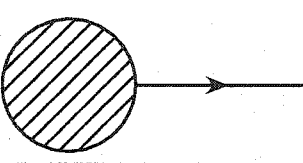
Incoming fermion	———▶ ⬯	$u(p)$
Outgoing fermion	⬯ ———▶	$\overline{u}(p)$

Table 1.2: Feynman rules for the external lines in a diagram.

The third set of Feynman rules, shown in Table 1.4, deals with the internal lines, better known as propagators, of a diagram. It is assumed that a four-momentum k flows through each line. The labels μ and ν denote four-component Lorentz indices and the labels a and b denote $SU(3)$ color indices. For the fermion propagators, the contraction $k_\mu \gamma^\mu$ is usually abbreviated as $\not{k}$. Aside from the color conservation factor δ^{ab}, the photon, gluon, and W boson propagators in Table 1.3 are all special cases of the general formula

$$\frac{-i}{k^2 - m^2 + i\varepsilon}\left[g_{\mu\nu} + (\xi - 1)\frac{k_\mu k_\nu}{k^2 - \xi m^2 + i\varepsilon}\right]. \tag{1.1}$$

Specifically, for the photon and gluon, we have $m = 0$ and we work in the Feynman-'t Hooft gauge where $\xi = 1$, and for the W boson we work in the unitary gauge by letting $\xi \to \infty$.

Conservation of energy and momentum at each interaction vertex is not sufficient to constrain the four-momentum of every internal line in a Feynman diagram with loops, therefore we must integrate over all undetermined loop momenta. The $+i\varepsilon$ in the denominator of each propagator is the pole term which provides the prescription for integration when the remainder of the propagator becomes singular. The location of these poles in the complex k_0-plane allows us to move from Minkowski space to Euclidean space by means of a Wick rotation $(k_0)_M \to i(k_0)_E$. This change of variables alters the denominators of our propagators from $(k_M^2 - m^2 + i\varepsilon)$ to $(-k_E^2 - m^2 + i\varepsilon)$ so that they are no longer singular, and thus, explicit reference to the pole prescription can be dropped. Henceforth, it will be assumed that any loop integrals we encounter will have already been Wick rotated into Euclidean space, unless explicitly stated otherwise.

Charged lepton-photon		$-ie\gamma^\mu$
Quark-gluon		$ig_s\gamma^\mu t^a$
Quark-quark-W boson		$\frac{ig_w}{2\sqrt{2}}\gamma^\mu(1-\gamma_5)V_{ij}$
3 gluons		$ig_s f^{abc}\left[(k_1-k_2)_\lambda g_{\mu\nu}\right.$ $+(k_2-k_3)_\mu g_{\nu\lambda}$ $\left.+(k_3-k_1)_\nu g_{\lambda\mu}\right]$
Gluon-ghost		$g_s f^{abc}p_\mu$

Table 1.3: Feynman rules for the interaction vertices in a diagram.

1.3 Perturbative Calculations

For a particular physical process, the basic calculational scheme is to group
Feynman diagrams, based on the number of interaction vertices, in order to
generate the terms of a perturbation series. Even the first term of such a series
is often a very accurate approximation. Subsequent terms in the series are sup-
pressed by powers of α_j, a dimensionless number that is related to the coupling
constant, g_j, of a particular interaction by

$$\alpha_j = \frac{g_j^2}{4\pi} , \tag{1.2}$$

where factors of $\hbar$ and c are taken to be 1. At this stage, two things should be
pointed out.

First, is that α_j, known in the context of electromagnetism as the fine-structure
constant, is not constant, but rather, depends on the characteristic scale of the
process. In QED, $\alpha^{-1} \sim 137$ at low energies, but the coupling increases to
$\alpha^{-1} \sim 128$ at energies characteristic of the masses of the weak bosons. In QCD,
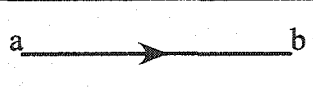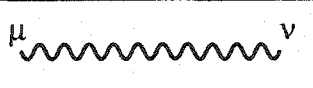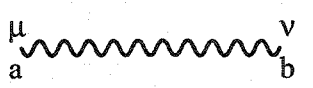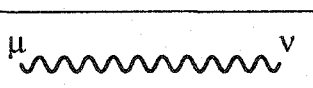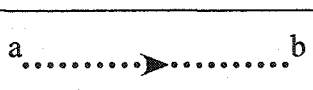
Lepton	———————➤———————	$\dfrac{i(k_\mu\gamma^\mu+m)}{k^2-m^2+i\varepsilon}$
Quark	a ———————➤——————— b	$\dfrac{i(k_\mu\gamma^\mu+m)\delta^{ab}}{k^2-m^2+i\varepsilon}$
Photon	μ ～～～～～～ ν	$\dfrac{-ig_{\mu\nu}}{k^2+i\varepsilon}$
Gluon	μ ～～～～～～ ν / a ～ b	$\dfrac{-ig_{\mu\nu}\delta^{ab}}{k^2+i\varepsilon}$
W boson	μ ～～～～～～ ν	$\dfrac{-i}{k^2-m^2+i\varepsilon}\left[g_{\mu\nu}-\dfrac{k_\mu k_\nu}{m^2}\right]$
Ghost	a ·········➤········· b	$\dfrac{-i\delta^{ab}}{k^2+i\varepsilon}$

Table 1.4: Feynman rules for the propagators in a diagram.

on the other hand, the analog to the fine-structure constant, α_s, is not nearly so small. Furthermore, α_s becomes increasingly large at lower energies so that perturbation theory cannot be used at all unless the characteristic energy of a process is sufficiently large. This property of QCD is known as asymptotic freedom.

Second, is that the factors that accompany α_j^n in the n-th term of a perturbation series are not necessarily such that the n-th term is smaller than its predecessor. This sort of behavior sometimes arises when the presence of additional loops in a diagram allows the inclusion of certain interaction vertices that were previously absent. It also occurs for diagrams with a very large number of loops ($n \sim \alpha^{-1}$) because the number of Feynman diagrams eventually increases far too quickly for their contributions to be suppressed by α^n. This is why we speak of a perturbation series as an asymptotic series.

Most of the pioneering work in quantum field theory was done in the context of the electromagnetic interaction and it was here that the term "radiative corrections" was first used to describe the perturbative adjustments to physical quantities that arose in the theory. The first successful calculation of this sort was Bethe's explanation [4] of the Lamb shift in 1947, followed the next year by Schwinger's calculation [5] of the electron anomalous magnetic moment. The electron anomalous magnetic moment was the subject of the first two-loop perturbative calculation, performed by Sommerfield [6] in 1957. QED remains the easiest sector of the Standard Model within which to perform perturbative

calculations, as might be attested to by the existence of a partial five-loop calculation [7]. As for the electroweak and QCD sectors of the Standard Model, perturbative calculations were underway by the end of the 1960s [8], several years before these theories were cast in a completed form. It should also be mentioned that many developments in perturbative quantum field theory have resulted from studies of simpler theories such as φ^3, $\lambda\phi^4$, or Yukawa theory. In the context of the latter, a recent publication [9] examines a mathematical technique for computing a particular class of 31-loop effects!

There are several motivations driving precision calculations in the Standard Model, the most exciting of which is the prospect of finding indirect evidence for physics beyond the Standard Model via small, systematic deviations between experimental measurements and the corresponding Standard Model predictions. Precise Standard Model calculations can also affect the systematic errors involved in experimental settings like the beam luminosity in a collider. Finally, from an aesthetic standpoint, it is only natural that we should want to extract as much as possible from such a predictive and successful theory.

So begins our journey into multiloop calculations in the Standard Model. The chapters ahead fall into two main classes: techniques and research. Chapters 2 through 10 provide a comprehensive description of an assortment of technical details that are used to facilitate the calculations ahead. Chapters 11, 12, and 13 each document the results of an original research project, and collectively, these chapters are the heart of this thesis. Following the conclusions in Chapter 14, the Appendix describes and catalogs the computer programs that have been written in conjunction with this work so that the results presented here can, if the need arises, be verified or extended.

"Somebody thought of that, and someone believed it; look what it's done so far."

Kermit the Frog (*The Rainbow Connection*)

Chapter 2

Dimensional Regularization

In Chapter 1, we saw how perturbative quantum field theory gives rise to loop integrals. Individually, these loop integrals may contain ultraviolet and infrared divergences, and while the sum of all diagrams of a given order in a renormalized quantum field theory must lead to finite physical predictions, it is simply not feasible to do such calculations all in one piece. Instead, we regularize individual loop integrals. More specifically, we artificially adjust loop integrals so that they produce finite results individually, but yield the same sum as the unregularized integrals.

There are a number of techniques available for regularizing loop integrals, some of which we will now discuss. Consider the Euclidean-space integral

$$\int \frac{d^4k}{(k^2 + m^2)^2} . \tag{2.1}$$

This integral has an ultraviolet divergence. Since the divergence arises from the high-momentum portion of the integral ($|k| \to \infty$), the most obvious solution would be to place a cutoff on the integral so that we only integrate over momentum values below some Λ. This method has its drawbacks, though, not the least of which is the loss of Lorentz invariance. A slightly more robust tactic is Pauli-Villars regularization, whereby we multiply the integral by an additional factor:

$$\int \frac{d^4k}{(k^2 + m^2)^2} \frac{\Lambda^2}{k^2 + \Lambda^2} . \tag{2.2}$$

If Λ is sufficiently large, the low-momentum region of the loop integral is unaffected, but the high-momentum region is suppressed by a factor of k^2, which in this case is enough to remove the divergence.

Meanwhile, there are also infrared divergences to deal with, such as the one

in the integral

$$\int \frac{d^4k}{k^4(k^2 + m^2)} \, . \tag{2.3}$$

Since this divergence arises from the low-momentum portion of an integral ($|k| \to 0$), we could place a lower cutoff on the integral so that we only integrate over momentum values above some μ. Alternatively, seeing as the source of the divergence is the k^4 factor which originated from the propagators of massless particles, we could add a tiny mass μ to these particles so that the integral becomes

$$\int \frac{d^4k}{(k^2 + \mu^2)^2(k^2 + m^2)} \, . \tag{2.4}$$

Using these methods, we can in principle obtain an explicit result for each loop integral in terms of the artificial parameters Λ and μ. After combining all the relevant contributions, we would then take the limits $\Lambda \to \infty$ and $\mu \to 0$ and expect to obtain a sensible result. The drawbacks to this approach are threefold: first, the calculations are more cumbersome than the simplicity of the methods suggest; second, the separation of ultraviolet and infrared divergences can sometimes be more of a nuisance than a virtue, especially for the types of calculations encountered in this thesis; finally, certain symmetries are violated by these methods, and hence the results are not always reliable.

A superior approach is the method of dimensional regularization [10], whereby we regard the loop momentum as a vector in a D-dimensional space. We will soon see how in this framework, divergences only arise when D is a positive integer such as 4. Conceptual abstractness notwithstanding, dimensional regularization is an extremely useful method that has become the standard for many classes of calculations in particle physics.

2.1 Basic Calculation

In this section, we will evaluate the most basic Euclidean-space loop integral,

$$I_n = \int \frac{d^4k}{(2\pi)^4} \frac{1}{(k^2 + m^2)^n} \, , \tag{2.5}$$

from first principles using the method of dimensional regularization. In conjunction with the techniques we will discuss in subsequent chapters, this result will be a central component of the solution of more complicated integrals.

After generalizing the dimension of the integral from 4 to D,

$$I_n = \int \frac{d^D k}{(2\pi)^D} \frac{1}{(k^2 + m^2)^n} \, , \tag{2.6}$$

our first step is to switch to a hyperspherical coordinate system. Assuming, for now, that D is a positive integer and that $(2n - D) > 0$, we have

$$(k_1, k_2, \ldots, k_D) \longrightarrow (K, \phi, \theta_1, \ldots, \theta_{D-2}) \tag{2.7}$$

via

$$
\begin{aligned}
k_1 &= K \cos \theta_1 , \\
k_2 &= K \sin \theta_1 \cos \theta_2 , \\
k_3 &= K \sin \theta_1 \sin \theta_2 \cos \theta_3 , \\
&\vdots \\
k_{D-1} &= K \sin \theta_1 \ldots \sin \theta_{D-2} \cos \phi , \\
k_D &= K \sin \theta_1 \ldots \sin \theta_{D-2} \sin \phi .
\end{aligned}
\tag{2.8}
$$

The Jacobian factor, J, which relates the integration elements of the two coordinate systems by

$$dk_1 \, dk_2 \, \ldots \, dk_D = J \, dK \, d\phi \, d\theta_1 \, \ldots \, d\theta_{D-2} , \tag{2.9}$$

is given by the determinant

$$
\begin{aligned}
J &= \begin{vmatrix} \frac{\partial k_1}{\partial K} & \cdots & \frac{\partial k_D}{\partial K} \\ \vdots & \ddots & \vdots \\ \frac{\partial k_1}{\partial \theta_{D-2}} & \cdots & \frac{\partial k_D}{\partial \theta_{D-2}} \end{vmatrix} \\
&= K^{D-1} \prod_{j=1}^{D-2} \sin^j \theta_j .
\end{aligned}
\tag{2.10}
$$

The loop integral can then be factored into angular and radial parts:

$$I_n = \int d\Omega_D \int_0^\infty \frac{dK}{(2\pi)^D} \frac{K^{D-1}}{(K^2 + m^2)^n} . \tag{2.11}$$

To evaluate the radial integral, we begin with the substitution

$$K = m\sqrt{x} \tag{2.12}$$

so that

$$I_n = \frac{m^{D-2n}}{2(2\pi)^D} \int d\Omega_D \int_0^\infty dx \, \frac{x^{D/2-1}}{(x+1)^n} . \tag{2.13}$$

The x-integral can then be evaluated in terms of a Beta function. We will look at Beta and Gamma functions more carefully in the next section, but in the mean-

time, borrowing (2.29) and (2.30), our loop integral can now be written as

$$I_n = \frac{m^{D-2n}}{2(2\pi)^D} \frac{\Gamma\left(\frac{D}{2}\right) \Gamma\left(n - \frac{D}{2}\right)}{\Gamma(n)} \int d\Omega_D .$$

(2.14)

Turning to the angular integral, we have

$$\int d\Omega_D = \int_0^{2\pi} d\phi \prod_{j=1}^{D-2} \left(\int_0^{\pi} \sin^j \theta_j d\theta_j \right) .$$

(2.15)

The ϕ-integral is simply 2π, and the θ_j-integrals can be handled by (2.32) so that

$$\int d\Omega_D = 2\pi \prod_{j=1}^{D-2} \frac{\Gamma\left(\frac{j+1}{2}\right) \Gamma\left(\frac{1}{2}\right)}{\Gamma\left(\frac{j+2}{2}\right)} .$$

(2.16)

When the product is expanded, the $\Gamma((j+2)/2)$ terms in the denominator will cancel the $\Gamma((j+1)/2)$ terms in the adjacent numerator. This observation, along with $\Gamma(1/2) = \sqrt{\pi}$ and $\Gamma(1) = 1$, allows us to write

$$\int d\Omega_D = \frac{2\pi^{D/2}}{\Gamma(\frac{D}{2})} .$$

(2.17)

Inserting this result into (2.14), we have our solution for the basic loop integral in dimensional regularization:

$$\int \frac{d^D k}{(2\pi)^D} \frac{1}{(k^2 + m^2)^n} = \frac{1}{(4\pi)^{D/2}} \frac{\Gamma\left(n - \frac{D}{2}\right)}{\Gamma(n)} \left(\frac{1}{m^2}\right)^{n-\frac{D}{2}} .$$

(2.18)

While we originally assumed that D was a positive integer and that $(2n-D) > 0$ in order to facilitate an explicit derivation, (2.18) can be extended by means of analytic continuation so as to be valid for any choice of D in the complex plane such that $\Gamma(n - D/2)$ is well-defined.

2.2   The Gamma Function

We have now seen that the solution for the basic loop integral in dimensional regularization (2.18) can be expressed in terms of Gamma functions. In this section, we will examine some of the properties of these functions (see [11] for more rigor).

The most common definition of the Gamma function is through the integral

$$\Gamma(z) = \int_0^\infty t^{z-1} e^{-t} dt \ . \tag{2.19}$$

This formulation quickly leads to a number of useful properties, such as

$$\Gamma(z+1) = z\Gamma(z) \ , \tag{2.20}$$

$$\Gamma(1/2) = \sqrt{\pi} \ , \tag{2.21}$$

$$\Gamma(n) = (n-1)! \ , \qquad n \in \{1, 2, 3, \ldots\} \ . \tag{2.22}$$

Mathematicians, meanwhile, tend to prefer the Weierstrassian product

$$\frac{1}{\Gamma(z)} = z e^{\gamma z} \prod_{n=1}^\infty \left\{ \left(1 + \frac{z}{n}\right) e^{-z/n} \right\} \ , \tag{2.23}$$

where γ is the Euler-Mascheroni constant, an irrational number defined by

$$\gamma = \lim_{m \to \infty} \left(\frac{1}{1} + \frac{1}{2} + \cdots + \frac{1}{m} - \log m \right) = 0.5772157 \ldots \ . \tag{2.24}$$

From (2.23) it is readily deduced that $\Gamma(z)$ is an analytic function of z with simple poles at $z = 0, -1, -2, \ldots$ Looking back at (2.18), it is now clear why we originally restricted ourselves to values of $(2n - D)$ that were greater than zero, as the Gamma function in the numerator is not well-behaved when $(n - D/2)$ is a negative integer. Of course, it is apparent that the original integral (2.5) has an ultraviolet divergence whenever $n \leq 2$.

We expect to encounter divergences, though, as that is the reason for which regularization is required in the first place. The structure of the Gamma function implies that so long as we steer clear of the poles, we can work with a well-behaved, analytic function. To accomplish this, we write

$$D = 4 - 2\epsilon \tag{2.25}$$

so that Gamma functions like $\Gamma(n - D/2)$ are well-behaved, since the argument, $n - 2 + \epsilon$, is never a non-positive integer. We can use (2.20) to write an arbitrary Gamma function $\Gamma(a + b\epsilon)$ in terms of $\Gamma(1 + b\epsilon)$, which in turn can be expressed as

$$\Gamma(1 + b\epsilon) = \exp\left\{ -(b\epsilon)\gamma + \frac{(b\epsilon)^2}{2} \zeta(2) - \frac{(b\epsilon)^3}{3} \zeta(3) + \ldots \right\} \ . \tag{2.26}$$

Expanding out the exponential in (2.26), we obtain $\Gamma(1 + b\epsilon)$ as a series in powers of ϵ. The coefficients of this expansion depend on the transcendental numbers

$\{\gamma, \zeta(2), \zeta(3), \ldots\}$, where γ was defined in (2.24) and $\zeta(n)$ is the Riemann zeta function defined by

$$\zeta(n) = \sum_{k=1}^{\infty} \frac{1}{k^n} \,. \tag{2.27}$$

We could easily evaluate $\zeta(n)$ to arbitrary precision numerically, but it is nevertheless worth noting that $\zeta(2) = \pi^2/6$ and $\zeta(4) = \pi^4/90$. The more general Gamma function $\Gamma(a + b\epsilon)$ can be expanded in ϵ as

$$\Gamma(a + b\epsilon) = P(a, b)\, \Gamma(1 + b\epsilon) \,, \tag{2.28}$$

where we use (2.26) for $\Gamma(1 + b\epsilon)$ and $P(a, b)$ is a Pochhammer symbol [12] that, by virtue of (2.20), is a rational function involving only a, b, and ϵ.

The Beta function, $B(a, b)$, occurs frequently when we use dimensional regularization to evaluate loop integrals, and it can be written in terms of Gamma functions as

$$B(a, b) = \frac{\Gamma(a)\Gamma(b)}{\Gamma(a + b)} \,. \tag{2.29}$$

In particular, Beta functions appear in the following commonly used integrals [13]:

$$\int_0^{\infty} \frac{x^{\mu-1}\, dx}{(1 + x)^{\nu}} = B(\mu, \nu - \mu) \,, \tag{2.30}$$

$$\int_0^1 x^{\mu-1}(1 - x)^{\nu-1} dx = B(\mu, \nu) \,, \tag{2.31}$$

$$\int_0^{\frac{\pi}{2}} \sin^{\mu-1} x \, \cos^{\nu-1} x \, dx = \frac{1}{2} B\left(\frac{\mu}{2}, \frac{\nu}{2}\right) \,. \tag{2.32}$$

The relation (2.32) can be used to establish a Gamma function identity, known as the doubling formula, which we will need to call upon later:

$$\Gamma(2x) = \frac{2^{2x-1}}{\sqrt{\pi}} \, \Gamma(x) \, \Gamma\left(x + \frac{1}{2}\right) \,. \tag{2.33}$$

We have now seen how dimensional regularization allows us to express individual loop integrals as series in powers of ϵ. Actually, we are dealing with a Laurent series — in other words a series with powers and inverse powers of ϵ — because the divergent diagrams will blow up if we take the physical limit of (2.25), namely, $\epsilon \to 0$. When all the relevant diagrams for a calculation are included and the theory is properly renormalized, we expect that the troublesome terms with inverse powers of ϵ will cancel, leaving us with a result that is finite and physical as $\epsilon \to 0$.

Looking at the Gamma functions in (2.18), we see that this particular integral will have precisely one factor of $\Gamma(1 + \epsilon)$ within which the transcendental constants in (2.26) appear. More complicated integrals will depend on more complex combinations of Gamma functions, but it turns out that if we remove a factor of

$$\mathcal{F} \equiv \frac{m^{-2\epsilon}\,\Gamma(1 + \epsilon)}{(4\pi)^{D/2}} \tag{2.34}$$

for each loop in the integral, the remainder of the solution will always be independent of γ. Meanwhile, (2.34) goes smoothly to $1/(4\pi)^2$ in the limit $\epsilon \to 0$, so it essentially allows us to remove some of the clutter that accompanies a typical loop integral.

2.3 Scaleless Integrals

In this section, we will prove an important result regarding the behavior of scaleless integrals like

$$J_n = \int \frac{d^4 k}{k^{2n}} \tag{2.35}$$

in dimensional regularization. Specifically, these integrals are zero. We will now justify this result in three different ways in order of increasing rigor and sophistication.

Intuitive Method

While we have already seen how dimensional regularization deals with loop integrals with ultraviolet divergences, the technique applies equally well when there are infrared divergences. Suppose we take $n = 2$ in (2.35) so that we wish to evaluate

$$J_2 = \int \frac{d^D k}{k^4} . \tag{2.36}$$

This integral has logarithmic divergences of both an ultraviolet and infrared nature. By treating both types of divergences simultaneously through a single artificial parameter ϵ, dimensional regularization allows the two types of divergences to cancel for scaleless integrals. Heuristically,

$$\int \frac{d^D k}{k^4} \sim \frac{1}{\epsilon_{UV}} - \frac{1}{\epsilon_{IR}} = 0 . \tag{2.37}$$

As this reasoning is less convincing for $n \neq 2$, we can also examine what happens when we make the substitution $k = \mu\ell$. Applying this to (2.35), we have

$$
\begin{aligned}
J_n &= \int \frac{d^D(\mu\ell)}{(\mu\ell)^{2n}} \\
&= \mu^{D-2n} \int \frac{d^D\ell}{\ell^{2n}} \\
&= \mu^{D-2n} J_n \,,
\end{aligned}
\tag{2.38}
$$

and so for (2.38) to hold for arbitrary values of μ, we can require that $J_n = 0$.

Brute Force Method

Borrowing a technique from the next chapter, we can show that scaleless integrals in dimensional regularization are zero based on the result of (2.18). The idea is to apply the time-honored physicist's technique of multiplying by 1 for a clever choice of 1. Specifically,

$$
J_n = \int \frac{d^D k}{k^{2n}} \frac{k^2 + m^2}{k^2 + m^2} \,.
\tag{2.39}
$$

We then combine the denominators with a Feynman parameter. Postponing an explanation of the details of this technique to the next chapter, we have

$$
J_n = \frac{\Gamma(n+1)}{\Gamma(n)\Gamma(1)} \int_0^1 (1-x)^{n-1} dx \int d^D k \; \frac{k^2 + m^2}{[x(k^2 + m^2) + (1-x)k^2]^{n+1}} \,.
\tag{2.40}
$$

Since we intend to show that $J_n = 0$, it will be convenient to discard multiplicative factors at the front of the expression as they arise. Writing the numerator as

$$
k^2 + m^2 = (k^2 + xm^2) + (1-x)m^2 \,,
\tag{2.41}
$$

$$
J_n \sim \int_0^1 (1-x)^{n-1} dx \int d^D k \; \left\{ \frac{1}{(k^2 + xm^2)^n} + \frac{(1-x)m^2}{(k^2 + xm^2)^{n+1}} \right\} \,.
\tag{2.42}
$$

At this stage, we can apply the basic result (2.18) to both of the terms in the braces, resulting in

$$
\begin{aligned}
J_n \;\sim\; \int_0^1 dx \Bigg\{ & (1-x)^{n-1} \frac{\Gamma(n - D/2)}{\Gamma(n)} \left(\frac{1}{xm^2} \right)^{n-D/2} \\
& + (1-x)^n m^2 \frac{\Gamma(n+1 - D/2)}{\Gamma(n+1)} \left(\frac{1}{xm^2} \right)^{n+1-D/2} \Bigg\} \,.
\end{aligned}
\tag{2.43}
$$

Next we use (2.20) in order to write the Gamma functions in the second term in the same form as those in the first:

$$J_n \sim \frac{\Gamma(n - \frac{D}{2})}{\Gamma(n)} \left(\frac{1}{m^2}\right)^{n - \frac{D}{2}}$$

$$\times \int_0^1 dx \left\{ x^{\frac{D}{2}-n}(1-x)^{n-1} + x^{\frac{D}{2}-n-1}(1-x)^n \frac{(n - \frac{D}{2})}{n} \right\}. \tag{2.44}$$

The x-integrals can be evaluated with the identity (2.31) so that

$$J_n \sim n B\left(\frac{D}{2} - n + 1, n\right) + \left(n - \frac{D}{2}\right) B\left(\frac{D}{2} - n, n + 1\right)$$

$$\sim \frac{n\Gamma\left(\frac{D}{2} - n + 1\right)\Gamma(n)}{\Gamma\left(\frac{D}{2} + 1\right)} - \frac{\left(\frac{D}{2} - n\right)\Gamma\left(\frac{D}{2} - n\right)\Gamma(n+1)}{\Gamma\left(\frac{D}{2} + 1\right)}$$

$$\sim \frac{\Gamma\left(\frac{D}{2} - n + 1\right)\Gamma(n+1)}{\Gamma\left(\frac{D}{2} + 1\right)} - \frac{\Gamma\left(\frac{D}{2} - n + 1\right)\Gamma(n+1)}{\Gamma\left(\frac{D}{2} + 1\right)}$$

$$\sim 0. \tag{2.45}$$

Elegant Method

The method we will now present (first used in [14]) is a proof that

$$J = \int_0^\infty x^\mu \, dx = 0 \tag{2.46}$$

in dimensional regularization. The generalization to scaleless D-dimensional loop integrals follows naturally, as the radial part of these integrals takes on the same form as (2.46). We start by breaking the integral into two parts,

$$J = J_1 + J_2 = \int_0^b x^\mu \, dx + \int_b^\infty x^\mu \, dx. \tag{2.47}$$

Looking at J_1, we will define the integral in a distributional sense, namely,

$$J_1 = \int_0^b x^\mu f(x) \, dx, \tag{2.48}$$

where $f(x)$ is a test function that is sufficiently well-behaved to be infinitely differentiable over the region $x \in [0, b]$. As a result, we can expand $f(x)$ in terms of a Taylor series,

$$f(x) = f(0) + f'(0)\, x + \frac{f''(0)}{2}\, x^2 + \ldots + \frac{f^n(0)}{n!}\, x^n + \ldots . \qquad (2.49)$$

Provided $\mathrm{Re}(\mu) > -1$, we can now integrate so that

$$J_1 = \frac{f(0)\, b^{\mu+1}}{\mu+1} + \frac{f'(0)\, b^{\mu+2}}{\mu+2} + \ldots + \frac{f^n(0)\, b^{\mu+n+1}}{(n-1)!(\mu+n+1)} + \ldots . \qquad (2.50)$$

While this expression is explicitly valid for $\mathrm{Re}(\mu) > -1$, we can use analytic continuation to define J_1 for all possible values of μ, aside from the simple poles that occur at $-1, -2, \ldots$. Finally, choosing a particularly simple test function, namely $f(x) = 1\ \forall x \in [0, b]$, we obtain

$$J_1 = \int_0^b x^\mu f(x)\, dx = \frac{b^{\mu+1}}{\mu+1}, \qquad \mu \in \mathcal{C}\backslash\{-1, -2, \ldots\}. \qquad (2.51)$$

Moving on to J_2, we will again define the integral in a distributional sense, and in addition, we will make the substitution $x = 1/y$, so that

$$J_2 = \int_b^\infty x^\mu f(x)\, dx = \int_0^{1/b} y^{-\mu-2} f(1/y)\, dy. \qquad (2.52)$$

Then we proceed, just as for J_1, by expanding f in a Taylor series, performing the integral under the assumption that μ lies in a safe range ($\mathrm{Re}(\mu) < -1$ in this case), extending the result to all values of μ by analytic continuation, and then setting the test function to 1. This gives us

$$J_2 = \frac{(1/b)^{-\mu-1}}{(-\mu-1)} = -\frac{b^{\mu+1}}{\mu+1}, \qquad \mu \in \mathcal{C}\backslash\{-1, -2, \ldots\}, \qquad (2.53)$$

and so J_1 and J_2 cancel to establish that J is zero and that scaleless integrals indeed vanish in dimensional regularization.

"Here is an ordinary square... but suppose we extend the square beyond the two dimensions of our universe, along the hypothetical Z axis, there. This forms a three-dimensional object known as a 'cube', or a 'Frinkahedron' in honor of its discoverer."

Professor Frink (*The Simpsons*)

Chapter 3

Parameter Tricks

In Chapter 2, we showed how dimensional regularization allows us to mitigate
the divergences that arise in loop integrals. On the other hand, the basic result
of (2.18) does not apply directly to most loop integrals, as they typically contain
a number of different denominator factors arising from the various propagators
in Feynman diagrams. For simplicity, we will loosely use the term "propaga-
tor" for the denominator factor associated with the full propagator arising from
the Feynman rules of Chapter 1. In this chapter, we will introduce a number of
ways of dealing with multiple propagators so that we can evaluate more elab-
orate loop integrals in terms of the basic integral (2.18). We will illustrate these
methods using classes of integrals that we will have further encounters with in
the chapters ahead.

3.1 Feynman Parameters

Consider the one-loop integral

$$\int \frac{[d^D k]}{(k^2 + 2kp)^a \; k^{2(b+c\epsilon)}} \qquad \text{where} \qquad [d^D k] = \frac{d^D k}{(2\pi)^D} \, . \qquad (3.1)$$

We denote this class of integrals by "onshell" and Figure 3.1 shows a sketch. By
sketch we mean a diagram that depicts the basic structure of the integral. While
this could be a Feynman diagram, it could also be the case that a class of inte-
grals — hereafter to be referred to as a topology — appears at an intermediate
stage of a calculation. The sketch of a topology merely indicates which propaga-
tors are present, but says nothing about how they got there, how many powers
of each factor exist, or what might be in the numerator. Note the presence of
the $k^{2c\epsilon}$ term in (3.1). While it is simple enough to set $c = 0$ for integrals that
originate from one-loop Feynman diagrams, such epsilon-propagators can arise

on massless lines in a multiloop diagram when we integrate over one or more subloops. We will see an example of this later in this section.
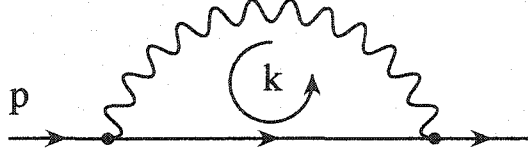
Figure 3.1: Sketch of the "onshell" topology.

The idea behind Feynman parameters is the identity

$$\frac{1}{AB} = \int_0^1 dx \, \frac{1}{[xA + (1-x)B]^2} \, . \tag{3.2}$$

This may seem like a frivolous complication, but if A and B are propagators in a loop integral, it is easier to perform the loop integration on the right-hand side of (3.2) than on the left. Before we apply this to the "onshell" topology, we will need a more general version of the identity (3.2) [1]:

$$\frac{1}{A_1^{m_1} A_2^{m_2} \cdots A_n^{m_n}} = \int_0^1 dx_1 \cdots dx_n \, \delta \left(\sum x_i - 1 \right) \frac{\prod x_i^{m_i - 1}}{[\sum x_i A_i]^{\sum m_i}} \frac{\Gamma(m_1 + \cdots + m_n)}{\Gamma(m_1) \cdots \Gamma(m_n)} \, . \tag{3.3}$$

When we apply (3.3) to (3.1), we obtain

$$\frac{\Gamma(a + b + c\epsilon)}{\Gamma(a)\Gamma(b + c\epsilon)} \int_0^1 dx \, x^{a-1} (1-x)^{b+c\epsilon-1} \int \frac{[d^D k]}{[x(k^2 + 2kp) + (1-x)k^2]^{a+b+c\epsilon}} \, . \tag{3.4}$$

The denominator terms can now be combined and we complete the square:

$$\begin{aligned} x(k^2 + 2kp) + (1-x)k^2 &= k^2 + 2xkp \\ &= (k + xp)^2 - x^2 p^2 \, . \end{aligned} \tag{3.5}$$

Note that in Euclidean space, $p^2 = -m^2$. We then shift the variable of integration to $\ell = k + xp$ so that we have

$$\frac{\Gamma(a + b + c\epsilon)}{\Gamma(a)\Gamma(b + c\epsilon)} \int_0^1 dx \, x^{a-1} (1-x)^{b+c\epsilon-1} \int \frac{[d^D \ell]}{[\ell^2 + x^2 m^2]^{a+b+c\epsilon}} \, . \tag{3.6}$$

Applying the basic dimensional regularization integral (2.18), we produce

$$\frac{\Gamma(a+b+c\epsilon)}{\Gamma(a)\Gamma(b+c\epsilon)} \int_0^1 dx\, x^{a-1}(1-x)^{b+c\epsilon-1} \left\{ \frac{\Gamma\left(a+b+c\epsilon-\frac{D}{2}\right)}{(4\pi)^{D/2}\Gamma(a+b+c\epsilon)} \left(\frac{1}{x^2 m^2}\right)^{a+b+c\epsilon-\frac{D}{2}} \right\}$$

(3.7)

or more simply,

$$\frac{\Gamma\left(a+b+c\epsilon-\frac{D}{2}\right)}{(4\pi)^{D/2}\Gamma(a)\Gamma(b+c\epsilon)m^{2(a+b+c\epsilon)-D}} \int_0^1 dx\, x^{D-1-a-2b-2c\epsilon}(1-x)^{b+c\epsilon-1}\,.$$

(3.8)

Using (2.31) to perform the x-integration, we have

$$\frac{\Gamma\left(a+b+c\epsilon-\frac{D}{2}\right)}{(4\pi)^{D/2}\Gamma(a)\Gamma(b+c\epsilon)m^{2(a+b+c\epsilon)-D}}\, B(D-a-2b-2c\epsilon, b+c\epsilon)\,.$$

(3.9)

Finally, using (2.29) to write the Beta function in terms of Gamma functions, we obtain

$$\frac{\Gamma\left(a+b+c\epsilon-\frac{D}{2}\right)\Gamma(D-a-2b-2c\epsilon)}{(4\pi)^{D/2}\Gamma(a)\Gamma(D-a-b-c\epsilon)m^{2(a+b+c\epsilon)-D}}$$

(3.10)

for a final result of

$$\int \frac{[d^D k]}{(k^2+2kp)^a\, k^{2(b+c\epsilon)}} = \frac{\Gamma\left(a+b-2+(c+1)\epsilon\right)\Gamma(4-a-2b-2(c+1)\epsilon)}{(4\pi)^{2-\epsilon}\Gamma(a)\Gamma(4-a-b-(c+2)\epsilon)\, m^{2(a+b-2+(c+1)\epsilon)}}\,.$$

(3.11)

Another common one-loop topology that can be handled with a Feynman parameter is "one":

$$\int \frac{[d^D k]}{(k+q)^{2(a+b\epsilon)}\, k^{2(c+d\epsilon)}}\,.$$

(3.12)

This topology is sketched in Figure 3.2. Note that both propagators are massless and can therefore have epsilon-pieces if subloops have already been integrated out. Also, there are no constraints on the external momentum q, unlike the case in "onshell' where we needed to know that $p^2 = -m^2$.
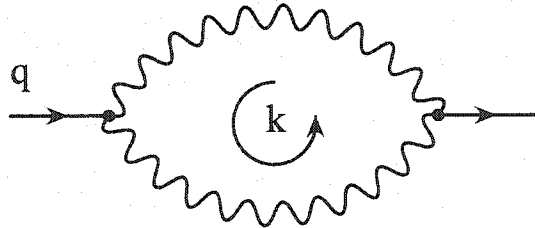
Figure 3.2: Sketch of the "one" topology.

We will not derive a general result for the "one" topology here, however we will now look at an example where we can integrate over a subloop in order to see how one-loop topologies can be nested. Consider the integral

$$J_{001} = \int \frac{[d^D k_1][d^D k_2]}{(k_1^2 + 2k_1 p)(k_1 + k_2)^2 k_2^2} \tag{3.13}$$

as depicted in Figure 3.3. Since we have routed k_2 through both of the massless
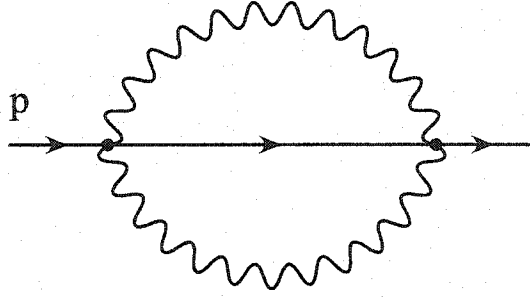
Figure 3.3: Sketch of the "J_{001}" topology.

lines, the k_2-dependent subloop belongs to the "one" topology. Introducing a Feynman parameter,

$$
\begin{aligned}
J_{001} &= \frac{\Gamma(2)}{\Gamma(1)\Gamma(1)} \int_0^1 dx \int \frac{[d^D k_1]}{k_1^2 + 2k_1 p} \int \frac{[d^D k_2]}{[x(k_1 + k_2)^2 + (1-x)k_2^2]^2} \\
&= \int_0^1 dx \int \frac{[d^D k_1]}{k_1^2 + 2k_1 p} \int \frac{[d^D k_2]}{[(k_2 + xk_1)^2 + x(1-x)k_1^2]^2} \; .
\end{aligned}
\tag{3.14}
$$

Next we identify $\ell = k_2 + xk_1$ and use (2.18) to evaluate the ℓ-integral, yielding

$$
\begin{aligned}
J_{011} &= \int_0^1 dx \int \frac{[d^D k_1]}{k_1^2 + 2k_1 p} \frac{\Gamma\left(2 - \frac{D}{2}\right)}{(4\pi)^{D/2} [x(1-x)k_1^2]^{2-D/2}} \\
&= \frac{\Gamma(\epsilon)}{(4\pi)^{D/2}} \int_0^1 dx \, x^{-\epsilon}(1-x)^{-\epsilon} \int \frac{[d^D k_1]}{(k_1^2 + 2k_1 p)\, k_1^{2\epsilon}} \; .
\end{aligned}
\tag{3.15}
$$

The remaining k_1-integral belongs to the "onshell" topology, and so when we substitute (3.11) and evaluate the x-integral with (2.31), we obtain

$$
\begin{aligned}
J_{011} &= \frac{\Gamma(\epsilon)}{(4\pi)^{D/2}} \frac{\Gamma(1-\epsilon)\Gamma(1-\epsilon)}{\Gamma(2-2\epsilon)} \frac{\Gamma(-1+2\epsilon)\Gamma(3-4\epsilon)}{(4\pi)^{D/2}\Gamma(3-3\epsilon)\, m^{2(-1+2\epsilon)}} \\
&= \left(\frac{m^{-2\epsilon}\Gamma(1+\epsilon)}{(4\pi)^{D/2}}\right)^2 m^2 \left\{ \frac{\Gamma^2(1-\epsilon)\Gamma(-1+2\epsilon)\Gamma(3-4\epsilon)}{\Gamma(2-2\epsilon)\Gamma(3-3\epsilon)\Gamma(1+\epsilon)\epsilon} \right\} \; .
\end{aligned}
\tag{3.16}
$$

Notice how we have explicitly separated the factor in the brackets at the front, in accordance with the convention (2.34). Expanding the Gamma functions in the braces as a Laurent series in ϵ and dividing out the loop factors, we obtain

$$\frac{J_{011}}{m^2\mathcal{F}^2} = -\frac{1}{2\epsilon^2} - \frac{5}{4\epsilon} + \left(-\frac{11}{8} - \frac{\pi^2}{3}\right) + \left(\frac{55}{16} - \frac{5\pi^2}{6} - 4\zeta(3)\right)\epsilon + \mathcal{O}\left(\epsilon^2\right), \quad (3.17)$$

in exact agreement with the result provided in [15].

3.2 Schwinger Parameters

While there are often several techniques that can be used to evaluate certain loop integrals — some one-loop integrals can even be solved in Minkowski space with direct contour integration — there are also loop integrals that do not yield to Feynman parameters in any obvious way. For example, the "gm3" topology,

$$\int \frac{[d^D k_1][d^D k_2]}{(k_1^2 + 1)^a(k_2^2 + 1)^b(k_1 - k_2)^{2c}}, \quad (3.18)$$

and depicted in Figure 3.4, is a vacuum bubble topology that often arises in calculations. Note that we have set $m = 1$ for convenience, since for integrals with a single external scale, the overall mass dependence is uniquely determined by dimensional considerations. Should we try to evaluate (3.18) using Feynman
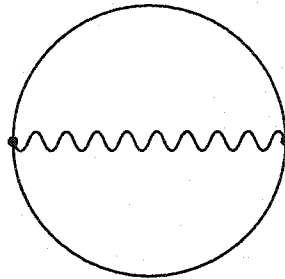
Figure 3.4: Sketch of the "gm3" topology.

parameters, we would find that although the loop integrals can be dealt with, the integrals over the Feynman parameters themselves are unusually difficult. An easier solution arises from a related technique: Schwinger parameters.

A Schwinger parameter, α, can be introduced via the identity

$$\frac{1}{A^a} = \frac{1}{\Gamma(a)} \int_0^\infty d\alpha \, \alpha^{a-1} e^{-\alpha A}. \quad (3.19)$$

This identity is then copied several times so that

$$\frac{1}{A^a B^b \cdots} = \frac{1}{\Gamma(a)\Gamma(b)\cdots} \int_0^\infty d\alpha \int_0^\infty d\beta \ \cdots \ \alpha^{a-1}\beta^{b-1} \cdots \ e^{-\alpha A - \beta B - \dots} \qquad (3.20)$$

and all the different propagators are additively combined in the argument of the exponential. Applying this to the "gm3" integral (3.18), we have

$$\frac{1}{\Gamma(a)\Gamma(b)\Gamma(c)} \int_0^\infty d\alpha \ d\beta \ d\gamma \ \alpha^{a-1}\beta^{b-1}\gamma^{c-1} \int [d^D k_1][d^D k_2]$$
$$\times \exp\left[-\alpha(k_1^2 + 1) - \beta(k_2^2 + 1) - \gamma(k_1 - k_2)^2\right] . \qquad (3.21)$$

Next, we rewrite the exponential as a product of Gaussians in the loop momenta:

$$\exp[\cdots] = e^{-(\alpha+\beta)} \exp\left[-(\alpha + \gamma)k_1^2 - (\beta + \gamma)k_2^2 + 2\gamma k_1 k_2\right]$$
$$= e^{-(\alpha+\beta)} e^{-(\alpha+\gamma)\left(k_1 - \frac{\gamma}{\alpha+\gamma}k_2\right)^2} e^{-\left(\frac{\alpha\beta+\alpha\gamma+\beta\gamma}{\alpha+\gamma}\right)k_2^2} . \qquad (3.22)$$

If we shift k_1 by an amount $\gamma k_2/(\alpha + \gamma)$, we have two Gaussian loop integrals of the form

$$G(\mu) = \int [d^D k] \ e^{-\mu k^2} . \qquad (3.23)$$

To evaluate $G(\mu)$, we work in hyperspherical coordinates and use (2.17) to evaluate the angular integral:

$$G(\mu) = \frac{2\pi^{D/2}}{\Gamma(D/2)} \frac{1}{(2\pi)^D} \int_0^\infty dk \ k^{D-1} e^{-\mu k^2} . \qquad (3.24)$$

Setting $x = \mu k^2$, we can use (2.19) to solve the x-integral:

$$G(\mu) = \frac{2}{(4\pi)^{D/2}\Gamma(D/2)} \frac{\mu^{-D/2}}{2} \int_0^\infty dx \ x^{\frac{D}{2}-1} e^{-x}$$
$$= \frac{\mu^{-D/2}}{(4\pi)^{D/2}\Gamma(D/2)} \Gamma(D/2)$$
$$= \frac{\mu^{-D/2}}{(4\pi)^{D/2}} . \qquad (3.25)$$

Returning to our "gm3" calculation, we can now insert (3.25) for the two Gaussian loop integrals, obtaining

$$\frac{1}{(4\pi)^D \Gamma(a)\Gamma(b)\Gamma(c)} \int_0^\infty d\alpha \ d\beta \ d\gamma \ \alpha^{a-1}\beta^{b-1}\gamma^{c-1} e^{-(\alpha+\beta)} (\alpha\beta + \alpha\gamma + \beta\gamma)^{-D/2} . \quad (3.26)$$

With the loop integrals out of the way, we are now left with integrals over the three Schwinger parameters. Starting with the γ-integral,

$$I_\gamma = \int_0^\infty d\gamma \; \gamma^{c-1} \left(\alpha\beta + (\alpha+\beta)\gamma\right)^{-D/2} , \tag{3.27}$$

into which we substitute $\gamma = \alpha\beta z/(\alpha+\beta)$, so that

$$I_\gamma = \frac{(\alpha\beta)^{c-D/2}}{(\alpha+\beta)^c} \int_0^\infty dz \; z^{c-1}(1+z)^{-D/2} . \tag{3.28}$$

Using (2.30) to solve the z-integral,

$$I_\gamma = \frac{(\alpha\beta)^{c-D/2}}{(\alpha+\beta)^c} \; B\left(c , \frac{D}{2} - c\right) , \tag{3.29}$$

and so the "gm3" integral now becomes

$$\frac{B\left(c , \frac{D}{2} - c\right)}{(4\pi)^D \; \Gamma(a)\Gamma(b)\Gamma(c)} \int_0^\infty d\alpha \, d\beta \; \alpha^{a-1+c-\frac{D}{2}} \beta^{b-1+c-\frac{D}{2}} (\alpha+\beta)^{-c} e^{-(\alpha+\beta)} . \tag{3.30}$$

At this stage, the astute substitutions are $\alpha = x\rho$ and $\beta = (1-x)\rho$, leading to

$$\frac{B\left(c , \frac{D}{2} - c\right)}{(4\pi)^D \; \Gamma(a)\Gamma(b)\Gamma(c)} \int_0^1 dx \; x^{a-1+c-\frac{D}{2}} (1-x)^{b-1+c-\frac{D}{2}}$$
$$\times \int_0^\infty d\rho \; \rho^{1+\left(a-1+c-\frac{D}{2}\right)+\left(b-1+c-\frac{D}{2}\right)-c} e^{-\rho} . \tag{3.31}$$

Solving the x-integral with (2.31) and the ρ-integral with (2.19), we finish with

$$\int \frac{[d^D k_1][d^D k_2]}{(k_1^2 + 1)^a (k_2^2 + 1)^b (k_1 - k_2)^{2c}} \tag{3.32}$$
$$= \frac{\Gamma\left(\frac{D}{2} - c\right) \Gamma\left(a + c - \frac{D}{2}\right) \Gamma\left(b + c - \frac{D}{2}\right) \Gamma(a + b + c - D)}{(4\pi)^D \; \Gamma(a)\Gamma(b)\Gamma\left(\frac{D}{2}\right) \Gamma(a + b + 2c - D)} .$$

Note that a, b, and c need not be integers. In all honesty, "gm3" is probably the most complicated integral for which we make use of a general solution. As we will see in the next chapter, there are methods by which we can write arbitrary integrals within a given topology in terms of a few specific integrals in the topology, and therefore general solutions are, fortunately, unnecessary.

3.3 Tomonaga Parameters

While Feynman and Schwinger parameters are usually versatile enough to help us evaluate many multiloop integrals, there is a third identity that is worth knowing about:

$$\frac{1}{A^\alpha B^\beta} = \frac{1}{B(\alpha,\beta)} \int_0^\infty d\lambda \, \frac{\lambda^{\beta-1}}{[A+B\lambda]^{\alpha+\beta}} \, . \tag{3.33}$$

The parameter λ in this identity does not have a commonly used name, and so we shall create a temporary name to be used within this thesis. It would seem fitting to name this parameter after Sin-Itiro Tomonaga who, along with Richard Feynman and Julian Schwinger, was awarded the Nobel Prize in Physics in 1965 for "fundamental work in quantum electrodynamics, with deep-ploughing consequences for the physics of elementary particles" [16].

To illustrate the application of Tomonaga parameters, consider the integral

$$J_1^+ = \int \frac{[d^D k_1][d^D k_2]}{(k_1 p + 1)(k_2^2)[(k_1+k_2)^2 + 1]} \, . \tag{3.34}$$

The unusual factor $(k_1 p + 1)$ is characteristic of a category of integrals known as eikonal integrals. We will encounter eikonal integrals again in Chapters 6 and 12, but for now, we will simply use J_1^+ as a representative example of the types of loop integrals where Tomonaga parameters are most useful.

We start by shifting k_1 in (3.34) to $k_1 - k_2$ and then introduce a Tomonaga parameter to combine the k_1-dependent factors:

$$\begin{aligned}
J_1^+ &= \int \frac{[d^D k_1][d^D k_2]}{(k_1 p - k_2 p + 1)(k_2^2)(k_1^2 + 1)} \\
&= \int \frac{[d^D k_1][d^D k_2]}{k_2^2} \int_0^\infty \frac{d\lambda}{[k_1^2 + 1 + \lambda(k_1 p - k_2 p + 1)]^2} \, . \tag{3.35}
\end{aligned}$$

Next, we complete the square of the new denominator and use $p^2 = -1$:

$$[k_1^2 + 1 + \lambda(k_1 p - k_2 p + 1)] = \left[\left(k_1 + \frac{\lambda p}{2}\right)^2 + \frac{\lambda^2}{4} + \lambda + 1 - \lambda k_2 p\right] \, . \tag{3.36}$$

After an obvious shift in k_1 we can perform the k_1-integral using (2.18), so that

$$J_1^+ = \frac{\Gamma(\epsilon)}{(4\pi)^{D/2}} \int_0^\infty d\lambda \int \frac{[d^D k_2]}{k_2^2 \left(\frac{\lambda^2}{4} + \lambda + 1 - \lambda k_2 p\right)^\epsilon} \, . \tag{3.37}$$

Introducing a second Tomonaga parameter to evaluate the k_2-integral,

$$
\begin{aligned}
J_1^+ &= \frac{\Gamma(\epsilon)}{(4\pi)^{D/2}} \int_0^\infty d\lambda \int_0^\infty \frac{d\rho\, \rho^{\epsilon-1}}{B(1,\epsilon)} \int \frac{[d^D k_2]}{\left[k_2^2 + \rho\left(\frac{\lambda^2}{4} + \lambda + 1 - \lambda k_2 p\right)\right]^{1+\epsilon}} \\
&= \frac{\Gamma(1+\epsilon)}{(4\pi)^{D/2}} \int_0^\infty d\lambda \int_0^\infty d\rho\, \rho^{\epsilon-1} \int \frac{[d^D k_2]}{\left[\left(k_2 - \frac{\lambda\rho}{2}p\right)^2 + \rho\left(\frac{\rho\lambda^2}{4} + \frac{\lambda^2}{4} + \lambda + 1\right)\right]^{1+\epsilon}} \\
&= \frac{\Gamma(-1+2\epsilon)}{(4\pi)^D} \int_0^\infty d\lambda \int_0^\infty \frac{d\rho\, \rho^{\epsilon-1}}{\rho^{-1+2\epsilon}} \left(\frac{\rho\lambda^2}{4} + \frac{\lambda^2}{4} + \lambda + 1\right)^{1-2\epsilon}.
\end{aligned}
\tag{3.38}
$$

At this stage, we encounter the crucial steps, as even Feynman and Schwinger parameters can cast loop integrals like J_1^+ in terms of an integral over some intricate function of parameters. Actually solving these final integrals analytically is the real challenge. For the task at hand, the substitutions

$$
\lambda = 2x, \qquad \rho = \frac{(x+1)^2}{x^2}\, z,
\tag{3.39}
$$

result in a complete separation of the x- and z-dependent factors, so that

$$
J_1^+ = \frac{2\Gamma(-1+2\epsilon)}{(4\pi)^D} \int_0^\infty dx\, \frac{x^{-2+2\epsilon}}{(x+1)^{-4+6\epsilon}} \int_0^\infty dz\, \frac{z^{-\epsilon}}{(1+z)^{-1+2\epsilon}}.
\tag{3.40}
$$

Using (2.30) to evaluate both integrals, the final result is

$$
J_1^+ = \frac{2}{(4\pi)^D} B(-1+2\epsilon, -3+4\epsilon)\Gamma(1-\epsilon)\Gamma(-2+3\epsilon).
\tag{3.41}
$$

3.4 Partial Fractions

Occasionally a set of propagators is not linearly independent, so that an obvious simplification is available. For example, the "gm2" topology

$$
\int \frac{[d^D k]}{(k^2 + m^2)^a\, k^{2b}},
\tag{3.42}
$$

as depicted in Figure 3.5, is a one-loop vacuum bubble topology in which the two propagators are not independent. As a result, we have a partial fraction identity

$$
\frac{1}{(k^2 + m^2)\, k^2} = \frac{1}{m^2}\left[\frac{1}{k^2} - \frac{1}{(k^2 + m^2)}\right]
\tag{3.43}
$$
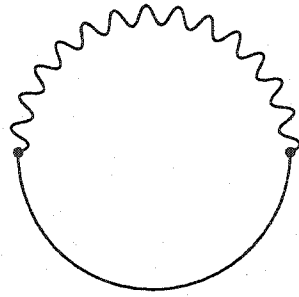
Figure 3.5: Sketch of the "gm2" topology.

which allows us to start with the general "gm2" integral (3.42) and whittle down the exponents a and b until one of them becomes zero. Note that for the purposes of this section, we assume that b is an integer, even though the most general "gm2" topology can also have an epsilon-propagator here. If the k^2 factors disappear, we are left with the basic integral (2.18), whereas if we eliminate the $(k^2 + m^2)$ factors, a scaleless integral remains.

A more efficient way of thinking about this technique is to write the explicit linear dependence of the propagators:

$$(k^2 + m^2) - (k^2) - m^2 = 0 \, . \tag{3.44}$$

If we rewrite this expression as

$$1 = \frac{1}{m^2} \left[(k^2 + m^2) - (k^2) \right] \, , \tag{3.45}$$

we can multiply by 1, in the form of the right-hand side of (3.45), as many times as is necessary to remove one of the propagators. In the next chapter, we will derive more sophisticated relationships which allow us to manipulate the exponents of propagators in loop integrals. This will become one of the most important methods in our arsenal.

"This day and age we're living in gives cause for apprehension, with speed and new invention, and things like third dimension, yet we get a trifle weary, with Mister Einstein's theory."

(*As Time Goes By*)

Chapter 4

Recurrence Relations

In Chapter 3, we described a number of techniques that can be used to evaluate loop integrals that contain several propagators. While the use of external parameters — Feynman, Schwinger, or Tomonaga — is the most aesthetically pleasing, the unfortunate fact of the matter is that often the resultant integrals over these parameters cannot be analytically solved, especially in a general form applicable to an entire topology. Section 3.4 introduced a simple identity that arises from a partial fraction decomposition and can be interpreted as a primitive recurrence relation, that is, a relationship between similar loop integrals that differ only in the explicit exponents of the propagators. In this chapter, we will derive a more sophisticated set of recurrence relations. Devising a recurrence relation algorithm to simplify integrals in a multiloop topology is one of the most tedious tasks associated with this kind of work, therefore, after we look at the basic concept behind recurrence relations, we will illustrate their use through a sequence of increasingly complicated examples.

4.1 Basic Concepts

The first use of recurrence relations to simplify loop integrals took place over twenty years ago in the context of calculating β-functions of massless scalar φ^3 theory [17,18]. While the computational resources available at that time were meager, these works were nearly clairvoyant in their assessment of the future applications of the method. To illustrate the basic idea, consider the n-loop integral

$$\int \frac{[d^D k_1][d^D k_2]\cdots[d^D k_n]}{\mathcal{D}(k_1, k_2, \ldots, k_n, p)} ,$$

(4.1)

where $\mathcal{D}(k_1, k_2, \ldots, k_n, p)$ denotes an unspecified collection of propagators. Now suppose, at the front of the integrand, we insert the operator

$$\frac{\partial}{\partial(k_i)_\mu} \ell_\mu \, , \tag{4.2}$$

where $i \in [1, n]$ and $\ell \in \{k_1, k_2, \ldots, k_n, p\}$. Stokes' Theorem then allows us to transform our integral:

$$\int \frac{\partial}{\partial(k_i)_\mu} \ell_\mu \frac{[d^D k_1][d^D k_2] \cdots [d^D k_n]}{\mathcal{D}(k_1, k_2, \ldots, k_n, p)}$$

$$= \oint_{k_i \to \infty} [d^{D-1} S^\mu] \ell_\mu \frac{[d^D k_1] \cdots [d^D k_{i-1}][d^D k_{i+1}] \cdots [d^D k_n]}{\mathcal{D}(k_1, k_2, \ldots, k_n, p)} . \tag{4.3}$$

Along the $(D-1)$-dimensional surface where $k_i \to \infty$, every k_i-dependent propagator in $\mathcal{D}$ will go to k_i^2, because the k_i terms will dominate anything else. As a result, the surface integral is a scaleless integral which, as we recall from Section 2.3, vanishes in dimensional regularization. In other words, we can generate recurrence relations from the identity

$$\int \frac{\partial}{\partial(k_i)_\mu} \ell_\mu \frac{[d^D k_1][d^D k_2] \cdots [d^D k_n]}{\mathcal{D}(k_1, k_2, \ldots, k_n, p)} = 0 \, . \tag{4.4}$$

It is interesting to note that these integration by parts identities in momentum space are equivalent, via Fourier transforms, to statements of translation invariance and momentum conservation in position space [18]. While that interpretation is much more intuitive, the momentum-space formulation is easier to work with.

Observe that the basic identity (4.4) does not address loop integrals containing numerator factors. Our derivation of recurrence relations is restricted to scalar integrals, wherein the integrals are completely characterized by the exponents of the propagators, positive or negative. Oftentimes, any numerator factors we might start with can be written as linear combinations of propagators so as to create scalar integrals. The examples in this chapter will all behave in this way. In Chapter 5, we will explore techniques that can be used when this method cannot adequately handle all numerator factors. For an n-loop integral, we have $(n + 1)(n + 2)/2$ independent scalar products that can be constructed from $\{k_1, k_2, \ldots, k_n, p\}$, but since $p^2 = -m^2$ can be pulled out of the integral, there are really only $n(n + 3)/2$ scalars that need to be expressed in terms of propagators. So long as the propagators are linearly independent, this means that we need 2 different propagators for a one-loop integral, 5 for a two-loop integral, 9 for a three-loop integral, and so on. While we are on the topic of com-

binatorics, we can see from (4.4) that with n choices for k_i and $(n+1)$ choices for ℓ, we can generate $n(n+1)$ independent recurrence relations, in other words, 2, 6, and 12, for one-, two-, and three-loop topologies, respectively.

At this stage, it would be wise to introduce some notation. Given that the scalar integrals we will be working with can be completely characterized by the exponents of the propagators, we can write an integral from a topology "I" as

$$I(a_1, a_2, a_3, a_4, a_5) = \int \frac{[d^D k_1][d^D k_2]}{[1]^{a_1} [2]^{a_2} [3]^{a_3} [4]^{a_4} [5]^{a_5}} , \qquad (4.5)$$

where factors like [1] are convenient shorthands for specific propagators. Looking back at the partial fraction identity (3.45) for the "gm2" topology, if we set $m = 1$, we can write this as

$$1 = [1] - [2] . \qquad (4.6)$$

All recurrence relations will look like $\{1 = \dots \}$ at the moment they are applied to an integral. Based on (4.4), however, recurrence relations are typically derived in the form $\{0 = \dots \}$, so it is useful to have an additional notation. Taking (3.44) as a starting point, we would write

$$0 = \mathbf{1}^- - \mathbf{2}^- - 1 , \qquad (4.7)$$

where the symbol $\mathbf{1}^-$ denotes the integral $gm2(a_1 - 1, a_2)$, so that (4.7) represents

$$0 = gm2(a_1 - 1, a_2) - gm2(a_1, a_2 - 1) - gm2(a_1, a_2) . \qquad (4.8)$$

To conclude this section, we will look at another type of recurrence relation. For the sake of simplicity, let us examine a one-loop topology where

$$\mathcal{T} = \frac{1}{[1]^{a_1} [2]^{a_2}} , \qquad (4.9)$$

so that the standard recurrence relation identity (4.4) reads

$$\int [d^D k] \frac{\partial}{\partial k_\mu} (q_\mu \mathcal{T}) = 0 \qquad (4.10)$$

for $q \in \{k, p\}$. Now consider the integral

$$\int [d^D k] \, q_\mu \mathcal{T} . \qquad (4.11)$$

Tensorially, this integral must be proportional to p_μ, as p is the only vector that remains after integration. Furthermore, to obtain the correct mass dimension,

we require a factor of

$$(-p^2)^{\frac{D}{2}-a_1-a_2} .$$ (4.12)

Finally, we will denote the dimensionless remaining pieces by $\mathcal{X}$, so that

$$\int [d^D k] \, q_\mu \mathcal{T} = p_\mu (-p^2)^{\frac{D}{2}-a_1-a_2} \mathcal{X} .$$ (4.13)

Note that $\mathcal{X}$ will turn out to be a combination of loop integrals, albeit ones in which the mass dimension is already factored out. If we assign q_μ in (4.13) as p_μ and contract both sides with p^μ, we obtain the trivial result that $\mathcal{X}$ corresponds exactly to the integral over $\mathcal{T}$, aside from the explicit mass dimension. Setting q_μ equal to k_μ and contracting both sides with p^μ, on the other hand, will provide us with a nontrivial result for $\mathcal{X}$ once we rewrite $(k \cdot p)$ in terms of propagators in $\mathcal{T}$. Having determined $\mathcal{X}$, we then return to (4.13), with $q_\mu = k_\mu$, and take the partial derivative of both sides with respect to p_μ. Since $\mathcal{X}$ is technically mass-independent, the partial derivative only sees the leading p-dependent factors on the right-hand side of (4.13). We will demonstrate this method explicitly in the next example. It is important to realize that the recurrence relations developed in this way will not be independent from the recurrence relations provided by the integration by parts technique (4.4). Instead, these "extra" recurrence relations correspond to particularly unusual combinations of the original recurrence relations. Since it is often the case that these unusual combinations are both useful and hard to construct from the original recurrence relations, it is worth knowing about the approach.

4.2 Simple One-Loop Example

For our first explicit example of recurrence relations, let us recall the "onshell" topology from Section 3.1. Restricting the exponents to integers, we have

$$I(a_1, a_2) = \int \frac{[d^D k]}{k^{2a_1} (k^2 + 2kp)^{a_2}} .$$ (4.14)

Based on (4.4), there will be two recurrence relations:

$$\int [d^D k] \, \frac{\partial}{\partial k_\mu} \frac{p_\mu}{k^{2a_1} (k^2 + 2kp)^{a_2}} = 0 ,$$ (4.15)

$$\int [d^D k] \, \frac{\partial}{\partial k_\mu} \frac{k_\mu}{k^{2a_1} (k^2 + 2kp)^{a_2}} = 0 .$$ (4.16)

Starting with (4.15), we find that

$$\int [d^D k] \left\{ -\frac{2a_1(k \cdot p)}{k^2} - \frac{2a_2(k \cdot p)}{(k^2 + 2kp)} - \frac{2a_2 p^2}{(k^2 + 2kp)} \right\} \frac{1}{k^{2a_1}(k^2 + 2kp)^{a_2}} = 0 \,.$$

(4.17)

Using

$$p^2 = -1 \,, \qquad k^2 = [1] \,, \qquad (k \cdot p) = \frac{1}{2}([2] - [1]) \,,$$

(4.18)

the recurrence relation becomes

$$\int [d^D k] \left\{ -\frac{a_1([2] - [1])}{[1]} - \frac{a_2([2] - [1])}{[2]} + \frac{2a_2}{[2]} \right\} \frac{1}{[1]^{2a_1}[2]^{a_2}} = 0 \,,$$

(4.19)

or more compactly,

$$\mathbf{R1}: \qquad (a_1 - a_2) - a_1 \mathbf{1}^+ \mathbf{2}^- + 2a_2 \mathbf{2}^+ + a_2 \mathbf{1}^- \mathbf{2}^+ = 0 \,.$$

(4.20)

Repeating the same sequence of steps for (4.16), we obtain

$$\int [d^D k] \left\{ D - \frac{2a_1 k^2}{k^2} - \frac{2a_2 k^2}{(k^2 + 2kp)} - \frac{2a_2(k \cdot p)}{(k^2 + 2kp)} \right\} \frac{1}{k^{2a_1}(k^2 + 2kp)^{a_2}} = 0 \,,$$

$$\int [d^D k] \left\{ D - 2a_1 - \frac{2a_2[1]}{[2]} - \frac{a_2([2] - [1])}{[2]} \right\} \frac{1}{[1]^{2a_1}[2]^{a_2}} = 0 \,,$$

$$\mathbf{R2}: \qquad (D - 2a_1 - a_2) - a_2 \mathbf{1}^- \mathbf{2}^+ = 0 \,.$$

(4.21)

Equations (4.20) and (4.21) are the two recurrence relations for the "onshell" topology. **R2** will be all we need to concentrate on, as it relates $I(a_1, a_2)$ to $I(a_1 - 1, a_2 + 1)$. Rewriting it as

$$1 = \frac{a_2}{D - 2a_1 - a_2} \frac{[1]}{[2]} \,,$$

(4.22)

we see that this recurrence relation can be applied as many times as necessary in order to reduce a_1 to 0. Once $a_1 = 0$, the "onshell" topology simplifies to

$$I(0, a_2) = \int \frac{[d^D k]}{(k^2 + 2kp)^{a_2}}$$

$$= \int \frac{[d^D k]}{[(k + p)^2 + 1]^{a_2}}$$

$$= \int \frac{[d^D k]}{(k^2 + 1)^{a_2}} , \qquad (4.23)$$

which we recognize as the most basic dimensionally regularized integral (2.18). Note that we have shifted k to $(k - p)$ in the last line. Even if (4.23) did not correspond to an exactly solvable loop integral, it does represent a subtopology that is simpler than the one we started with. If need be, we can repeat the recurrence relation process for any subtopology we encounter until we either obtain integrals that we have previously solved or a set of so-called master integrals. Master integrals, which in some sense represent the boundary conditions of a set of recurrence relations, will arise in the example in Section 4.4.

Before moving on to a more complicated example, though, we will examine the extra recurrence relation that was discussed at the end of the previous section. Applying (4.13) to the "onshell" topology, we have

$$\int [d^D k] \frac{k_\mu}{k^{2a_1}(k^2 + 2kp)^{a_2}} = p_\mu (-p^2)^{\frac{D}{2} - a_1 - a_2} \mathcal{X} . \qquad (4.24)$$

By contracting both sides with p^μ and using (4.18) we find that

$$\mathcal{X} = \frac{1}{2}(\mathbf{1}^- - \mathbf{2}^-) . \qquad (4.25)$$

Taking the partial derivative of both sides of (4.24) with respect to p_μ leads to

$$\int [d^D k] \frac{-2a_2 k^\mu k_\mu}{k^{2a_1}(k^2 + 2kp)^{a_2 + 1}}$$

$$= D(-p^2)^{\frac{D}{2} - a_1 - a_2} \mathcal{X} - 2\left(\frac{D}{2} - a_1 - a_2\right) p_\mu p^\mu (-p^2)^{\frac{D}{2} - a_1 - a_2 - 1} \mathcal{X}$$

$$= 2(D - a_1 - a_2)(-p^2)^{\frac{D}{2} - a_1 - a_2} \mathcal{X} . \qquad (4.26)$$

Using (4.18) on the left-hand side, (4.25) on the right, and setting $p^2 = -1$, the extra recurrence relation can be written as

$$\mathbf{X1}: \qquad -2a_2 \mathbf{1}^- \mathbf{2}^+ - (D - a_1 - a_2)\mathbf{1}^- + (D - a_1 - a_2)\mathbf{2}^- = 0 . \qquad (4.27)$$

We now wish to show that this recurrence relation can be constructed from the ones that we derived earlier ((4.20) and (4.21)):

$$\mathbf{R1}: \qquad (a_1 - a_2) - a_1 \mathbf{1}^+ \mathbf{2}^- + 2a_2 \mathbf{2}^+ + a_2 \mathbf{1}^- \mathbf{2}^+ = 0 ,$$

$$\mathbf{R2}: \qquad (D - 2a_1 - a_2) - a_2 \mathbf{1}^- \mathbf{2}^+ = 0 .$$

First, we will add **R1** and **R2** in order to cancel the 1^-2^+ terms:

$$\mathbf{R1 + R2}: \qquad (D - a_1 - 2a_2) - a_1 1^+ 2^- + 2a_2 2^+ = 0. \qquad (4.28)$$

Next we apply 1^- to this, so that

$$(D + 1 - a_1 - 2a_2)1^- - (a_1 - 1)2^- + 2a_2 1^- 2^+ = 0. \qquad (4.29)$$

Notice that we also shifted $a_1 \to (a_1 - 1)$. This is because applying 1^- lowers the exponent of [1] in the loop integral, and since the explicit factors of a_1 in the recurrence relations refer to this exponent, they must be shifted also. For the same reason, the application of 1^+ would entail the shift $a_1 \to (a_1 + 1)$.

Next, we apply 2^- to **R2**, obtaining

$$(D + 1 - 2a_1 - a_2)2^- - (a_2 - 1)1^- = 0. \qquad (4.30)$$

Finally, subtracting (4.29) from (4.30), we have

$$-2a_2 1^- 2^+ - (D - a_1 - a_2)1^- + (D - a_1 - a_2)2^- = 0, \qquad (4.31)$$

which is exactly what we obtained in (4.27) using the other method. In other words,

$$\mathbf{X1 = 2^- R2 - 1^- (R1 + R2)}, \qquad (4.32)$$

and the extra recurrence relation is not independent of the others.

4.3   Simple Two-Loop Example

Now we are ready to look at a two-loop example. Consider the "N5c" topology, as sketched in Figure 4.1 and defined by the integral

$$N5c(a_1, a_2, a_3, a_4, a_5) = \int \frac{[d^D k_1][d^D k_2]}{k_1^{2a_1} k_2^{2a_2} (k_1 + p)^{2a_3} (k_2 + p)^{2a_4} (k_1 + k_2 + p)^{2a_5}}. \qquad (4.33)$$

With any new topology, the first steps should be to decide how to route the momenta and to express all possible scalar products in terms of the propagators so that recurrence relations can be derived. For "N5c", the recurrence relations
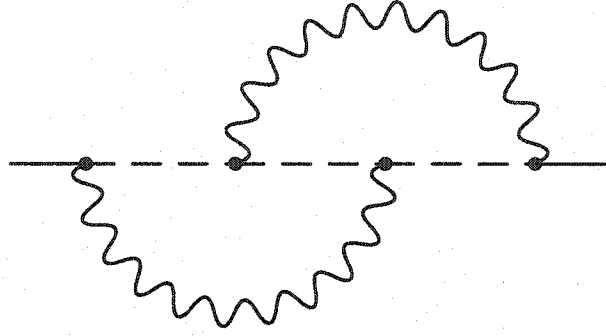
Figure 4.1: Sketch of the "N5c" topology.

are:

$$\mathbf{R1}:\quad a_3 3^+(-1-1^-)+a_5 5^+(-1^-+4^-)+(D-2a_1-a_3-a_5)=0\,,$$

$$\mathbf{R2}:\quad a_1 1^+(1+3^-+4^--5^-)$$
$$+a_3 3^+(2^--5^-)+a_5 5^+(-2^-+3^-)+(a_3-a_5)=0\,,$$

$$\mathbf{R3}:\quad a_1 1^+(-1-3^-)$$
$$+a_3 3^+(1+1^-)+a_5 5^+(1^-+2^--3^--4^-)+(a_1-a_3)=0\,,$$

$$\mathbf{R4}:\quad a_2 2^+(1+3^-+4^--5^-)$$
$$+a_4 4^+(1^--5^-)+a_5 5^+(-1^-+4^-)+(a_4-a_5)=0\,,$$

$$\mathbf{R5}:\quad a_4 4^+(-1-2^-)+a_5 5^+(-2^-+3^-)+(D-2a_2-a_4-a_5)=0\,,$$

$$\mathbf{R6}:\quad a_2 2^+(-1-4^-)$$
$$+a_4 4^+(1+2^-)+a_5 5^+(1^-+2^--3^--4^-)+(a_2-a_4)=0\,.$$

(4.34)

Before scrutinizing the recurrence relations, the next step is to determine what kind of simplification will occur if one of the propagators is removed from the topology. For "N5c" integrals, the removal of any propagator leads to a two-loop integral with four massless propagators. Since one of the loops will have only two propagators, this subloop belongs to the "one" topology, and following the evaluation of this subloop, the remaining loop integral will also be a "one" integral. Most topologies are not this simple — the more common situation is that there are one or two propagators whose removal does not simplify things appreciably. In addition, the removal of a propagator often leads to a simpler topology with the same number of loops, as opposed to the sequence of trivial one-loop integrals that we have with "N5c".

Having looked at the effects of removing any particular propagator, the next step is to check for symmetries in the loop integral. For the "N5c" topology, the integral is unchanged by the swap $k_1 \leftrightarrow k_2$, so that a_1 and a_3 can be interchanged with a_2 and a_4, respectively. This simplifies our task somewhat, since a quick perusal of the recurrence relations in (4.34) indicates that **R4**, **R5**, and **R6** can be obtained directly from **R2**, **R1**, and **R3**, respectively, by such a symmetry. As a result, we need only consider **R1**, **R2**, and **R3**.

Now it is time to look at the recurrence relations. Notice that if we were to apply **R1** directly,

$$1 = \frac{1}{(D - 2a_1 - a_3 - a_5)} \left\{ \frac{a_3}{[3]}(1 + [1]) + \frac{a_5}{[5]}([1] - [4]) \right\} , \qquad (4.35)$$

the $a_3/[3]$ term would increase a_3 indefinitely without lowering any of the other exponents. Similarly, we cannot use **R2** or **R3** in isolation. The problems, evidently, are the solitary raising terms like $a_3 3^+$, and one solution would be to look for a linear combination of recurrence relations in which these terms cancel. **R1 + R2 + R3**,

$$a_1 1^+ (4^- - 5^-) + a_3 3^+ (2^- - 5^-) + (D - a_1 - a_3 - 2a_5) = 0 , \qquad (4.36)$$

is such a linear combination, leading to the useful relationship

$$1 = \frac{1}{(D - a_1 - a_3 - 2a_5)} \left\{ \frac{a_1}{[1]}([5] - [4]) + \frac{a_3}{[3]}([5] - [2]) \right\} . \qquad (4.37)$$

Repeated applications of (4.37) will eventually bring either a_2, a_4, or a_5 to zero, at which point the "N5c" topology can be solved in terms of simpler topologies.

4.4 Complicated One-Loop Example

In the two previous examples, we were able to construct a single recurrence relation that was guaranteed to reduce one of the exponents in the integral until one of the propagators was removed and the topology was simplified. If this were always the case, any multiloop topology could eventually be reduced to a nesting of one-loop subtopologies and a number of physicists would get more sleep. Instead, we often find that there are certain integrals in a topology, known as master integrals, that cannot be reduced any further by the recurrence relations. We will discuss methods of evaluating master integrals in Chapter 6. Now we shall look at an example of a topology containing a master integral in order to illustrate some of the additional techniques that can be used to construct a

solution algorithm with recurrence relations.

Consider the one-loop topology "M3", as sketched in Figure 4.2 and defined by the integral

$$M3(a_1, a_2, a_3) = \int \frac{[d^D k]}{k^{2a_1}(k^2 + 2kp)^{a_2}(k + p)^{2a_3}} \, . \tag{4.38}$$
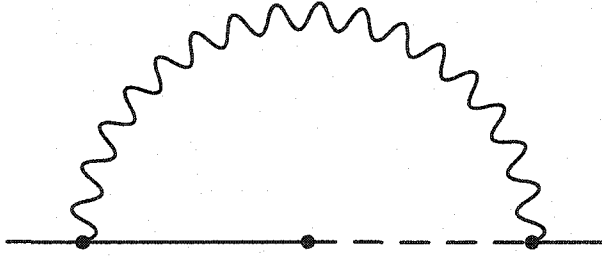
Figure 4.2: Sketch of the "M3" topology.

If the exponents are all integers, this is a very simple integral to solve — simply construct a partial fraction identity relating [2] and [3] and apply it until one of these propagators is removed so that the remaining integral belongs to either the "one" or "onshell" topologies. The "M3" topology can also arise from a multiloop topology, though, after one or more subloops have been integrated out, in which case one or both of the massless propagators [1] and [3] will have a non-integer exponent. If only one of these exponents is non-integer, the solution is still straightforward, so we will focus on the case where both [1] and [3] have non-integer exponents. Assuming that we started from a three-loop integral and have integrated over two subloops, we can rewrite (4.38) as

$$M3(a_1, a_2, a_3) = \int \frac{[d^D k]}{k^{2(a_1+\epsilon)}(k^2 + 2kp)^{a_2}(k + p)^{2(a_3+\epsilon)}} \, . \tag{4.39}$$

where now a_1, a_2, and a_3 are all integers. The recurrence relations for this topology are

$$\mathbf{R1}: \quad a_2 2^+ 1^- + (a_3 + \epsilon)3^+(1^- + 2^-) + (2a_1 + a_2 - D + 2\epsilon) = 0 \, ,$$

$$\mathbf{R2}: \quad -(a_1 + \epsilon)1^+ 2^- + a_2 2^+(2 + 1^-)$$
$$+(a_3 + \epsilon)3^+(2 + 1^- - 2^-) + (a_1 - a_2 + \epsilon) = 0 \, . \tag{4.40}$$

If we remove [2], the topology simplifies to a "one" integral. The presence of the ϵ-propagators, however, prevents us from removing [1] or [3]. The strategy, then,

will be to lower a_2 as much as possible while keeping a_1 and a_3 from running off to arbitrarily large positive or negative values.

Let us start by trying to lower a_2. Both recurrence relations contain 2^+ terms, so we certainly do not want to apply these directly. We could, however, apply 2^- to R2 in order to "invert" the $2a_2 2^+$ term. Unfortunately, R2 also contains an $a_2 2^+ 1^-$ term, so that $2^- R2$ will have a 1^- term which will allow a_1 to become increasingly negative without doing anything about a_2. Fortunately, there is also a $a_2 2^+ 1^-$ term in R1, so that this problematic term is canceled in

$$(R2 - R1): \quad -(a_1 + \epsilon)1^+ 2^- + 2a_2 2^+ \\ +2(a_3 + \epsilon)3^+(1 - 2^-) + (D - a_1 - 2a_2 - \epsilon) = 0 \,. \tag{4.41}$$

Now we can apply 2^- in order to invert the $2a_2 2^+$ term, so that

$$1 = \frac{[2]}{2(1 - a_2)} \left\{ (D - a_1 - 2a_2 + 2 - \epsilon) - (a_1 + \epsilon)\frac{[2]}{[1]} + 2(a_3 + \epsilon)\frac{1 - [2]}{[3]} \right\} \,. \tag{4.42}$$

This identity will lower a_2 every time it is applied, but notice that the $(1 - a_2)$ factor in the denominator precludes us from using it when $a_2 = 1$. This is a general feature of recurrence relation algorithms, namely, that whenever we try to lower an integer exponent by inverting a term with a raising operator for that propagator, we cannot lower the exponent past 1. Although some of our integrals might have $a_2 = 0$ as a consequence of the $[2]^2$ terms in (4.42), we have to continue the algorithm with the worst-case scenario in mind, specifically, integrals of the form $M3(a_1, 1, a_3)$ for arbitrary values of a_1 and a_3.

With $a_2 = 1$, let us now concentrate on focusing a_3 towards zero. The linear dependence of [2] and [3],

$$1 = [2] - [3] \,, \tag{4.43}$$

can be used directly when $a_3 > 0$, as it will either lower a_3 towards zero or, better yet, give us $a_2 = 0$. Alternatively, if $a_3 < 0$, we simply divide the identity (4.43) by [3] and rearrange the terms so that

$$1 = \frac{[2] - 1}{[3]} \,. \tag{4.44}$$

This will certainly increase a_3 and it may or may not lower a_2 to zero.

At this stage, we need to deal with a_1 in integrals of the form $M3(a_1, 1, 0)$ in an attempt to focus a_1 to a single value. We are going to aim for $a_1 = 1$, for reasons that will become clearer in Chapter 6, so that our master integral is

$M3(1, 1, 0)$. If $a_1 > 1$, we can simply apply **R1**:

$$1 = \frac{1}{(D - 2a_1 - a_2 - 2\epsilon)} \left\{ a_2 \frac{[1]}{[2]} + (a_3 + \epsilon) \frac{[1] + [2]}{[3]} \right\} . \qquad (4.45)$$

All three of the terms in (4.45) lead to good things. The $[1]/[2]$ term lowers a_1, and even though a_2 is increased to 2, it can be lowered again with (4.42) so that, at worst, a_3 is raised instead. The $[1]/[3]$ term lowers a_1 and the corresponding increase in a_3 can be reversed with (4.43). Finally, the $[2]/[3]$ term sends a_2 to zero.

All that remains is to address integrals where $a_1 < 1$. This is the most non-trivial step of the algorithm because while it is extremely easy to increase a_1, we cannot increase a_2 without encountering an infinite loop once the $[2]$ term in (4.42) lowers a_2 back to 1. No direct combination of **R1** and **R2** is free of 2^+ factors, and since $a_2 = 1$, we are not allowed to apply a 2^- operator either. The solution is to create a hybrid combination of recurrence relations, whereby we apply raising or lowering operators only to some of the recurrence relations in a well-chosen combination. For instance, consider

$$\mathbf{1^+ R1} : \quad a_2 \mathbf{2^+} + (a_3 + \epsilon) \mathbf{3^+}(1 + \mathbf{1^+ 2^-}) + (2a_1 + a_2 - D + 2 + 2\epsilon)\mathbf{1^+} = 0 . \qquad (4.46)$$

This relation only contains a single $\mathbf{2^+}$ term, just like the relation $(\mathbf{R2 - R1})$ in (4.41), which suggests that we can cancel the offending term with an appropriate combination of the two,

$$(\mathbf{R2 - R1}) - 2\mathbf{1^+}(\mathbf{R1}) : \quad \begin{aligned} &-2(a_3 + \epsilon)\mathbf{3^+ 2^-}(1 + \mathbf{1^+}) \\ &+2(D - 2 - 2a_1 - a_2 - 2\epsilon)\mathbf{1^+} \\ &-(a_1 + \epsilon)\mathbf{1^+ 2^-} + (D - a_1 - 2a_2 - \epsilon) = 0 , \end{aligned} \qquad (4.47)$$

or equivalently,

$$1 = \frac{1}{(a_1 + 2a_2 - D + \epsilon)} \left\{ -2(a_3 + \epsilon) \frac{[2]}{[3]} \left(1 + \frac{1}{[1]}\right) \right. \qquad (4.48)$$
$$\left. + \frac{2(D - 2 - 2a_1 - a_2 - 2\epsilon) - (a_1 + \epsilon)[2]}{[1]} \right\} .$$

It is clear that this relation will increase a_1 without any drawbacks. As a result, any "M3" integral with two epsilon-propagators can be cast in terms of "one" integrals and the master integral

$$M3(1, 1, 0) = \int \frac{[d^D k]}{k^{2(1+\epsilon)}(k^2 + 2kp)(k + p)^{2\epsilon}} . \qquad (4.49)$$

This is not a particularly pleasant master integral to solve, and we will see exactly why in Chapter 6, but at least there is only the one.

4.5 Complicated Two-Loop Example

To complete the sequence of examples illustrating the construction of recurrence relation algorithms, consider the two-loop topology "T1ep", as sketched in Figure 4.3 and defined by the integral

$$T1ep(a_1, a_2, a_3, a_4, a_5) = \int \frac{[d^D k_1][d^D k_2]}{k_1^{2a_1} k_2^{2(a_2+\epsilon)}(k_1 - k_2)^{2a_3}(k_1 + p)^{2a_4}(k_2^2 + 2k_2 p)^{a_5}}. \tag{4.50}$$

The wavy line in Figure 4.3 is the epsilon-propagator. If any of the other four
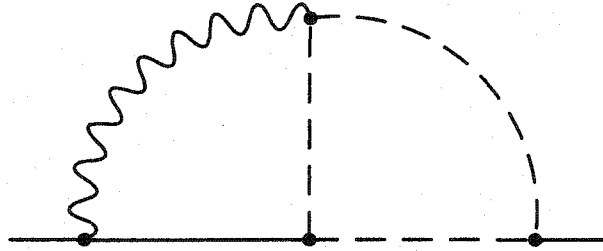
Figure 4.3: Sketch of the "T1ep" topology.

propagators are removed, the topology immediately unravels into a pair of one-loop integrals, and so our task is clear: lower a_1, a_3, a_4, and a_5 without letting a_2 run away in either direction. We might well end up with a master integral such as $T1ep(1, 0, 1, 1, 1)$.

First we need the recurrence relations. When dealing with two-loop topologies, let alone three-loop topologies, it is important to print out the recurrence relations in a format that emphasizes their basic behavior without distractions from less important features. In this spirit, here are the recurrence relations for the "T1ep" topology, printed in a convenient format:

$$\begin{aligned}
\mathbf{R1}: \quad &+[3+] * (-[1-] + [2-]) \\
&+[4+] * (-1 - [1-]) \\
&-2 * a1 - a3 - a4 + D
\end{aligned} \tag{4.51}$$

$$\begin{aligned}
\mathbf{R2}: \quad &+[1+] * (-[2-] + [3-]) \\
&+[3+] * (-[1-] + [2-])
\end{aligned} \tag{4.52}$$

$$+[4+] * (-[1-] + [3-] - [5-])$$
$$-a1 + a3$$

R3 : $+[1+] * (-1 - [4-])$
$$+[3+] * (-1 + [1-] - [2-] - [4-] + [5-]) \qquad (4.53)$$
$$+[4+] * (1 + [1-])$$
$$+a1 - a4$$

R4 : $+[2+] * (-[1-] + [3-])$
$$+[3+] * ([1-] - [2-]) \qquad (4.54)$$
$$+[5+] * (-1 - [2-] + [3-] - [4-])$$
$$-a2 + a3 - ep$$

R5 : $+[3+] * ([1-] - [2-])$
$$+[5+] * (-[2-]) \qquad (4.55)$$
$$-2 * a2 - a3 - a5 + D - 2 * ep$$

R6 : $+[2+] * (-[5-])$
$$+[3+] * (1 - [1-] + [2-] + [4-] - [5-]) \qquad (4.56)$$
$$+[5+] * (2 + [2-])$$
$$+a2 - a5 + ep$$

In addition to a wise use of brackets and the omission of the obvious "= 0" pieces, the raising operators implicitly contain the appropriate coefficient, namely, $[1+] = a_1 1^+$ and $[2+] = (a_2 + \epsilon)2^+$.

Now let us get to work. Even though the order is usually somewhat arbitrary, as our first task we will try to lower a_5. R4 and R6 both contain solitary $[5+]$ terms that we might invert. Unfortuantely, R6 is not a good choice, because the $[3+]$ term will lead to a $[5]/[3]$ term that does not provide a net-lowering of the exponents $\{a_1, a_3, a_4, a_5\}$. Meanwhile, the $[5+][2-]$ term in R4 will create a $[2]$ term that lowers a_2 indefinitely. Fortunately, such a term also appears in R5, and so the combination

R4 − R5 : $+[2+] * (-[1-] + [3-])$
$$+[5+] * (-1 + [3-] - [4-])$$
$$+a2 + 2 * a3 + a5 - D + ep \qquad (4.57)$$

can be used to lower a_5:

$$1 = [3] - [4] + \frac{[5]}{(a_5 - 1)} \left\{ (a_2 + 2a_3 + a_5 - 5 + 3\epsilon) \right.$$
$$\left. + (a_2 + \epsilon)\frac{[3] - [1]}{[2]} \right\} . \tag{4.58}$$

Turning to a_4, we need look no further than 4^-R1:

$$1 = -[1] + \frac{[4]}{(a_4 - 1)} \left\{ (5 - 2a_1 - a_3 - a_4 - 2\epsilon) + a_3\frac{[2] - [1]}{[3]} \right\} . \tag{4.59}$$

Since the $[4][2]/[3]$ term in (4.59) is not net-lowering in $\{a_1, a_3, a_4, a_5\}$, we will need to make sure that when we lower a_3, we do not generate a similar $[3][2]/[4]$ term which would essentially create a runaway scenario by means of a net $[2][2]$ term. After looking carefully at the recurrence relations in order to find a combination which cancels dangerous $[n+]$ and $[n+][2-]$ terms, we find that

$$\mathbf{2R4 - R5 + R6} : \quad +[2+] * (-2 * [1-] + 2 * [3-] - [5-])$$
$$+[3+] * (1 + [4-] - [5-])$$
$$+[5+] * (2 * [3-] - 2 * [4-])$$
$$+a2 + 3 * a3 - D + ep \tag{4.60}$$

fits the bill perfectly, leading to

$$1 = [5] - [4] + \frac{[3]}{(1 - a_3)} \left\{ (a_2 + 3a_3 - 7 + 3\epsilon) + 2a_5\frac{[3] - [4]}{[5]} \right.$$
$$\left. - (a_2 + \epsilon)\frac{[5] + 2[1] - 2[3]}{[2]} \right\} . \tag{4.61}$$

This leaves us with the task of lowering a_1, and after a bit of searching, we obtain a relation

$$\mathbf{R1 + R3 + 2R4 - R5 + R6} : \quad +[1+] * (-1 - [4-])$$
$$+[2+] * (-2 * [1-] + 2 * [3-] - [5-])$$
$$+[5+] * (2 * [3-] - 2 * [4-])$$
$$-a1 + a2 + 2 * a3 - 2 * a4 + ep \tag{4.62}$$

in which we can invert a $[1+]$ term without running into other difficulties, so

that

$$1 \;=\; -[4] + \frac{[1]}{(a_1 - 1)} \left\{ (1 - a_1 + a_2 + 2a_3 - 2a_4 + \epsilon) + 2a_5 \frac{[3] - [4]}{[5]} \right.$$
$$\left. + (a_2 + \epsilon)\frac{2[3] - [5] - 2[1]}{[2]} \right\} . \tag{4.63}$$

We can use the preceding relations to lower a_1, a_3, a_4, and a_5 all to 1 so that we are now faced with integrals of the form $T1ep(1, a_2, 1, 1, 1)$. Although we cannot remove $[2]$, we can focus the exponent a_2 towards a specific value such as 0. If $a_2 > 0$, a direct application of **R5**,

$$1 \;=\; \frac{1}{(4 - 2a_2 - a_3 - a_5 - 2\epsilon)} \left\{ a_5 \frac{[2]}{[5]} - a_3 \frac{[1] - [2]}{[3]} \right\} , \tag{4.64}$$

will either lower a_2 or send a_1 to 0. It does not matter that a_3 or a_5 might be raised to 2, as we can easily reapply relations (4.61) or (4.58) to return these exponents to 1 without running into an infinite loop.

Raising negative values of a_2, on the other hand, is a considerably more difficult job, as none of the original recurrence relations are free of $[2-]$ terms and we cannot invert these on account of the $[n+]$ factors that accompany them, given that $a_n = 1 \; \forall n \in \{1, 3, 4, 5\}$. There are two options available to us here. The first is to construct a hybrid recurrence relation like (4.47), whereby we find an elaborate combination of recurrence relations within which raising and lowering operators act on only some of the relations. This is the most elegant method, but it can also be extremely difficult to come up with such a relation. The alternative involves brute force, but it is at least guaranteed to work, and so in the interests of obtaining a solution without wasting an inordinate amount of time, it can be used as a last resort. Here is how it works. We know that **R5** can lower positive values of a_2 in integrals of the form $T1ep(1, a_2, 1, 1, 1)$. Suppose a_2 is negative, though, and we apply **R5** once anyways. We would probably expect to have, after settling a_3 and a_5 back down to 1, a term like $T1ep(1, a_2 - 1, 1, 1, 1)$. If, on paper, we work out this connection, for arbitrary values of a_2, we can take the $T1ep(1, a_2 - 1, 1, 1, 1)$ term that we generate and solve for it in terms of everything else. Then, by shifting a_2 to $a_2 + 1$, we will have a relation which increases negative values of a_2. It takes a page or so of shorthand to work out the details, but in this particular case a remarkable thing happens: the $T1ep(1, a_2 - 1, 1, 1, 1)$ terms all cancel! As a result, we simply collect all the other things we generate from applying **R5** to $T1ep(1, a_2, 1, 1, 1)$ and come up with

$$1 \;=\; \frac{1}{2(a_2 - 1 + 2\epsilon)} \left\{ (a_2 - 1 + \epsilon)([3] - [1] - [5]) + \frac{[1]}{[3]} \right.$$

$$+[2]\left(\frac{[3]-[4]}{[5]}+\frac{[4]-[5]}{[3]}\right)\Bigg\} \ . \qquad (4.65)$$

This relation can be used for all values of a_2 in $T1ep(1, a_2, 1, 1, 1)$ integrals, and so the "T1ep" topology has no master integrals.

4.6 Additional Comments

We have now looked at a number of examples of how to use recurrence relations to simplify the loop integrals in a topology. When properly applied, these procedures allow us to write an arbitrary loop integral in terms of loop integrals belonging to simpler topologies and, perhaps, master integrals within the same topology.

At the end of the example in the previous section, we briefly described a brute force method of generating the hard-to-find recurrence relations that are often needed in the final stages of an algorithm. Since this particular case turned out to be easier than we had any right to expect, it is worth discussing the method further. The most common application of this method occurs when the application of any recurrence relation, in combination with the relations previously used, leads to an infinite loop wherein a term in one of the relations exactly reverses the effect of another relation. In cases like this, by starting with an integral and applying a recurrence relation on paper, we will soon generate additional factors of the original integral, so that schematically,

$$(\text{Original Integral}) = (\text{Simpler Integrals}) + (\text{Constant}) * (\text{Original Integral}) . \quad (4.66)$$

Once an equation like this is obtained, it is obvious that an infinite loop can be avoided simply by moving all the (Original Integral) terms to the same side of the equation. Another common situation is that

$$\begin{aligned}(\text{Original Integral}) \ = \ &(\text{Simpler Integrals}) + (\text{Constant}) * (\text{Original Integral}) \\ &+ (\text{Constant}) * (\text{More Complicated Integral}) . \qquad (4.67)\end{aligned}$$

In this case, solve for the (More Complicated Integral) and shift the exponents so that this becomes the (Original Integral) and the initial (Original Integral) looks simpler in comparison. It must be stressed, though, that this method is a last resort and should only be used when the integral under consideration has one free parameter, otherwise there will be several calculations required and they might be rather unwieldy.

While paper can be used to explain the ideas in this chapter, it would be foolish to attempt to calculate multiloop integrals on paper in this way. Beyond its

numerous other virtues, symbolic computation, which we will discuss in Chapter 10, becomes an indispensable tool for implementing recurrence relation algorithms. Once an algorithm is created, we can double-check it by ensuring that the original recurrence relations are satisfied for a large assortment of specific integrals. Basically, these tests consist of choosing one specific integral from the topology, expressing each recurrence relation in terms of this integral and some other specific integrals with similar parameters, evaluating the integrals using the programmed algorithm, and then checking to see that all recurrence relations are satisfied by the explicit calculation even though some of them might not have been used to construct the recurrence relation algorithm. Since the creation of these algorithms is perhaps the most difficult aspect of this work, it is quite reassuring to have these kinds of tests available to us.

"Though at first it seems as though it doesn't show, like a tree, ability will bloom and grow."

The Aristocats (*Scales and Arpeggios*)

Chapter 5

Tensor Reduction

In Chapter 4, we saw how recurrence relations provide a powerful method for dealing with loop integrals so that we do not need to construct general solutions. Since the method assumes that we have scalar integrals, we need to rewrite numerator factors in terms of existing propagators. Unfortunately, it is not always possible to do this directly. This chapter explores a subtle technique that can be used to accomplish the same objective.

5.1 One-Loop Procedure

Consider the integral

$$\int \frac{[d^D k]\, k^2}{(k^2 + m^2)^n}. \tag{5.1}$$

Aside from the additional numerator factor of k^2, this corresponds to the "gm2" topology that we first encountered in Section 3.4. This numerator does not cause much trouble, though, as it can easily be written as

$$k^2 = (k^2 + m^2) - m^2 \tag{5.2}$$

so that

$$\int \frac{[d^D k]\, k^2}{(k^2 + m^2)^n} = \int [d^D k] \left\{ \frac{1}{(k^2 + m^2)^{n-1}} - \frac{m^2}{(k^2 + m^2)^n} \right\} \tag{5.3}$$

and both terms on the right-hand side are scalar integrals.

Now consider the integral

$$\int \frac{[d^D k]\, (k \cdot p)}{(k^2 + m^2)^n}. \tag{5.4}$$

It is obviously impossible to write $(k \cdot p)$ as a linear combination of existing propagators and k-independent constants. In principle, we could introduce an additional propagator such as $(k^2 + 2kp)$, but then we would no longer be deal-

ing with the "gm2" topology. Instead, there is a clever way. Since we are integrating over all possible values of k and the denominator is quadratic in k, the substitution $k \to -k$ leads to

$$\int \frac{[d^D k]\,(k \cdot p)}{(k^2 + m^2)^n} = \int \frac{[d^D k]\,(-k \cdot p)}{(k^2 + m^2)^n}\,, \tag{5.5}$$

and so (5.4) is in fact zero. This argument holds whenever we have an odd number of powers of k in the numerator of a loop integral whose denominator is quadratic in k.

A more complicated situation arises with the integral

$$\int \frac{[d^D k]\,(k \cdot p)^2}{(k^2 + m^2)^n}\,, \tag{5.6}$$

as symmetry arguments like the one above no longer demand that this integral vanish. Rewriting (5.6) as

$$p_\mu p_\nu \int \frac{[d^D k]\,k^\mu k^\nu}{(k^2 + m^2)^n}\,, \tag{5.7}$$

we will now construct an identity for $k^\mu k^\nu$ that, while not true in isolation, is true for our purposes because we are integrating over all possible values of k. We start by noting that the k-integral must yield a k-independent tensor that is symmetric in μ and ν. The only candidate is $g^{\mu\nu}$. Next, any replacement of $k^\mu k^\nu$ must maintain both the correct mass dimension and the same number of k-factors in the numerator. As a result,

$$k^\mu k^\nu \propto g^{\mu\nu} k^2\,. \tag{5.8}$$

We determine the constant of proportionality by contracting both sides of (5.8) with $g_{\mu\nu}$ and noting that in dimensional regularization $g_{\mu\nu} g^{\mu\nu} = D$. Then we have

$$k^\mu k^\nu \sim \frac{g^{\mu\nu} k^2}{D}\,. \tag{5.9}$$

The $\sim$ reminds us that while (5.9) is not explicitly true by itself, the two sides are equivalent after integration over all possible values of k. Substituting (5.9) back into (5.7), we obtain

$$\int \frac{[d^D k]\,(k \cdot p)^2}{(k^2 + m^2)^n} = \frac{p^2}{D} \int \frac{[d^D k]\,k^2}{(k^2 + m^2)^n}\,, \tag{5.10}$$

and we can use (5.3) to solve the k-integral on the right-hand side. Introducing

a more compact notation, we can write our newfound identity as

$$\langle k^{\mu,2} \rangle = \frac{g^{\mu_1 \mu_2}}{D} \langle k^2 \rangle \,, \tag{5.11}$$

where

$$\langle k^{\mu,n} \rangle \equiv \int \frac{[d^D k] \, k^{\mu_1} \cdots k^{\mu_n}}{\mathcal{D}(k^2, m^2)} \,, \tag{5.12}$$

$$\langle k^2 \rangle \equiv \int \frac{[d^D k] \, k^2}{\mathcal{D}(k^2, m^2)} \,, \tag{5.13}$$

and $\mathcal{D}$ represents some collection of propagators. The generalization of (5.11) is

$$\langle k^{\mu,n} \rangle = \frac{G^{\mu_1 \cdots \mu_n}}{f(n, D)} \langle k^n \rangle \,, \tag{5.14}$$

where $G^{\mu_1 \cdots \mu_n}$ denotes a sum of products of $n/2$ $g^{\alpha\beta}$ tensors that is completely symmetric in the indices $\{\mu_1, \ldots, \mu_n\}$. We have already shown that

$$f(2, D) = D \,, \tag{5.15}$$

and we wish to construct a general formula. For $n = 4$,

$$\langle k^{\mu,4} \rangle = \frac{g^{\mu_1 \mu_2} g^{\mu_3 \mu_4} + g^{\mu_1 \mu_3} g^{\mu_2 \mu_4} + g^{\mu_1 \mu_4} g^{\mu_2 \mu_3}}{f(4, D)} \langle k^4 \rangle \,. \tag{5.16}$$

Contracting both sides with $g_{\mu_1 \mu_2} g_{\mu_3 \mu_4}$ and noting that $g_\alpha^\beta g_\beta^\alpha = D$, we obtain

$$\langle k^4 \rangle = \frac{D^2 + D + D}{f(4, D)} \langle k^4 \rangle \tag{5.17}$$

so that

$$f(4, D) = D(D + 2) \,. \tag{5.18}$$

At this stage, we might guess that

$$f(n, D) = D(D + 2)(D + 4) \cdots (D + (n - 2)) \,. \tag{5.19}$$

This turns out to be the correct expression for $f(n, D)$ and we can prove it by induction. Having established (5.19) for $n = 2, 4$, we now need to show that if it is true, as written, for n, then it necessarily follows that it is also true for $n + 2$.

To begin, we observe that $G^{\mu_1 \cdots \mu_{n+2}}$ has $(n + 1)!!$ terms. This is because the order of the $g^{\alpha\beta}$ factors is irrelevant, so we might as well write the one involving μ_1 at the front. There are then $(n + 1)$ other μ indices that can be paired with μ_1 in this leading g-tensor. Then, we write the g-tensor containing the lowest

remaining μ index, leaving $(n - 1)$ other indices to pair with it, and so forth, yielding $(n + 1)(n - 1) \ldots = (n + 1)!!$ terms.

Now, of the $(n + 1)!!$ terms, $(n - 1)!!$ will contain $g^{\mu_1 \mu_2}$ and the remaining $n(n - 1)!!$ will not. When we contract $G^{\mu_1 \cdots \mu_{n+2}}$ with $g_{\mu_1 \mu_2} g_{\mu_3 \mu_4} \cdots g_{\mu_{n+1} \mu_{n+2}}$, those terms containing $g^{\mu_1 \mu_2}$ will yield D times the full contraction over the remaining n indices. As for the terms without $g^{\mu_1 \mu_2}$, we can assume, without loss of generality, that the leading term is $g^{\mu_1 \mu_3}$. In this case, our contraction involves

$$g_{\mu_1 \mu_2} g^{\mu_1 \mu_3} g^{\mu_2 \mu_j} = g_{\mu_2}^{\mu_3} g^{\mu_2 \mu_j} = g^{\mu_3 \mu_j} . \tag{5.20}$$

Since $j > 3$, we have $f(n, D)$ remaining once μ_1 and μ_2 are out of the picture. In other words,

$$
\begin{aligned}
f(n + 2, D) &= Df(n, D) + n \left\{ Df(n - 2, D) + (n - 2) \{ \ldots \} \right\} \\
&= Df(n, D) + n \left\{ f(n, D) \right\} \\
&= (D + n) f(n, D) \\
&= D(D + 2)(D + 4) \cdots (D + [(n + 2) - 2]) . \tag{5.21}
\end{aligned}
$$

We can also write $f(n, D)$ as $(D + n - 2)!!$. This is not only more compact, but by virtue of the identity (2.22), it suggests that we should be able to cast our result in terms of the ubiquitous Gamma functions. Explicitly,

$$
\begin{aligned}
f(n, D) &= D(D + 2)(D + 4) \cdots (D + (n - 2)) \\
&= 2^{n/2}(D/2)(D/2 + 1) \cdots (D/2 + n/2 - 1) \\
&= \frac{2^{n/2} \, \Gamma\left(\frac{D+n}{2}\right)}{\Gamma\left(\frac{D}{2}\right)} . \tag{5.22}
\end{aligned}
$$

This process of tensor reduction on one-loop integrals is so useful that we automatically incorporate it into the three major one-loop topologies — "one", "onshell", and "gm2" — that were introduced in Chapter 3.

5.2 Multiloop Procedure

While the method we developed in the previous section works extremely well at the one-loop level, things become increasingly complicated when we have two or more loops. In particular, we often encounter topologies with fewer propagators than is necessary to be able to rewrite every possible numerator factor. In this section we will examine, through a sequence of increasingly difficult examples, how tensor reduction can be implemented in multiloop integrals.

One-Loop Subloop

Consider the "T2" topology, as sketched in Figure 5.1, and defined by

$$T2(a_1, a_2, a_3, a_4) = \int \frac{[d^D k_1][d^D k_2]}{k_1^{2a_1} k_2^{2a_2} (k_1 + p)^{2a_3} [(k_1 + k_2 + p)^2 + 1]^{a_4}} \tag{5.23}$$

$$\equiv \int \frac{[d^D k_1][d^D k_2]}{[1]^{a_1} [2]^{a_2} [3]^{a_3} [4]^{a_4}} .$$
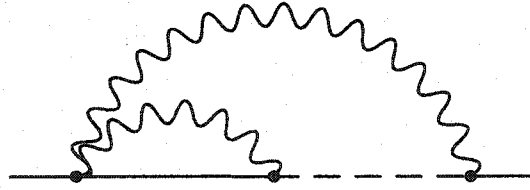
Figure 5.1: Sketch of the "T2" topology.

First, notice that the k_2-dependent subloop cannot be evaluated on its own, even though it looks a lot like "onshell". This is because the external momentum that flows through the massive line of the k_2-loop is $(k_1 + p)$, instead of just p, and since the 1 in the mass term of [4] is actually $m^2 = -p^2$, the k_2-loop depends nontrivially on two different external scales. This is a major reason why massive lines are more of a nuisance than massless lines.

Next, observe that the four propagators of (5.23) are insufficient to handle all possible numerator factors that depend on k_1, k_2, and p. Specifically,

$$p^2 = -1, \quad k_1^2 = [1], \quad k_2^2 = [2], \quad k_1 \cdot p = ([3] - [1] + 1)/2, \tag{5.24}$$

leaving only [4] to handle both $(k_2 \cdot p)$ and $(k_1 \cdot k_2)$, which is clearly insufficient.

The solution to this problem relies on the fact that the only part of the k_2-integral that is not quadratic in k_2 is the $2k_2 \cdot (k_1 + p)$ term that arises in [4]. Therefore, suppose we break k_2 into two pieces — one that is parallel to $(k_1 + p)$ and the other that is perpendicular to it:

$$k_2 = k_2^{\|} + k_2^{\perp} = \frac{k_2 \cdot (k_1 + p)}{(k_1 + p)^2} (k_1 + p) + k_2^{\perp} . \tag{5.25}$$

Now observe what happens to the two k_2-dependent propagators using this representation of k_2:

$$[2] = \left(k_2^{\|}\right)^2 + \left(k_2^{\perp}\right)^2 , \tag{5.26}$$

$$[4] = \left(k_2^{\|}\right)^2 + \left(k_2^{\perp}\right)^2 + 2k_2^{\|} \cdot (k_1 + p) + (k_1 + p)^2 + 1 . \tag{5.27}$$

Both of these factors are quadratic in $k_2^\perp$, precisely because of the specific form of (5.25). Once we know that the propagators of (5.23) are quadratic in $k_2^\perp$, we do not actually need to write them as in (5.26) and (5.27), but we will use (5.25) to rewrite the k_2 factors appearing in the numerator via $(k_2 \cdot p)$ and $(k_1 \cdot k_2)$. At first glance, this might seem like a rather futile thing to do, as $k_2^\parallel$ contains the exact same $(k_2 \cdot p)$ and $(k_1 \cdot k_2)$ terms that we are trying to deal with in the first place. The loophole, though, is that $k_2^\parallel$ doesn't really depend on $(k_2 \cdot p)$ and $(k_1 \cdot k_2)$ — it depends on $(k_2 \cdot (k_1 + p))$, and we can deal with this particular scalar product:

$$k_2 \cdot (k_1 + p) = ([4] - [2] - [3] - 1)/2 . \tag{5.28}$$

At this stage, then, we have managed to rewrite all possible numerator factors in terms of the propagators [1], [2], [3], and [4], along with $k_2^\perp$. Since these propagators only depend on $k_2^\perp$ via $(k_2^\perp)^2$, we can average over the directions of $k_2^\perp$ in an analogous fashion to the one-loop tensor reduction technique we developed in the previous section. The only difference is that $k_2^\perp$ lies in a $(D-1)$-dimensional subspace because it is orthogonal to $(k_1 + p)$. Once we have averaged over the directions of $k_2^\perp$, we might still have factors of $k_2^\perp$ in the numerator, but they can only appear as powers of $(k_2^\perp)^2$. These can be expressed in terms of propagators by solving (5.25) for $k_2^\perp$, so that

$$(k_2^\perp)^2 = k_2^2 - \frac{[k_2 \cdot (k_1 + p)]^2}{(k_1 + p)^2} . \tag{5.29}$$

This example represents the main way in which tensor reduction arises at the two-loop level, wherein there is only one situation in which things become more complicated. If the propagator [3] had been a massive line instead, the factors of $(k_1 + p)^2$ created by the tensor reduction would correspond to a fifth type of propagator which we shall label as [5]. This fifth propagator is not independent of the others, though, and a partial fraction identity could be used to eliminate either [3] or [5] at any stage of the calculation so that there would be two closely related types of two-loop, four-propagator integrals to solve.

At the three-loop level, however, things can become more complicated. The next three examples illustrate the ways in which tensor reduction can be used to deal with the more difficult situations that arise with three loops.

Separate Subloops

Consider the "X7" topology, as sketched in Figure 5.2, and defined by

$$X7(a_1, a_2, a_3, a_4, a_5, a_6) = \int \frac{[d^D k_1][d^D k_2][d^D k_3]}{k_1^{2a_1}(k_1 + p)^{2a_2} k_2^{2a_3} k_3^{2a_4}} \tag{5.30}$$

$$\times \frac{1}{[(k_1 + k_2 + p)^2 + 1]^{a_5} \, [(k_1 + k_3 + p)^2 + 1]^{a_6}} \, .$$
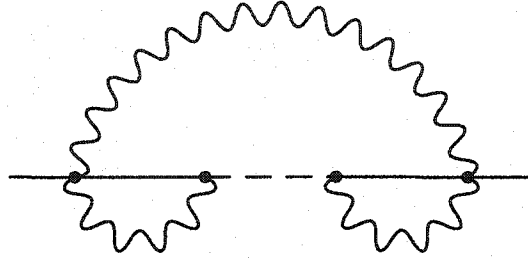
Figure 5.2: Sketch of the "X7" topology.

Although we only have six independent propagator factors to try to cope with nine possible numerator factors, we can apply the tensor reduction procedure to the k_2- and k_3-subloops simultaneously:

$$k_2 \;=\; \frac{k_2 \cdot (k_1 + p)}{(k_1 + p)^2} \, (k_1 + p) + k_2^\perp \, , \tag{5.31}$$

$$k_3 \;=\; \frac{k_3 \cdot (k_1 + p)}{(k_1 + p)^2} \, (k_1 + p) + k_3^\perp \, . \tag{5.32}$$

Every propagator is either independent of or quadratic in $k_2^\perp$ and $k_3^\perp$, therefore we can average over the directions of both of these $(D-1)$-dimensional vectors in order to handle scalar products in the numerator involving k_2 or k_3.

Nested Subloops

The "X1" topology, as sketched in Figure 5.3, is defined by the integral

$$X1(a_1, a_2, a_3, a_4, a_5, a_7, a_8) \;=\; \int \frac{[d^D k_1][d^D k_2][d^D k_3]}{k_1^{2a_1} (k_1 + p)^{2a_2} (k_1 + k_3)^{2a_3} k_2^{2a_4}} \tag{5.33}$$

$$\times \frac{1}{[(k_2 + k_3)^2 + 1]^{a_5} \, k_3^{2a_7} (k_3^2 + 1)^{a_8}} \, .$$

For the small subloop at the top, it is clear that we need to assign

$$k_2 = \frac{k_2 \cdot k_3}{k_3^2} \, k_3 + k_2^\perp \, . \tag{5.34}$$

Both k_2-dependent propagators will be quadratic in $k_2^\perp$, so we can average over
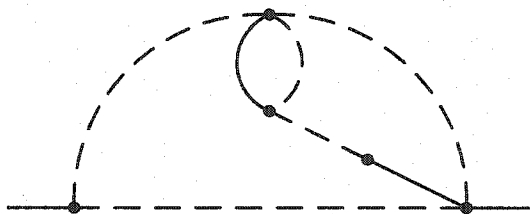
Figure 5.3: Sketch of the "X1" topology.

the directions of this $(D - 1)$-dimensional vector. Although we do not actually solve the k_2-integral at this stage, we know that if we did, the result could only generate additional factors of k_3^2. As a result, the k_3-integral would then involve the three factors k_3^2, $(k_3^2 + 1)$, and $(k_1 + k_3)^2$, so we can now apply the tensor reduction procedure to k_3:

$$k_3 = \frac{k_3 \cdot k_1}{k_1^2} \, k_1 + k_3^{\perp} \,. \tag{5.35}$$

As far as the details of the application are concerned, the nested subloops work the same as the separate subloops because we simultaneously project two of the loop momenta. The main difference between the two is the subtle reasoning needed to establish that the nested subloops do in fact behave in this way.

Two-Loop Subloop

For our final example, we consider the "T3m" topology, as sketched in Figure 5.4, and defined by the integral

$$T3m(a_1, a_2, a_3, a_4, a_5, a_6, a_7) \;=\; \int \frac{[d^D k_1][d^D k_2][d^D k_3]}{k_1^{2a_1}(k_1 + p)^{2a_2}(k_1 + k_2 + p)^{2a_3}} \tag{5.36}$$

$$\times \frac{1}{(k_1 + k_2 + k_3 + p)^{2a_4}(k_1 + k_3 + p)^{2a_5} k_2^{2a_6} k_3^{2a_7}} \,.$$

Now things look somewhat ominous, as there is no subloop that contains only two propagators. Instead, we will need to consider the k_2-k_3-subloop as a whole, beginning with the observation that the propagators in this subloop only depend on k_1 and p through the combination $(k_1 + p)$. Since we can express the scalar products $k_2 \cdot (k_1 + p)$ and $k_3 \cdot (k_1 + p)$ in terms of existing propagators, we can write $p = (k_1 + p) - k_1$ so that the only troublesome scalar products are $(k_1 \cdot k_2)$ and $(k_1 \cdot k_3)$. Then, we take the rather unusual step of projecting k_1 along $(k_1 + p)$:

$$k_1 = \frac{k_1 \cdot (k_1 + p)}{(k_1 + p)^2} \, (k_1 + p) + k_1^{\perp} \,. \tag{5.37}$$
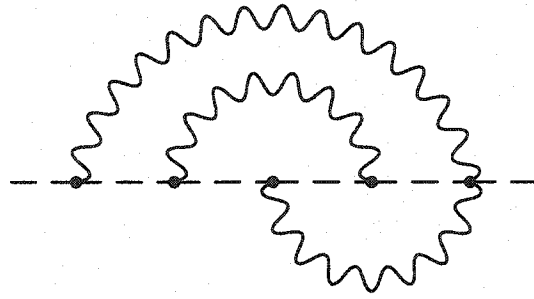
Figure 5.4: Sketch of the "T3m" topology.

Each of the propagators, except for k_1^2, already depends on k_1 via $(k_1 + p)$, and so the only propagator in which $k_1^{\perp}$ can appear is k_1^2. The $k_1^{\perp}$ dependence here will obviously be quadratic, thus we can legitimately average over the directions of $k_1^{\perp}$, and consequently, we can express all possible scalar products in terms of existing propagators in the "T3m" topology.

5.3 Auxiliary Propagators

As we have seen, the tensor reduction procedure can quickly become intricate and abstract. There is an alternative, which we shall now examine, that is conceptually simpler. The idea is to create an auxiliary propagator in order to handle any numerator factor that cannot be expressed as a linear combination of propagators. As an explicit example, we reexamine the "T2" topology from earlier in this section:

$$T2(a_1, a_2, a_3, a_4) = \int \frac{[d^D k_1][d^D k_2]}{k_1^{2a_1} k_2^{2a_2} (k_1 + p)^{2a_3} [(k_1 + k_2 + p)^2 + 1]^{a_4}} . \tag{5.38}$$

Rather than invoke a tensor reduction scheme in order to manage five potential scalar products in the numerator in terms of the four propagators, we simply introduce a fifth propagator,

$$[5] = k_2 \cdot p , \tag{5.39}$$

so that every scalar product is now under control. While it is clear that this auxiliary propagator sits in the numerator, it can be incorporated into a set of recurrence relations without any conceptual difficulties.

While any topology to which we can apply a tensor reduction could instead be handled with auxiliary propagators, the converse is not true. For example, the "X13" topology, as sketched in Figure 5.5, does not contain any subloops for which we can construct a tensor reduction scheme that would enable us

to express nine possible scalar products in terms of the seven propagators in the topology. In this case, we have no choice but to introduce two auxiliary propagators.
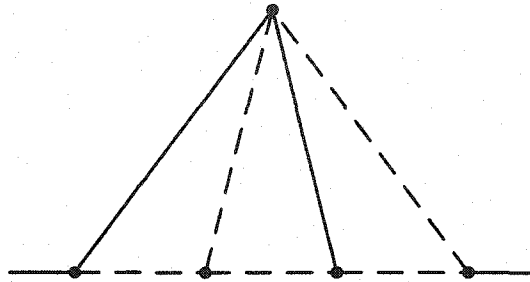
Figure 5.5: Sketch of the "X13" topology.

One might wonder why we went to so much trouble describing the tensor reduction procedure when the auxiliary propagator method can solve the same problems with much less mess and is sufficiently robust so as to apply to all topologies. Given that some experts rely on auxiliary propagators entirely [19] and others use a mix of tensor reduction and auxiliary propagators [20], the choice is an aesthetic one. When we use auxiliary propagators, we find that the recurrence relations are easy to derive and simple to write. On the other hand, it does no good to lower the negative exponent on the auxiliary propagator even further, and so it is often more difficult to construct an effective algorithm that uses the recurrence relations to simplify a topology. Conversely, the tensor reduction method makes it difficult to derive and write recurrence relations. It is almost always the case, though, that there is a modest subset of recurrence relations or linear combinations of recurrence relations that can be written quite compactly. With no auxiliary propagators to worry about, the removal of any propagator will then lead to a simplification of the original topology. It is for this reason that the tensor reduction procedure is the preferred approach here whenever subloops are present.

"Once you have eliminated the impossible, whatever remains, however unlikely, must be the truth."

Sherlock Holmes

Chapter 6

Master Integrals

In Chapter 4, we saw how to construct recurrence relations that allow us to write an arbitrary loop integral in terms of loop integrals belonging to simpler topologies and, perhaps, master integrals within the same topology. While this procedure undoubtedly makes some of the most complicated loop calculations more manageable, we are still left with the task of evaluating the master integrals. In this chapter, we will illustrate a variety of techniques that can be used to obtain explicit solutions for master integrals.

6.1 One-Loop Examples

M2 Master Integral

Consider the "M2" topology, as sketched in Figure 6.1, and defined by the integral

$$M2(a_1, a_2) = \int \frac{[d^D k]}{(k^2 + 2kp)^{a_1}(k^2 + 1)^{a_2}} .$$
(6.1)

Although this may look like an innocent one-loop topology, the presence of two
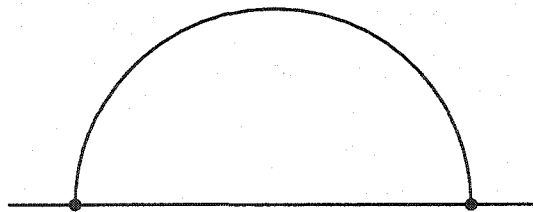
Figure 6.1: Sketch of the "M2" topology.

massive lines makes it quite difficult to solve. Recurrence relations can be used

to lower the exponents a_1 and a_2 to 1, so that we will have to evaluate the master integral

$$M2(1,1) = \int \frac{[d^D k]}{(k^2 + 2kp)(k^2 + 1)} . \tag{6.2}$$

Introducing a Feynman parameter, we obtain

$$
\begin{aligned}
M2(1,1) &= \Gamma(2) \int_0^1 dx \int \frac{[d^D k]}{[x(k^2 + 2kp) + (1-x)(k^2 + 1)]^2} \\
&= \int_0^1 dx \int \frac{[d^D k]}{[(k + xp)^2 + (x^2 - x + 1)]^2} \\
&= \frac{\Gamma(\epsilon)}{(4\pi)^{D/2}} \int_0^1 dx \, (x^2 - x + 1)^{-\epsilon} .
\end{aligned} \tag{6.3}
$$

The x-integral in (6.3) is surprisingly difficult to solve analytically. Recognizing that this integral is finite, we will expand the integrand in powers of ϵ:

$$
\begin{aligned}
(x^2 - x + 1)^{-\epsilon} &= \exp\left[-\epsilon \ln(x^2 - x + 1)\right] \\
&= 1 - \epsilon \ln(x^2 - x + 1) + \frac{\epsilon^2}{2} \ln^2(x^2 - x + 1) - \ldots \quad . \tag{6.4}
\end{aligned}
$$

Removing a loop factor of $\mathcal{F} = \Gamma(1 + \epsilon)/(4\pi)^{D/2}$ from (6.3), the master integral can then be expanded in powers of ϵ as

$$\frac{M2(1,1)}{\mathcal{F}} = \frac{1}{\epsilon} - \int_0^1 dx \, \ln(x^2 - x + 1) + \frac{\epsilon}{2} \int_0^1 dx \, \ln^2(x^2 - x + 1) + \mathcal{O}(\epsilon^2) . \tag{6.5}$$

The Feynman parameter integrals are now free of external parameters like ϵ, and so they can be evaluated numerically if necessary. With a bit of work, though, analytic solutions can also be obtained. For the first integral, we write

$$(x^2 - x + 1) = \left(x - e^{i\pi/3}\right)\left(x - e^{-i\pi/3}\right) , \tag{6.6}$$

split the logarithm into two terms, integrate each term by parts, and find that

$$\int_0^1 dx \, \ln(x^2 - x + 1) = -2 + \frac{\pi}{\sqrt{3}} . \tag{6.7}$$

The second integral is substantially harder to evaluate; the result is

$$\int_0^1 dx \, \ln^2(x^2 - x + 1) = 2\left(4 + \frac{\pi}{\sqrt{3}} \ln 3 - 9S_2 - \frac{2\pi}{\sqrt{3}}\right) . \tag{6.8}$$

This is our first example of a loop integral whose solution contains constants like $\sqrt{3}$, ln 3, and S_2, in addition to the $\zeta(n)$ and γ that we first saw in Section 2.2. S_2, defined by

$$S_2 = \frac{4}{9\sqrt{3}} \, \text{Cl}_2\left(\frac{\pi}{3}\right) = 0.2604341376\ldots , \tag{6.9}$$

is a constant that arises frequently in loop integrals with more than one massive line. Unraveling the notation [21], $\text{Cl}_2(x)$ is known as the Clausen function and it can be written as

$$\text{Cl}_2(x) = \text{Im}\left[\text{Li}_2\left(e^{i\theta}\right)\right] = \sum_{k=1}^{\infty} \frac{\sin kx}{k^2} . \tag{6.10}$$

Meanwhile, $\text{Li}_2(x)$ is the dilogarithm, defined by

$$\text{Li}_2(x) = -\int_0^x \frac{\log(1-z)}{z} \, dz = -\int_0^x \frac{dz}{z} \int_0^z \frac{dy}{1-y} . \tag{6.11}$$

The dilogarithm is often written in terms of Spence functions, and based on the right-most term of (6.11), it is not surprising that these functions will sometimes arise in conjunction with Feynman parameter integrals. Returning from the digression, we have obtained the "M2" master integral and can write it as

$$\frac{M2(1,1)}{\mathcal{F}} = \frac{1}{\epsilon} + \left(2 - \frac{\pi}{\sqrt{3}}\right) + \epsilon\left(4 - \frac{2\pi}{\sqrt{3}} + \frac{\pi}{\sqrt{3}} \ln 3 - 9S_2\right) + \mathcal{O}(\epsilon^2) . \tag{6.12}$$

While this result took some effort to obtain, the existence of a recurrence relation algorithm has at least prevented us from having to evaluate "M2" integrals for the general case.

M3 Master Integral

In Section 4.4, we used recurrence relations to solve the "M3" topology in terms of the master integral

$$M3(1,1,0) = \int \frac{[d^D k]}{k^{2(1+\epsilon)}(k^2 + 2kp)(k+p)^{2\epsilon}} . \tag{6.13}$$

To evaluate it, we first combine the p-dependent propagators with a Feynman parameter x, and then combine the resulting

$$x(k+p)^2 + (1-x)(k^2 + 2kp) = (k+p)^2 + (1-x) \tag{6.14}$$

factor with the p-independent propagator using an additional Feynman parameter y:

$$
\begin{aligned}
M3(1,1,0) &= \frac{\Gamma(1+\epsilon)}{\Gamma(\epsilon)\Gamma(1)}\frac{\Gamma(2+2\epsilon)}{\Gamma(1+\epsilon)\Gamma(1+\epsilon)}\int_0^1 dx\, x^{\epsilon-1}\int_0^1 dy\, y^\epsilon(1-y)^\epsilon \\
&\quad \times \int \frac{[d^D k]}{[(k+yp)^2 + y(y-x)]^{2+2\epsilon}} \\
&= \frac{\Gamma(2+2\epsilon-D/2)}{\Gamma(\epsilon)\Gamma(1+\epsilon)(4\pi)^{D/2}}\int_0^1 dx\int_0^1 dy\, \frac{x^{\epsilon-1}y^\epsilon(1-y)^\epsilon}{[y(y-x)]^{2+2\epsilon-D/2}} \\
&= \frac{\mathcal{F}\,\Gamma(3\epsilon)}{\Gamma(\epsilon)\Gamma^2(1+\epsilon)}\int_0^1 dx\int_0^1 dy\, \frac{x^{\epsilon-1}y^{-2\epsilon}(1-y)^\epsilon}{(y-x)^{3\epsilon}}\,.
\end{aligned}
\tag{6.15}
$$

Note that we have expressed the loop factor of $\Gamma(1+\epsilon)/(4\pi)^{D/2}$ as $\mathcal{F}$ in the last line of (6.15). At this stage, we will divide the Feynman parameter integrals into two parts: I_1 for $y > x$ and I_2 for $x > y$, so that

$$
M3(1,1,0) = \frac{\mathcal{F}\,\Gamma(3\epsilon)}{\Gamma(\epsilon)\Gamma^2(1+\epsilon)}(I_1 + I_2)\,.
\tag{6.16}
$$

Starting with I_1, we will write $x = yz$, where $z \in [0,1]$. This leads to

$$
\begin{aligned}
I_1 &= \int_0^1 dy \int_0^1 y\, dz\, \frac{(yz)^{\epsilon-1}y^{-2\epsilon}(1-y)^\epsilon}{(y-yz)^{3\epsilon}} \\
&= \int_0^1 dy\, y^{-4\epsilon}(1-y)^\epsilon \int_0^1 dz\, z^{\epsilon-1}(1-z)^{-3\epsilon} \\
&= B(1+\epsilon, 1-4\epsilon)B(1-3\epsilon, \epsilon) \\
&= \frac{1}{\epsilon} + 3 + \left(9 + \frac{7\pi^2}{6}\right)\epsilon + \left(27 + \frac{7\pi^2}{2} + 18\zeta(3)\right)\epsilon^2 + \mathcal{O}(\epsilon^3)\,,
\end{aligned}
\tag{6.17}
$$

where we have used (2.31) to evaluate the integrals in the second line. Turning to I_2, we start by rewriting the denominator as

$$
\begin{aligned}
(y-x)^{-3\epsilon} &= (-1)^{-3\epsilon}(x-y)^{-3\epsilon} \\
&= e^{3i\pi\epsilon}(x-y)^{-3\epsilon}\,,
\end{aligned}
\tag{6.18}
$$

where we have used $-1 \to e^{-i\pi}$, a step which we will justify more carefully in Section 6.3. Then, we can use $y = xz$, for $z \in [0,1]$, so that

$$
I_2 = e^{3i\pi\epsilon}\int_0^1 dx\int_0^1 x\, dz\, \frac{x^{\epsilon-1}(xz)^{-2\epsilon}(1-xz)^\epsilon}{(x-xz)^{3\epsilon}}
$$

$$= e^{3i\pi\epsilon} \int_0^1 dx \int_0^1 dz \, x^{-4\epsilon} z^{-2\epsilon} (1-z)^{-3\epsilon} (1-xz)^{\epsilon} . \qquad (6.19)$$

Since this integral is finite, we can now expand the integrand as a series in ϵ and evaluate the integral term by term. Incidentally, this is why we have chosen $M3(1,1,0)$ as our master integral. Other choices, while superficially finite, would lead to divergences in the integral I_2 that prevent an expansion of the integrand in powers of ϵ. The result for the first few terms of (6.19) is

$$I_2 = e^{3i\pi\epsilon} \left\{ 1 + \left(7 + \frac{\pi^2}{6} \right) \epsilon + \left(37 - \frac{\pi^2}{6} + 11\zeta(3) \right) \epsilon^2 + \mathcal{O}(\epsilon^3) \right\} . \qquad (6.20)$$

Combining the results of (6.16), (6.17), (6.19), and (6.20), we have

$$\frac{M3(1,1,0)}{\mathcal{F}} = \frac{1}{3\epsilon} + \frac{4}{3} + \left(\frac{16}{3} + \frac{11\pi^2}{18} + i\pi \right) \epsilon$$
$$+ \left(\frac{64}{3} + \frac{5\pi^2}{18} + 7\zeta(3) + i\pi \left(7 + \frac{\pi^2}{6} \right) \right) \epsilon^2 + \mathcal{O}(\epsilon^3) . \qquad (6.21)$$

The imaginary terms arise from the expansion of $e^{3i\pi\epsilon}$ in (6.20). In Section 6.3, we will explore the origin and meaning of the imaginary parts of loop integrals.

6.2 Eikonal Integrals

In Section 3.3, we showed how Tomonaga parameters can be used to evaluate the J_1^+ integral:

$$J_1^+ = \int \frac{[d^D k_1][d^D k_2]}{(k_1 p + 1)(k_2^2)[(k_1 + k_2)^2 + 1]}$$
$$= \frac{2}{(4\pi)^D} B(-1 + 2\epsilon, -3 + 4\epsilon)\Gamma(1 - \epsilon)\Gamma(-2 + 3\epsilon) . \qquad (6.22)$$

The propagator $(k_1 p + 1)$ is known as an eikonal propagator, and consequently, J_1^+ is an eikonal integral. The meaning of this term stems from the Greek root *eiko-*, meaning weak or yielding, since the eikonal propagator depends weakly on the loop momentum. In the context of the method of asymptotic expansions, which we shall examine carefully in Chapter 7, eikonal propagators arise from the region of a loop integral where $|k| < |p|$, so that $(k^2 + 2kp) \to (2kp)$. The additional $+1$ term is merely a consequence of a shift of k to $(k - p)$:

$$(2kp) \to 2((k-p)p) = 2(kp - p^2) = 2(kp + 1) . \qquad (6.23)$$

As we saw in Chapter 1, the Minkowski-space definition of a propagator includes an infinitesimal pole term $+i\delta$ (previously written as $+i\varepsilon$) in order to prescribe a method for integrating near the poles of the propagator. Based on the locations of these poles, we can justify a Wick rotation to Euclidean space. When we combine a set of propagators with $+i\delta$ pole terms using one of the parameters from Chapter 3, the composite denominator factor will also have a $+i\delta$ pole term, so that we usually regard the $+i\delta$ as implicit and we Wick rotate at an early stage in the calculation. With asymptotic expansions, the situation becomes more delicate due to the possibility of $-i\delta$ pole terms. Whenever such terms might arise, we must remain in Minkowski space until the pole situation is clarified. For small loop momenta, the Minkowski-space propagators $(k^2 + 2kp + i\delta)$ and $(k^2 - 2kp + i\delta)$ would be expanded as

$$\frac{1}{(k^2 + 2kp + i\delta)} = \frac{1}{(2kp + i\delta)} - \frac{k^2}{(2kp + i\delta)^2} + \dots , \tag{6.24}$$

$$\frac{1}{(k^2 - 2kp + i\delta)} = -\frac{1}{(2kp - i\delta)} - \frac{k^2}{(2kp - i\delta)^2} - \dots . \tag{6.25}$$

As we can see, the propagator in (6.24) retains the $+i\delta$ pole term and therefore a Euclidean-space calculation will be appropriate. The propagator in (6.25), on the other hand, now has a $-i\delta$ pole term and therefore a permanent Wick rotation cannot be used to evaluate the loop integral.

With these developments in mind, the original loop integral in (6.22) is actually ill-defined, as we do not know the sign of the pole term in the eikonal propagator. The "+" in J_1^+ indicates that the pole term was indeed $+i\delta$, which is why we were able to evaluate the integral in Euclidean space using the techniques of Chapter 3. Conversely, we can also have a J_1^- integral, wherein the eikonal propagator carries a $-i\delta$ pole term. A Wick rotation is therefore prohibited, but fortunately we are rescued by an identity from complex analysis [22]:

$$\int_{-\infty}^{\infty} \frac{f(x)\,dx}{x - a \pm i\delta} = P \int_{-\infty}^{\infty} \frac{f(x)\,dx}{x - a} \mp i\pi f(a) . \tag{6.26}$$

Rearranging this slightly,

$$\int_{-\infty}^{\infty} \frac{f(x)\,dx}{x - a - i\delta} = \int_{-\infty}^{\infty} \frac{f(x)\,dx}{x - a + i\delta} + 2\pi i f(a) , \tag{6.27}$$

or in other words, a loop integral in which only a single propagator has a $-i\delta$ pole term can be related to the corresponding integral where all propagators have $+i\delta$ pole terms and an additional integral that is also free of $-i\delta$ pole terms.

Quantitatively, this means that

$$J_1^- = J_1^+ + \Delta J_1 \qquad (6.28)$$

where

$$\Delta J_1 = 2\pi i \int_M \frac{[d^D k_1][d^D k_2]}{(k_2^2 + i\delta)[(k_1 + k_2)^2 - 1 + i\delta]} \delta(k_1^0 - 1) . \qquad (6.29)$$

Although we will stay in Minkowski space, as denoted by the label M on the loop integral, the remaining poles are conventionally located and will hereafter be suppressed. Combining the denominators with a Feynman parameter, we have

$$\Delta J_1 = 2\pi i \int_0^1 dx \int_M \frac{[d^D k_1][d^D k_2]}{[(k_2 + x k_1)^2 + x(1 - x)k_1^2 - x]^2} \delta(k_1^0 - 1) . \qquad (6.30)$$

After shifting k_2 to $k_2 - x k_1$, we can evaluate the k_2-integral by converting (2.18) back to Minkowski space:

$$\int_M \frac{d^D k}{(2\pi)^D} \frac{1}{(k^2 - m^2)^n} = \frac{(-1)^n i}{(4\pi)^{D/2}} \frac{\Gamma\left(n - \frac{D}{2}\right)}{\Gamma(n)} \left(\frac{1}{m^2}\right)^{n - \frac{D}{2}} . \qquad (6.31)$$

This leads to

$$
\begin{aligned}
\Delta J_1 &= 2\pi i \int_0^1 dx \int_M [d^D k_1] \delta(k_1^0 - 1) \frac{i\Gamma(\epsilon)}{(4\pi)^{D/2}} \frac{1}{[x - x(1 - x)k_1^2]^\epsilon} \\
&= \frac{-2\pi\Gamma(\epsilon)}{(4\pi)^{D/2}(2\pi)^D} \int_0^1 dx \int \frac{d^{D-1}\mathbf{k}}{[x - x(1 - x) + x(1 - x)\mathbf{k}^2]^\epsilon} ,
\end{aligned}
\qquad (6.32)
$$

where $\mathbf{k}$ denotes the $(D-1)$-dimensional spatial momentum associated with k_1. Working in hyperspherical coordinates, the integration element becomes

$$\int d^{D-1}\mathbf{k} = \int d\Omega_{D-1} \int_0^\infty k^{D-2} \, dk , \qquad (6.33)$$

where $k = |\mathbf{k}|$. Using (2.17) to evaluate the angular integral in (6.32),

$$\Delta J_1 = -\frac{4\sqrt{\pi}}{(4\pi)^D} \frac{\Gamma(\epsilon)}{\Gamma\left(\frac{3}{2} - \epsilon\right)} \int_0^1 dx \int_0^\infty \frac{k^{D-2} \, dk}{[x^2 + x(1 - x)k^2]^\epsilon} . \qquad (6.34)$$

With the substitution

$$k = \sqrt{\frac{x}{1 - x}} \, z , \qquad (6.35)$$

the x- and z-integrals can be evaluated in terms of Beta functions via (2.31) and (2.30), respectively, resulting in

$$
\begin{aligned}
\Delta J_1 &= -\frac{2\sqrt{\pi}}{(4\pi)^D}\frac{\Gamma(\epsilon)}{\Gamma\left(\frac{3}{2}-\epsilon\right)}B\left(\frac{5}{2}-3\epsilon,-\frac{1}{2}+\epsilon\right)B\left(\frac{3}{2}-\epsilon,-\frac{3}{2}+2\epsilon\right)\\
&= -\frac{2\sqrt{\pi}}{(4\pi)^D}\Gamma\left(-\frac{3}{2}+2\epsilon\right)B\left(\frac{5}{2}-3\epsilon,-\frac{1}{2}+\epsilon\right).
\end{aligned}
\tag{6.36}
$$

There are two nontrivial sets of eikonal master integrals that we will encounter in Chapter 12, $J_1^{\pm}$ and $J_2^{\pm}$. The calculation of $J_2^{\pm}$ follows the same procedures as we have used for $J_1^{\pm}$, and for completeness, the results are:

$$
\begin{aligned}
J_1^{\pm} &= \int_M \frac{[d^D k_1][d^D k_2]}{(k_1 p - 1 \pm i\delta)(k_2^2 + i\delta)[(k_1 + k_2)^2 - 1 + i\delta]}\\
&= \frac{1}{(4\pi)^D}\bigg\{2\Gamma(1-\epsilon)\Gamma(-2+3\epsilon)B(-3+4\epsilon,-1+2\epsilon)\\
&\quad -(1\mp1)\sqrt{\pi}\Gamma\left(-\frac{3}{2}+2\epsilon\right)B\left(\frac{5}{2}-3\epsilon,-\frac{1}{2}+\epsilon\right)\bigg\},
\end{aligned}
\tag{6.37}
$$

$$
\begin{aligned}
J_2^{\pm} &= \int_M \frac{[d^D k_1][d^D k_2]}{(k_1 p \pm i\delta)(k_2^2 - 1 + i\delta)[(k_1 + k_2)^2 - 1 + i\delta]}\\
&= \pm\frac{\sqrt{\pi}}{(4\pi)^D}\Gamma\left(-\frac{3}{2}+2\epsilon\right)B\left(-\frac{1}{2}+\epsilon,-\frac{1}{2}+\epsilon\right).
\end{aligned}
\tag{6.38}
$$

Meanwhile, the following eikonal integrals are scaleless integrals, and so in accordance with the results of Section 2.3, they are zero in dimensional regularization:

$$
\int_M \frac{[d^D k]}{(k^2 + i\delta)^{a_1}(2kp \pm i\delta)^{a_2}},
\tag{6.39}
$$

$$
\int_M \frac{[d^D k_1][d^D k_2]}{(k_1^2 + i\delta)^{a_1}(k_2^2 + i\delta)^{a_2}((k_1 - k_2)^2 + i\delta)^{a_3}(2k_1 p \pm i\delta)^{a_4}(2k_2 p \pm i\delta)^{a_5}}.
\tag{6.40}
$$

6.3   Imaginary Terms

Let us have a closer look at the "one" topology that we briefly saw in Section 3.1. The integral, defined in Minkowski space as

$$
\int_M \frac{[d^D k]}{((k+p)^2 + i\delta)^{a_1}(k^2 + i\delta)^{a_2}},
\tag{6.41}
$$

is sketched in Figure 6.2. Note that a_1 and a_2 need not be integer exponents and that the external momentum p obeys the onshell condition $p^2 = m^2$. Even
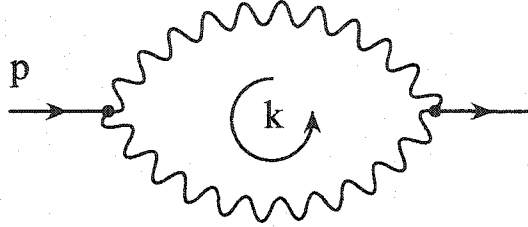
Figure 6.2: Sketch of the "one" topology.

though we could Wick rotate this integral and evaluate it, the Minkowski-space pole terms produce a subtle effect. With a Feynman parameter, the denominators are combined as

$$
\begin{aligned}
x((k+p)^2 + i\delta) + (1-x)(k^2 + i\delta) &= k^2 + 2xkp + xp^2 + i\delta \\
&= (k+xp)^2 + x(1-x)p^2 + i\delta .
\end{aligned}
\tag{6.42}
$$

By shifting k to $(k-xp)$, the k-integral can be evaluated using the basic Minkowski-space result (6.31), giving rise to a factor of

$$
\left(\frac{1}{-x(1-x)p^2 - i\delta} \right)^{a_1 + a_2 - D/2} .
\tag{6.43}
$$

Ordinarily, we take the limit $\delta \to 0$ as soon as possible, but for this case we will keep δ around a little while longer. If we factor out $x(1-x)p^2$, a term which is non-negative, the term containing δ still must go to 0 as $\delta \to 0$, so we will rescale δ and examine the factor

$$
(-1 - i\delta)^{D/2 - a_1 - a_2} .
\tag{6.44}
$$

Writing the argument of the exponent as $(a - b\epsilon)$ for integers a and b, we have

$$
(-1 - i\delta)^a \left[(-1 - i\delta)^{-\epsilon} \right]^b .
\tag{6.45}
$$

We can smoothly take the limit $\delta \to 0$ for the first factor to produce $(-1)^a$, but in the second factor, the non-integer exponent ϵ makes $(-1)^{-\epsilon}$ ambiguous. Instead, the δ suggests that we should write

$$
\lim_{\delta \to 0} (-1 - i\delta) = e^{-i\pi} ,
\tag{6.46}
$$

and so the "one" topology gives rise to factors of $e^{i\pi\epsilon}$ which, when expanded in ϵ as

$$e^{i\pi\epsilon} = 1 + i\pi\epsilon - \frac{\pi^2\epsilon^2}{2} - \frac{i\pi^3\epsilon^3}{6} + \cdots , \qquad (6.47)$$

give rise to imaginary terms in the loop integrals.

The Optical Theorem

The amplitudes that we compute for various classes of Feynman diagrams are connected to the probabilities for certain physical processes to occur. These probabilities must have a sensible physical interpretation, and as a direct consequence, the amplitudes are constrained by a relationship known as the optical theorem [1]. Quantitatively, the optical theorem states that

$$\text{Im}\,\mathcal{M}(\mathcal{A} \to \mathcal{A}) = C \sum_{\mathcal{B}} |\mathcal{M}(\mathcal{A} \to \mathcal{B})|^2 , \qquad (6.48)$$

where $\mathcal{A}$ and $\mathcal{B}$ both represent a set of particles with specific identities and momenta and C is a constant which depends on a set of external parameters relating to the particles in $\mathcal{A}$. The sum is over any possible set of particles $\mathcal{B}$ which can simultaneously be put onshell. Customizing (6.48) to the case where $\mathcal{A}$ is a single particle of mass m, the constant is simply $\frac{1}{2}$. Then, we can separate the sum over $\mathcal{B}$ into a sum over specific particles and an integral over the physically allowed phase space of these particles. As a result of the techniques that we will describe in Chapter 7, we will always be able to reduce our work to single-scale diagrams, and thus $\mathcal{B}$ must consist of massless particles only, lest we end up turning one massive particle into another equally massive particle plus some others. As a result, for a specific diagram that specifies $\mathcal{M}$, we need only sum over the ways in which the diagram can be "cut" in two by only cutting through massless lines. Thinking of the optical theorem in this way, we have

$$\text{Im}\,\mathcal{M} = \frac{1}{2} \sum_{\text{cuts}} \int d\Pi_{\text{cut}}\, \mathcal{M}_1 \mathcal{M}_2^* , \qquad (6.49)$$

where $\mathcal{M}_1$ and $\mathcal{M}_2$ correspond to the two pieces of $\mathcal{M}$ that are produced by the cut. The phase space integral involves a factor of

$$\frac{d^3\mathbf{q}}{(2\pi)^3 2E} \qquad (6.50)$$

for every particle involved in a given cut, along with a δ-function to conserve overall four-momentum. It was shown by the aptly-named Cutkosky [23] that

this cutting procedure is applicable to diagrams with an arbitrary number of loops. Over forty years later, this powerful idea is still elusive to some [24].

After deriving several important phase space factors, we will illustrate this method through an extensive series of examples. Be forewarned that this will be a very intricate and lengthy section in order to supply details that are completely absent in the literature. These techniques are required to obtain the master integrals encountered in Chapter 13.

Phase Space Factors

Define **P2** as the phase space of two massless scalars, assuming that the initial particle has mass m. This situation is depicted by Figure 6.3. Quantitatively,
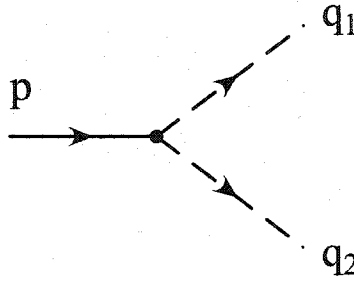
Figure 6.3: Origin of the **P2** phase space factor.

$$\mathbf{P2} = \int \frac{d^{D-1}\mathbf{q_1}}{(2\pi)^{D-1}\,2E_1} \frac{d^{D-1}\mathbf{q_2}}{(2\pi)^{D-1}\,2E_2}\, (2\pi)^D\, \delta^{(D)}(p - q_1 - q_2)\,, \qquad (6.51)$$

where we have generalized to D dimensions. Working in the rest frame of the incident particle,

$$\delta^{(D)}(p - q_1 - q_2) = \delta(m - E_1 - E_2)\, \delta^{(D-1)}(-\mathbf{q_1} - \mathbf{q_2}) \qquad (6.52)$$

and the second δ-function can be used to set $\mathbf{q_2} = -\mathbf{q_1}$, so that

$$\mathbf{P2} = \frac{1}{4(2\pi)^{D-2}} \int \frac{d^{D-1}\mathbf{q_1}}{E_1 E_2}\, \delta(m - E_1 - E_2)\,. \qquad (6.53)$$

Since the final particles are massless, $E_1 = |\mathbf{q_1}|$ and $E_2 = |\mathbf{q_2}| = |-\mathbf{q_1}| = E_1$, leading to

$$\mathbf{P2} = \frac{1}{4(2\pi)^{D-2}} \int \frac{d^{D-1}\mathbf{q_1}}{|\mathbf{q_1}|^2}\, \delta(m - 2|\mathbf{q_1}|)\,. \qquad (6.54)$$

Moving to spherical coordinates, where $\int d^{D-1}\mathbf{q_1} = \int d\Omega_{D-1} \int q_1^{D-2} \, dq_1$, and using (2.17) to evaluate the angular integral,

$$\mathbf{P2} = \frac{2^{(1-D)}\pi^{(3-D)/2}}{\Gamma\left(\frac{D-1}{2}\right)} \int q_1^{D-4} \, \delta(m - 2q_1) \, dq_1 \, . \tag{6.55}$$

Finally, using the δ-function identity

$$\delta\left(f(x)\right) = \sum_i \frac{\delta(x - x_i)}{|f'(x_i)|} \, , \quad \forall i \text{ such that } f(x_i) = 0 \, , \tag{6.56}$$

we obtain

$$\int q_1^{D-4} \, \delta(m - 2q_1) \, dq_1 = \frac{m^{D-4}}{2^{D-3}} \tag{6.57}$$

so that

$$\mathbf{P2} = \frac{m^{(D-4)}2^{(4-2D)}\pi^{(3-D)/2}}{\Gamma\left(\frac{D-1}{2}\right)} \, . \tag{6.58}$$

Setting $D = 4 - 2\epsilon$ and removing the loop factor of $\mathcal{F} = m^{-2\epsilon}\Gamma(1 + \epsilon)/(4\pi)^{D/2}$ in accordance with (2.34), our final result for the phase space of two massless particles is

$$\mathbf{P2} = \frac{\mathcal{F} \, 2^{2\epsilon}\pi^{3/2}}{\Gamma(1 + \epsilon)\Gamma(3/2 - \epsilon)} \, . \tag{6.59}$$

Although we could proceed in a similar fashion to derive **P3**, the phase space of three massless scalars, it will be worth the extra effort if we add a complication to the derivation: we will allow one of the particles to have a non-zero mass. At the end of the derivation, we can recover **P3** by taking this mass to be zero, but otherwise, this non-zero mass will allow us to obtain an expression for the four-body phase space **P4** that arises in many three-loop master integrals. Let **P3m** denote this generalized three-body phase space, as depicted in Figure 6.4. Taking $q_2^2 = y$ to be the mass of particle 2 and using the external particle mass as the unit of energy (so that $y = m_2^2/M^2$), we have

$$\begin{aligned}
\mathbf{P3m} &= \int \frac{d^{D-1}\mathbf{q_1}}{(2\pi)^{D-1} \, 2E_1} \frac{d^{D-1}\mathbf{q_2}}{(2\pi)^{D-1} \, 2E_2} \frac{d^{D-1}\mathbf{q_3}}{(2\pi)^{D-1} \, 2E_3} \, (2\pi)^D \, \delta^{(D)}(p - q_1 - q_2 - q_3) \\
&= \frac{1}{8(2\pi)^{2D-3}} \int \frac{d^{D-1}\mathbf{q_1} d^{D-1}\mathbf{q_2}}{|\mathbf{q_1}||\mathbf{q_2}||\mathbf{q_1} + \mathbf{q_2}|} \, \delta(1 - |\mathbf{q_1}| - |\mathbf{q_2}| - |\mathbf{q_1} + \mathbf{q_2}|) \, . \tag{6.60}
\end{aligned}$$

If we write $\mathbf{q_1}$ and $\mathbf{q_2}$ in hyperspherical coordinates, only the angle θ between these two vectors remains in the integral. Letting q_1 and q_2 denote the magni-
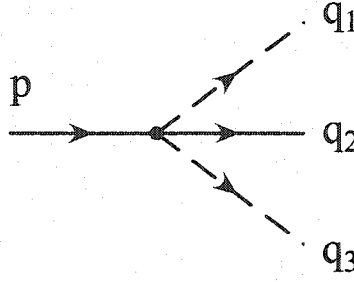
Figure 6.4: Origin of the **P3m** phase space factor.

tudes of q_1 and q_2, we obtain

$$\mathbf{P3m} \;=\; \frac{\Omega_{D-1}\Omega_{D-2}}{8(2\pi)^{2D-3}} \int \frac{(q_1^{D-3}dq_1)(q_2^{D-2}dq_2)\sin^{D-3}\theta\, d\theta}{\sqrt{q_2^2+y}\sqrt{q_1^2+q_2^2+2q_1q_2\cos\theta}}$$

$$\times\, \delta\!\left(1-q_1-\sqrt{q_2^2+y}-\sqrt{q_1^2+q_2^2+2q_1q_2\cos\theta}\right). \tag{6.61}$$

Before we roll up our sleeves to evaluate the integral, let us rewrite the factors in front in a more convenient form. Using (2.17), we see that

$$\frac{\Omega_{D-1}\Omega_{D-2}}{8(2\pi)^{2D-3}} \;=\; \frac{1}{8(2\pi)^{2D-3}}\left(\frac{2\pi^{\frac{3}{2}-\epsilon}}{\Gamma(3/2-\epsilon)}\right)\left(\frac{2\pi^{1-\epsilon}}{\Gamma(1-\epsilon)}\right)$$

$$=\; \frac{2^{-6+4\epsilon}\pi^{-\frac{5}{2}+2\epsilon}}{\Gamma(3/2-\epsilon)\Gamma(1-\epsilon)}. \tag{6.62}$$

Using the doubling formula (2.33), we can write

$$\frac{1}{\Gamma(1-\epsilon)} \;=\; \frac{\Gamma(2-2\epsilon)}{\Gamma(1-\epsilon)\Gamma(1-\epsilon)}\frac{\Gamma(1-\epsilon)}{\Gamma(2-2\epsilon)}$$

$$=\; \frac{1}{B(1-\epsilon,1-\epsilon)}\frac{\sqrt{\pi}}{2^{1-2\epsilon}\,\Gamma(3/2-\epsilon)}, \tag{6.63}$$

so that

$$\frac{\Omega_{D-1}\Omega_{D-2}}{8(2\pi)^{2D-3}} \;=\; \frac{2^{-7+6\epsilon}\pi^{-2+2\epsilon}}{B(1-\epsilon,1-\epsilon)\,\Gamma^2(3/2-\epsilon)}. \tag{6.64}$$

Abbreviating $B(1-\epsilon,1-\epsilon)$ by B_{11}, removing two loop factors of $\mathcal{F}$, and using our result (6.59) for **P2**, we conclude that

$$\frac{\Omega_{D-1}\Omega_{D-2}}{8(2\pi)^{2D-3}} \;=\; \frac{2^{1-2\epsilon}\,(\mathbf{P2})^2}{\pi B_{11}}. \tag{6.65}$$

Returning to the integral in (6.61), we will use the δ-function to perform the integral over θ. In order to rewrite the δ-function as $\delta(\theta - \theta_0)$, the identity (6.56) requires us to divide the integrand by a factor of

$$\left| \frac{d}{d\theta} \left(1 - q_1 - \sqrt{q_2^2 + y} - \sqrt{q_1^2 + q_2^2 + 2q_1 q_2 \cos\theta} \right) \right| = \frac{q_1 q_2 \sin\theta}{\sqrt{q_1^2 + q_2^2 + 2q_1 q_2 \cos\theta}} \, . \tag{6.66}$$

Our phase space factor now looks like

$$\mathbf{P3m} = \frac{2^{1-2\epsilon} \, (\mathbf{P2})^2}{\pi B_{11}} \int \frac{(q_1^{D-4} dq_1)(q_2^{D-3} dq_2) \sin^{D-4}\theta \, d\theta}{\sqrt{q_2^2 + y}} \, \delta(\theta - \theta_0) \, . \tag{6.67}$$

At this stage we will change variables from the momentum magnitudes q_1 and q_2 to the mass invariants z and u, defined by

$$z = (q_2^\mu + q_3^\mu)^2 = (p^\mu - q_1^\mu)^2 = 1 - 2q_1 \, , \tag{6.68}$$

$$u = (q_1^\mu + q_3^\mu)^2 = (p^\mu - q_2^\mu)^2 = 1 + y - 2\sqrt{q_2^2 + y} \, , \tag{6.69}$$

where an index μ in the equations above indicates a four-vector. From (6.68), it is easy to see that

$$
\begin{aligned}
q_1 &= \frac{1-z}{2} \, , \\
q_1^{D-4} dq_1 &= -\frac{(2q_1)^{-2\epsilon} \, dz}{2^{1-2\epsilon}} \, ,
\end{aligned}
\tag{6.70}
$$

whereas (6.69) leads to

$$
\begin{aligned}
q_2^2 &= \left(\frac{1+y-u}{2} \right)^2 - y \, , \\
2q_2 dq_2 &= 2 \left(\frac{1+y-u}{2} \right) \left(-\frac{du}{2} \right) \, , \\
\frac{q_2^{D-3} dq_2}{\sqrt{q_2^2 + y}} &= -\frac{du}{2} \, q_2^{-2\epsilon} \, .
\end{aligned}
\tag{6.71}
$$

The $q_1^{-2\epsilon}$ and $q_2^{-2\epsilon}$ factors are left unsubstituted in anticipation of a future cancellation. Substituting (6.70) and (6.71) into (6.67), we obtain

$$\mathbf{P3m} = \frac{(\mathbf{P2})^2}{2\pi B_{11}} \int du \, dz \, (2q_1 q_2)^{-2\epsilon} \, (\sin^2\theta_0)^{-\epsilon} \, . \tag{6.72}$$

The compactness of this expression is somewhat deceiving, as $\sin\theta_0$ is implicitly fixed by the δ-function in (6.61). Specifically,

$$\left(1 - q_1 - \sqrt{q_2^2 + y}\right) = \sqrt{q_1^2 + q_2^2 + 2q_1q_2\cos\theta_0}\,,$$

$$1 + y - 2q_1 - 2\sqrt{q_2^2 + y} + 2q_1\sqrt{q_2^2 + y} = 2q_1q_2\cos\theta_0\,, \tag{6.73}$$

and with $\cos\theta_0 = 1 - 2\sin^2(\theta_0/2)$, we have

$$\sin^2(\theta_0/2) = \frac{1}{4q_1q_2}\left[2q_1q_2 - \left(1 - 2q_1 + y + 2(q_1 - 1)\sqrt{q_2^2 + y}\right)\right]\,. \tag{6.74}$$

Using $\sin^2\theta_0 = 4\sin^2(\theta_0/2)(1 - \sin^2(\theta_0/2))$,

$$(\sin^2\theta_0)^{-\epsilon} = \frac{1}{(2q_1q_2)^{-2\epsilon}}\left[2q_1q_2 - \left(1 - 2q_1 + y + 2(q_1 - 1)\sqrt{q_2^2 + y}\right)\right]^{-\epsilon}$$

$$\times \left[2q_1q_2 + \left(1 - 2q_1 + y + 2(q_1 - 1)\sqrt{q_2^2 + y}\right)\right]^{-\epsilon}\,. \tag{6.75}$$

As anticipated, when we substitute this result into (6.72), the $(2q_1q_2)^{-2\epsilon}$ factors cancel. To finish the derivation, we will need to use (6.68) and (6.69) to write the terms in the square brackets of (6.75) in terms of z and u. After a lengthy sequence of tedious but straightforward algebraic manipulations, we find that

$$\mathbf{P3m} = \frac{(\mathbf{P2})^2}{2\pi B_{11}}\int du\, dz\, u^{-\epsilon}\, z^{-\epsilon}\left(\frac{(1-z)(z-y)}{z} - u\right)^{-\epsilon}\,. \tag{6.76}$$

Setting $y = 0$, we obtain the phase space factor **P3** for three massless scalars:

$$\mathbf{P3} = \frac{(\mathbf{P2})^2}{2\pi B_{11}}\int du\, dz\, u^{-\epsilon}\, z^{-\epsilon}\,(1 - z - u)^{-\epsilon}\,. \tag{6.77}$$

The limits of integration for **P3** are

$$\int_0^1 dz \int_0^{1-z} du \quad\text{or}\quad \int_0^1 du \int_0^{1-u} dz\,. \tag{6.78}$$

Supposing we have four massless scalars, we can group two of them together (particles 2 and 4, for instance) and integrate over the two-body phase space of the pair. The resulting invariant, $y = (q_2^\mu + q_4^\mu)^2$, can then be regarded as a single massive particle. Together with particles 1 and 3, this "massive particle" forms a three-body phase space of the form (6.76). This can be expressed

as

$$\mathbf{P4} = \frac{(\mathbf{P2})^3}{4\pi^2 B_{11}} \int du\, dz\, dy\, u^{-\epsilon}\, z^{-\epsilon}\, y^{-\epsilon}\, \left(\frac{(1-z)(z-y)}{z} - u\right)^{-\epsilon}, \qquad (6.79)$$

where the extra $\mathbf{P2}/2\pi$ in front, relative to $\mathbf{P3m}$, arises from

$$
\begin{aligned}
(2\pi)^D \delta^{(D)}(p - q_1 - q_2 - q_3 - q_4) &= \int d^D q_{24}\, (2\pi)^D \delta^{(D)}(p - q_1 - q_3 - q_{24}) \\
&\qquad \times \delta^{(D)}(q_{24} - q_2 - q_4) \\
&= \frac{1}{2\pi} \int dy\, (2\pi)^D \delta^{(D)}(p - q_1 - q_3 - q_{24}) \\
&\qquad \times \left[\int \frac{d^{D-1}\mathbf{q_{24}}}{(2\pi)^{D-1}} (2\pi)^D \delta^{(D)}(q_{24} - q_2 - q_4)\right].
\end{aligned}
\qquad (6.80)
$$

There are six ways to express the limits of integration for P4. Two of them are

$$\int_0^1 dz \int_0^z dy \int_0^{(1-z)(z-y)/z} du \qquad \text{and} \qquad \int_0^1 dz \int_0^{1-z} du \int_0^{z(1-z-u)/(1-z)} dy\,. \qquad (6.81)$$

Fortunately, these expressions are easier to apply than they are to derive. The proper use of these formulas will now be displayed with some examples.

Simple Example of a 2-Particle Cut

Let us consider an integral from the "one" topology wherein we have exactly one factor of each propagator:

$$one(1,1) = \int \frac{[d^D k]}{(k+p)^2 k^2}\,. \qquad (6.82)$$

Removing the loop factor $\mathcal{F} = m^{-2\epsilon} \Gamma(1+\epsilon)/(4\pi)^{D/2}$ and using $(-1)^{-\epsilon} = e^{i\pi\epsilon}$ from (6.46), we can evaluate the entire integral explicitly:

$$\frac{one(1,1)}{\mathcal{F}} = \frac{1}{\epsilon} + (2 + i\pi) + \left(4 + 2i\pi - \frac{2\pi^2}{3}\right)\epsilon + \mathcal{O}(\epsilon^2)\,. \qquad (6.83)$$

Using the optical theorem, we will now evaluate the imaginary part of this integral directly. Figure 6.5 shows how the integral can be split into two by cutting across massless lines. Each side is a trivial vertex which contributes nothing to
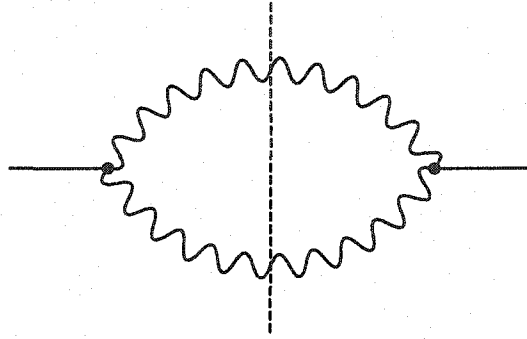
Figure 6.5: Illustration of a cut through the massless lines of a "one" integral.

a loop integral, thus from (6.49) we have

$$\mathrm{Im}\ one(1,1) = \frac{1}{2}\,\mathbf{P2}\ .$$

(6.84)

Substituting (6.59) for **P2** and expanding the result as a series in ϵ, we have

$$\frac{\mathrm{Im}\ one(1,1)}{\mathcal{F}} = \pi + 2\pi\epsilon + \mathcal{O}(\epsilon^2)\ ,$$

(6.85)

in agreement with the complete result (6.83).

Simple Example of a 3-Particle Cut

A simple example of a two-loop integral whose imaginary part can be evaluated with the optical theorem is

$$J_{000}(1,1,1) = \int \frac{[d^D k_1][d^D k_2]}{k_1^2 k_2^2 (k_1 + k_2 + p)^2}\ .$$

(6.86)

The complete solution for this integral, obtained from a sequence of two simple massless one-loop integrals, is

$$\frac{J_{000}(1,1,1)}{\mathcal{F}^2} = \frac{1}{4\epsilon} + \left(\frac{13}{8} + \frac{i\pi}{2}\right) + \left(\frac{115}{16} - \frac{7\pi^2}{12} + \frac{13i\pi}{4}\right)\epsilon + \mathcal{O}(\epsilon^2)\ .$$

(6.87)

As shown in Figure 6.6, the cut is obvious. As with the previous example, each side is just a trivial vertex, therefore

$$\mathrm{Im}\ J_{000}(1,1,1) = \frac{1}{2}\,\mathbf{P3}\ .$$

(6.88)
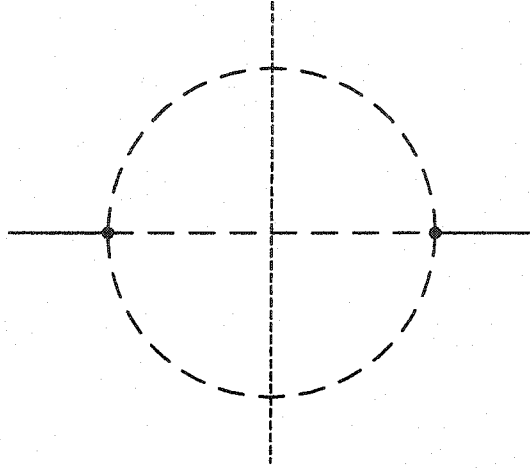
Figure 6.6: Illustration of a cut through the massless lines of a "J_{000}" integral.

Substituting (6.77) for **P3**, we have

$$\mathrm{Im}\, J_{000}(1,1,1) = \frac{(\mathbf{P2})^2}{4\pi B_{11}} \int_0^1 du \int_0^{1-u} dz\, u^{-\epsilon}\, z^{-\epsilon}\, (1-z-u)^{-\epsilon}. \qquad (6.89)$$

With the substitution $z = (1-u)w$, the integrals can be evaluated explicitly as

$$\int_0^1 du \int_0^{1-u} dz\, u^{-\epsilon}\, z^{-\epsilon}\, (1-z-u)^{-\epsilon} = \int_0^1 du\, u^{-\epsilon}(1-u)^{1-2\epsilon} \int_0^1 dw\, w^{-\epsilon}(1-w)^{-\epsilon}$$
$$= B(1-\epsilon, 2-2\epsilon)B(1-\epsilon, 1-\epsilon) \qquad (6.90)$$

so that

$$\frac{\mathrm{Im}\, J_{000}(1,1,1)}{\mathcal{F}^2} = \frac{(\mathbf{P2})^2}{4\pi\mathcal{F}^2} B(1-\epsilon, 2-2\epsilon)$$
$$= \frac{\pi}{2} + \frac{13\pi}{4}\,\epsilon + \mathcal{O}(\epsilon^2), \qquad (6.91)$$

which agrees with (6.87).

Simple Example of a 4-Particle Cut

The simplest example of a loop integral whose imaginary part can be evaluated with a four-particle cut is

$$J4 = \int \frac{[d^D k_1][d^D k_2][d^D k_3]}{k_1^2 k_2^2 k_3^2 (k_1 + k_2 + k_3 + p)^2}. \qquad (6.92)$$

This integral is sketched in Figure 6.7, where we refrain from drawing the obvious cut. This integral can be evaluated exactly as a sequence of three massless

Figure 6.7: Sketch of the "J4" integral.

one-loop integrals, with the result

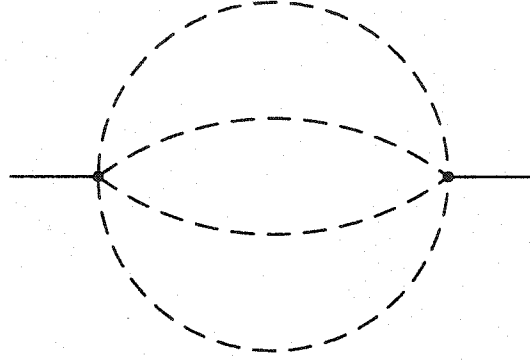$$\frac{J4}{\mathcal{F}^3} = \frac{1}{36\epsilon} + \left(\frac{71}{216} + \frac{i\pi}{12}\right) + \left(\frac{3115}{1296} - \frac{5\pi^2}{36} + \frac{71i\pi}{72}\right)\epsilon + \mathcal{O}(\epsilon^2). \tag{6.93}$$

Alternatively, we can obtain the imaginary part of this integral using the formula (6.79) for **P4**:

$$\mathrm{Im}\, J4 = \frac{(\mathbf{P2})^3}{8\pi^2 B_{11}} \int_0^1 dz \int_0^z dy \int_0^{u_m} du\, u^{-\epsilon}\, z^{-\epsilon}\, y^{-\epsilon}\, (u_m - u)^{-\epsilon} \tag{6.94}$$

where $u_m = (1 - z)(z - y)/z$. With the substitution $u = u_m w$, the u-integral is $u_m^{1-2\epsilon} B_{11}$, so that

$$\mathrm{Im}\, J4 = \frac{(\mathbf{P2})^3}{8\pi^2} \int_0^1 dz\, z^{-1+\epsilon}\, (1 - z)^{1-2\epsilon} \int_0^z dy\, y^{-\epsilon}\, (z - y)^{1-2\epsilon}. \tag{6.95}$$

With the substitution $y = zx$, the x- and z-integrals are $B(1 - \epsilon, 2 - 2\epsilon)$ and $B(2 - 2\epsilon, 2 - 2\epsilon)$, respectively, so that our final result is

$$\frac{\mathrm{Im}\, J4}{\mathcal{F}^3} = \frac{\pi}{12} + \frac{71\pi}{72}\epsilon + \mathcal{O}(\epsilon^2), \tag{6.96}$$

in agreement with the complete result (6.93).

These first three examples of how to apply the optical theorem to obtain the imaginary part of a loop integral are somewhat unimpressive, as we are only confirming results that we can more easily obtain with more conventional methods. Think of these examples as a calibration of the method. The utility

of these new methods occurs when we encounter more complicated integrals in which we do not know anything about the exact result.

More Difficult Example of a 2-Particle Cut

Our first non-trivial example of a master integral evaluated via cuts is the "N5a" master integral,

$$N5a(1,1,1,1,1) = \int \frac{[d^D k_1][d^D k_2]}{k_1^2 k_2^2 (k_1^2 + 2k_1 p)(k_2 + p)^2 \left[(k_1 + k_2)^2 + 2(k_1 + k_2)p\right]} , \quad (6.97)$$

and sketched in Figure 6.8.
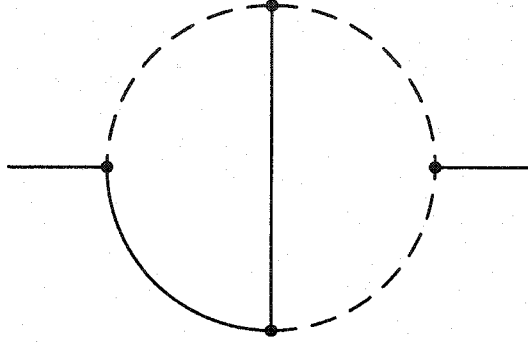
Figure 6.8: Sketch of the "N5a" master integral.

After cutting through the two massless lines on the right, we see that a one-loop integral still remains to the left of the cut. The general procedure is to evaluate an integral such as this and to put the external lines on mass shell. Then, this result is to be folded into the integration of the phase space calculation. For two particle cuts, however, there are no remaining integrals to be performed in P2 because there is only one way in which two particles can partition the available phase space. As a result, calculations with two-particle cuts reduce to a multiplication of P2/2 with the remaining loop integral. For the "N5a" integral currently under consideration, this loop integral is

$$L = \int \frac{[d^D k]}{k^2(k^2 + 2kp)\left[(k+q)^2 + 1\right]} , \quad (6.98)$$

as pictured in Figure 6.9.

We begin evaluating L by combining the two massive propagators with a Feynman parameter,

$$x(k^2 + 2kp) + (1-x)\left[(k+q)^2 + 1\right] = k^2 + 2k\left(xp + (1-x)q\right) + (1-x)(q^2 + 1)$$
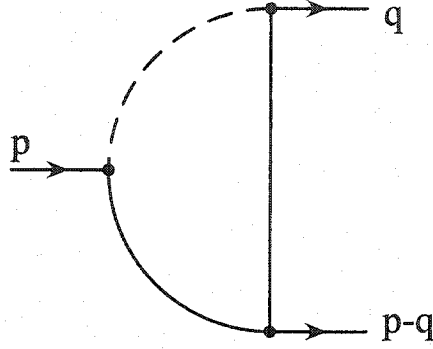
Figure 6.9: Sketch of the remaining loop integral after cutting the "N5a" master integral.

$$= k^2 + 2kt + (1 - x), \qquad (6.99)$$

where $t = (xp + (1-x)q)$ and we have used $q^2 = 0$ in the last line. Next, we introduce a second Feynman parameter in order to fold in the massless propagator in L:

$$
\begin{aligned}
y\left[k^2 + 2kt + (1 - x)\right] + (1 - y)k^2 &= k^2 + 2ykt + y(1 - x) \\
&= (k + yt)^2 + y(1 - x) - y^2 t^2 . \quad (6.100)
\end{aligned}
$$

But

$$
\begin{aligned}
t^2 &= [xp + (1 - x)q]^2 \\
&= x^2 p^2 + (1 - x)^2 q^2 + 2x(1 - x)pq \\
&= x^2(-1) + (1 - x)^2(0) + x(1 - x)\left[p^2 + q^2 - (p - q)^2\right] \\
&= -x^2 - x(1 - x) \\
&= -x , \qquad (6.101)
\end{aligned}
$$

and so

$$
\begin{aligned}
L &= \Gamma(3) \int_0^1 y\, dy \int_0^1 dx \int \frac{[d^D k]}{\left[(k + yt)^2 + y(1 - x) + xy^2\right]^3} \\
&= \frac{\Gamma(3 - D/2)}{(4\pi)^{D/2}} \int_0^1 dy \int_0^1 dx \frac{y^{-\epsilon}}{(1 - x + xy)^{1+\epsilon}} . \qquad (6.102)
\end{aligned}
$$

After pulling out the standard loop factor (2.34), we can evaluate the Feynman

parameter integrals, resulting in

$$L = \mathcal{F}\left[\frac{\pi^2}{6} + 3\zeta(3)\,\epsilon + \mathcal{O}(\epsilon^2)\right]. \tag{6.103}$$

The imaginary part of the "N5a" master integral is then

$$\text{Im } N5a(1,1,1,1,1) = \frac{\mathbf{P2}}{2} L$$

$$= \mathcal{F}^2\left[\frac{\pi^3}{6} + \left(3\pi\zeta(3) + \frac{\pi^3}{3}\right)\epsilon + \mathcal{O}(\epsilon^2)\right]. \tag{6.104}$$

More Difficult Example of a 3-Particle Cut

With cuts of three or more particles the partition of the total phase space is not unique, and hence, integrals over mass invariants appear in (6.77) and (6.79). Any propagators and loops that are not severed by a particular cut will also depend on these integration parameters. This can be seen in the "N5d" topology, as sketched in Figure 6.10.
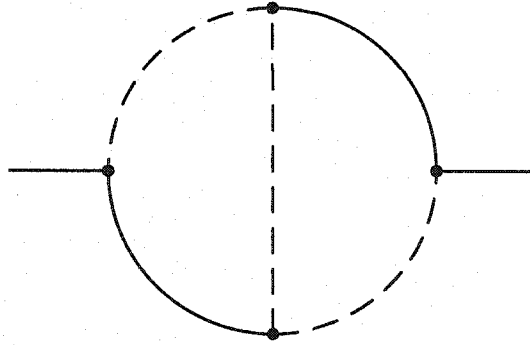
Figure 6.10: Sketch of the "N5d" master integral.

In this particular case, all that remains after the cut are two massive propagators. Since they each split into a pair of massless lines which are cut, the four-momenta of these massive propagators are related to the mass invariants, z and u, of (6.77):

$$\frac{1}{k_1^2 + 1} = \frac{1}{1-z}, \tag{6.105}$$

$$\frac{1}{k_2^2 + 1} = \frac{1}{1-u}. \tag{6.106}$$

The minus signs are required to reconcile the Minkowski-space formulation of

the phase space formulas with the Euclidean-space formulation of our loop integrals. The "N5d" master integral is therefore

$$\text{Im } N5d(1,1,1,1,1) = \frac{(\mathbf{P2})^2}{4\pi B_{11}} \int_0^1 du \int_0^{1-u} dz \, \frac{u^{-\epsilon} z^{-\epsilon} (1-z-u)^{-\epsilon}}{(1-z)(1-u)}$$

$$= \mathcal{F}^2 \left[\frac{\pi^3}{6} + \left(7\pi\zeta(3) + \frac{\pi^3}{3} \right) \epsilon + \mathcal{O}(\epsilon^2) \right] . \qquad (6.107)$$

More Difficult Example of a 4-Particle Cut

For our final example, we shall consider the "M11" master integral, as sketched in Figure 6.11. This integral is very closely related to the "Y9" topology described in the Appendix.
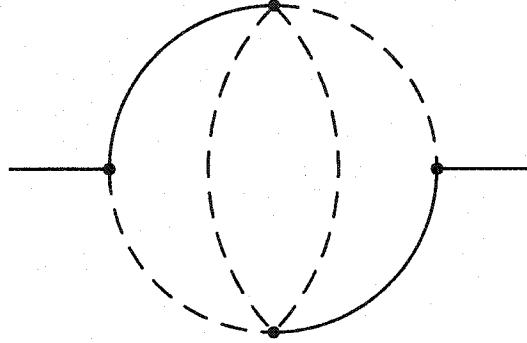
Figure 6.11: Sketch of the "M11" master integral.

On each side of the cut we have a massive propagator. As might be expected when cutting through four lines in a planar three-loop diagram, there are no loop integrals remaining. We would like to apply our four-body phase space expression (6.79) to this integral, but first we will need to change one of the integration variables. Specifically, we need to replace the invariant $u = (q_1 + q_3)^2$ with $v = (q_1 + q_2)^2$ since the massless loop corresponds to a massive q_2 and thus the massive propagators beside the cut carry momenta $(q_1 + q_2)$ and $(q_2 + q_3)$. With

$$u + v + z = 1 + y , \qquad (6.108)$$

we can rewrite (6.79) as

$$\mathbf{P4} = \frac{(\mathbf{P2})^3}{4\pi^2 B_{11}} \int_0^1 dy \int_y^1 dz \int_{y/z}^{1+y-z} dv \, y^{-\epsilon} z^{-\epsilon} (1+y-z-v)^{-\epsilon} \left(v - \frac{y}{z} \right)^{-\epsilon} . \qquad (6.109)$$

The integral we need to evaluate has the additional propagator factors $(1-v)^{-1}$

and $(1 - z)^{-1}$, and as before, can be expanded in ϵ and evaluated term by term, thereby leading to

$$
\mathrm{Im}\, M11 = \pi \mathcal{F}^3 \left[\left(-1 + \frac{\pi^2}{6} \right) + \left(-14 + \frac{7\pi^2}{6} + 9\zeta(3) \right) \epsilon \right. \tag{6.110}
$$
$$
\left. + \left(-119 + \frac{15\pi^2}{2} + 63\zeta(3) + \frac{41\pi^4}{180} \right) \epsilon^2 + \mathcal{O}\left(\epsilon^3 \right) \right] .
$$

Although some of the master integrals that arise in Chapter 13 are even more elaborate than the examples considered here, the general ideas are the same. Be forewarned, though, that not all papers in this field treat imaginary terms properly. For example, the master integrals for any two-loop topology, such as the ones used in the preceding examples, have been calculated in [15]. While this paper is a valuable reference, there are errors in the signs of the imaginary terms in some of these integrals [25].

Additional Trick

Consider the "Y2a" master integral,

$$
Y2a(0, 1, 1, 1) = \int \frac{[d^D k_1][d^D k_2]}{k_1^{2\epsilon} k_2^2 (k_1 + p)^2 \left[(k_1 + k_2 + p)^2 + 1 \right]} , \tag{6.111}
$$

as shown in Figure 6.12. The epsilon-propagator $k_1^{2\epsilon}$ indicates that this is a
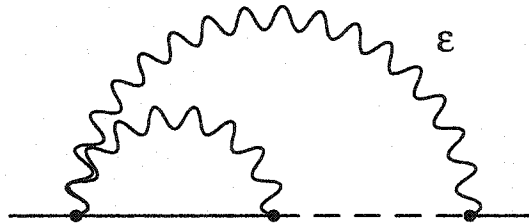
Figure 6.12: Sketch of the "Y2a" master integral.

subtopology of a three-loop topology. Although a two-loop diagram — even one with an epsilon-propagator — is usually simpler than a three-loop diagram, it appears as if we cannot evaluate the imaginary part of the master integral (6.111) using cuts, since the epsilon-propagator does not really correspond to a well-defined virtual particle that can be put on mass shell. One option would be to "undo" the epsilon-propagator by replacing it with a massless subloop so that we could make a three-particle cut on a three-loop integral. There is an easier method that can be applied to this particular topology, though.

Since the k_2-dependent subloop sits entirely on the $(k_1 + p)$-line, any cut through the $(k_1 + p)^2$ propagator will result in the onshell condition $(k_1 + p)^2 = 0$ in the k_2-loop. Our inability to cut through the $k_1^{2\epsilon}$ line is irrelevant to the k_2-integral, which with the aforementioned onshell constraint, is identical to a much simpler integral:

$$\int \frac{[d^D k_2]}{[(k_1 + k_2 + p)^2 + 1]\,k_2^2} \quad \xrightarrow{(k_1+p)^2=0} \quad \int \frac{[d^D k_2]}{(k_2^2 + 1)k_2^2}. \tag{6.112}$$

This new k_2-integral is a simple one-loop vacuum bubble integral, which together with the remaining massless k_1-dependent loop, can easily be solved in order to obtain the imaginary part of the "Y2a" master integral:

$$\frac{\text{Im}\, Y2a(0,1,1,1)}{\mathcal{F}^2} = \frac{\pi}{2} + \frac{11\pi}{4}\epsilon + \left(\frac{85\pi}{8} - \frac{5\pi^3}{12}\right)\epsilon^2 + \mathcal{O}(\epsilon^3). \tag{6.113}$$

Of course, the real part of $Y2a(0,1,1,1)$ cannot be obtained in this way, but if the imaginary terms are all we are interested in then this "cut-free cutting" technique is a useful trick to know about.

Vacuum Bubbles

Diagrams without external lines are known as vacuum bubbles. Although the exponentiation of disconnected diagrams identity [1] allows us to discard vacuum bubble diagrams generated directly from the Feynman rules of Chapter 1, such diagrams can be legally obtained in other contexts. Recurrence relations, for instance, can sometimes eliminate one or more propagators in such a way that vacuum bubble integrals are produced. Also, as we shall see in Chapter 7, it is sometimes useful to consider the behavior of a loop integral when the loop momenta are so much larger than the external momenta that the external lines might just as well not exist.

While vacuum bubble integrals are slightly easier to solve than propagator-type integrals with the same number of loops, we can often save unnecessary work by realizing that vacuum bubble integrals are purely real. This is most obviously seen by observing that if we were to cut through a vacuum bubble diagram, there would be no way to put all the cut particles on mass shell and still conserve energy. In other words, an isolated vacuum cannot generate physical particles and physical particles cannot annihilate into nothing.

6.4   Advanced Techniques

The arsenal of techniques we have discussed in this chapter is powerless to evaluate many of the master integrals that we often encounter. More sophisticated mathematical techniques can be used to obtain analytic results like [26]

$$N5(1,1,1,1,1) = \int \frac{[d^D k_1][d^D k_2]}{k_1^2 k_2^2 (k_1^2 + 2k_1 p)(k_2^2 + 2k_2 p)[(k_1 + k_2)^2 + 2(k_1 + k_2)p]}$$

$$= \mathcal{F}^2 \left[\frac{3}{2} \zeta(3) - \pi^2 \ln 2 + \mathcal{O}(\epsilon) \right]. \tag{6.114}$$

Another useful technique is the method of differential equations [27], whereby the onshell condition $p^2 = -m^2$ is suspended long enough to use recurrence relations to express $d/d(m^2)$ of a master integral in terms of the master integral itself and known integrals from subtopologies. While the differential equation method is fraught with its own complications, it can be used to obtain the coefficient of any particular power of ϵ in the Laurent series expansion of a master integral.

Finite loop integrals can, of course, be evaluated numerically even without recourse to Feynman parameters, although some sort of technique is typically used to reduce the number of integration variables so that computing time is optimized for a given level of precision. With a sufficiently precise computation, a numerical result can be converted to a quasi-analytic form by using an integer relation algorithm [28] to express the master integral as a simple linear combination of products of the various irrational numbers (such as π, $\zeta(3)$, $\ln 2$, and S_2) that the solution is expected to depend on. This technique was used [15, 29] to evaluate the complete set of two-loop self-energy onshell master integrals.

"I knew scientists wasted their lives but geez..."

Homer Simpson (*The Simpsons*)

Chapter 7

Loop Integrals With Multiple Scales

Up to this point, we have been discussing loop integrals depending on only one mass scale. With this restriction, we have presented a plethora of tools that can be used to simplify and evaluate loop integrals. Unfortunately, many realistic calculations are more complicated than this, as propagators from two or more different kinds of massive particles can appear in loop integrals. In this chapter, we will illustrate methods with which multi-scale loop integrals can be evaluated in terms of single-scale loop integrals. Given the power of the techniques of the previous chapters, the ability to handle multi-scale loop integrals essentially gives us a license to attempt any multiloop calculation that we wish in perturbative quantum field theory.

7.1 Exactly Solvable Example

Consider the integral

$$\int \frac{[d^D k]}{(k^2 + m^2)(k^2 + M^2)} , \tag{7.1}$$

where $M > m$. Using a partial fraction decomposition, as discussed in Section 3.4, we can write (7.1) in terms of a pair of single-scale integrals:

$$\int \frac{[d^D k]}{(k^2 + m^2)(k^2 + M^2)} = \frac{1}{M^2 - m^2} \left\{ \int \frac{[d^D k]}{k^2 + m^2} - \int \frac{[d^D k]}{k^2 + M^2} \right\} . \tag{7.2}$$

Each of the single-scale loop integrals can be solved explicitly using the basic dimensional regularization result (2.18) so that

$$\int \frac{[d^D k]}{(k^2 + m^2)(k^2 + M^2)} = \frac{\Gamma(-1 + \epsilon)}{(4\pi)^{D/2}} \frac{1}{M^2 - m^2} \left\{ (m^2)^{(1-\epsilon)} - (M^2)^{(1-\epsilon)} \right\} . \tag{7.3}$$

If we remove an overall loop factor of $M^{-2\epsilon}\Gamma(1+\epsilon)/(4\pi^2)^{D/2}$, (7.3) can be expanded in powers of ϵ as

$$\frac{1}{\epsilon} + \left(1 - \frac{\frac{m^2}{M^2}\ln\left(\frac{m^2}{M^2}\right)}{\frac{m^2}{M^2} - 1}\right) + \mathcal{O}(\epsilon) . \tag{7.4}$$

In the next two sections, we will obtain this result using other techniques. While these techniques add a layer of intricacy to the calculation, we are not trying to overcomplicate things merely for fun. Rather, these new techniques are readily applicable to less trivial loop integrals for which exact solutions are extremely difficult to obtain by any other means.

7.2 Taylor Expansions

The two mass scales appearing in a loop integral like (7.1) can alternatively be regarded as one mass scale and a dimensionless number:

$$m^2 = rM^2 , \quad r \in (0,1) . \tag{7.5}$$

This suggests that if we use (7.5) to cast (7.1) in terms of r and M, the integral might become much simpler when r is very close to zero. A close inspection of

$$\int \frac{[d^D k]}{(k^2 + m^2)(k^2 + M^2)} = \int \frac{[d^D k]}{(k^2 + rM^2)(k^2 + M^2)} , \tag{7.6}$$

however, suggests that the rM^2 term in the denominator might not necessarily be smaller than the k^2 term. Suppose, instead, that we are interested in what happens when r is very close to 1, in other words, when m is not much smaller than M. Equivalently, we can define another dimensionless number x via

$$m^2 = (1 - x)M^2 , \quad x \in (0,1) , \tag{7.7}$$

and consider the behavior of the integral when x is very close to zero. In this case,

$$\int \frac{[d^D k]}{(k^2 + m^2)(k^2 + M^2)} = \int \frac{[d^D k]}{(k^2 + M^2 - xM^2)(k^2 + M^2)} , \tag{7.8}$$

and we are guaranteed that the xM^2 term will be substantially smaller than $(k^2 + M^2)$, regardless of the size of k^2. This implies that the Taylor series expansion

$$\frac{1}{(k^2 + M^2 - xM^2)} = \frac{1}{(k^2 + M^2)} + \frac{xM^2}{(k^2 + M^2)^2} + \frac{(xM^2)^2}{(k^2 + M^2)^3} + \cdots$$

$$= \sum_{n=0}^{\infty} \frac{(xM^2)^n}{(k^2 + M^2)^{n+1}} \tag{7.9}$$

will converge. Assuming that we can safely interchange the order of the summation and integration, (7.8) becomes

$$\int \frac{[d^D k]}{(k^2 + m^2)(k^2 + M^2)} = \sum_{n=0}^{\infty} (xM^2)^n \int \frac{[d^D k]}{(k^2 + M^2)^{n+2}} . \tag{7.10}$$

At this stage the loop integral, while dependent on an integer n over which we will eventually sum, is of the simple type (2.18), so that

$$\int \frac{[d^D k]}{(k^2 + m^2)(k^2 + M^2)} = \frac{M^{-2\epsilon}}{(4\pi)^{D/2}} \sum_{n=0}^{\infty} \left(1 - \frac{m^2}{M^2}\right)^n \frac{\Gamma(n+\epsilon)}{\Gamma(n+2)} . \tag{7.11}$$

It is not at all obvious that this result agrees with the exact solution (7.3), but an explicit expansion of both formulas in powers of ϵ and $x = (1 - m^2/M^2)$ confirms that they are indeed the same.

In most realistic multi-scale problems, we will not have an exact solution to compare with. Furthermore, when we apply a Taylor expansion to the integrand, it will usually not even be possible to obtain a general solution for the remaining loop integral in terms of the summation index n. Instead, we expand the integrand to a finite number of terms and evaluate each loop integral separately. Using this tactic, the accuracy of the truncated sum comes into question. From the Taylor-expanded solution (7.11), if we remove a loop factor of $M^{-2\epsilon}\Gamma(1 + \epsilon)/(4\pi)^{D/2}$, we are left with

$$\sum_{n=0}^{\infty} \left(1 - \frac{m^2}{M^2}\right)^n \frac{\Gamma(n+\epsilon)}{\Gamma(n+2)\Gamma(1+\epsilon)} . \tag{7.12}$$

The $n = 0$ term, via the $\Gamma(n + \epsilon)$ factor, provides the only ϵ^{-1} contribution, in agreement with (7.4), while the next term in an ϵ-expansion receives contributions from all values of n. Suppose we truncate the series at $n = N$ and plot the finite part of (7.12) as a function of m^2/M^2 for various choices of N. Figure 7.1 shows these plots, along with the exact result of (7.4). Since the expansion parameter $(1 - m^2/M^2)$ is small for $m \simeq M$, it is not surprising that even the severe $N = 1$ truncation provides reliable results near $m^2/M^2 = 1$. As we move to smaller values of m^2/M^2, more terms are needed in the series in order to follow the exact result accurately. With a sufficiently large number of terms, we can obtain a reliable result in the extreme limit of $m^2/M^2 = 0$. Alternatively, we could try to find a way to create an expansion about the $m^2/M^2 = 0$ limit. This will be the topic of the next section.
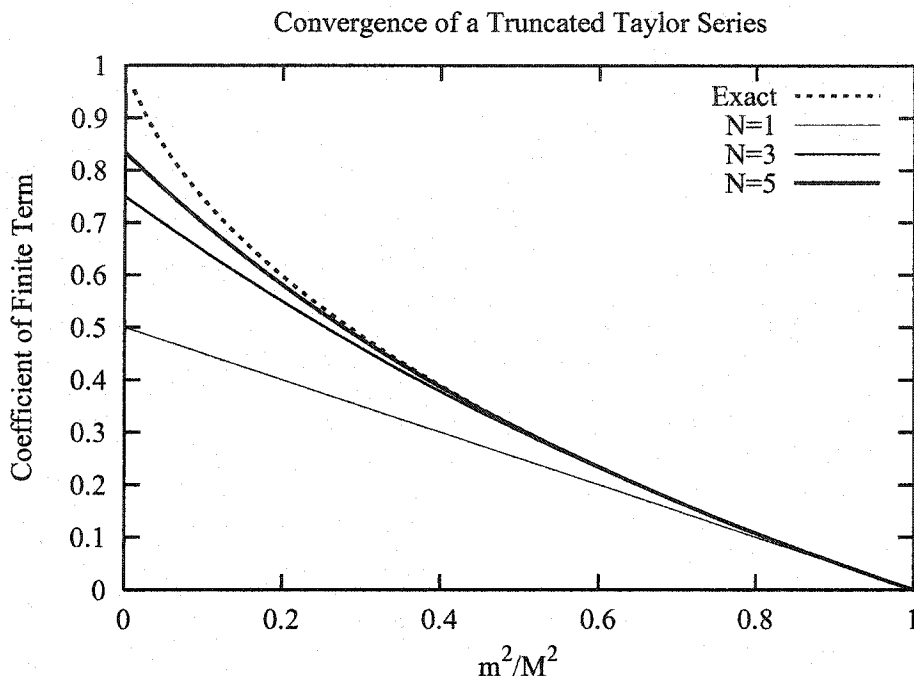
Figure 7.1: Plot of the finite part of a Taylor series expansion of a simple loop integral as a function of the mass-square ratio m^2/M^2. The solid lines represent the functions obtained by truncating the series after 1, 3, and 5 terms, respectively. The dashed line denotes the exact solution.

7.3   Method of Asymptotic Expansions

Inspired by the success of the Taylor expansion method, we would now like to expand the simple integral (7.1) about the $m^2/M^2 = 0$ limit. At the beginning of the previous section, however, we noted that the integral

$$\int \frac{[d^D k]}{(k^2 + m^2)(k^2 + M^2)} = \int \frac{[d^D k]}{(k^2 + rM^2)(k^2 + M^2)} \qquad (7.13)$$

does not appear to permit a simplification because k^2 may or may not be larger than rM^2, even if r is quite small. Suppose that we divide the integral into two parts based on the magnitude of k,

$$\int \frac{[d^D k]}{(k^2 + m^2)(k^2 + M^2)} = \left(\int_{|k|<\mu} + \int_{|k|>\mu} \right) \frac{[d^D k]}{(k^2 + m^2)(k^2 + M^2)} , \qquad (7.14)$$

where $m < \mu < M$. For the small-k integral, $k^2 < M^2$ so that we can expand the M-dependent propagator as

$$\frac{1}{(k^2 + M^2)} = \frac{1}{M^2} - \frac{k^2}{(M^2)^2} + \frac{(k^2)^2}{(M^2)^3} - \cdots$$

$$= \sum_{n=0}^{\infty} \frac{(-1)^n (k^2)^n}{(M^2)^{n+1}} . \tag{7.15}$$

Similarly, for the large-k integral, $k^2 > m^2$ so that we can expand the m-dependent propagator as

$$\frac{1}{(k^2 + m^2)} = \frac{1}{k^2} - \frac{m^2}{(k^2)^2} + \frac{(m^2)^2}{(k^2)^3} - \cdots$$

$$= \sum_{n=0}^{\infty} \frac{(-1)^n (m^2)^n}{(k^2)^{n+1}} . \tag{7.16}$$

Either expansion allows one of the mass scales to be factored out of the integral so that a single-scale integral remains. Unfortunately, the limits of integration are restricted so that we do not have a solution available. Let us then add and subtract integrals so that our expanded integrands can be integrated over all possible values of k,

$$\int \frac{[d^D k]}{(k^2 + m^2)(k^2 + M^2)} = \mathcal{A} + \mathcal{B} - \mathcal{C} - \mathcal{D} , \tag{7.17}$$

where

$$\mathcal{A} = \sum_{n=0}^{\infty} \frac{(-1)^n}{(M^2)^{n+1}} \int \frac{[d^D k] \, (k^2)^n}{(k^2 + m^2)} , \tag{7.18}$$

$$\mathcal{B} = \sum_{n=0}^{\infty} (-1)^n (m^2)^n \int \frac{[d^D k]}{(k^2)^{n+1}(k^2 + M^2)} , \tag{7.19}$$

$$\mathcal{C} = \sum_{n=0}^{\infty} \frac{(-1)^n}{(M^2)^{n+1}} \int_{|k|>\mu} \frac{[d^D k] \, (k^2)^n}{(k^2 + m^2)} , \tag{7.20}$$

$$\mathcal{D} = \sum_{n=0}^{\infty} (-1)^n (m^2)^n \int_{|k|<\mu} \frac{[d^D k]}{(k^2)^{n+1}(k^2 + M^2)} . \tag{7.21}$$

The integrals $\mathcal{A}$ and $\mathcal{B}$ are now solvable. Although the expansions by which they were generated do not converge over the entire integration region, any spurious divergences that this might create in $\mathcal{A}$ or $\mathcal{B}$ will be absent in the overall result of $(\mathcal{A} + \mathcal{B} - \mathcal{C} - \mathcal{D})$. Looking more closely at $\mathcal{C}$ and $\mathcal{D}$, we see that the integration

regions are such that an additional expansion is possible. Specifically, since $\mathcal{C}$ depends on only large values of k, the $(k^2 + m^2)$ propagator can be expanded without additional convergence problems:

$$\mathcal{C} = \sum_{j=0}^{\infty}\sum_{n=0}^{\infty} \frac{(-1)^{j+n}(m^2)^j}{(M^2)^{n+1}} \int_{|k|>\mu} \frac{[d^D k]\,(k^2)^n}{(k^2)^{j+1}} . \tag{7.22}$$

Similarly, since $\mathcal{D}$ depends on only small values of k, the $(k^2 + M^2)$ propagator can be expanded:

$$\mathcal{D} = \sum_{j=0}^{\infty}\sum_{n=0}^{\infty} \frac{(-1)^{j+n}(m^2)^n}{(M^2)^{j+1}} \int_{|k|<\mu} \frac{[d^D k]\,(k^2)^j}{(k^2)^{n+1}} . \tag{7.23}$$

After swapping the dummy summation indices in $\mathcal{D}$, we see that the only difference between $\mathcal{C}$ and $\mathcal{D}$ is the region of integration. Together, they are

$$\mathcal{C} + \mathcal{D} = \sum_{j=0}^{\infty}\sum_{n=0}^{\infty} \frac{(-1)^{j+n}(m^2)^n}{(M^2)^{j+1}} \int \frac{[d^D k]\,(k^2)^j}{(k^2)^{n+1}} \tag{7.24}$$

which is identically zero on account of the scaleless loop integrals. This rather fortuitous result means that the correct solution to (7.17) will be obtained merely from $(\mathcal{A} + \mathcal{B})$. In other words, when we break a loop integral into two regions in order to facilitate various expansions of the integrand, whatever additional contribution we obtain by integrating one of the expanded integrands over the entire integration volume will be exactly canceled by the additional contribution that we obtain from integrating the other expanded integrand over the entire integration volume.

By evaluating $\mathcal{A}$ and $\mathcal{B}$ explicitly, we can verify that we obtain the correct result (7.1). For $\mathcal{A}$, we will rewrite the k^2 factors in the numerator of (7.18) as $((k^2+m^2)-m^2)$. When we multiply out the n copies of this factor, we will obtain a scaleless integral if we have so much as one $(k^2 + m^2)$ factor in the numerator, therefore we need only consider the $(-m^2)$ contributions:

$$\begin{aligned}
\mathcal{A} &= \sum_{n=0}^{\infty} \frac{(-1)^n}{(M^2)^{n+1}} \int \frac{[d^D k]\,(-m^2)^n}{(k^2 + m^2)} \\
&= \frac{\Gamma(-1+\epsilon)\,m^{-2\epsilon}}{(4\pi)^{D/2}} \sum_{n=0}^{\infty} \frac{m^{2(n+1)}}{M^{2(n+1)}} \\
&= \frac{\Gamma(-1+\epsilon)\,m^{-2\epsilon}}{(4\pi)^{D/2}} \frac{\frac{m^2}{M^2}}{1 - \frac{m^2}{M^2}}
\end{aligned}$$

$$= \frac{\Gamma(-1+\epsilon)}{(4\pi)^{D/2}} \frac{m^{2(1-\epsilon)}}{M^2 - m^2} . \tag{7.25}$$

This is exactly the first term of (7.3). As for $\mathcal{B}$, for arbitrary values of n, we can obtain a solution with the help of a Feynman parameter:

$$\begin{aligned}
\mathcal{B} &= \sum_{n=0}^{\infty} (-m^2)^n \int \frac{[d^D k]}{k^{2(n+1)}(k^2 + M^2)} \\
&= \sum_{n=0}^{\infty} \frac{\Gamma(n+2)}{\Gamma(n+1)} (-m^2)^n \int_0^1 dx \, (1-x)^n \int \frac{[d^D k]}{(k^2 + xM^2)^{n+2}} \\
&= \sum_{n=0}^{\infty} \frac{\Gamma(n+2-D/2)}{\Gamma(n+1)} \frac{(-m^2)^n}{(4\pi)^{D/2}} \int_0^1 dx \, \frac{(1-x)^n}{(xM^2)^{n+2-D/2}} \\
&= \frac{M^{-2\epsilon}}{(4\pi)^{D/2}} \sum_{n=0}^{\infty} \frac{\Gamma(n+\epsilon)}{\Gamma(n+1)} \left(-\frac{m^2}{M^2}\right)^n \int_0^1 dx \, x^{-n-\epsilon} (1-x)^n .
\end{aligned}$$

Using (2.31), the x-integral can be solved in terms of a Beta function, and in addition, we will make use of the identity [13]

$$\Gamma(x)\Gamma(1-x) = \frac{\pi}{\sin \pi x} , \tag{7.26}$$

so that

$$\begin{aligned}
\mathcal{B} &= \frac{M^{-2\epsilon}}{(4\pi)^{D/2}} \sum_{n=0}^{\infty} \frac{\Gamma(n+\epsilon)}{\Gamma(n+1)} \left(-\frac{m^2}{M^2}\right)^n \frac{\Gamma(n+1)\Gamma(1-n-\epsilon)}{\Gamma(2-\epsilon)} \\
&= \frac{M^{-2\epsilon}}{(4\pi)^{D/2}} \sum_{n=0}^{\infty} \left(-\frac{m^2}{M^2}\right)^n \frac{\pi}{\sin \pi(n+\epsilon)} \frac{1}{\Gamma(2-\epsilon)} .
\end{aligned}$$

With $\sin \pi(n+\epsilon) = (-1)^n \sin \pi\epsilon$ and another application of (7.26) with $x = 2 - \epsilon$, we have

$$\begin{aligned}
\mathcal{B} &= \frac{M^{-2\epsilon}}{(4\pi)^{D/2}} \sum_{n=0}^{\infty} \left(\frac{m^2}{M^2}\right)^n \frac{\pi}{\sin \pi\epsilon} \frac{1}{\Gamma(2-\epsilon)} \\
&= -\frac{M^{-2\epsilon}}{(4\pi)^{D/2}} \sum_{n=0}^{\infty} \left(\frac{m^2}{M^2}\right)^n \Gamma(-1+\epsilon) \\
&= -\frac{\Gamma(-1+\epsilon)}{(4\pi)^{D/2}} \frac{M^{2(1-\epsilon)}}{M^2 - m^2} , \tag{7.27}
\end{aligned}$$

which is exactly the second term in (7.3). Together with (7.25), (7.27) proves that it is possible to expand a two-scale loop integral about the limit $m^2/M^2 = 0$. This is an example of an asymptotic expansion. As we did with the Taylor ex-

pansions of the previous section, it is useful to look at the convergence of an expansion about $m^2/M^2 = 0$. Using the finite term of (7.4),

$$\left(1 - \frac{\frac{m^2}{M^2} \ln\left(\frac{m^2}{M^2}\right)}{\frac{m^2}{M^2} - 1} \right) ,$$

(7.28)

we can expand the denominator as a series in m^2/M^2 and then truncate the overall result at $(m^2/M^2)^N$, keeping in mind that there are also logarithmic factors in the expansion. In a realistic calculation, we could only expect to obtain the leading terms of such a series, and the effects of the large logarithms on the convergence of the expansion are important. Figure 7.2 compares the functions obtained for various values of N with the exact solution. Although the trun-
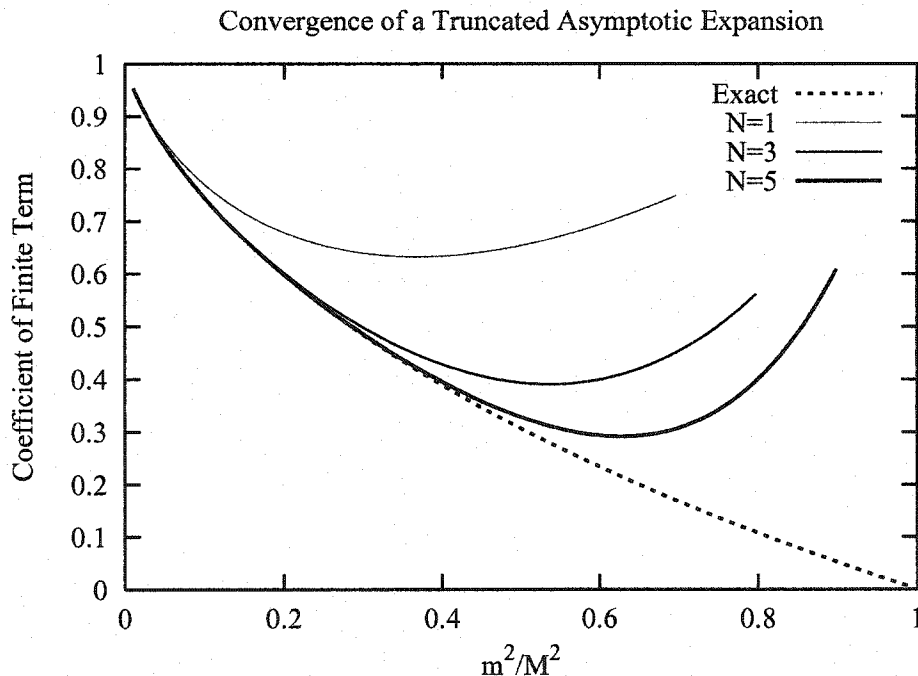

Figure 7.2: Plot of the finite part of an asymptotic series expansion of a simple loop integral as a function of the mass-square ratio m^2/M^2. The solid lines represent the functions obtained by truncating the series after 1, 3, and 5 terms, respectively. The dashed line denotes the exact solution.

cated series work well for small values of m^2/M^2, as expected, the convergence becomes quite poor as this parameter increases. Additional terms in the series would certainly extend the range for which accurate results are obtained, but

we should keep in mind that for sufficiently large values of m^2/M^2, the Taylor expansion about $m^2/M^2 = 1$ will be more reliable. In fact, if we splice the $N = 5$ asymptotic expansion to the $N = 5$ Taylor expansion at a point such as $m^2/M^2 = 0.3$, as shown in Figure 7.3, we can see that the two expansions match up almost seamlessly. Not only does this confirm that we can accurately
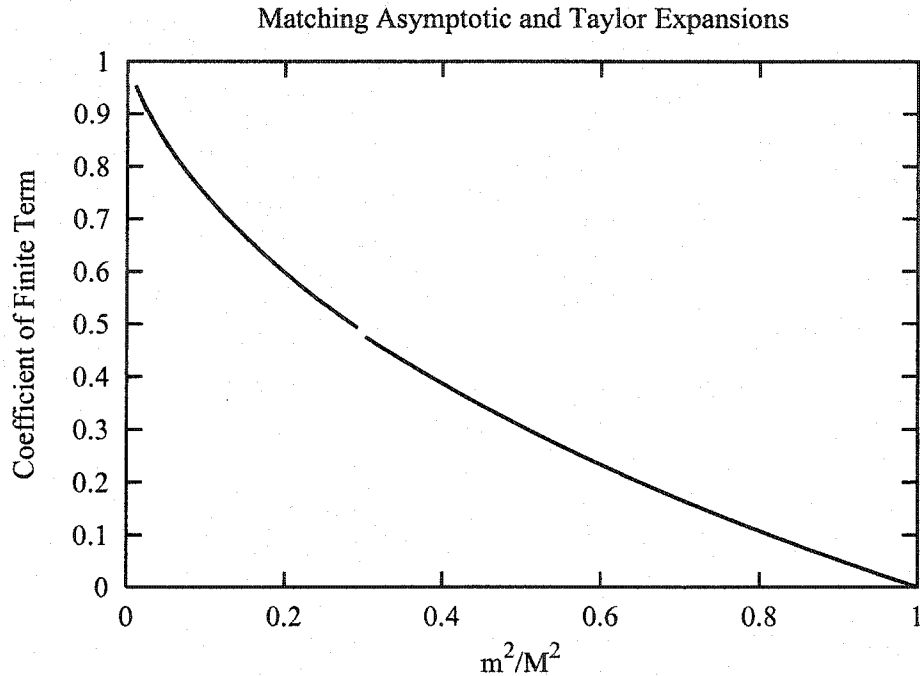

Figure 7.3: Plot of the finite part of series expansions of a simple loop integral as a function of the mass-square ratio m^2/M^2. For $m^2/M^2 < 0.3$, the $N = 5$ asymptotic expansion about $m^2/M^2 = 0$ is used, while for $m^2/M^2 > 0.3$, the $N = 5$ Taylor expansion about $m^2/M^2 = 1$ is used.

calculate the original loop integral (7.1) for any choice of m and M, but it provides an important consistency check on our calculation. For more realistic and more difficult calculations, such consistency checks are hard to come by, and are therefore quite reassuring.

General Procedure

Having illustrated the use of asymptotic expansions with an explicit example, we will now enumerate a simple five-step algorithm [30] which can be applied to a general two-scale loop integral. For integrals with more than two scales,

we could either apply this procedure recursively [31] or in combination with a Taylor expansion, as we will see in Chapter 11.

Step 1: Identify the large and small external scales in the integrals.

Step 2: Divide the integration volume into regions so that within each region, the loop momentum flows through the various propagators are of the order of one of the external scales. More specifically, the statement $k \sim M$ asserts that $k^2 > m^2$ in Euclidean space.

Step 3: Within every region, expand any propagators within which there are terms that depend differently on the external scales.

Step 4: Remove the constraints on the regions and integrate each expanded integrand over the original integration volume.

Step 5: Add the contributions from each region to obtain the final result.

The fourth step of this algorithm requires further explanation, since by ignoring the constraints on the individual regions, it may appear as if contributions to the total integral are counted more than once. As we saw explicitly in the previous example, this does not happen because the extra contributions to the total integral that are introduced by removing the constraints on individual regions can be expressed as scaleless integrals which vanish in dimensional regularization. This implies that the integrals from the various regions are different analytic functions of the parameters of the problem.

Two-Loop Implementation

For a problem with two external scales, the method of asymptotic expansions leads to two momentum regions for one-loop integrals: $k \sim m$ and $k \sim M$. For two-loop integrals, however, we cannot simply assign regions for k_1 and k_2 separately because there will be one or more propagators that depend on both k_1 and k_2. For simplicity, let us denote the combination of k_1 and k_2 by k_3 — in practice, k_3 is almost always $k_1 + k_2$ or $k_1 - k_2$. Naively, k_1, k_2, and k_3 could each be either soft ($\sim m$) or hard ($\sim M$), but since the three momenta are not independent, it is not possible to have two of them soft while the third is hard. It is, of course, permissible to have all three soft, all three hard, or one soft and two hard. This leads to five momentum regions for two-loop integrals, as depicted in Figure 7.4.

Oftentimes, an expansion of the integrand within one of the momentum regions leads to a scaleless integral. While this is certainly convenient, it is also

$|k_2|$

M

$|k_1|$

$1 \quad (k_3 \sim M)$

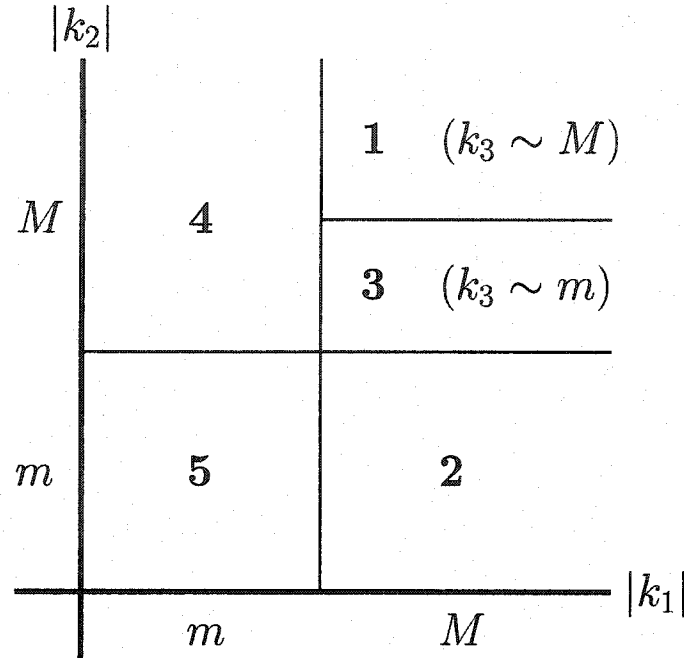$3 \quad (k_3 \sim m)$

4

5

2

m

M

Figure 7.4: Sketch of the five momentum regions required for a two-loop calculation using the method of asymptotic expansions.

related to a potential pitfall. Consider a two-loop integral containing the following five propagators:

$$
\begin{aligned}
[\mathbf{1}] &= k_1^2 \,, \\
[\mathbf{2}] &= k_2^2 \,, \\
[\mathbf{3}] &= (k_1^2 + 2k_1 p) \,, \\
[\mathbf{4}] &= (k_1 + k_2)^2 + 2(k_1 + k_2)p \,, \\
[\mathbf{5}] &= (k_1^2 + 2k_1 P) \,,
\end{aligned}
$$

where the external momenta p and P are related by $p = (m/M)P$. In Region 2, where $k_1 \sim M$, $k_2 \sim m$, and $k_1 + k_2 \sim M$, propagators [3] and [4] are expanded in terms of k_1^2 denominator factors. This leaves only $[\mathbf{2}] = k_2^2$ for k_2-dependence in the denominator, so that the k_2-integral is scaleless and this region does not contribute. In Region 1, where k_1, k_2, and $k_1 + k_2$ are all $\sim M$, [3] and [4] become k_1^2 and $(k_1 + k_2)^2$, respectively. This region contributes a non-zero result, and if we look carefully, we can see that we never explicitly took advantage of the assumption that $k_2 \sim M$, hence this latter region should automatically include the special case of the former region where k_1 and $k_1 + k_2$ were $\sim M$ but $k_2 \sim m$. In other words, we are getting away with a double-counting in this

particular case. Unfortunately, this is not an unassailable feature of the method of asymptotic expansions. As a counterexample, consider the two-loop integral containing:

$$
\begin{aligned}
[1] &= k_1^2 + m^2 \,, \\
[2] &= k_2^2 \,, \\
[3] &= (k_1 + p)^2 \,, \\
[4] &= (k_1 + k_2 + p)^2 \,, \\
[5] &= (k_2^2 + 2k_2 p) \,,
\end{aligned}
$$

where $p^2 = -M^2$. This integral arises in the context of the top quark decays that we will discuss in Chapter 13. Suppose that k_1 and k_2 are both $\sim M$, so that [1] becomes k_1^2. Without making any assumptions about the size of $k_1 + k_2$, we can already solve this integral in terms of the "T1" topology. Indeed, the region where $k_1 + k_2$ is also assumed to be $\sim M$ (Region 1) would lead to no further expansions. If, however, we assume that $k_1 + k_2 \sim m$ (Region 3), [4] becomes p^2, and the k_1- and k_2-integrals factor. Neither of them are scaleless, though, and thus the double-counting is no longer benign. From this example, we are forced to adopt an additional proviso:

Proviso to Step 3: If the propagators in a loop integral are such that all allowed expansions within one region are consistent with the momentum assignments of another region, discard the latter region in order to avoid double-counting. In other words, once an integral can be solved in terms of single-scale integrals, additional expansions (if available) should be avoided.

To conclude this section, we will look at an example which features another superficial difficulty. Consider a two-loop integral containing seven propagators:

$$
\begin{aligned}
[1] &= k_1^2 \,, \\
[2] &= k_2^2 \,, \\
[3] &= (k_1 + k_2)^2 \,, \\
[4] &= (k_1^2 + 2k_1 p) \,, \\
[5] &= (k_1 + k_2)^2 + 2(k_1 + k_2)p \,, \\
[6] &= (k_1^2 + 2k_1 P) \,, \\
[7] &= (k_2^2 - 2k_2 P) \,,
\end{aligned}
$$

where, as before, the external momenta p and P are related by $p = (m/M)P$. Integrals like this arise in the context of the recoil corrections to the bound state energy levels we will discuss in Chapter 12. In the region where k_1 and k_2 are both $\sim M$ but $k_1 + k_2 \sim m$ (Region 3), the only propagator that permits an obvious expansion is [4] $\rightarrow k_1^2$. At this stage, the integral still depends on both

external scales. This would be acceptable if the k_1- and k_2-integrals factored so that one of the integrals only depended on the soft scale and the other integral only depended on the hard scale, but that is clearly not the case here. Instead, suppose we try to factor the two-loop integral into a k_1-integral depending on the hard scale and a $(k_1 + k_2)$-integral depending on the soft scale. This can be accomplished by writing k_2 as $(k_1+k_2)-k_1$ so that [2] $\rightarrow k_1^2$ and [7] $\rightarrow (k_1^2+2k_1P)$. In other words, the soft and hard scales will only decouple once we express the loop integral in terms of loop momenta which are soft and hard.

7.4 Convergence Improvement

Although asymptotic expansions allow us, in principle, to obtain an arbitrary number of terms in a series which approximates the exact result, limitations in computational resources frequently prevent us from calculating as many terms as we would sometimes like. In particular, we are often interested in checking the behavior of the series as the expansion parameter increases, in which case the series might converge quite slowly. Fortunately, there are

> ... powerful methods to recover an accurate approximation to an exact answer from a few terms of a slowly convergent or divergent perturbation series if these terms can be supplemented by some analytic information about the answer. [32]

We will briefly outline two such techniques — the Shanks method and Padé approximants — that can be used to improve the accuracy of a result obtained from a truncated series.

Shanks Method

The basic idea behind the Shanks method is that many series have a transient behavior that is predominantly that of a geometric series. Quantitatively, this implies that the n-th partial sum of the series, A_n, can be well-approximated by

$$A_n \simeq A + \alpha q^n \tag{7.29}$$

for some appropriate choice of A, α, and q. Insofar that this assumption is accurate, the true limit of the series, A, can be more easily pinpointed by creating a new series, $S(A_n)$, which attempts to remove the transient behavior induced by α and q:

$$S(A_n) = \frac{A_{n-1}A_{n+1} - A_n^2}{A_{n-1} + A_{n+1} - 2A_n} . \tag{7.30}$$

The series (7.30), which can be constructed directly from the original series A_n, will converge more quickly and therefore reduce the error induced by truncating A_n after a finite number of terms. If necessary, the process can be nested so as to produce even better convergence via the series $S^2(A_n) = S[S(A_n)]$, $S^3(A_n)$, and so on.

Padé Approximants

A more powerful procedure for dealing with truncated series involves Padé approximants, as they are not only capable of accelerating the convergence of many slowly converging series, but they can often handle divergent series as well! Divergences in a power series arise from the presence of singularities so that any simple polynomial will be an inadequate approximation near such a singularity. A Padé approximant is a rational function — in other words, a ratio of two polynomials — whose coefficients are chosen so that when the approximant is expanded, it matches the original power series order by order. For a polynomial of order T in the variable x, we can construct the Padé approximants

$$\mathcal{P}_M^N(x) = [N/M] = \frac{\sum_{n=0}^N A_n x^n}{\sum_{n=0}^M B_n x^n} \tag{7.31}$$

provided that $M + N = T$. Without loss of generality, we set $B_0 = 1$.

Whenever we have reason to believe that a power series we are generating is arising from an analytic function, Padé approximants are likely to be of use, as they explicitly incorporate the effects of simple poles. This technique applies to multiloop calculations at a much deeper level than the artificial expansions we introduce in order to cope with multiple scale problems. Indeed, the basic structure of perturbative quantum field theory is such that we can, at best, express physical quantities as asymptotic series [33] in the coupling parameter. Padé approximants can then be used [34, 35] to estimate the effects of higher-order terms, particularly in QCD where the expansion parameter α_s is sufficiently large that the perturbation series does not converge very quickly.

"They all laughed at Christopher Columbus when he said the world was round."

George and Ira Gershwin (*They All Laughed*)

Chapter 8

Color Factors

In Chapter 1, we saw that the Feynman rules for perturbative QCD contain 3-by-3 color matrices t^a, in addition to the γ-matrices that also appear in QED. The effects of these two types of matrices can be factored completely, so that a QCD diagram gives rise to the product of a color factor and a colorless QED-like amplitude. As a result, aside from the non-Abelian diagrams that begin to appear at the two-loop level, QCD calculations are essentially just QED calculations multiplied by the appropriate color factors. In this chapter, we will review some of the group theory behind color factors [1, 36] and then we will calculate several color factors explicitly.

8.1 Lie Algebras

Suppose that we have a Lagrangian from which we will construct a quantum field theory and that this Lagrangian is invariant under a certain class of unitary transformations. While discrete unitary transformations such as time reversal, charge conjugation, and parity provide deep insights into the nature of the theory, we will focus on continuous transformations containing elements arbitrarily close to the identity transformation. Within such groups, more properly known as Lie groups, every element can be expressed in terms of a product of infinitesimal elements. We can write an infinitesimal group element $\mathcal{G}$ as

$$\mathcal{G}(\varepsilon) = 1 + i\varepsilon^a t^a + \mathcal{O}(\varepsilon^2) \,, \tag{8.1}$$

where t^a are Hermitian operators that generate the symmetry group and ε^a are infinitesimal parameters which specify the group element. Near the identity element, where global topological structure is irrelevant, we can use (8.1) to describe the features of the Lie group in terms of the Lie algebra which governs the generators t^a. Specifically, since the product of any two group elements is

itself a group element, the product of generators must be a linear combination
of generators. The same is true for the commutator of generators,

$$\left[t^a, t^b\right] = i f^{abc} t^c \,, \tag{8.2}$$

where f^{abc} denotes a collection of numbers known as structure constants. The
commutation relation (8.2) and the set of generators to which it applies consti-
tute a Lie algebra.

One particular family of Lie algebras is used throughout the Standard Model
and it is based on the Lie group $SU(N)$, the set of all $N \times N$ unitary transfor-
mations U such that $\det(U) = 1$. We can represent the generators of $SU(N)$ by a
set of $(N^2 - 1)$ traceless Hermitian N-dimensional matrices t^a. This is known as
the fundamental representation. Of the many technical results associated with
the theory of Lie algebras, there are a few identities which are indispensable for
calculating color factors. We will now discuss the origin of these identities.

Trace Normalization

Although the $SU(N)$ generators are traceless in isolation,

$$\mathrm{Tr}\left(t^a\right) = 0 \,, \tag{8.3}$$

this need not be the case for products of two or more generators. By selecting an
appropriate basis, the trace of a product of two generators can be normalized as

$$\mathrm{Tr}\left(t^a t^b\right) = T_R \, \delta^{ab} \,. \tag{8.4}$$

The trace normalization factor, T_R, takes on a unique value in $SU(N)$ Lie alge-
bras in the fundamental representation,

$$T_R = \frac{1}{2} \,, \tag{8.5}$$

as can be checked explicitly using the $SU(2)$ generators

$$t^1 = \frac{1}{2}\begin{pmatrix} 0 & 1 \\ 1 & 0 \end{pmatrix}, \qquad t^2 = \frac{1}{2}\begin{pmatrix} 0 & -i \\ i & 0 \end{pmatrix}, \qquad t^3 = \frac{1}{2}\begin{pmatrix} 1 & 0 \\ 0 & -1 \end{pmatrix}. \tag{8.6}$$

At this stage, we can show that f^{abc} in (8.2) is antisymmetric in all its indices,
and not just a and b. Simply multiply (8.2) from the right with t^d, take a trace of
both sides, and then use (8.4) on the right hand side to see that

$$\mathrm{Tr}\left(\left[t^a, t^b\right] t^d\right) = i f^{abc} \, T_R \, \delta^{cd} \,, \tag{8.7}$$

and so

$$f^{abc} = -\frac{i}{T_R} \text{Tr} \left(\left[t^a, t^b \right] t^c \right) . \tag{8.8}$$

Clearly f^{abc} is antisymmetric in a and b. Using the cyclic property of the trace, we see that

$$
\begin{aligned}
\text{Tr} \left(\left[t^a, t^b \right] t^c \right) &= \text{Tr} \left(\left[t^a t^b - t^b t^a \right] t^c \right) \\
&= \text{Tr} \left(t^a t^b t^c \right) - \text{Tr} \left(t^b t^a t^c \right) \\
&= \text{Tr} \left(t^b t^c t^a \right) - \text{Tr} \left(t^c t^b t^a \right) \\
&= -\text{Tr} \left(\left[t^c, t^b \right] t^a \right) ,
\end{aligned}
\tag{8.9}
$$

and so f^{abc} is antisymmetric in a and c as well. A similar calculation confirms that f^{abc} is antisymmetric in b and c.

Casimir Operator in the Fundamental Representation

Consider the operator

$$t^2 = t^a t^a , \tag{8.10}$$

where we are summing over the $(N^2 - 1)$ possible values of a. If we calculate the commutator of t^2 with any particular generator, say t^b, we find that

$$
\begin{aligned}
\left[t^2, t^b \right] &= t^a t^a t^b - t^b t^a t^a \\
&= t^a \left(t^b t^a + i f^{abc} t^c \right) - \left(t^a t^b + i f^{bac} t^c \right) t^a \\
&= t^a \left(i f^{abc} t^c \right) + \left(i f^{abc} t^c \right) t^a \\
&= i f^{abc} \{ t^a, t^c \} \\
&= 0 .
\end{aligned}
\tag{8.11}
$$

Since the anticommutator is symmetric in a and c while f^{abc} is antisymmetric in these indices, we conclude that t^2 commutes with every generator and is therefore an invariant of the algebra. This is why, for instance, the ℓ in the $\ell(\ell+1)$ eigenvalue of the angular momentum operator L^2 is an acceptable quantum number for the electron in a hydrogen atom. The invariance of t^2 allows us to write

$$t^a t^a = C_F \, \mathbf{1} , \tag{8.12}$$

where $\mathbf{1}$ is the $N \times N$ unit matrix and C_F is known as the Casimir operator in the fundamental representation of $SU(N)$. The Casimir operator is a constant within any particular representation; we can determine C_F by taking the trace

of (8.12) and using (8.4) to evaluate the left hand side:

$$
\begin{aligned}
\mathrm{Tr}\left(t^a t^a\right) &= C_F\,\mathrm{Tr}(1)\,, \\
T_R\,\delta^{aa} &= C_F N\,, \\
T_R\left(N^2 - 1\right) &= C_F N\,,
\end{aligned}
\tag{8.13}
$$

and since $T_R = 1/2$,

$$
C_F = \frac{N^2 - 1}{2N}\,.
\tag{8.14}
$$

Casimir Operator in the Adjoint Representation

So far, we have used the fundamental representation of $SU(N)$, wherein each of the $(N^2 - 1)$ generators is mapped to an $N \times N$ traceless Hermitian matrix such that the commutation relation (8.2) is satisfied. Another important group representation is the adjoint representation, where the generators are simply written in terms of the structure constants:

$$
\left(t_A^b\right)_{ac} = i f^{abc}\,.
\tag{8.15}
$$

The commutation relation (8.2) follows directly from the Jacobi identity

$$
f^{ade} f^{bcd} + f^{bde} f^{cad} + f^{cde} f^{abd} = 0\,,
\tag{8.16}
$$

or equivalently,

$$
\left[t^a, \left[t^b, t^c\right]\right] + \left[t^b, \left[t^c, t^a\right]\right] + \left[t^c, \left[t^a, t^b\right]\right] = 0\,.
\tag{8.17}
$$

In the adjoint representation, the trace normalization factor in

$$
\mathrm{Tr}\left(t_A^a t_A^b\right) = T_A\,\delta^{ab}
\tag{8.18}
$$

is

$$
T_A = N\,,
\tag{8.19}
$$

as can be seen by explicit calculation in the $SU(2)$ case where

$$
\left[\frac{\sigma^i}{2}, \frac{\sigma^j}{2}\right] = i\varepsilon^{ijk}\,\frac{\sigma^k}{2}\,.
\tag{8.20}
$$

The Casimir operator in the adjoint representation of $SU(N)$, denoted by C_A, is defined by

$$
t_A^a t_A^a = C_A\,\mathbf{1}\,,
\tag{8.21}
$$

where 1 is the $(N^2-1) \times (N^2-1)$ unit matrix. Just as we obtained C_F before, we can take the trace of both sides and use the trace normalization (8.18) to obtain

$$C_A = N \, . \tag{8.22}$$

Useful Identities

Consider the double contraction $f^{acd} f^{bcd}$. We can use (8.15) to interpret the f factors as generators in the adjoint representation, so that

$$
\begin{aligned}
f^{acd} f^{bcd} &= -f^{acd} f^{dcb} \\
&= \left(t_A^c\right)_{ad} \left(t_A^c\right)_{db} \\
&= \left(t_A^c t_A^c\right)_{ab} \\
&= C_A \, 1_{ab} \\
&= C_A \, \delta^{ab} \, .
\end{aligned} \tag{8.23}
$$

Another useful simplification occurs for the contraction of an f with two generators:

$$
\begin{aligned}
f^{abc} t^b t^c &= \frac{1}{2}\left(f^{abc} t^b t^c + f^{acb} t^c t^b\right) \\
&= \frac{1}{2}\left(f^{abc} t^b t^c - f^{abc} t^c t^b\right) \\
&= \frac{f^{abc}}{2}\left[t^b, t^c\right] \\
&= \frac{i}{2} f^{abc} f^{bcd} t^d \\
&= \frac{iC_A}{2} t^a \, ,
\end{aligned} \tag{8.24}
$$

where in the last line, we have applied the identity (8.23). Finally, we can consider the product $t^a t^b t^a$ of generators, assumed to be in the fundamental representation:

$$
\begin{aligned}
t^a t^b t^a &= \left(t^b t^a + \left[t^a, t^b\right]\right) t^a \\
&= t^b t^a t^a + i f^{abc} t^c t^a \\
&= \left(C_F - \frac{C_A}{2}\right) t^b \, .
\end{aligned} \tag{8.25}
$$

Note that we have used (8.12) and (8.24) to obtain the last line of (8.25). We now have all the tools we need to calculate color factors.

8.2 Calculation of Color Factors

There are systematic methods available [37] for calculating color factors in non-Abelian gauge theories. In this section, we will use the results of the previous section to obtain the $SU(N)$ color factors for basic one- and two-loop diagrams in detail.

In general, physically measurable quantities are obtained from Feynman diagrams by taking a trace over factors associated with a particular fermion line. For simplicity, let us assume that we have a single fermion line running through each diagram, as is the case with the top quark decays of Chapter 13. The color factor will then contain an overall factor of $1/N$ in order to average over the initial colors of the fermion. This $1/N$ will inevitably be canceled by a factor of N resulting from the $\text{Tr}(1)$ that remains once all the color matrices are rewritten in terms of C_F and C_A.
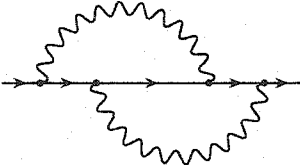
In the examples ahead, remember that we are working backwards along a fermion line in order to accumulate color matrices in the trace. Every basic gluon-fermion vertex contributes a single t^a factor, and we will automatically apply the δ^{ab} factors from the gluon propagators which enforce color conservation between vertices. In order to make all our color factors real, we will assign $-if^{abc}$ from the three-gluon vertex Feynman rule of Table 1.3 towards the color factor. Note that the gluons are labeled a, b, and c in a counterclockwise order.

At the one-loop level, there is only one color factor to calculate:

$$
\begin{aligned}
&= \frac{1}{N}\,\text{Tr}\,(t^a t^a) \\
&= \frac{1}{N}\,\text{Tr}\,(C_F\,\mathbf{1}) \\
&= C_F\,.
\end{aligned}
\tag{8.26}
$$
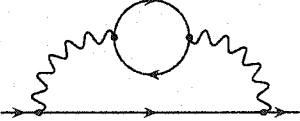
At the two-loop level, we can start with the following simple Abelian diagrams:

$$
\begin{aligned}
&= \frac{1}{N}\,\text{Tr}\left(t^a t^b t^b t^a\right) \\
&= \frac{1}{N}\,\text{Tr}\,(t^a C_F t^a) \\
&= C_F^2\,,
\end{aligned}
\tag{8.27}
$$
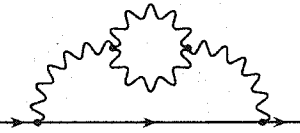
$$= \frac{1}{N} \operatorname{Tr}\left(t^a t^b t^a t^b\right)$$

$$= \frac{1}{N} \operatorname{Tr}\left((C_F - C_A/2)t^b t^b\right)$$

$$= C_F(C_F - C_A/2) . \tag{8.28}$$

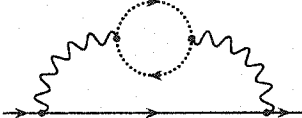The other Abelian diagram involves a second fermion loop and therefore a second trace:

$$= \frac{1}{N} \operatorname{Tr}\left(t^a t^b\right) \operatorname{Tr}\left(t^a t^b\right)$$

$$= \frac{1}{N} \operatorname{Tr}\left(t^a t^b\right) T_R \, \delta^{ab}$$

$$= \frac{T_R}{N} \operatorname{Tr}\left(t^a t^a\right)$$

$$= C_F T_R . \tag{8.29}$$

Similarly, there is a non-Abelian diagram with a subloop:

$$= \frac{1}{N} \operatorname{Tr}\left(t^a t^b\right) \left(-i f^{cda}\right) \left(-i f^{bdc}\right)$$

$$= \frac{1}{N} \operatorname{Tr}\left(t^a t^b\right) C_A \, \delta^{ab}$$

$$= \frac{C_A}{N} \operatorname{Tr}\left(t^a t^a\right)$$

$$= C_F C_A . \tag{8.30}$$

This diagram also requires an overall symmetry factor of $1/2$ due to the indistinguishability of the gluons in the subloop. In order to cancel the unphysical polarization modes of the gluon subloop, we will also need to consider diagrams with a ghost loop. Provided we assign the same $-i f^{abc}$ part of the interaction term towards the color factor as we did for the three-gluon vertex, and provided we incorporate the ghost loop factor of (-1) elsewhere, the ghost loop diagram will have the same color factor as the gluon loop diagram:

$$= C_F C_A . \tag{8.31}$$

Finally, there is a diagram with a single non-Abelian vertex:

$$
\begin{aligned}
&= \frac{1}{N}\, \mathrm{Tr}\left(t^a t^b t^c\right)\left(-if^{cba}\right) \\
&= \frac{i}{N}\, \mathrm{Tr}\left(t^a t^b t^c\right) f^{abc} \\
&= \frac{i}{N}\, \mathrm{Tr}\left(t^a\, \frac{iC_A}{2}\, t^a\right) \\
&= -\frac{C_F C_A}{2}\,.
\end{aligned}
\tag{8.32}
$$

At the three-loop level, the number of types of diagrams proliferates rapidly — including diagrams with four-gluon vertices — but the techniques we are using still apply. As we will not require three-loop color factors for the top quark decay calculation in Chapter 13, we shall stop here.

Since QCD is based on an $SU(3)$ gauge symmetry, we can assign specific numerical values to the three constants on which our color factors depend:

$$
\begin{aligned}
T_R &= 1/2\,, & (8.33) \\
C_F &= 4/3\,, & (8.34) \\
C_A &= 3\,. & (8.35)
\end{aligned}
$$

It is in our best interests, though, not to make these substitutions until the very end of a calculation. Instead, we can group our calculation into various subsets, each with a specific dependence on T_R, C_F, and C_A. As the cancellation of divergences or gauge parameters cannot rely on a coincidence between specific numerical values of these three constants, each individual subset must be well-behaved in isolation. This provides a valuable method with which to check a difficult calculation.

"In every job that must be done there is an element of fun."
                                          Mary Poppins (*A Spoonful of Sugar*)

Chapter 9

Renormalization Factors

So far, we have painted a picture of perturbative quantum field theory in which we can approximate nature by calculating sets of Feynman diagrams of increasing complexity. This is an oversimplification. The problem is that the particles with which we do our experiments already incorporate virtual effects at all possible scales and there is simply no way to turn these interactions off. The parameters, such as coupling constants and particle masses, upon which the predictions of quantum field theory depend, are naively extracted from simple processes involving these complicated particles. Therefore, if we are going to calculate perturbative corrections to a physical process induced by virtual particles, it is absolutely essential that we do not double-count the virtual effects that are implicitly present in the parameters of the theory. Renormalization is the name for the quantitative procedure we follow in order to accomplish this goal. In this chapter, we will show how the formal ideas of renormalization can be cast in a convenient form suitable for practical implementation in a multiloop calculation.

9.1 Formalities

For the purposes of this chapter, we shall restrict ourselves to the renormalization of Quantum Electrodynamics. Our first objective is to clarify what we mean when we measure the parameters of the theory using low-energy experiments. The QED Lagrangian consists of three terms; two are kinetic terms which lead to propagators for the photon and electron and the other is an interaction term between a photon and an electron. This is fine for the theory end of things, but in an experiment, we can only measure what goes in and what comes out. The physically realistic propagators and vertices should therefore look something like the sketches in Figure 9.1. We can describe the shaded blobs quantitatively
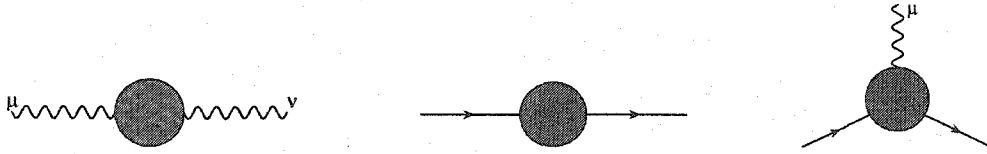
Figure 9.1: Sketch of the physically realistic propagators and interaction vertex in Quantum Electrodynamics. The shaded blobs represent processes that our experiments cannot detect.

using the Feynman rules of Chapter 1 and in this way, we obtain expressions for the effective propagators and vertices as series in powers of α. In order to justify using the physically measured electron mass and charge in the basic Feynman rules, we need to place constraints on the expressions for the effective propagators and vertices. These constraints are known as renormalization conditions, and in order to satisfy them, we are forced to add additional Feynman rules to the theory. Such additional Feynman rules are called counterterms; Table 9.1 lists the counterterms for Quantum Electrodynamics. The counterterm param-

	$-i(g^{\mu\nu}q^2 - q^\mu q^\nu)\delta_3$
	$i(\not{p}\delta_2 - \delta_m)$
	$-ie\gamma^\mu\delta_1$

Table 9.1: Feynman rules for counterterms in Quantum Electrodynamics.

eters δ_1, δ_2, δ_3, and δ_m can be obtained, to any desired order in α, from explicit loop calculations. To leading order, the results are derived in [1], and when adjusted to match our conventions, they are:

$$\delta_1 = \frac{e^2\Gamma(1+\epsilon)m^{-2\epsilon}}{(4\pi)^{D/2}}\left(-\frac{3}{\epsilon} - \frac{4}{1-2\epsilon}\right), \qquad (9.1)$$

$$\delta_2 = \frac{e^2\Gamma(1+\epsilon)m^{-2\epsilon}}{(4\pi)^{D/2}}\left(-\frac{3}{\epsilon} - \frac{4}{1-2\epsilon}\right), \qquad (9.2)$$

$$\delta_3 = \frac{e^2\Gamma(1+\epsilon)m^{-2\epsilon}}{(4\pi)^{D/2}}\left(-\frac{4}{3\epsilon}\right), \qquad (9.3)$$

$$m\delta_2 - \delta_m = \frac{e^2\Gamma(1+\epsilon)m^{1-2\epsilon}}{(4\pi)^{D/2}}\left(\frac{3}{\epsilon} + \frac{4}{1-2\epsilon}\right). \tag{9.4}$$

Notice that $\delta_1 = \delta_2$. This is not a coincidence, as the Ward-Takahashi identity guarantees that this must be true to all orders in α. It might seem alarming that these counterterm coefficients are divergent. This is a consequence of the fact that the one-loop contributions to the shaded blobs of Figure 9.1 are themselves divergent, and if contributions from these shaded blobs are implicitly present in the physical parameters of the theory, then these divergences are necessarily canceled by the various δ factors. Without renormalization, we would be trying to do perturbative calculations using parameters that are not appropriate to the scale at which we perform our experiments. Thinking of renormalization in terms of scale-dependent parameters is a very powerful idea which has many applications outside of particle physics.

9.2 A More Useful Translation

The justification for counterterms presented in the previous section is a heuristic one. More typically, a "top down" approach is employed in which the initial Lagrangian is separated into two parts through a rescaling of fields. One of these parts gives rise to the familiar Feynman rules in terms of physical parameters and the other part produces the counterterms. Either way, the existence of counterterms is required. We shall now see how these counterterms are used, and in the process, we will point out a cancellation which allows us to incorporate renormalization effects more efficiently.

We will start with δ_3. When we use the Feynman rule in Table 9.1, we must keep in mind that the counterterm is sandwiched between two regular photon propagators. The resulting product is

$$\left(\frac{-ig_{\mu\alpha}}{q^2}\right)\left[-i(g^{\alpha\beta}q^2 - q^\alpha q^\beta)\delta_3\right]\left(\frac{-ig_{\beta\nu}}{q^2}\right) = \frac{i\delta_3}{q^4}\left(g^\beta_\mu q^2 - q_\mu q^\beta\right)g_{\beta\nu}$$

$$= \frac{i\delta_3}{q^2}\left(g_{\mu\nu} - \frac{q_\mu q_\nu}{q^2}\right). \tag{9.5}$$

When this product of propagators is used as one piece of a Feynman diagram, the $q_\mu q_\nu$ terms vanish as a consequence of the Ward identity [1]. This means that the photon propagator counterterm, when sandwiched between two ordinary photon propagators, behaves like a single photon propagator multiplied by $-\delta_3$. We will call this the charge renormalization factor and denote it by PH:

$$\text{PH} = -\delta_3. \tag{9.6}$$

Next we consider the counterterm for the electron propagator. Taking the Feynman rule from Table 9.1 and sandwiching it between two regular electron propagators, we have

$$\left(\frac{i(\not{p}+m)}{p^2-m^2}\right)[i(\not{p}\delta_2-\delta_m)]\left(\frac{i(\not{p}+m)}{p^2-m^2}\right)\ . \tag{9.7}$$

If we split the counterterm into two parts via

$$[i(\not{p}\delta_2-\delta_m)]=[i(m\delta_2-\delta_m)]+[i\delta_2(\not{p}-m)] \tag{9.8}$$

and recognize that $(\not{p}-m)(\not{p}+m)=(p^2-m^2)$, we can write (9.7) as

$$\left(\frac{i(\not{p}+m)}{p^2-m^2}\right)[i(m\delta_2-\delta_m)]\left(\frac{i(\not{p}+m)}{p^2-m^2}\right)-\left(\frac{i(\not{p}+m)}{p^2-m^2}\right)\delta_2\ . \tag{9.9}$$

We call the factor between the propagators in the first term of (9.9) the mass renormalization constant and denote it by MC:

$$\mathrm{MC}=i(m\delta_2-\delta_m)\ . \tag{9.10}$$

Meanwhile, in the second term of (9.9), we have $-\delta_2$ multiplied by a single electron propagator. Every electron propagator in a QED diagram sits between two electron-photon vertices, though, and so the total number of vertices in a diagram minus the total number of electron propagators will always equal one-half the number of external electron lines in the diagram. This is very useful because the vertex counterterm in Table 9.1 is such that we need only multiply the corresponding diagram by δ_1. Since the Ward-Takahashi identity asserts that $\delta_1 = \delta_2$, most of the δ_1 contributions from the vertex counterterms will cancel the $-\delta_2$ contributions from the electron propagator counterterms. All that will remain is a factor of δ_1, for every pair of external electron lines, which we call the wavefunction renormalization factor WF:

$$\mathrm{WF}=\delta_1=\delta_2\ . \tag{9.11}$$

The term wavefunction renormalization is used because it is possible to regard this factor as being associated with the wavefunctions of the external electron lines:

$$u(p)\rightarrow\sqrt{1+\delta_2}\,u(p)\qquad\qquad\overline{u}(p)\rightarrow\sqrt{1+\delta_2}\,\overline{u}(p)\ . \tag{9.12}$$

To summarize, we have shown how the four counterterm parameters δ_1, δ_2, δ_3, and δ_m can be replaced by the three renormalization factors PH, MC, and WF. Furthermore, two of these new factors — PH and WF — can be directly
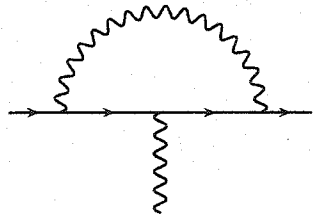
multiplied with the result from an ordinary diagram. The mass renormalization constant, on the other hand, still carries a feature of the original sandwiching procedure, so that MC must be multiplied by a diagram in which an electron propagator is used twice in a row. We represent this by an $\times$ on an electron line:

$$\longrightarrow \!\!\!\times\!\!\! \longrightarrow \quad = \mathrm{MC} \left(\frac{i(\not{p} + m)}{p^2 - m^2} \right)^2 . \tag{9.13}$$

One final remark about renormalization factors is that usually we do not need to calculate them ourselves. Regardless of the physical process under consideration, there is only one set of PH, MC, and WF factors for a given theory, and hence, the results are transcribed directly from the literature whenever possible.

A Simple Example

We conclude this chapter with an explicit example of how to apply renormalization factors correctly in a physical calculation. As a preview for Chapter 11, we will consider the $\mathcal{O}\left(\alpha^2\right)$ QED calculation of the anomalous magnetic moment of the electron. The leading contribution to a_e is at $\mathcal{O}\left(\alpha\right)$:

$$(a_e)_1 = \left(\frac{\alpha}{\pi} \right) \left(\frac{1}{2} + 2\epsilon + \mathcal{O}\left(\epsilon^2\right) \right) . \tag{9.14}$$

The leading term, $\alpha/2\pi$, is Schwinger's famous result [5], and the $\mathcal{O}\left(\epsilon\right)$ term will be needed for the $\mathcal{O}\left(\alpha^2\right)$ result due to the presence of $1/\epsilon$ in the counterterms.

At $\mathcal{O}\left(\alpha^2\right)$, there are 7 two-loop diagrams to consider, as shown in Figure 9.2. In general, the loop in diagram (g) could also be a muon or tau, but we shall restrict ourselves to QED with only electrons. Notice that diagrams (c) and (d) are mirror images of each other. This means that we need only calculate one of them and multiply the result by 2; the same is true for diagrams (e) and (f). The total contribution from the diagrams in Figure 9.2 is

$$(a_e)_2^{diagrams} = \left(\frac{\alpha}{\pi} \right)^2 \left[\frac{23}{24\epsilon} + \left(\frac{641}{144} + \frac{\pi^2}{12} + \frac{3\zeta(3)}{4} - \frac{\pi^2}{2} \ln 2 \right) \right] . \tag{9.15}$$

We expect the divergence in (9.15) to cancel once we incorporate the renormalization factors. Expressed in terms of α and to finite order in ϵ, we obtain the
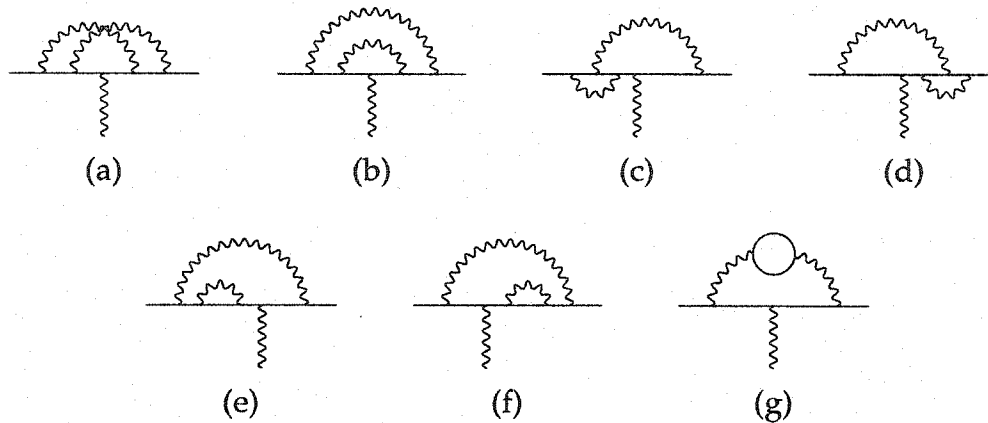
Figure 9.2: $\mathcal{O}\left(\alpha^2\right)$ diagrams that contribute to a_e.

renormalization factors WF, PH, and MC from (9.2), (9.3), and (9.4):

$$\text{WF} = \left(\frac{\alpha}{\pi}\right)\left(-\frac{3}{4\epsilon}-1\right), \tag{9.16}$$

$$\text{PH} = \left(\frac{\alpha}{\pi}\right)\left(\frac{1}{3\epsilon}\right), \tag{9.17}$$

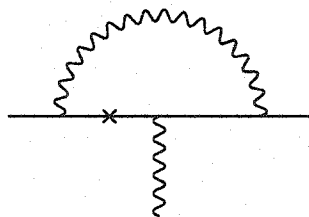$$\text{MC} = im_e\left(\frac{\alpha}{\pi}\right)\left(\frac{3}{4\epsilon}+1\right). \tag{9.18}$$

The WF and PH renormalization factors simply multiply the $\mathcal{O}\left(\alpha\right)$ result in (9.14):

$$(a_e)_2^{\text{WF}} = \text{WF}\,(a_e)_1 = \left(\frac{\alpha}{\pi}\right)^2\left(-\frac{3}{8\epsilon}-2\right), \tag{9.19}$$

$$(a_e)_2^{\text{PH}} = \text{PH}\,(a_e)_1 = \left(\frac{\alpha}{\pi}\right)^2\left(\frac{1}{6\epsilon}+\frac{2}{3}\right). \tag{9.20}$$

The MC factor, meanwhile, is to be multiplied by a one-loop diagram in which there is an extra electron propagator,

$$(a_e)_{1m} = \frac{i}{m_e}\left(\frac{\alpha}{\pi}\right)\left(\frac{1}{2}+\frac{\epsilon}{2}+\mathcal{O}\left(\epsilon^2\right)\right), \tag{9.21}$$

so that

$$(a_e)_2^{\mathrm{MC}} = 2\,\mathrm{MC}\,(a_e)_{1m} = \left(\frac{\alpha}{\pi}\right)^2 \left(-\frac{3}{4\epsilon} - \frac{7}{4}\right) . \qquad (9.22)$$

The factor of 2 in (9.22) accounts for the mirror image of the diagram in (9.21). Combining (9.22) with (9.19) and (9.20), we have the renormalization contributions to $(a_e)_2$,

$$(a_e)_2^{renorm} = \left(\frac{\alpha}{\pi}\right)^2 \left(-\frac{23}{24\epsilon} - \frac{37}{12}\right) . \qquad (9.23)$$

Adding this to the contributions from the two-loop diagrams in (9.15), we obtain the finite final result

$$(a_e)_2 = \left(\frac{\alpha}{\pi}\right)^2 \left(\frac{197}{144} + \frac{\pi^2}{12} + \frac{3\zeta(3)}{4} - \frac{\pi^2}{2}\ln 2\right) , \qquad (9.24)$$

as first obtained by Sommerfield [6].

Although the preceding example was a fairly simple one, the main ideas extend to more difficult calculations. In Chapter 13, for example, we will be using the $\mathcal{O}\left(\alpha_s^2\right)$ QCD renormalization factors as part of a calculation involving the decay of a top quark.

"Anything that happens, happens. Anything that, in happening, causes something else to happen, causes something else to happen. Anything that, in happening, causes itself to happen again, happens again. It doesn't necessarily do it in chronological order, though."

(Hitch Hiker's Guide to the Galaxy)

Chapter 10

Symbolic Computation

Symbolic computation is an indispensable tool for performing most multiloop calculations. In this chapter, we will have a brief look at a few of the main ideas associated with symbolic computation, the specific programming environments that have been used to obtain the results in this thesis, and some of the challenges associated with especially large computations. The Centre for Symbolic Computation at the University of Alberta provides an excellent environment for applying these computational techniques to a number of research frontiers, and in particular, to the calculations presented in this thesis.

10.1 Basic Ideas

The use of symbols in place of specific numbers was a very fruitful abstraction for ancient mathematicians, but only in the last few decades has this idea been carried over to the realm of machine computation. For certain types of problems in various branches of science, the benefits have been enormous. Suppose, for example, that in the context of some physical problem, we would like to solve a set of equations for one or more functions f_i which depend on one or more variables x_j. If the equations cannot be solved by hand conveniently, a very common approach involves writing a computer program in a language such as FORTRAN or C and solving the equations numerically for each specific point in a grid of possible values of the variables. If the grid is sufficiently dense, the interpolations between the grid points will usually provide a good approximation to the exact solution. With symbolic computation, on the other hand, the goal would be to obtain the exact functional form of the solution. An exact solution has several advantages over a numerical solution. First, specific numerical values can always be obtained from an exact solution, whereas the reverse is not true. Secondly, an exact solution is free of the numerical errors that accrue in a

numerical calculation, both from the approximations that result from a discrete grid and the rounding of intermediate floating point numbers in the program. Finally, the functional form of an exact solution often provides insights into the problem that might easily be overlooked from a plot of an accurate numerical solution.

The desire for exact solutions is natural, but how can a computer deliver them? It all starts with the basic representation of data. In a typical numerical programming language, computer memory is set aside to keep track of a list of variables. These variables can encode things like integers, floating point numbers, or character strings, and they are repeatedly modified by the specific instructions of a computer program. In a typical symbolic programming language, the basic object is a term. A term consists of a rational number coefficient and one or more algebraic variables with various integer exponents. Terms are grouped together to form an expression and it is the expression which is dynamically altered over the course of a symbolic program. Terms can be created, destroyed, combined, or split, and so the size of an expression can change. The principal way to modify an expression is through pattern matching. Suppose, for example, that we have an expression, f, whose terms make up a polynomial in the symbol x, and that we would like to differentiate $f(x)$. Schematically, the computer will represent each term as:

$$\text{Term} = (\text{Numerator, Denominator, Exponent of Symbol 1}, \ldots).$$

Each of the elements is an integer and we will assume that x is the only symbol in this particular program, so that the term $3x^{14}$ will be represented in memory as

$$3x^{14} \longrightarrow (3, 1, 14).$$

The differentiation instruction $(a/b)x^c \to (ac/b)x^{c-1}$ can easily be implemented as

$$(\text{a}, \text{b}, \text{c}) \Rightarrow (\text{a} * \text{c}, \text{b}, \text{c} - 1).$$

Of course, the program should know how to simplify the fraction (ac/b) if there are common factors in the numerator and denominator. Other functions of x — $\sin x$, for example — would be stored as separate symbols and additional rules would be necessary to handle them. In principle, all of this can be done if the programmer is sufficiently diligent. Not every scientist has the time or inclination to be a diligent programmer, though, and with this point we segue into a look at the relative strengths of a few symbolic algebra programs.

10.2 Computer Algebra Programs

Of the dozens of computer algebra systems in existence, three have been used extensively in conjunction with this thesis: Maple [38], Mathematica [39], and FORM [40]. Maple and Mathematica are conceptually very similar. Both systems incorporate massive amounts of built-in knowledge and a fancy user-interface. A useful analogy is to think of each of these systems as a sort of mathematical Swiss Army Knife. These are very convenient programs to use for certain tasks. For example, Maple was used at the end of Section 3.1 to expand the Gamma functions in (3.16) as a Laurent series in ϵ. Specifically, the command

> simplify(series(GAMMA(1 − ep) ∗ GAMMA(1 − ep) ∗ GAMMA(−1 + 2 ∗ ep)
> ∗GAMMA(3 − 4 ∗ ep)/GAMMA(2 − 2 ∗ ep)/GAMMA(3 − 3 ∗ ep)
> /GAMMA(1 + ep)/ep, ep = 0, 4));

yields

$$-\tfrac{1}{2}\mathsf{ep}^{-2} - \tfrac{5}{4}\mathsf{ep}^{-1} + \left(-\tfrac{1}{3}\pi^2 - \tfrac{11}{8}\right) + \left(-4\zeta(3) - \tfrac{5}{6}\pi^2 + \tfrac{55}{16}\right)\mathsf{ep} + O(\mathsf{ep}^2) \ .$$

Mathematica, meanwhile, is particularly good at providing analytic solutions for the parameter integrals that are required for our master loop integrals. For example, the integral (6.19) in Section 6.1 can be evaluated using the command

> Integrate[Series[x ∧ (−4 ∗ ep) ∗ z ∧ (−2 ∗ ep) ∗ (1 − z) ∧ (−3 ∗ ep)
> ∗(1 − x ∗ z) ∧ ep, {ep, 0, 2}], {x, 0, 1}, {z, 0, 1}]

with the result
$$\frac{6 + \mathsf{ep}(42 + \mathsf{Pi}^2) + \mathsf{ep}^2(222 - \mathsf{Pi}^2 + 66\mathsf{Zeta}[3])}{6} \ .$$

For all their bells and whistles, Maple and Mathematica come up short in the most crucial area for multiloop calculations: large problems. These two systems are slow, inefficient, and cannot accomodate problems which exceed certain memory requirements. For this reason, FORM is the program of choice for the majority of the work in this thesis. Developed by a fellow particle physicist, but applicable to any field of research, FORM has very little in the way of built-in knowledge. It is up to the user to add everything that is needed and only what is needed. The key feature of the program, though, is the ability to handle expressions of immense size by using large sections of hard disk space for temporary storage. This, along with the austere design, makes it extremely efficient, and thus well-suited to work on difficult multiloop calculations.

10.3   Very Large Calculations

Inevitably, research-level problems usually manage to saturate all available computing resources. In multiloop calculations, the culprits are threefold. The first two are directly related to the number of loops, as both the overall number of diagrams and the typical complexity of each diagram increases dramatically with each extra loop. These two factors are fixed in advance by the scope of the problem. The third culprit in our multiloop computations is the series expansion of a multi-scale problem, as described in Chapter 7. An approximate rule of thumb is that the computing time needed to generate N terms of such a series expansion grows as the factorial of N. No matter how powerful the computer being used, it is not hard to pick a value of N sufficiently large to put the computation out of reach. In general, when expanding loop integrals from opposite ends of a kinematic region, roughly five terms of each expansion are sufficient to produce a region of overlap where the two expansions agree. For two-loop calculations, five terms can usually be obtained on a desktop computer (circa 2004) without any extraordinary optimization efforts, and so it is not particularly important to try to extract one or two additional terms. At three loops, on the other hand, even the first few terms are hard to get, thus further efforts are justified.

Typically, the primary method of extending a very large calculation is to optimize the computer code. This is often done by analyzing the flow of a program and then trying to improve the efficiency at one or more key bottlenecks through small modifications in the code. The next level of optimization involves adjusting the system settings that govern the various levels of memory allocation. Having maximized the performance of a particular program on a particular machine, the next escalation of effort might involve other computers. The various diagrams in a multiloop calculation can be distributed among a set of machines, for instance. Often, though, there are one or two diagrams whose difficulty exceed that of all the others combined, so that distributed computing is not necessarily much of an improvement. Instead, one might consider parallel computing, where a set of computers is used to evaluate a single diagram. The latest version of FORM supports parallel processing [41], and thus provides a less expensive alternative to high-performance workstations.

Recently, an alternative paradigm has been implemented by Laporta [19] to solve the large systems of recurrence relations that arise in multiloop calculations. In place of the manually constructed algorithms described in Chapter 4, this new approach uses the Gaussian elimination procedure in a brute force way. Instead of applying the recurrence relations selectively to create an efficient algorithm that is valid for arbitrary exponents of the propagators, the Laporta method picks a specific range of exponents and writes every possible recurrence relation for every possible loop integral in the range. The loop inte-

grals are then ranked by "difficulty" and the large list of recurrence relations is used to remove the loop integrals one by one, starting with the most difficult. When every recurrence relation is used up, whichever loop integrals remain are regarded as master integrals. Spurious master integrals can arise if the initial range of loop integrals is not sufficiently large. This algorithm is applied only to the top-level topologies that follow directly from the original diagrams, and while some of the master integrals identified by the algorithm will consist of products of smaller integrals or loop integrals with integrable subloops, there is no need to work through a sequence of subtopologies. The initial implementation of the Laporta algorithm involves sophisticated programming techniques, but once the core of the algorithm is designed, it can quickly be adapted to address any other given topology. Given the manual effort required to construct recurrence relation algorithms for three-loop topologies, the lure of a computer-generated algorithm is apparent. What might not be apparent, though, is that the Laporta algorithm, while admittedly slow and inefficient for simple problems, is actually faster at obtaining additional terms deep within an expansion. In Chapter 13, for instance, this algorithm was used to obtain the ω^5 terms for the contribution to top quark decay from the two most difficult diagrams [43]. The key feature of the Laporta algorithm which seems to provide this improvement is the use of very large tables to store the results of each specific loop integral. The generation of such large tables, in place of strict real-time algorithms, is likely to facilitate substantial improvements [44] in programs written with the traditional recurrence relation algorithms. This is an avenue that will soon be explored, and in the immediate future, it is likely that both algorithms will be employed in order to determine the ultimate potential of each.

"I predict that within 100 years computers will be twice as powerful, 10 000 times larger, and so expensive that only the five richest kings of Europe will own them."

Professor Frink (*The Simpsons*)

Chapter 11

Muon $g - 2$

Measurements of the anomalous magnetic moments of the electron and muon provide us with extremely sensitive tests of the Standard Model. Minute deviations between the experimental measurements and the corresponding Standard Model predictions might be indicative of New Physics. In this chapter, we will outline the components of the Standard Model prediction for the muon anomalous magnetic moment and explain how preliminary deviations between theory and experiment were distorted by three distinct calculational errors. Most significant among these was an error in the light-by-light scattering contributions; the paper [45] on which Section 11.2 is based was instrumental in settling this issue. We conclude with an update on the current status of the theory and experiment.

11.1 Background

A charged lepton, such as an electron or muon, can interact with an electromagnetic field in one of two parity-conserving ways, so that the most general interaction vertex is

$$-ie\gamma_\mu F_1(q^2) + \frac{e}{2m}\sigma_{\mu\nu}q^\nu F_2(q^2) \,. \tag{11.1}$$

In relativistic quantum mechanics, $F_1 = 1$ and $F_2 = 0$, therefore only the Dirac term $-ie\gamma_\mu$ is present; the Pauli term is absent because it is proportional to the anomalous magnetic moment, which in Dirac theory is

$$a \equiv \frac{g - 2}{2} \equiv F_2(0) = 0 \,. \qquad \text{(Dirac theory)} \tag{11.2}$$

A nonzero anomalous magnetic moment can arise from the radiative corrections induced by a quantum field theory, as was first calculated by Schwinger [5].

For any charged lepton, the QED contribution to the anomalous magnetic moment can be calculated as a series in powers of the fine-structure constant:

$$a^{\mathrm{QED}} = A_1 \left(\frac{\alpha}{\pi}\right) + A_2 \left(\frac{\alpha}{\pi}\right)^2 + A_3 \left(\frac{\alpha}{\pi}\right)^3 + \cdots , \tag{11.3}$$

where the dimensionless numerical coefficients A_i depend, at most, on m_e, m_μ, and m_τ. The contribution to the anomalous magnetic moment from any other kind of physics is characteristically suppressed by the ratio m^2/Λ^2, where m is the mass of the lepton under consideration and Λ is the mass scale at which the other kind of physics resides (with the assumption that $\Lambda > m$). As a result, even though a_e has been measured about 150 times as precisely as a_μ ($\delta a_e \simeq 0.4 \times 10^{-11}$ and $\delta a_\mu \simeq 60 \times 10^{-11}$) [46, 47], the ratio $m_\mu^2/m_e^2 \simeq 43\,000$ indicates that a_μ is almost 300 times more sensitive than a_e to non-QED physics. It is for this reason that a_μ is so important. The measurement of a_e is not discarded, however, because it can be used, along with (11.3), to determine a value for α that is more precise than is currently possible using any other means.

There are three classes of contributions to a_μ from the Standard Model. We will describe them only briefly here, but a more detailed discussion and additional references can be found in [48]. The largest Standard Model contribution to a_μ is due to QED:

$$
\begin{aligned}
a_\mu^{\mathrm{QED}} &= \frac{\alpha}{2\pi} + 0.765\,857\,376\,(27) \left(\frac{\alpha}{\pi}\right)^2 + 24.050\,508\,98\,(44) \left(\frac{\alpha}{\pi}\right)^3 \\
&\quad + 126.07\,(41) \left(\frac{\alpha}{\pi}\right)^4 + 930\,(170) \left(\frac{\alpha}{\pi}\right)^5 \\
&= 116\,584\,719.4\,(1.4) \times 10^{-11} .
\end{aligned}
\tag{11.4}
$$

This result has been obtained analytically through three loops [49] (the uncertainties arise from lepton mass uncertainties), the complete four-loop calculation has been evaluated numerically [50], and the five-loop diagrams have been estimated numerically [7, 51]. The important thing to note is that the uncertainty in a_μ^{QED} is significantly smaller than the current experimental uncertainty of 60×10^{-11}.

The next largest Standard Model contribution to a_μ comes from QCD, or more specifically, from the effects of virtual hadrons. The primary component of a_μ^{had} arises from the vacuum polarization diagram of Figure 11.1. Since we cannot use perturbative QCD to evaluate the vacuum polarization contribution, we must instead employ the optical theorem to derive a dispersion relation that relates the "stuffed" photon propagator in Figure 11.1 to the experimentally mea-
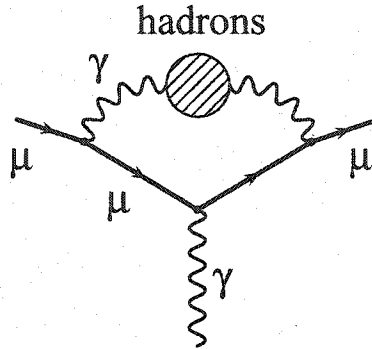
Figure 11.1: Vacuum polarization contribution to a_μ^{had}.

sured cross section for $e^+e^- \to$ hadrons. Using this approach, a recent analysis of the vacuum polarization effects [52] leads to

$$a_\mu^{\text{had}} = 6\,938\,(80) \times 10^{-11}\,.$$ (11.5)

The uncertainty in this contribution is obviously quite substantial. Note that there is an alternate method for obtaining the vacuum polarization contributions which relies on experimental data for τ decays (see, for example, [53] for a discussion).

The third and smallest Standard Model contribution to a_μ is caused by the electroweak sector, involving virtual Z^0, $W^\pm$, and H bosons. This contribution has been obtained analytically through two loops [54], resulting in

$$\begin{aligned}
a_\mu^{\text{EW}} &= \frac{5G_\mu m_\mu^2}{24\sqrt{2}\pi^2} \left\{ \frac{1}{5}\left(1 - 4\sin^2\theta_w\right)^2 + 1 + \mathcal{O}\left(\frac{m_\mu^2}{M_W^2}\right) \right\} \\
&\quad + a_\mu^{\text{EW}}(2\,\text{loops}) \\
&= 152\,(4) \times 10^{-11}\,.
\end{aligned}$$ (11.6)

As was the case with the QED contribution, the uncertainty in the electroweak contribution to a_μ is significantly smaller than the experimental uncertainty.

Combining these three classes of contributions, we obtain the current Standard Model prediction for the muon anomalous magnetic moment:

$$\begin{aligned}
a_\mu^{\text{SM}} &= a_\mu^{\text{QED}} + a_\mu^{\text{had}} + a_\mu^{\text{EW}} \\
&= 116\,591\,809\,(80) \times 10^{-11}\,.
\end{aligned}$$ (11.7)

Let us now backtrack to the year 2000. At the time, the best experimental

determination of a_μ dated back to a 1977 experiment at CERN [55]:

$$\left(a_\mu^{exp}\right)_{1977} = 116\,592\,300\,(840) \times 10^{-11}\,. \tag{11.8}$$

While this was an impressive measurement for its time, a more precise experiment began collecting data in 1998 at the Brookhaven National Laboratory. At this time, the theoretical prediction was

$$\left(a_\mu^{SM}\right)_{2000} = 116\,591\,597\,(67) \times 10^{-11}\,, \tag{11.9}$$

in agreement with the CERN measurement. The BNL experiment, E821, aspired to reduce the experimental uncertainty by more than an order of magnitude, though, and in February of 2001, the most recent E821 analysis [56] had modified the world-average experimental result to

$$\left(a_\mu^{exp}\right)_{2001} = 116\,592\,023\,(151) \times 10^{-11}\,. \tag{11.10}$$

Although the absolute discrepancy between theory and experiment had decreased, the significance of the discrepancy had become substantial,

$$a_\mu^{exp} - a_\mu^{SM} = (426 \pm 165) \times 10^{-11} \Rightarrow 2.6\sigma\,, \tag{11.11}$$

and scores of particle physicists scrambled into action to try to account for the discrepancy. Much of the theoretical effort involved contributions from various kinds of New Physics that would exactly produce such a discrepancy. Others set about double-checking the Standard Model calculations and their efforts paid off when it was suggested that the light-by-light scattering contributions to a_μ^{had} had been incorporated with the wrong sign [57,58]. The previous contribution,

$$a_\mu^{LBL} = -85\,(25) \times 10^{-11}\,, \tag{11.12}$$

resulted from the combined efforts of two independent groups [59,60]. It can be seen from (11.11) that if we change the sign of a_μ^{LBL}, the resulting increase in a_μ^{SM} decreases the discrepancy between theory and experiment by about one standard deviation.

11.2 Light-By-Light Scattering

The light-by-light scattering contributions to a_μ^{had} arise from diagrams like the one in Figure 11.2. Here, the virtual hadrons are irreducibly connected to four photons and there is no known way to relate these contributions directly to experimental observables. Instead, the diagrams must be calculated with the help
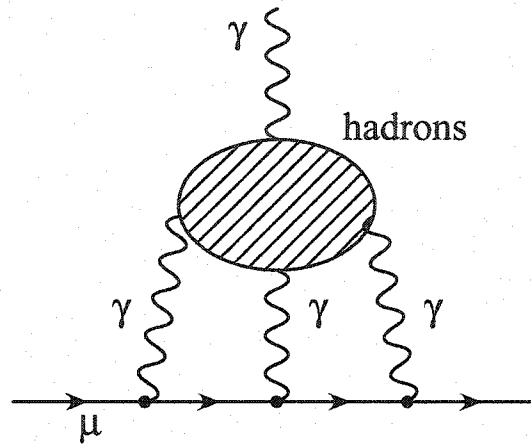
Figure 11.2: Light-by-light scattering contribution to a_μ^{had}.

of specific models of hadron physics. The choice of model will undoubtedly affect the magnitude of the contributions, but the overall sign should be model-independent, and thus we shall restrict ourselves to a specific model for our own calculation of the light-by-light scattering contribution.

The hadronic blob interacting with four photons in Figure 11.2 can be modeled as the exchange of a neutral hadron between pairs of photons. Since the π^0 is by far the lightest neutral hadron, and thereby provides the dominant contribution to a_μ^{LBL}, we will ignore the other neutral hadrons and model the light-by-light scattering by the two diagrams in Figure 11.3. To calculate the

(a)   (b)
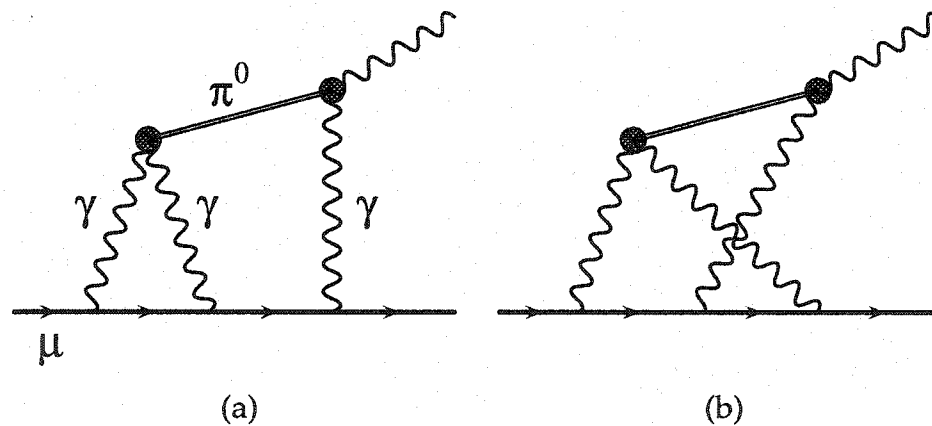
Figure 11.3: Pion pole contributions to a_μ^{LBL}.

contribution from the "giraffe" diagrams of Figure 11.3, we require a Feynman rule for the interaction of a pion with two photons. This interaction results from

the Adler-Bell-Jackiw anomaly [61,62], and at low energies, it is described by the Wess-Zumino-Witten Lagrangian [63,64],

$$\mathcal{L}_{\text{WZW}} = -\frac{\alpha N_c}{12\pi F_\pi} F_{\mu\nu} \widetilde{F}^{\mu\nu} \pi^0 , \tag{11.13}$$

where $N_c = 3$ is the number of colors in QCD and $F_\pi \simeq 92.4$ MeV is the pion decay constant. This interaction is only valid at low energies, and so it should not be surprising that we would obtain ultraviolet divergences if we naively used it in the loop diagrams of Figure 11.3. We can tame the incorrect high-energy behavior in an approximate way by multiplying the $\pi^0\gamma\gamma$ interaction vertex by a form factor whose value is essentially 1 at low energies and 0 at high energies. This transforms the $\pi^0\gamma\gamma$ interaction vertex to

$$\frac{\alpha N_c}{3\pi F_\pi} F_{\pi^0\gamma\gamma}(q_1^2, q_2^2) \, i\epsilon_{\mu\nu\alpha\beta} \, q_1^\alpha q_2^\beta , \tag{11.14}$$

where q_1 and q_2 are the outgoing momenta of the two photons and $F_{\pi^0\gamma\gamma}(q_1^2, q_2^2)$ is the form factor. The simplest choice for $F_{\pi^0\gamma\gamma}(q_1^2, q_2^2)$ is the Vector Meson Dominance form factor,

$$F_{\pi^0\gamma\gamma}(q_1^2, q_2^2) = \frac{M^2}{M^2 - q_1^2} \frac{M^2}{M^2 - q_2^2} , \tag{11.15}$$

where the parameter M is phenomenologically determined to be very close to the mass of the ρ meson:

$$M \approx m_\rho \simeq 769 \text{ MeV} . \tag{11.16}$$

This form factor, as its name suggests, has a nice physical interpretation. The denominator factors of $(M^2 - q^2)$ can be regarded as ρ meson propagators, so that we can think of one vector particle (the photon) behaving like another vector particle (the ρ) when interacting with the π^0.

At this stage, we have now reduced the light-by-light scattering contributions of Figure 11.3 to calculating a pair of two-loop integrals. The main complication is that these loop integrals depend on three external scales: m_μ, m_π, and M. To solve these integrals analytically, we will employ the expansion techniques of Chapter 7. Since m_μ and m_π are fairly close together, we can perform the expansion procedure in two stages.

In the first stage, we use a Taylor expansion to remove m_π from the loop integrals:

$$\frac{1}{k^2 + m_\pi^2} = \frac{1}{k^2 + m_\mu^2 - m_\mu^2 + m_\pi^2}$$

$$= \frac{1}{k^2 + m_\mu^2} - \left(\frac{m_\pi^2 - m_\mu^2}{m_\mu^2} \right) \frac{m_\mu^2}{\left(k^2 + m_\mu^2 \right)^2} + \cdots . \tag{11.17}$$

We will denote this first expansion parameter by δ,

$$\delta = \frac{m_\pi^2 - m_\mu^2}{m_\mu^2} , \tag{11.18}$$

and we can see that δ is only small because of the proximity of m_μ and m_π; an extension to η meson exchange, for instance, would require a different expansion procedure.

For the second stage, we will employ an asymptotic expansion in the small parameter m_μ^2/M^2. To do this, we need to divide the loop integrals into five regions based on the scales of the two loop momenta. As explained in Section 7.3, within each of the regions, one or more propagators will contain both soft ($\mathcal{O}(m_\mu)$) and hard ($\mathcal{O}(M)$) terms. After expanding these propagators, the original two-scale, two-loop integrals in each region will simplify to either single-scale two-loop integrals or products of a soft-scale one-loop integral with a hard-scale one-loop integral. Integrations in all five regions can then be carried out analytically, and the coefficients of the two expansion parameters, δ and m_μ^2/M^2, can be obtained to an arbitrary order.

The result can be written as

$$a_\mu^{\mathrm{LBL},\pi^0} = \left(\frac{\alpha}{\pi} \right)^3 \frac{m_\mu^2}{F_\pi^2} \left(\frac{N_c}{\pi} \right)^2 X_{\pi^0}, \tag{11.19}$$

and we find

$$
\begin{aligned}
X_{\pi^0} =\ & \frac{1}{48} L^2 + \left(\frac{1}{96} - \frac{\pi}{48\sqrt{3}} \right) L - \frac{277}{10368} \\
& + \frac{\pi}{24\sqrt{3}} S_2 - \frac{17\pi}{3456\sqrt{3}} + \frac{19}{128} S_2 - \frac{\zeta(3)}{288} - \frac{11\pi^2}{15552} \\
& + \frac{m_\mu^2}{M^2} \left[\frac{155}{1296} L^2 - \left(\frac{65}{1296} + \frac{\pi}{16\sqrt{3}} \right) L - \frac{11915}{62208} \right. \\
& \left. + \frac{\pi}{24\sqrt{3}} S_2 + \frac{\pi}{36\sqrt{3}} + \frac{39}{64} S_2 - \frac{\zeta(3)}{288} + \frac{347\pi^2}{93312} \right] \\
& + \delta \left[\left(\frac{1}{72} - \frac{\pi}{72\sqrt{3}} \right) L - \frac{1}{1296} + \frac{5}{96} \frac{\pi}{\sqrt{3}} S_2 - \frac{11\pi}{864\sqrt{3}} \right. \\
& \left. - \frac{1}{384} S_2 - \frac{\zeta(3)}{216} + \frac{53\pi^2}{31104} \right] + \mathcal{O} \left(\frac{m_\mu^4}{M^4}, \delta^2 \right) , \tag{11.20}
\end{aligned}
$$

where $L = \log(M/m_\mu)$, $\zeta(3) \simeq 1.202057$ is the Riemann zeta function, and $S_2 = \frac{4}{9\sqrt{3}}\mathrm{Cl}_2\left(\frac{\pi}{3}\right) \simeq 0.260434$. The positive sign of the coefficient of L^2 in the leading order in m_μ/M confirms the result of [57,58]. Using terms in (11.20) to $(m_\mu^2/M^2)^3$ and δ^6 and substituting $\alpha = 1/137.036$, $N_c = 3$, $M = 769$ MeV, $m_\mu = 105.66$ MeV, $m_\pi = 134.98$ MeV, and $F_\pi = 92.4$ MeV into (11.19) we obtain

$$a_\mu^{\mathrm{LBL},\pi^0} \simeq +56 \times 10^{-11} \, . \tag{11.21}$$

The key feature of this result is that the light-by-light scattering contribution is indeed positive and that the discrepancy between the Standard Model and experiment is thereby reduced.

Our result can be checked in several ways, in particular to ensure the correct treatment of the Feynman rules in our computer programs. For example, using the WZW Lagrangian (11.13) one can evaluate the vacuum polarization contribution to a_μ where the virtual photon splits into a π^0 and a γ, as shown in Figure 11.4. The contribution of this diagram to a_μ should be positive, since a
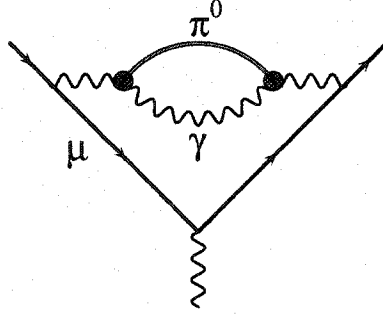
Figure 11.4: Vacuum polarization contribution of the neutral pion.

dispersion relation relates it to the cross section $\sigma(e^+e^- \to \pi^0\gamma)$. We find

$$a_\mu^{\mathrm{vp},\pi^0\gamma} = \left(\frac{\alpha}{\pi}\right)^3 \frac{m_\mu^2}{F_\pi^2} \left(\frac{N_c}{\pi}\right)^2 X_{\pi^0\gamma}, \tag{11.22}$$

where

$$X_{\pi^0\gamma} = \frac{L}{1296} + \frac{181}{15552} - \frac{\pi}{96\sqrt{3}} + \frac{7\pi^2}{7776} + \mathcal{O}\left(\frac{m_\mu^2}{M^2}, \delta\right) . \tag{11.23}$$

Including several more terms in the m_μ/M and δ expansions, we obtain

$$a_\mu^{\mathrm{vp},\pi^0\gamma} \simeq +3.7 \times 10^{-11} \, , \tag{11.24}$$

a positive contribution which lends further proof to the assertion that a_μ^{LBL} is positive.

11.3 $g − 2$ Epilogue

Shortly after our confirmation [45] of the positive sign in a_μ^{LBL}, the validity of the revised result was reinforced by a chiral perturbation theory calculation [65]. Meanwhile, the errors in the original negative-sign determinations of a_μ^{LBL} were traced to a misunderstanding of how the Levi-Civita tensor is normalized in FORM [66, 67]. A subsequent investigation [68], in which perturbative QCD is used to constrain the form factors of (11.14) at high energies, has suggested that the magnitude of the light-by-light scattering contribution may be larger than previously thought.

Meanwhile, the increased scrutiny of the Standard Model prediction for a_μ uncovered two other errors. The first of these was a minor adjustment of the $\mathcal{O}(\alpha^4)$ QED contribution which was found to have been in error due to problems with the numerical integration of the loop integrals [70]. The other was an error in the experimental determination of the cross section $\sigma(e^+ e^- \to \text{hadrons})$ used for the vacuum polarization contributions to a_μ^{had} resulting from luminosity miscalibrations at the CMD-2 experiment [71].

With all three corrections in place, we restate (11.7) as the current Standard Model prediction for the anomalous magnetic moment of the muon,

$$
\begin{aligned}
a_\mu^{\mathrm{SM}} &= 116\,591\,809 \pm 72_{\mathrm{VP}} \pm 35_{\mathrm{LBL}} \pm 4_{\mathrm{QED+EW}} \\
&= 116\,591\,809\,(80) \times 10^{-11},
\end{aligned}
\tag{11.25}
$$

where in the first line, we have provided a breakdown of the sources of the theoretical uncertainties.

On the experimental side, E821 continued to collect data until 2001. In this final year of running, negatively-charged muons were used in place of the positively-charged muons that had been measured previously. Based on the analysis of the final data set at E821 [47], the current experimental determination of the anomalous magnetic moment of the muon is

$$
a_\mu^{\mathrm{exp}} = 116\,592\,080\,(60) \times 10^{-11}.
\tag{11.26}
$$

From (11.25) and (11.26), we see that the current discrepancy between experiment and theory is

$$
a_\mu^{\mathrm{exp}} - a_\mu^{\mathrm{SM}} = (271 \pm 100) \times 10^{-11} \Rightarrow 2.7\sigma.
\tag{11.27}
$$

Although this discrepancy could stem from still undiscovered errors, or perhaps be just a statistical noncoincidence, it is hard not to consider it as a tantalizing hint for New Physics beyond the Standard Model. For example, supersymmet-

ric models typically [48] provide a contribution at the one-loop level of

$$\left| a_\mu^{\text{SUSY}} \right| \simeq 130 \times 10^{-11} \left(\frac{100 \text{ GeV}}{\widetilde{m}} \right)^2 \tan\beta , \tag{11.28}$$

where $\widetilde{m}$ is roughly the mass of the supersymmetric particles in the loop and $\tan\beta$ is the ratio of the vacuum expectation values of the Higgs doublets. For plausible regions of supersymmetric parameter space [72], (11.28) has both the correct sign and magnitude needed to account for the discrepancy in (11.27). Pending a possible direct observation at the LHC, this is only speculation of course, but hopefully we will soon have the concrete evidence available to look back fondly at the muon $g-2$ saga.

"They are illusions, they're not the solutions they promised to be, the answer was here all the time."

Evita (*Don't Cry For Me Argentina*)

Chapter 12

Energy Levels of QED Bound States

Bound states formed by the attractive force between oppositely charged particles provide us with a sensitive test of Quantum Electrodynamics via precise measurements of the energy levels; such measurements are often very impressive, owing to the characteristically low energies of these processes. In this chapter, we shall explore the energy levels of a general QED bound state formed between two particles whose charges, e and Ze, and masses, m and M, are arbitrary. After reviewing the basic hierarchy of energy level corrections, we will see how the techniques of perturbative quantum field theory can be used to evaluate new classes of energy level corrections for a general QED bound state. In particular, two new classes of results — the $\mathcal{O}\left(\alpha(Z\alpha)^5\right)$ radiative recoil and $\mathcal{O}\left((Z\alpha)^6\right)$ pure recoil corrections — are evaluated in this chapter, as first presented in the paper [73].

12.1 Classification of Energy Level Corrections

Let us begin by looking at a simple hydrogen atom consisting of an electron of mass m and charge $-|e|$ and a proton of mass M and charge $+|e|$. The Coulomb attraction between them is responsible for the binding of the particles and in the absence of any other complications, there is a set of energy levels

$$E_{binding} = -\frac{m\alpha^2}{2n^2} , \tag{12.1}$$

where n is a positive integer and $\alpha \simeq 1/137$ is the fine-structure constant. Roughly speaking, we can interpret (12.1) as implying that the speed of the electron (in units of c) is

$$v \sim \frac{\alpha}{n} , \tag{12.2}$$

which suggests that the electron is, to a good approximation, non-relativistic. Relativistic effects can thus be treated as a small perturbation to the Schrödinger equation, and since the relativistic kinetic energy is

$$
\begin{aligned}
KE &= m\left(\frac{1}{\sqrt{1 - v^2}} - 1\right) \\
&= \frac{1}{2}mv^2 + \frac{3}{8}mv^4 + \dots,
\end{aligned}
\tag{12.3}
$$

we expect the leading relativistic effect to be $\mathcal{O}\left(m\alpha^4\right)$. The contribution of the spin-orbit interaction is also of the same order and these two $\mathcal{O}\left(m\alpha^4\right)$ effects are known collectively as fine structure. Beyond this, we have two more effects to consider: hyperfine splitting and the Lamb shift. Hyperfine splitting, arising from a spin-spin interaction, is analogous to the spin-orbit effect, only now the angular momentum to which the electron spin couples is suppressed by the ratio m/M. The Lamb shift, meanwhile, is an $\mathcal{O}\left(m\alpha^5\right)$ effect whose origin is irreducibly field-theoretic. The hierarchy of these effects is summarized in Table 12.1. Strictly speaking, these effects refer to experimentally measured differences between specific energy levels. The leading-order contributions of Table 12.1 to these effects are supplemented by higher-order contributions.

	Binding energy	$\mathcal{O}\left(m\alpha^2\right)$
Relativistic Correction	Fine Structure	$\mathcal{O}\left(m\alpha^4\right)$
Spin-Orbit Interaction		
	Hyperfine Structure	$\mathcal{O}\left(m\alpha^4(m/M)\right)$
	Lamb Shift	$\mathcal{O}\left(m\alpha^5\right)$

Table 12.1: Energy hierarchy for a non-relativistic QED bound state.

Now let us generalize the problem. First, we will allow the magnitudes of the two charges to differ from each other. Specifically, we will keep the magnitude of the first charge as e and we will denote the magnitude of the second charge by Ze. Although Z has an obvious interpretation as the number of protons in a hydrogen-like atom, we will soon see how its inclusion is useful even for the ubiquitous systems in which $Z = 1$, such as positronium (e^+e^-), muo-

nium (μe), or muonic hydrogen (μp).

The second generalization we would like to make is that the pertinent mass scale should not be m, but rather, the reduced mass

$$\mu = \frac{mM}{m + M} \,. \tag{12.4}$$

When $m \ll M$, $\mu \simeq m$, but eventually we are going to derive results that are valid for any choices of m and M, and thus it is important to incorporate μ. This does not mean that m and M are absent, though. For example, the $\mathcal{O}(\alpha^4)$ hyperfine splitting for structureless spin-1/2 particles, as was first derived by Fermi [74], is

$$E_F = \frac{8}{3} \frac{\mu^3}{mM} (Z\alpha)^4 \,. \tag{12.5}$$

The factors of m and M in the denominator of (12.5) arise directly from the dipole moments of the particles, while the μ^3 must be present to provide E_F with an overall dimension of energy.

At this stage, we have three small parameters in the problem: α, $Z\alpha$, and either m/M or $(1 - m/M)$. While the entries in Table 12.1 summarize the leading order effects, there will be additional corrections that can be expressed in terms of one or more of these three small parameters. These additional corrections are given descriptive names based on which of the small parameters they incorporate. Energy level contributions that only depend on additional factors of $Z\alpha$ are known as binding corrections or, occasionally, relativistic corrections. Radiative corrections, meanwhile, depend on both α and $Z\alpha$ and are a result of Quantum Electrodynamics. Recoil corrections depend on m and M in a nontrivial way that cannot be derived directly in terms of μ. Finally, radiative recoil corrections are those which depend on all three of the small parameters.

We can also distinguish energy level corrections based on the source of the contribution, rather than the form of the result. With the lowest-order binding effect known exactly, every additional contribution will be obtained via traditional time-independent quantum-mechanical perturbation theory. The "soft" contributions arise from the long-range interactions of the bound state constituents, whereas the "hard" contributions correspond to the short-range interactions characterized by $\delta(r)$ terms in the perturbing potential. The soft contributions can be evaluated for arbitrary masses of the constituent particles because the essential soft dynamics of a non-relativistic bound state, as described by the Schrödinger equation, are characterized by the reduced mass of the system rather than the individual masses of the constituents. As a result, once the soft contributions are obtained in the equal mass case [75,76], the more general mass case follows easily. The hard contributions, on the other hand, result

from the relativistic region of loop-momentum integrals, and they are usually obtained as Taylor expansions of scattering amplitudes in terms of the spatial momentum components of the external particles, which are taken to be on mass shell. At lowest order in α, the hard diagrams should be evaluated exactly at threshold, whereby the constituents have zero relative velocity. This implies that the relevant loop-momentum integrals depend on only two scales: m and M. The hard contributions have a much more complicated dependence on the mass scales than the soft contributions do, and this is why we will expand the hard scattering diagrams in powers of either m/M or $(1 - m/M)$. In the next section, we will see in detail how to calculate these hard contributions.

12.2 Calculational Method

Consider the scattering amplitude between particles of masses m and M in Figure 12.1. We can construct the amplitude for this process by assembling the
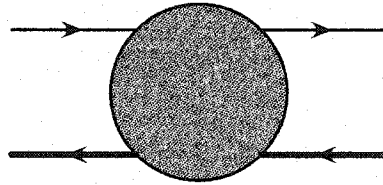
Figure 12.1: Sketch of a general scattering amplitude which produces corrections to the energy levels of a QED bound state. The thin and thick lines denote particles of mass m and M, respectively, and the central blob represents an unspecified QED interaction.

Feynman rules while moving backwards along each fermion line:

$$\mathcal{M} = i\left[\bar{u}(p)\mathcal{Q}_1 u(p)\right]\left[\bar{v}(P)\mathcal{Q}_2 v(P)\right] . \tag{12.6}$$

$\mathcal{Q}_1$ and $\mathcal{Q}_2$ incorporate every Feynman rule needed to describe the interactions in the blob. $\bar{u}(p)$ and $u(p)$ are the spinors for the light particle and in Minkowski space, the onshell condition is $p^2 = m^2$. Similarly, $\bar{v}(P)$ and $v(P)$ are the spinors for the heavy particle and $P^2 = M^2$. Since we are working at threshold, where the particles have no relative velocity, we do not allow a net momentum transfer from one particle to the other. This assumption already requires that the blob in Figure 12.1 contain at least one loop, since the propagator for a single photon, $-ig_{\mu\nu}/q^2$, would be singular when we constrain q^2 to be zero.

The amplitude (12.6) can be regarded as a perturbing potential via

$$\Delta U = -\mathcal{M} . \tag{12.7}$$

Since we work with momentum-space Feynman rules, we will need a Fourier transformation in order to obtain the configuration-space potential:

$$\Delta V = \Delta U \, \delta^3(\mathbf{r}) \, . \tag{12.8}$$

As anticipated in the previous section, these hard contributions are characterized by the δ-function in the perturbing potential. The energy shift induced by the perturbation ΔV is simply

$$\begin{aligned} \Delta E &= \langle \psi(\mathbf{r}) \, |\Delta V| \, \psi(\mathbf{r}) \rangle \\ &= -\mathcal{M} \, |\psi(0)|^2 \, . \end{aligned} \tag{12.9}$$

All hydrogenic wavefunctions vanish at the origin except for the S states ($\ell = 0$), and if we further restrict ourselves to the $1S$ states, we have

$$|\psi_{1S}(0)|^2 = \frac{(Z\alpha)^3 \mu^3}{\pi} \, . \tag{12.10}$$

Already we can see that a minimal two photon exchange in Figure 12.1 will lead to $\mathcal{O}\left((Z\alpha)^5\right)$ energy level shifts. Depending on the relative alignment of the spins of the constituent particles, a $1S$ state can either belong to the $J = 1$ triplet or the $J = 0$ singlet. The triplet and singlet states are often represented by the prefixes ortho- and para-, respectively. The hyperfine splitting represents the energy gap between these formerly degenerate states:

$$E_{\text{hfs}} = E_{\text{triplet}} - E_{\text{singlet}} \, . \tag{12.11}$$

The average energy shift — which is very closely related to Lamb shift — will be defined as

$$E_{\text{aver}} = \frac{E_{\text{triplet}} \, d + E_{\text{singlet}}}{d+1} \, , \tag{12.12}$$

where $d = 3 - 2\epsilon$ is the number of spatial directions, in dimensional regularization, in which the polarization vector of the triplet state can point.

We now have most of the formalism in place except for one key point: how do we choose the spinors $\overline{u}$, u, $\overline{v}$, and v in (12.6) so that the incoming and outgoing pairs of particles have a well-defined total spin? With the particles at rest, we can define a bound state wavefunction $\psi = u\overline{v}$ so that $\psi^\dagger = v\overline{u}$ and (12.6) becomes

$$\mathcal{M} = i \, \text{Tr} \left\{ \psi^\dagger \mathcal{Q}_1 \psi \mathcal{Q}_2 \right\} \, . \tag{12.13}$$

The wavefunctions can be expressed [75] as

$$\psi_p = \frac{1+\gamma_0}{2\sqrt{2}}\gamma_5 \,, \tag{12.14}$$

$$\psi_o = \frac{1+\gamma_0}{2\sqrt{2}}\gamma\cdot\xi \,, \tag{12.15}$$

where ξ is the polarization vector. We will average over the d directions of ξ immediately after taking the trace in (12.13) by creating the polarization four-vector $\xi = (0,\xi)$ and using the identity

$$\langle (\xi\cdot A)(\xi\cdot B)\rangle = \frac{1}{d}\left(A_0 B_0 - A\cdot B\right). \tag{12.16}$$

Note that since $p = (m,0)$, we can remove any explicit reference to the zeroth component of the four-vectors in (12.14), (12.15), and (12.16) via $\gamma_0 = \not{p}/m$ and $A_0 = A\cdot p/m$, leaving us with scalar products that are much more convenient to work with than specific components of vectors.

One-Loop Results

Recapitulating the formalism of the previous section, we can calculate the energy level shifts to the $1S$ singlet and triplet states with the expression

$$\Delta E = -i\frac{(Z\alpha)^3\mu^3}{\pi}\,\mathrm{Tr}\left\{\psi^\dagger Q_1\psi Q_2\right\}\,, \tag{12.17}$$

where ψ is taken to be either ψ_p or ψ_o depending on the spin of the bound state, and Q_1 and Q_2 depend on the specific structure of the scattering diagram. We will now illustrate this procedure by calculating the $\mathcal{O}\left((Z\alpha)^5\right)$ energy level shifts induced by the one-loop diagrams in Figure 12.2.
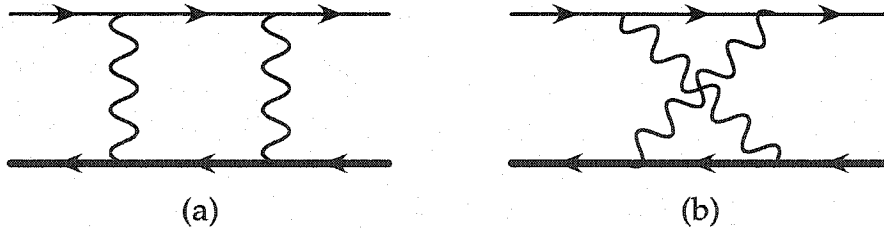
Figure 12.2: Diagrams contributing to the $\mathcal{O}\left((Z\alpha)^5\right)$ energy level shifts of a QED bound state.

The contribution to the energy shift from diagram (a) is

$$\Delta E_{1a} = -i\frac{(Z\alpha)^3\mu^3}{\pi}\int[d^Dk]\,\frac{-ig_{\mu\alpha}}{k^2}\,\frac{-ig_{\nu\beta}}{k^2}\,(-ie)^2(-iZe)^2 \qquad (12.18)$$

$$\times\,\mathrm{Tr}\left\{\psi^\dagger\gamma^\mu\frac{i(\not k+\not p+m)}{k^2+2kp}\gamma^\nu\psi\gamma^\beta\frac{i(\not k-P+M)}{k^2-2kP}\gamma^\alpha\right\}\,.$$

Notice that the incoming momentum P runs backward with respect to the arrow in the propagator for the heavy fermion, but since the loop momentum k is circulating clockwise, the denominator is $(k-P)^2+M^2$, or more compactly, k^2-2kP.

The next steps are to insert either the spin-zero or spin-one wavefunctions and to take the trace. This will lead to various scalar products involving p, P, and k, all of which are either constant or can be expressed in terms of existing denominator factors, thereby leaving us with loop integrals of the form

$$\int\frac{[d^Dk]}{k^{2a}(k^2+2kp)^b(k^2-2kP)^c}\,. \qquad (12.19)$$

Since $p=(m,0)$ and $P=(M,0)$, the partial fraction identity

$$\frac{1}{(k^2+2kp)(k^2-2kP)}=\frac{1}{k^2(M+m)}\left\{\frac{m}{k^2+2kp}+\frac{M}{k^2-2kP}\right\} \qquad (12.20)$$

allows us to express the original two-scale integral as a pair of one-scale integrals, each of which can then be solved exactly. The integrals with p will finish with a factor of $m^{-2\epsilon}$, whereas the integrals with P will produce a factor of $M^{-2\epsilon}$. If the integrals were finite, these factors could be set to 1, but since the contributions of the individual loop integrals are typically divergent, we will need to be more careful. By writing

$$M^{-2\epsilon}=m^{-2\epsilon}\left(\frac{M}{m}\right)^{-2\epsilon}=m^{-2\epsilon}\left(1-2\epsilon\ln\frac{M}{m}+2\epsilon^2\ln^2\frac{M}{m}+\mathcal{O}\left(\epsilon^3\right)\right)\,, \qquad (12.21)$$

we can collect a factor of $m^{-2\epsilon}$ from every loop, regardless of how the integral is calculated.

Our final result for the hyperfine splitting due to the diagrams in Figure 12.2 is

$$\delta E_{\mathrm{hfs}}^1=-\frac{3mM}{M^2-m^2}\frac{Z\alpha}{\pi}\ln\frac{M}{m}E_F\,, \qquad (12.22)$$

in agreement with the result first obtained by [77], as expressed in the encyclopedic review article [78]. Notice that (12.22) is symmetric in m and M, as well

as finite in the limits $m \ll M$ and $m = M$.

Expansions in Mass Ratios

With an additional loop in the calculation, it will no longer be feasible to obtain compact solutions for the energy level shifts that are valid for any possible values of m and M. Instead, we will employ the expansion techniques of Chapter 7. In particular, we will consider two types of expansions.

If $m \sim M$, we will use the Taylor expansion technique of Section 7.2 to write

$$
\frac{1}{k^2 + 2kp} = \frac{1}{k^2 + 2kP(1-y)}
$$

$$
= \frac{1}{k^2 + 2kP} + y\,\frac{2kP}{(k^2 + 2kP)^2} + y^2\,\frac{(2kP)^2}{(k^2 + 2kP)^3} + \cdots , \quad (12.23)
$$

where the expansion parameter y is defined by

$$
y = 1 - \frac{m}{M} . \tag{12.24}
$$

This allows us to remove the small scale p from the loop integrals so that they only depend on the large scale P. Our result for the hyperfine splitting is

$$
\delta E^1_{\text{hfs}} = E_F\,\frac{Z\alpha}{\pi}\,\left(-\frac{3}{2} + \frac{y^2}{4} + \frac{y^3}{4} + \frac{y^4}{5} + \ldots \right) , \tag{12.25}
$$

which, after a bit of algebra, can be shown to be in agreement with the exact result of (12.31). If the constituents of the bound state are a particle-antiparticle pair, for example positronium, we can simply set $y = 0$, although it must be emphasized that we are including neither the annihilation diagram nor the anomalous magnetic moment diagram in Figure 12.3.

If $m \ll M$, we will use the asymptotic expansion technique of Section 7.3. At the one-loop level, this entails dividing the loop integrals into two regions: $k \sim m$ and $k \sim M$. When $k \sim M$, we can expand the light fermion propagator via

$$
\frac{1}{k^2 + 2kp} = \frac{1}{k^2 + 2rkP}
$$

$$
= \frac{1}{k^2} - r\,\frac{2kP}{k^4} + r^2\,\frac{(2kP)^2}{k^6} - \cdots , \tag{12.26}
$$
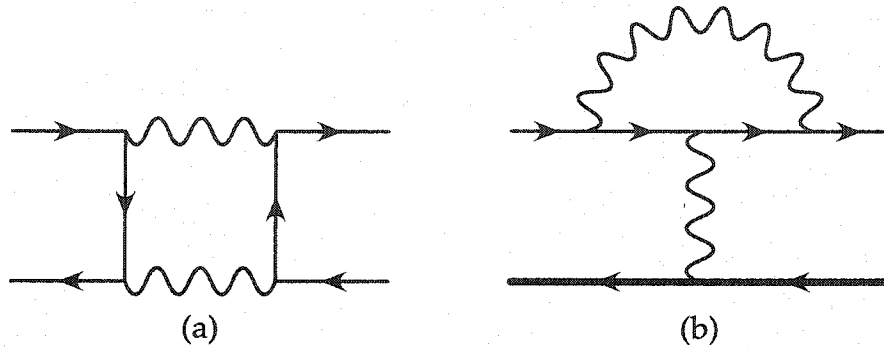
Figure 12.3: Annihilation and anomalous magnetic moment diagrams — contributing to the $\mathcal{O}\left((Z\alpha)^5\right)$ energy level shifts of a QED bound state — that we do not consider here.

where the expansion parameter r is defined by

$$r = \frac{m}{M}. \tag{12.27}$$

This allows us to remove the small scale p from the loop integrals so that they only depend on the large scale P. Turning to the other region, when $k \sim m$ we must expand the heavy fermion propagator:

$$\frac{1}{k^2 - 2kP} = -\frac{1}{2kP} - \frac{k^2}{(2kP)^2} - \frac{k^4}{(2kP)^3} - \cdots$$

$$= -r\frac{1}{2kp} - r^2\frac{k^2}{(2kp)^2} - r^3\frac{k^4}{(2kp)^3} - \cdots. \tag{12.28}$$

Although we have succeeded in removing the large scale P from the loop integrals, it has come at the price of eikonal propagators. As explained in Section 6.2, the pole terms of these propagators require extra attention. At the one-loop level, eikonal propagators are not much of a concern, since the partial fraction identity

$$\frac{1}{(2kp)(k^2 + 2kp)} = \frac{1}{k^2}\left(\frac{1}{2kp} - \frac{1}{k^2 + 2kp}\right) \tag{12.29}$$

allows us to remove either the eikonal propagator or the light fermion propagator. In the case of the former, this leads to a simple one-loop integral. In the case of the latter, the p in the eikonal propagator does not provide a true scale to the loop integral when $p = 0$, and so the scaleless loop integral is discarded, in accordance with the discussion in Section 2.3. Pictorially, we will denote eikonal

propagators with a double line so that

$$\Rightarrow \int \frac{[d^D k]}{k^{2a}(2kp \pm i\delta)^b} = 0 . \tag{12.30}$$

After calculating and combining the contributions from both regions, we obtain

$$\delta E^1_{\text{hfs}} = 3E_F \frac{Z\alpha}{\pi} \ln r \left(r + r^3 + r^5 + r^7 + \dots\right) , \tag{12.31}$$

in agreement with the exact result of (12.22). Although the asymptotic expansion method (around $m/M = 0$) is more difficult to implement than the Taylor expansion technique (around $m/M = 1$), it is extremely useful given the small m/M ratios which characterize most of the phenomenologically important QED bound states. For example, in ordinary hydrogen $m_e/m_p \simeq 1/2000$, in muonium $m_e/m_\mu \simeq 1/200$, and in muonic hydrogen $m_\mu/m_p \simeq 1/9$.

12.3 Radiative Recoil Corrections

The first class of two-loop contributions we will consider are the $\mathcal{O}\left(\alpha(Z\alpha)^5\right)$ radiative recoil corrections to the bound state energy levels. The additional factor of α relative to the $\mathcal{O}\left((Z\alpha)^5\right)$ corrections of Section 12.2 suggests that the additional photon will couple entirely to the light fermion, and thus we need to consider the 6 diagrams in Figure 12.4. We will multiply diagrams (c) and (f) by 2 in lieu of calculating their mirror images. In addition, we will need to incorporate renormalization contributions in accordance with the methods of Chapter 9. Specifically, this entails a wavefunction renormalization on the light fermion line of the one-loop diagrams in Figure 12.2, as well as a mass renormalization on the light fermion propagators in those diagrams.

Expansion About $m/M = 1$

Starting with the case of $m \simeq M$, we can expand each of the light fermion propagators as a Taylor series in $y = (1 - m/M)$ so that the small scale is removed from the loop integrals. At this stage, the most general loop integral we can have is from diagram (c) in Figure 12.4, containing the denominator factors:

$$k_1^2 \quad k_2^2 \quad k_2^2 + 2k_2P \quad (k_1 + k_2)^2 + 2(k_1 + k_2)P \quad k_1^2 + 2k_1P \quad k_1^2 - 2k_1P .$$
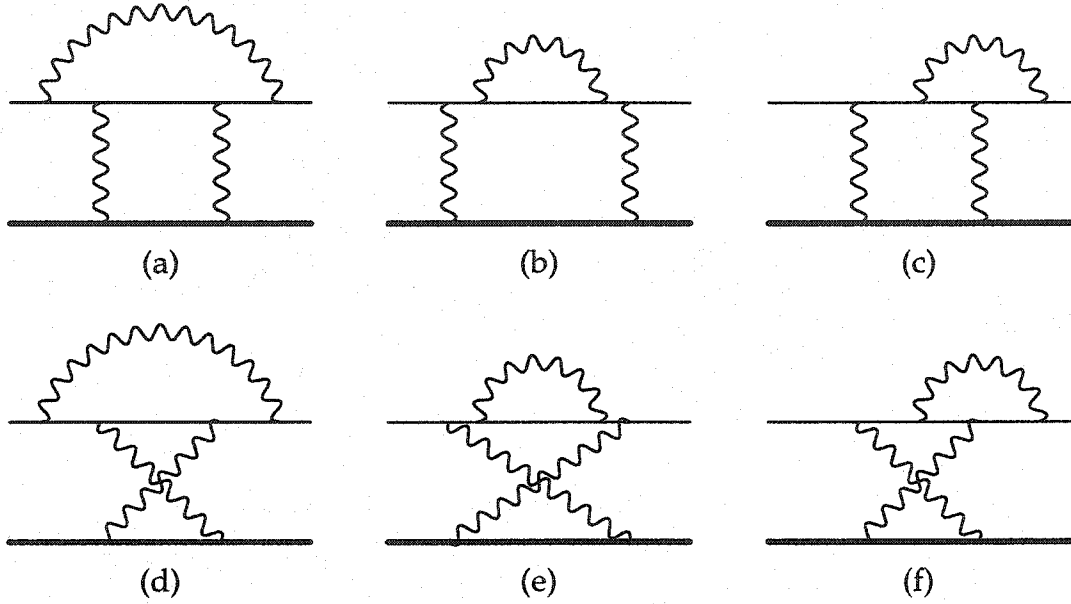
Figure 12.4: Diagrams contributing to the $\mathcal{O}\left(\alpha(Z\alpha)^5\right)$ radiative recoil corrections to the energy levels of a QED bound state. Diagrams (c) and (f) are multiplied by 2 for symmetry.

The partial fraction identity

$$\frac{1}{(k_1^2 - 2k_1 P)(k_1^2 + 2k_1 P)} = \frac{1}{2k_1^2}\left\{\frac{1}{(k_1^2 - 2k_1 P)} + \frac{1}{(k_1^2 + 2k_1 P)}\right\} \qquad (12.32)$$

can be used to remove one of the propagators so that the remaining five propagators constitute an integral of either the "N5" or "NP" type. These topologies are listed in the Appendix. The remainder of the calculation is straightforward and so we shall skip right to the results. Restoring the explicit mass dependence, we find for the hyperfine splitting that

$$\begin{aligned}
\delta E_{\text{hfs}}^{\text{rad rec}} \simeq{} & \frac{8(Z\alpha)^4 \mu^3}{3mM}\alpha(Z\alpha)\left\{\left(\frac{3\zeta(3)}{4\pi^2} + \frac{7}{8\pi^2} + 2\ln 2 - \frac{79}{32}\right)\right.\\
& + \left(1 - \frac{m}{M}\right)\left(-\frac{3\zeta(3)}{4\pi^2} - \frac{21}{8\pi^2} - \frac{3}{4}\ln 2 + \frac{25}{96}\right)\\
& + \left(1 - \frac{m}{M}\right)^2\left(-\frac{19}{24\pi^2} - \frac{3}{8}\ln 2 - \frac{19}{384}\right)\\
& + \left(1 - \frac{m}{M}\right)^3\left(-\frac{1}{8\pi^2} - \frac{3}{16}\ln 2 - \frac{55}{576}\right)
\end{aligned}$$

$$+ \left(1 - \frac{m}{M}\right)^4 \left(\frac{57}{400\pi^2} - \frac{3}{32}\ln 2 - \frac{2147}{23040}\right)$$

$$+ \left(1 - \frac{m}{M}\right)^5 \left(\frac{11}{40\pi^2} - \frac{3}{64}\ln 2 - \frac{631}{7680}\right)$$

$$+ \left(1 - \frac{m}{M}\right)^6 \left(\frac{41389}{117600\pi^2} - \frac{3}{128}\ln 2 - \frac{46679}{645120}\right)$$

$$+ \left(1 - \frac{m}{M}\right)^7 \left(\frac{141709}{352800\pi^2} - \frac{3}{256}\ln 2 - \frac{10561}{161280}\right) \qquad (12.33)$$

$$+ \left(1 - \frac{m}{M}\right)^8 \left(\frac{5539481}{12700800\pi^2} - \frac{3}{512}\ln 2 - \frac{157753}{2580480}\right) \Bigg\} ,$$

and for the spin-independent energy shift we obtain

$$\delta E_{\text{aver}}^{\text{rad rec}} \simeq \alpha(Z\alpha)^5 \frac{\mu^3}{m^2} \Bigg\{ \left(\frac{9\zeta(3)}{2\pi^2} - \frac{35}{4\pi^2} + \frac{31}{12}\right)$$

$$+ \left(1 - \frac{m}{M}\right) \left(-\frac{9\zeta(3)}{2\pi^2} + \frac{39}{2\pi^2} - \frac{7}{2}\ln 2 + \frac{45}{32}\right)$$

$$+ \left(1 - \frac{m}{M}\right)^2 \left(\frac{61}{24\pi^2} + \frac{9}{4}\ln 2 - \frac{119}{72}\right)$$

$$+ \left(1 - \frac{m}{M}\right)^3 \left(-\frac{29}{24\pi^2} + \frac{1}{8}\ln 2 + \frac{31}{288}\right)$$

$$+ \left(1 - \frac{m}{M}\right)^4 \left(\frac{233}{600\pi^2} + \frac{1}{16}\ln 2 - \frac{571}{11520}\right)$$

$$+ \left(1 - \frac{m}{M}\right)^5 \left(\frac{509}{1200\pi^2} + \frac{1}{32}\ln 2 - \frac{187}{3840}\right)$$

$$+ \left(1 - \frac{m}{M}\right)^6 \left(\frac{135311}{352800\pi^2} + \frac{1}{64}\ln 2 - \frac{13439}{322560}\right)$$

$$+ \left(1 - \frac{m}{M}\right)^7 \left(\frac{39721}{117600\pi^2} + \frac{1}{128}\ln 2 - \frac{1427}{40320}\right) \qquad (12.34)$$

$$+ \left(1 - \frac{m}{M}\right)^8 \left(\frac{5683891}{19051200\pi^2} + \frac{1}{256}\ln 2 - \frac{16901}{552960}\right) \Bigg\} .$$

There is, however, another set of diagrams that produces $\mathcal{O}\left(\alpha(Z\alpha)^5\right)$ effects. The vacuum polarization diagrams in Figure 12.5, along with a charge renormalization factor applied to the photons in the one-loop diagrams, should also be considered. This additional class of contributions will be separately finite, as can be justified using the group theoretical considerations of Chapter 8. By including these vacuum polarization effects and setting $m = M$, we can obtain
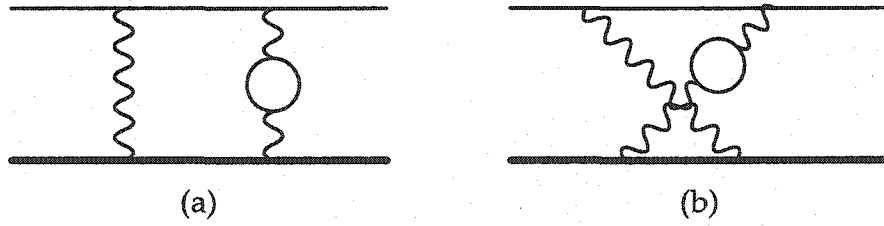
Figure 12.5: Vacuum polarization diagrams contributing to the $\mathcal{O}\left(\alpha(Z\alpha)^5\right)$ energy level shifts of a QED bound state.

the energy level corrections for positronium, provided we multiply our results by 2 to allow the radiative photon to couple to either line and we do not double-count the vacuum polarization contributions. With $\mu = m/2$, we obtain

$$\delta E_{\text{hfs}}^{\text{rad rec}} = m\alpha^6 \left\{ \frac{\zeta(3)}{2\pi^2} - \frac{79}{48} + \frac{41}{36\pi^2} + \frac{4}{3}\ln 2 \right\}, \tag{12.35}$$

$$\delta E_{\text{aver}}^{\text{rad rec}} = m\alpha^6 \left\{ \frac{9\zeta(3)}{8\pi^2} + \frac{97}{144} - \frac{1025}{432\pi^2} \right\}, \tag{12.36}$$

in complete agreement with the analytic result first derived in [79].

Expansion About $m/M = 0$

Now that we have checked our $(1-m/M)$ calculations against the known positronium results, the next step will be to examine the $m \ll M$ limit using an expansion in m/M. Our goal is to show that the two expansions match for a range of intermediate values of m/M so that for any choice of m and M, at least one of the expansions will produce reliable results. For consistency with (12.33) and (12.34), we will not include the vacuum polarization contributions of Figure 12.5. This will allow us to focus on the most difficult aspects of the calculation for which our method can provide new results.

In order to apply the asymptotic expansion techniques of Section 7.3, we will need to consider five distinct momentum regions of the loop integrals, as shown in Figure 7.4. Since the expansion procedure is somewhat subtle, we will take a moment to describe the process for each of the five regions. As before, the most general integral that we must consider is from diagram (c) in Figure 12.4, and prior to any expansions, it contains the denominator factors

$$k_1^2 \qquad k_2^2 \qquad k_2^2 + 2k_2 p \qquad (k_1 + k_2)^2 + 2(k_1 + k_2)p \qquad k_1^2 + 2k_1 p \qquad k_1^2 - 2k_1 P \,.$$

In Region 1, we have k_1, k_2, and $(k_1 + k_2)$ all $\sim M$, and therefore we can

expand all of the light fermion propagators,

$$\frac{1}{\ell^2 + 2\ell p} = \frac{1}{\ell^2} - \left(\frac{m}{M}\right)\frac{2\ell P}{\ell^4} + \left(\frac{m}{M}\right)^2\frac{(2\ell P)^2}{\ell^6} - \cdots ,\tag{12.37}$$

where ℓ represents k_1, k_2, or $(k_1 + k_2)$. These expansions will hereafter be abbreviated as $(\ell^2 + 2\ell p) \to \ell^2$ since we are primarily concerned with the set of denominator factors which might appear in the loop integrals. After the expansions, the set of denominator factors in Region 1 is transformed to

$$k_1^2 \quad k_2^2 \quad (k_1 + k_2)^2 \quad k_1^2 - 2k_1 P ,$$

so that we can first evaluate the k_2-integral as a massless subloop and then solve the k_1-integral.

In Region 2, $k_1 \sim M$ and $k_2 \sim m$. Here, we will expand $(k_1^2 + 2k_1 p) \to k_1^2$ and $((k_1 + k_2)^2 + 2(k_1 + k_2)p) \to k_1^2$, leaving us with

$$k_1^2 \quad k_2^2 \quad k_2^2 + 2k_2 p \quad k_1^2 - 2k_1 P .$$

The k_1- and k_2-integrals have factored and can easily be evaluated.

In Region 3, k_1 and k_2 are $\sim M$ but $(k_1 + k_2) \sim m$. This situation was discussed in detail at the end of Section 7.3, where we found that the expansions $(k_1^2 + 2k_1 p) \to k_1^2$, $(k_2^2 + 2k_2 p) \to k_2^2$, and $k_2^2 \to k_1^2$ were required, so that we have

$$k_1^2 \quad (k_1 + k_2)^2 + 2(k_1 + k_2)p \quad k_1^2 - 2k_1 P .$$

After the shift $k_2 \to (k_2 - k_1)$, we can see that the k_1- and k_2-integrals have been factored.

In Region 4, $k_1 \sim m$ and $k_2 \sim M$. After the expansions $(k_2^2 + 2k_2 p) \to k_2^2$ and $((k_1 + k_2)^2 + 2(k_1 + k_2)p) \to k_2^2$, the only k_2-dependent denominator factor is k_2^2. We can therefore discard Region 4 due to the presence of such scaleless integrals.

In Region 5, k_1 and k_2 are both $\sim m$. Here, we can only expand the heavy fermion propagator $(k_1^2 - 2k_1 P) \to 2k_1 P$. This eikonal propagator can be written in terms of $2k_1 p$ so that only the small scale remains in the integral. The resulting two-loop eikonal integrals belong to the "E2" topology. This topology, as defined in the Appendix, was solved for the first time in conjunction with this calculation.

We can assemble the contributions from the four nontrivial regions to produce the final result. For the hyperfine splitting we obtain

$$\delta E_{\mathrm{hfs}}^{\mathrm{rad\ rec}} \simeq \frac{8(Z\alpha)^4\mu^3}{3mM}\alpha(Z\alpha)\left\{\ln 2 - \frac{13}{4}\right.$$

$$+ \left(\frac{m}{M}\right)\left(\frac{15}{4\pi^2}\ln\frac{M}{m} + \frac{1}{2} + \frac{6\zeta(3)}{\pi^2} + \frac{17}{8\pi^2} + 3\ln 2\right)$$

$$- \left(\frac{m}{M}\right)^2\left(\frac{3}{2} + 6\ln 2\right)$$

$$+ \left(\frac{m}{M}\right)^3\left(\frac{61}{12\pi^2}\ln^2\frac{M}{m} + \frac{1037}{72\pi^2}\ln\frac{M}{m}\right.$$

$$\left. + \frac{133}{72} + \frac{9\zeta(3)}{2\pi^2} + \frac{5521}{288\pi^2} + 3\ln 2\right)$$

$$- \left(\frac{m}{M}\right)^4\left(\frac{163}{48} + 6\ln 2\right)$$

$$+ \left(\frac{m}{M}\right)^5\left(\frac{331}{40\pi^2}\ln^2\frac{M}{m} + \frac{5761}{300\pi^2}\ln\frac{M}{m} + \frac{691}{240}\right.$$

$$\left. + \frac{9\zeta(3)}{2\pi^2} + \frac{206653}{8000\pi^2} + 3\ln 2\right)$$

$$\left. - \left(\frac{m}{M}\right)^6\left(\frac{577}{120} + 6\ln 2\right)\right\}, \tag{12.38}$$

while for the spin-independent energy shift we find

$$\delta E_{\text{aver}}^{\text{rad rec}} \simeq \alpha(Z\alpha)^5\frac{\mu^3}{m^2}\left\{\frac{139}{32} - 2\ln 2\right.$$

$$+ \left(\frac{m}{M}\right)\left(\frac{3}{4} + \frac{6\zeta(3)}{\pi^2} - \frac{14}{\pi^2} - 2\ln 2\right)$$

$$+ \left(\frac{m}{M}\right)^2\left(-\frac{127}{32} + 8\ln 2\right)$$

$$+ \left(\frac{m}{M}\right)^3\left(-\frac{8}{3\pi^2}\ln^2\frac{M}{m} - \frac{55}{18\pi^2}\ln\frac{M}{m} + \frac{47}{36}\right.$$

$$\left. - \frac{3\zeta(3)}{\pi^2} - \frac{85}{9\pi^2} - 2\ln 2\right)$$

$$+ \left(\frac{m}{M}\right)^4\left(-\frac{55}{24} + 4\ln 2\right)$$

$$+ \left(\frac{m}{M}\right)^5\left(\frac{37}{60\pi^2}\ln^2\frac{M}{m} + \frac{29}{900\pi^2}\ln\frac{M}{m} + \frac{1027}{360}\right.$$

$$\left. - \frac{3\zeta(3)}{\pi^2} - \frac{370667}{36000\pi^2} - 2\ln 2\right)$$

$$+ \left(\frac{m}{M}\right)^6\left(-\frac{67}{20} + 4\ln 2\right)$$

$$+ \left(\frac{m}{M}\right)^7 \left(\frac{199}{70\pi^2} \ln^2 \frac{M}{m} - \frac{1759}{7350\pi^2} \ln \frac{M}{m} + \frac{887}{210}\right.$$

$$\left.\left. -\frac{3\zeta(3)}{\pi^2} - \frac{241491119}{18522000\pi^2} - 2\ln 2\right)\right\} . \tag{12.39}$$

The terms up to $\mathcal{O}\left((m/M)^2\right)$ were known previously [78] and the remaining terms of the expansions, save for the last one, were first presented in [80]. The coefficient of the $\mathcal{O}(m/M)$ term in (12.39) was the subject of some controversy, since two different numerical results have been reported, [81–83] and [84]. Our result for this term,

$$\alpha(Z\alpha)^5 \frac{\mu^3}{m^2} \frac{m}{M} \left(\frac{3}{4} + \frac{6\zeta(3)}{\pi^2} - \frac{14}{\pi^2} - 2\ln 2\right) \simeq -1.32402796 \, \alpha(Z\alpha)^5 \frac{\mu^3}{m^2} \frac{m}{M} , \tag{12.40}$$

is in excellent agreement with the numerical result of [84] where the coefficient $-1.324029(2)$ was obtained, and has since been confirmed in an independent analytical calculation [85].

Computationally, it becomes quite expensive to calculate additional terms in the expansions of (12.38) and (12.39). Furthermore, the presence of large logarithms in these results does not bode well for the convergence of these expressions for moderate values of m/M. Comparing the results from the m/M expansion with those of the $(1 - m/M)$ expansion, as expressed in (12.33) and (12.34), we find that we do have a region of overlap where the two expansions match, but that the region is very narrow. In Figure 12.6, we show this matching for both the hyperfine splitting and the average energy shift by plotting the m/M expansion from the left and the $(1-m/M)$ expansion from the right. The two expansions match at $m/M = 0.15$, a reflection of the poor convergence of the m/M expansions resulting from the large logarithms. Nevertheless, we have achieved our goal of calculating the radiative recoil corrections for arbitrary values of m and M.

12.4   Pure Recoil Corrections

Now that we have carefully constructed a procedure by which we can calculate certain classes of corrections to the energy levels of QED bound states, we will now use this machinery to evaluate the $\mathcal{O}\left((Z\alpha)^6\right)$ pure recoil corrections generated by the diagrams in Figure 12.7.

Unlike the radiative recoil contributions of Section 12.3, these $\mathcal{O}\left((Z\alpha)^6\right)$ pure recoil corrections require no renormalization factors. This is because the one-loop results, to which the renormalization factors will be applied, are $\mathcal{O}\left((Z\alpha)^5\right)$ and all possible renormalization factors are either $\mathcal{O}(\alpha)$ or $\mathcal{O}(Z^2\alpha)$, thereby
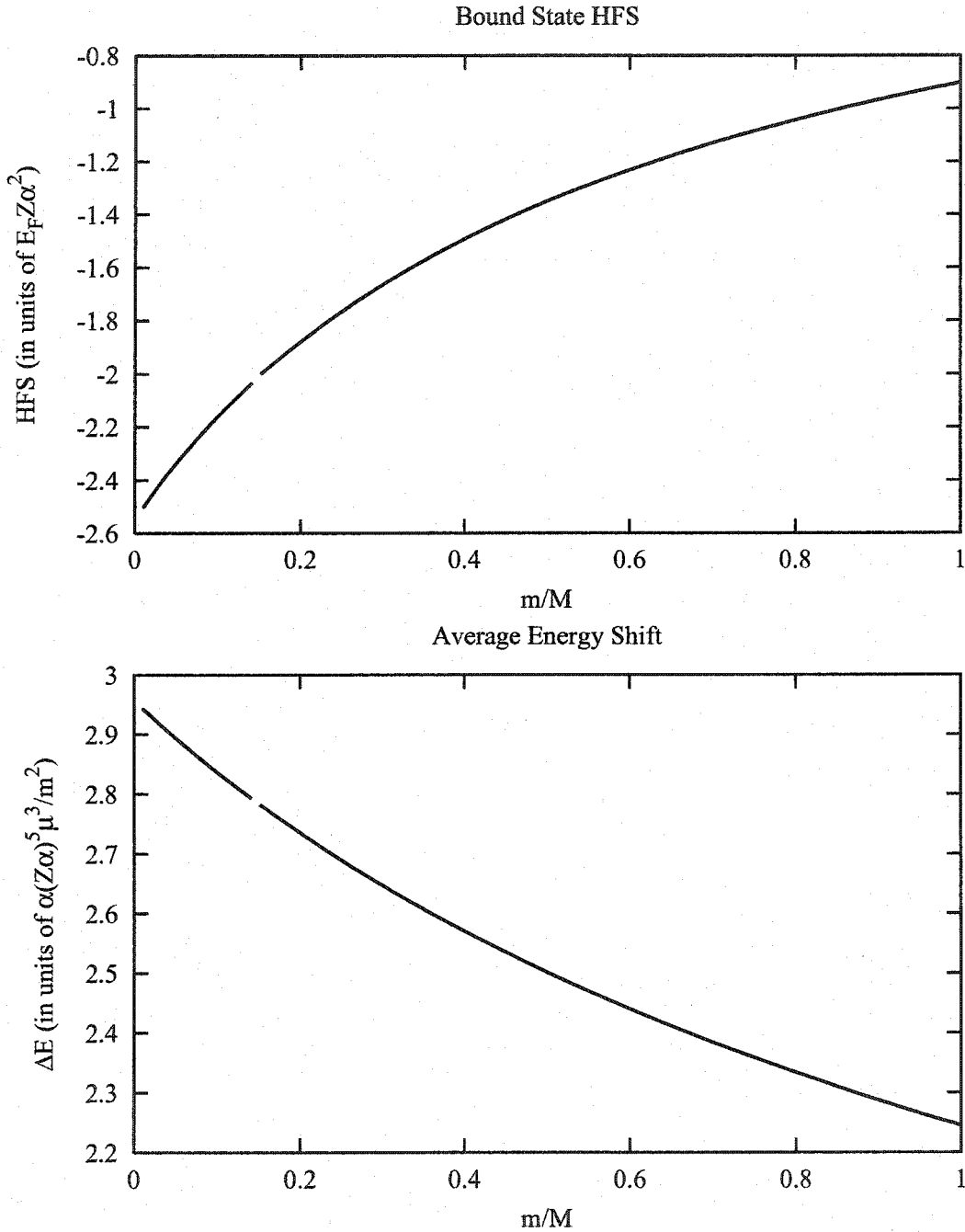
Figure 12.6: $\mathcal{O}(\alpha(Z\alpha)^5)$ radiative recoil contributions to the hyperfine splitting and average energy shift for arbitrary values of m and M. The curves from the left, taken from the m/M expansion, match at $m/M = 0.15$ with the curves from the right, obtained by the expansion in $(1 - m/M)$.
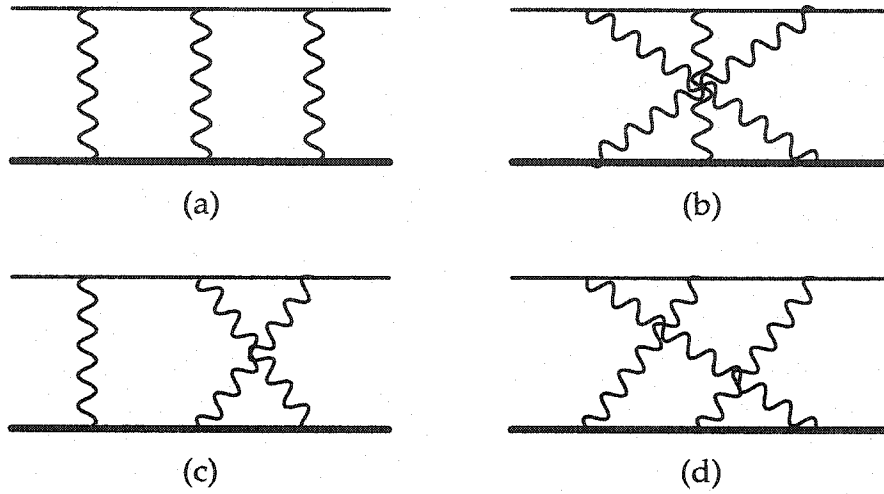
Figure 12.7: Diagrams contributing to the $\mathcal{O}\left((Z\alpha)^6\right)$ pure recoil corrections to the energy levels of a QED bound state. Diagrams (c) and (d) are multiplied by 2 for symmetry.

making it impossible to generate any contributions of $\mathcal{O}\left((Z\alpha)^6\right)$. On the other hand, the soft-scale effects that we discussed at the end of Section 12.1 can generate $\mathcal{O}\left((Z\alpha)^6\right)$ corrections, and thus the hard-scale contributions that we are about to calculate need not be finite. The $\mathcal{O}\left(\alpha(Z\alpha)^5\right)$ radiative recoil corrections of Section 12.3, conversely, receive no such soft-scale contributions and therefore these hard-scale effects must be finite.

Expansion About $m/M = 1$

As before, the $m \simeq M$ limit suggests an expansion in $(1 - m/M)$ which removes the small scale p from the light fermion propagators. The only complication that arises is that there are as many as seven different types of propagators for each diagram after the expansion. Since a two-loop topology only has five nontrivial scalar products, we will be able to construct partial fraction identities that reduce the number of propagators in each loop integral to five.

The result for this contribution to the hyperfine splitting is

$$
\begin{aligned}
\delta E_{\text{hfs}}^{\text{rec soft}} \;\simeq\; & \frac{8(Z\alpha)^6\mu^3 m^{-4\epsilon}}{3mM} \left\{ \left(-\frac{1}{8\epsilon} - \frac{51\zeta(3)}{8\pi^2} + \frac{5}{4\pi^2} - \frac{3}{4}\ln 2 \right) \right. \\
& + \left(1 - \frac{m}{M}\right)\left(\frac{1}{4}\right) \\
& \left. + \left(1 - \frac{m}{M}\right)^2 \left(\frac{1}{32\epsilon} + \frac{21\zeta(3)}{32\pi^2} + \frac{1}{48\pi^2} + \frac{1}{16}\ln 2 + \frac{2}{9} \right) \right)
\end{aligned}
\tag{12.41}
$$

$$+ \left(1 - \frac{m}{M}\right)^3 \left(\frac{1}{32\epsilon} + \frac{21\zeta(3)}{32\pi^2} + \frac{1}{48\pi^2} + \frac{1}{16}\ln 2 + \frac{17}{144}\right)$$

$$+ \left(1 - \frac{m}{M}\right)^4 \left(\frac{3}{128\epsilon} + \frac{63\zeta(3)}{128\pi^2} - \frac{2633}{43200\pi^2} + \frac{3}{64}\ln 2 + \frac{667}{11520}\right)$$

$$+ \left(1 - \frac{m}{M}\right)^5 \left(\frac{1}{64\epsilon} + \frac{21\zeta(3)}{64\pi^2} - \frac{3083}{21600\pi^2} + \frac{1}{32}\ln 2 + \frac{37}{1152}\right) ,$$

and for the spin-independent energy shift we obtain

$$\delta E_{\text{aver}}^{\text{rec hard}} \simeq (Z\alpha)^6 \frac{\mu^3}{m^2} \left\{ \left(-\frac{3\zeta(3)}{\pi^2} - \frac{11}{2\pi^2} - \frac{13}{24}\right) \right.$$

$$+ \left(1 - \frac{m}{M}\right) \left(\frac{3\zeta(3)}{\pi^2} + \frac{11}{2\pi^2} + \frac{13}{24}\right)$$

$$+ \left(1 - \frac{m}{M}\right)^2 \left(-\frac{3\zeta(3)}{2\pi^2} + \frac{1}{12\pi^2} - \ln 2 + \frac{275}{288}\right)$$

$$+ \left(1 - \frac{m}{M}\right)^4 \left(\frac{413}{1800\pi^2} - \frac{203}{5760}\right)$$

$$+ \left.\left(1 - \frac{m}{M}\right)^5 \left(\frac{413}{1800\pi^2} - \frac{203}{5760}\right) . \right. \tag{12.42}$$

By setting $Z = 1$, $m = M$, and $\mu = m/2$ in (12.41) and (12.42), we produce expressions for positronium,

$$\delta E_{\text{hfs}}^{\text{rec hard}} = m\alpha^6 \left\{ -\frac{1}{24\epsilon} + \frac{1}{6}\ln m - \frac{17\zeta(3)}{8\pi^2} + \frac{5}{12\pi^2} - \frac{1}{4}\ln 2 \right\} , \tag{12.43}$$

$$\delta E_{\text{aver}}^{\text{rec hard}} = m\alpha^6 \left\{ -\frac{3\zeta(3)}{8\pi^2} - \frac{11}{16\pi^2} - \frac{13}{192} \right\} , \tag{12.44}$$

in agreement with [75, 76].

Expansion About $m/M = 0$

Turning to the $m \ll M$ limit, we construct an expansion in m/M by following a similar procedure to the one we discussed in Section 12.3 for the radiative recoil contributions. Since none of the four diagrams in Figure 12.7 is more general than the others, it is easiest to devise an algorithm for diagrams (a) and (b) first and then to construct an algorithm for diagrams (c) and (d). The most notable complication is that with two distinct heavy fermion lines in each diagram, we encounter a new class of eikonal integrals; a detailed listing of these integrals can be found in the Appendix.

Our result for the hyperfine splitting is

$$
\delta E_{\text{hfs}}^{\text{rec hard}} \simeq \frac{8(Z\alpha)^6 \mu^3 m^{-4\epsilon}}{3mM} \left\{ \frac{m}{M} \left(-\frac{1}{2\epsilon} - 6\ln 2 + \frac{5}{12} \right) \right.
$$
$$
+ \left(\frac{m}{M} \right)^2 \left(\frac{1}{\epsilon} + \frac{9}{2\pi^2} \ln^2 \frac{M}{m} + \left(\frac{27}{2\pi^2} - 1 \right) \ln \frac{M}{m} - \frac{23}{12} + \frac{33\zeta(3)}{\pi^2} + \frac{93}{4\pi^2} \right)
$$
$$
\left. + \left(\frac{m}{M} \right)^3 \left(-\frac{3}{2\epsilon} - 6\ln 2 + \frac{25}{12} \right) \right\} . \tag{12.45}
$$

The divergences in this result, as well as those in (12.41), are canceled by soft-scale terms, which can be calculated by extending the calculation of [75,76] to the unequal mass case, resulting in

$$
\delta E_{\text{hfs}}^{\text{rec soft}} = \frac{(Z\alpha)^6 \mu^5}{m^2 M^2} \left[-\frac{16}{3} \left(\log(2\mu Z\alpha) - \frac{1}{4\epsilon} \right) + \frac{4mM}{\mu^2} + \frac{230}{27} \right] . \tag{12.46}
$$

Combining the results of (12.45) and (12.46), we find that the total $\mathcal{O}\left((Z\alpha)^6\right)$ pure recoil contribution to the hyperfine splitting is

$$
\delta E_{\text{hfs}}^{\text{rec}} \simeq \frac{8(Z\alpha)^6 \mu^3}{3mM} \left\{ \frac{3}{2} + \frac{\mu^2}{mM} \left[\left(\frac{65}{18} - 8\ln 2 + 2\ln(Z\alpha)^{-1} \right) \right. \right. \tag{12.47}
$$
$$
+ \left(\frac{m}{M} \right) \left(\frac{9}{2\pi^2} \ln^2 \frac{M}{m} + \left(\frac{27}{2\pi^2} - 1 \right) \ln \frac{M}{m} - 12\ln 2 - \frac{13}{12} + \frac{33\zeta(3)}{\pi^2} + \frac{93}{4\pi^2} \right)
$$
$$
\left. \left. + \left(\frac{m}{M} \right)^2 \left(\frac{9}{\pi^2} \ln^2 \frac{M}{m} + \left(\frac{27}{2\pi^2} - 2 \right) \ln \frac{M}{m} - 13\ln 2 - \frac{4}{3} + \frac{66\zeta(3)}{\pi^2} + \frac{93}{2\pi^2} \right) \right] \right\} .
$$

The terms in the first line of (12.47) are in agreement with the result first obtained in [86]. The remaining terms, arising solely from the hard-scale contributions in (12.45), can be used to obtain an analytic approximation to the function $f(x)$ near $x = 1$ in Equation (72) of [87].

For the hard-scale contribution to the spin-independent energy shift we find

$$
\delta E_{\text{aver}}^{\text{rec hard}} \simeq (Z\alpha)^6 \frac{\mu^3}{m^2} \left\{ \frac{m}{M} \left(4\ln 2 - \frac{7}{2} \right) \right.
$$
$$
+ \left(\frac{m}{M} \right)^2 \left(\left(\frac{4}{\pi^2} - \frac{8}{3} \right) \ln \frac{M}{m} - \frac{12\zeta(3)}{\pi^2} + \frac{3}{\pi^2} + \frac{8}{3} \right)
$$
$$
+ \left(\frac{m}{M} \right)^3 \left(4\ln 2 - \frac{31}{6} \right) \tag{12.48}
$$
$$
\left. + \left(\frac{m}{M} \right)^4 \left(-\frac{11}{3\pi^2} \ln^2 \frac{M}{m} - \left(\frac{113}{18\pi^2} + 2 \right) \ln \frac{M}{m} - \frac{6\zeta(3)}{\pi^2} - \frac{1565}{72\pi^2} + \frac{62}{9} \right) \right\} .
$$

Average Energy Shift
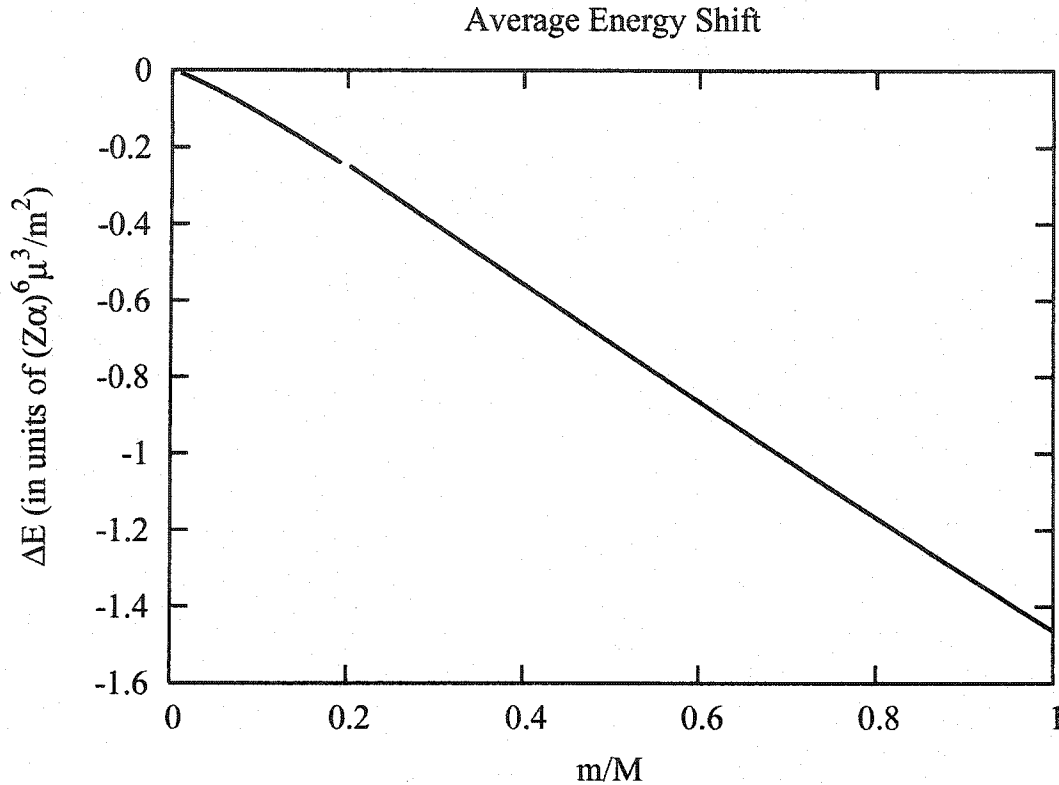
Figure 12.8: Finite portion of the $\mathcal{O}((Z\alpha)^6)$ hard-scale radiative recoil contributions to the hyperfine splitting and average energy shift for arbitrary values of m and M.

The m/M term of this expansion is in agreement with a calculation in [88]. To the best of our knowledge, the subsequent terms of this expansion are new. The computational overhead is greater for the pure recoil corrections than it was for the radiative recoil corrections and thus the expansions in this section contain fewer terms than their counterparts in Section 12.3. Nevertheless, we are still able to splice the two expansions together to produce smooth functions that are valid over the entire range of m/M. Figure 12.8 illustrates this behavior for the expressions for the average energy shift in (12.42) and (12.48).

In spite of the fact that the hard-scale contribution to the average energy shift given by (12.48) is finite at this order, soft contributions are also present and are needed to arrive at the physical result for this quantity. These soft contributions can be obtained by a calculation completely analogous to the one that produced (12.46).

12.5 Summary

In this chapter, we have demonstrated a method by which the corrections to the energy levels of a QED bound state, with constituents of mass m and M, can be expanded in either powers of m/M or $(1 - m/M)$. Both expansions are applied directly to the integrands of the loop integrals arising from the hard-scale contributions to the energy shifts. We have demonstrated the utility of these procedures by computing several terms in the expansions for the $\alpha(Z\alpha)^5$ radiative recoil and $(Z\alpha)^6$ pure recoil corrections to both the average energy shift and the hyperfine splitting of a general QED bound state. The $\mathcal{O}\left(\alpha(Z\alpha)^5\mu^3/(mM)\right)$ term in our result for the radiative recoil corrections to the average energy shift has resolved a discrepancy between two previous numerical results in the literature.

Further studies of QED bound state problems, using the methods described in this chapter, might involve higher-order corrections to the energy level shifts. Even in the absence of a complete calculation of such terms, it might be feasible to extract the terms enhanced by one or more factors of $\ln(M/m)$ by examining the singularities of the contributions from different expansion regions. Since these singularities must cancel in the complete result, their coefficients can be found by a partial calculation of the divergent parts of those contributions which can be evaluated most easily.

"They'll learn much more than I'll ever know and I think to myself what a wonderful world."

Louis Armstrong (*What a Wonderful World*)

Chapter 13

Top Quark Decay

The penultimate piece of the Standard Model — the top quark — was finally discovered in 1995 at Fermilab. Its unusually large mass, comparable to that of a large atom like tungsten, gives it a special status relative to the other quarks [89]. The Large Hadron Collider will produce about a million top quarks per day, therefore it is important to understand top quark behavior in order to distinguish this background from possible New Physics signals. This chapter deals with the decay of a top quark. After using the previously known tree-level and $\mathcal{O}(\alpha_s)$ results to explain the method of calculation, new $\mathcal{O}(\alpha_s^2)$ analytic results [90] are presented in Section 13.3.

13.1 Tree-Level Decay Rate

The top quark primarily decays into a b quark and a W boson, as shown in Figure 13.1. It is a simple textbook exercise [1] to calculate the decay rate,
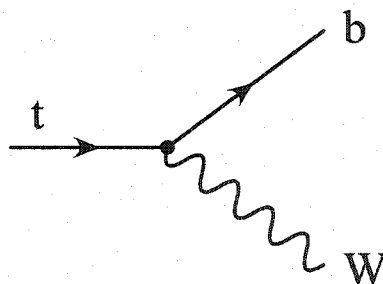
Figure 13.1: The tree-level decay $t \to bW$.

$\Gamma(t \to bW)$, for this process. Neglecting m_b, the result is

$$\Gamma(t \to bW) = \frac{G_F \left|V_{tb}\right|^2 m_t^3}{8\sqrt{2}\pi} \left(1 - \frac{m_W^2}{m_t^2}\right)^2 \left(1 + \frac{2m_W^2}{m_t^2}\right) , \qquad (13.1)$$

where G_F is the Fermi constant defined by

$$G_F = \frac{\sqrt{2}g_w^2}{8m_W^2} . \qquad (13.2)$$

If we rewrite (13.1) as

$$\Gamma(t \to bW) = \Gamma_0 \left[1 - 3\left(\frac{m_W^2}{m_t^2}\right)^2 + 2\left(\frac{m_W^2}{m_t^2}\right)^3\right] , \qquad (13.3)$$

where

$$\Gamma_0 = \frac{G_F \left|V_{tb}\right|^2 m_t^3}{8\sqrt{2}\pi} , \qquad (13.4)$$

we see that the analytic behavior of $\Gamma(t \to bW)$ with respect to the two mass scales m_W and m_t is that of a series in powers of (m_W^2/m_t^2). Hereafter denoting this ratio as

$$\omega \equiv \frac{m_W^2}{m_t^2} , \qquad (13.5)$$

we anticipate that perturbative corrections will modify (13.3) to

$$\Gamma(t \to bW) = \Gamma_0 \left[X_0 + \frac{\alpha_s}{\pi}X_1 + \left(\frac{\alpha_s}{\pi}\right)^2 X_2 + \mathcal{O}\left(\alpha_s^3\right)\right] , \qquad (13.6)$$

where X_0 is already known to be

$$X_0 = 1 - 3\omega^2 + 2\omega^3 \qquad (13.7)$$

and the higher-order corrections X_1 and X_2 will also be polynomials in ω. Unfortunately, it is not particularly convenient to evaluate the higher-order corrections in terms of $t \to bW$ diagrams like Figure 13.1 because in addition to gluon loops, we will have to consider diagrams with one or more gluons in the final state. We can circumvent this complication by using the optical theorem, the details of which we introduced in Section 6.3. The optical theorem asserts that we can obtain the decay width from

$$\Gamma = \frac{\mathrm{Im}(\Sigma)}{m_t} . \qquad (13.8)$$

The Γ in (13.8) includes decay modes with one or more low-energy gluons in the final state. The Σ in (13.8) denotes top quark self-energy diagrams with a b quark and W boson appearing as virtual particles in a loop. At tree-level, no gluons are present, and thus we need only consider the diagram in Figure 13.2. Applying the Feynman rules from Chapter 1, we find that
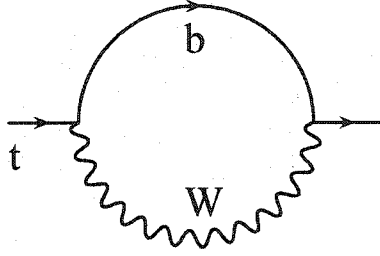
Figure 13.2: The self-energy diagram corresponding to the tree-level decay $t \to bW$.

$$i\Sigma = \int \frac{d^D k}{(2\pi)^D} \, \overline{u}(p) \left(\frac{ig_w V_{tb}}{2\sqrt{2}} \gamma^\mu (1 - \gamma_5) \right) \left(\frac{i(\not{k} + \not{p})}{(k+p)^2 + i\delta} \right) \left(\frac{ig_w V_{tb}^*}{2\sqrt{2}} \gamma^\nu (1 - \gamma_5) \right)$$
$$\times \left(\frac{-i(g_{\mu\nu} - k_\mu k_\nu / m_W^2)}{k^2 - m_W^2 + i\delta} \right) u(p) . \tag{13.9}$$

By the conditions of the optical theorem, the t quark spinors $\overline{u}(p)$ and $u(p)$ represent identical states, and therefore if we average over the initial spin states of the decaying quark, we can use a completeness relation [1] to replace the spinors in (13.9):

$$\overline{u}(p)[\cdots]u(p) \to \frac{1}{2} \text{Tr} \left\{ (\not{p} + m_t)[\cdots] \right\} . \tag{13.10}$$

Employing this simplification and using (13.2) to write g_w in terms of G_F, (13.9) becomes

$$\Sigma = \frac{iG_F |V_{tb}|^2}{2\sqrt{2}} \int \frac{d^D k}{(2\pi)^D} \frac{1}{[(k+p)^2 + i\delta] [k^2 - m_W^2 + i\delta]} \tag{13.11}$$
$$\times \text{Tr} \left\{ (\not{p} + m_t)\gamma^\mu (1 - \gamma_5)(\not{k} + \not{p})\gamma^\nu (1 - \gamma_5)(m_W^2 g_{\mu\nu} - k_\mu k_\nu) \right\} .$$

After evaluating the trace, Wick rotating, and writing the numerical factor at the front in terms of the Γ_0 defined in (13.4), we have

$$\Sigma = \frac{32\pi\Gamma_0}{m_t^3} \int [d^D k] \frac{[k^2(k \cdot p) + m_t^2 k^2 - 2m_W^2(k \cdot p) + 2(k \cdot p)^2 + 2m_W^2 m_t^2]}{(k+p)^2(k^2 + m_W^2)} . \tag{13.12}$$

The loop integral in (13.12) depends on two scales — m_W and m_t (via $p^2 = -m_t^2$) — and thus we will apply the asymptotic expansion method described in Chapter 7 to reduce the loop integrals to single-scale topologies. Specifically, we will divide the loop integral into two regions based on the magnitude of the loop momentum relative to the external scales. We use the term "soft" when the loop momentum is comparable to the scale of m_W (or more rigorously, $|k| < m_t$), and "hard" when the loop momentum is comparable to the scale of m_t ($|k| > m_W$).

For the soft region, the b quark propagator contains terms of different scales, thereby allowing us to expand

$$\frac{1}{(k+p)^2} = \frac{1}{p^2} \sum_{n=0}^{\infty} \left(-\frac{k^2 + 2k \cdot p}{p^2} \right)^n$$

$$= -\frac{1}{m_t^2} \sum_{n=0}^{\infty} \left(\frac{k^2 + 2k \cdot p}{m_t^2} \right)^n . \tag{13.13}$$

This leaves the W propagator $1/(k^2 + m_W^2)$ as the only denominator factor in the loop integral of (13.12). Due to the absence of p, this is a vacuum bubble integral, and as we saw at the end of Section 6.3, such integrals are strictly real. Since we are only interested in $\text{Im}(\Sigma)$, we can therefore discard the soft region at tree-level.

In the hard region, it is the W propagator that contains terms of different scales, thereby leading to the expansion

$$\frac{1}{k^2 + m_W^2} = \frac{1}{k^2} \sum_{n=0}^{\infty} \left(-\frac{m_W^2}{k^2} \right)^n . \tag{13.14}$$

The denominator factors of the loop integral (13.12) are now $(k+p)^2$ and k^2, and as we showed in Section 6.3, such integrals can produce imaginary terms. Using (13.5) to write $m_W^2 = \omega m_t^2$, we see that the loop integral now depends on the hard scale only. Writing all momenta in units of m_t, we obtain

$$\Sigma = 32\pi \Gamma_0 m_t^{D-3} \sum_{n=0}^{\infty} (-\omega)^n \int [d^D k] \frac{[k^2(k \cdot p) + k^2 - 2\omega(k \cdot p) + 2(k \cdot p)^2 + 2\omega]}{(k+p)^2 k^{2(n+1)}} . \tag{13.15}$$

It is clear from (13.15) that we will be able to write Σ as a series in powers of ω. As we first noted in Section 6.3, the imaginary terms for this particular class of loop integrals arise from an overall factor of

$$e^{i\pi\epsilon} = 1 + i\pi\epsilon - \frac{\pi^2\epsilon^2}{2} - \frac{i\pi^3\epsilon^3}{6} + \dots , \tag{13.16}$$

and thus, the only non-zero imaginary contributions to Σ correspond to $1/\epsilon$ divergences in the loop integral. An explicit calculation shows that only three terms in the ω-series diverge, with the result that

$$\text{Im}(\Sigma) = \frac{m_t^{-2\epsilon}\,\Gamma(1+\epsilon)}{(4\pi)^{D/2}}\,32\pi^2 m_t \Gamma_0 \left(\frac{1}{2} - \frac{3}{2}\omega^2 + \omega^3\right) . \tag{13.17}$$

Substituting this into (13.8) and sending $D \to 4$, we obtain the final result for the tree-level decay width,

$$\Gamma = \Gamma_0 \left(1 - 3\omega^2 + 2\omega^3\right) , \tag{13.18}$$

in agreement with (13.3).

For the tree-level computation, the optical theorem formalism is admittedly more cumbersome than the traditional calculation. In particular, we have added a loop integral where there was not one before. The utility of this approach will only become evident when we extend the calculation to $\mathcal{O}(\alpha_s)$ contributions and beyond. Essentially, we are willing to pay the price of an additional loop in exchange for being able to cast our results in terms of the self-energy-type loop integrals for which we have such a large number of techniques available to us (namely, Chapters 2-10).

13.2 $\mathcal{O}(\alpha_s)$ Corrections to the Decay Rate

With the optical theorem formalism for the tree-level calculation in place, it turns out that the $\mathcal{O}(\alpha_s)$ corrections are relatively easy to obtain. In order to generate $\mathcal{O}(\alpha_s)$ corrections from a self-energy diagram, we need only consider the different ways that a single gluon can be added to the tree-level diagram of Figure 13.2. Figure 13.3 shows the only three diagrams of this type. We multiply the contribution from the (a) diagram by 2 to account for its mirror image whereby a gluon runs from the b line to the outgoing t line.
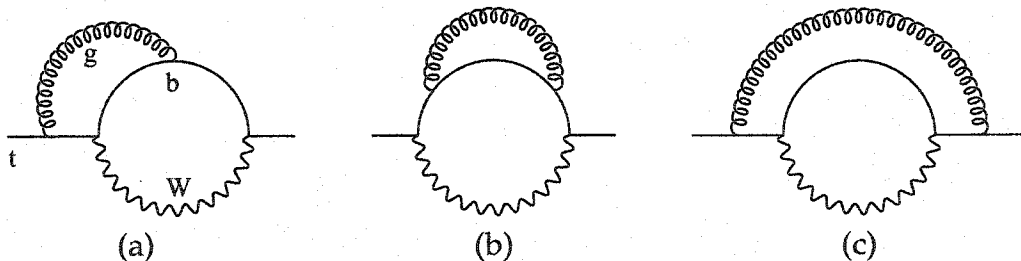
Figure 13.3: Diagrams contributing to top quark decay at $\mathcal{O}(\alpha_s)$.

As far as the loop integrals are concerned, diagrams (b) and (c) are specific cases of diagram (a), and thus we will focus on the latter. In Section 7.3, we saw how the method of asymptotic expansions gives rise to five momentum regions when applied to a two-loop integral with two scales. As we will soon see, only two of these are non-zero for the $\mathcal{O}(\alpha_s)$ diagrams of Figure 13.3. We will route the momenta through the diagrams as follows: k_1 will run clockwise through the W and b lines; k_2 will run counterclockwise through the gluon, t, and b; p will flow along the quark lines (t or b) from left to right. The five propagators are:

$$(k_1^2 + m_W^2) \qquad (k_1 + p)^2 \qquad (k_1 + k_2 + p)^2 \qquad (k_2^2 + 2k_2 p) \qquad k_2^2 \,. \qquad (13.19)$$

Labeling the regions using the convention in Figure 7.4, we will now discuss the five regions in sequential order.

In Region 1, k_1, k_2, and $(k_1 + k_2)$ are all hard. This allows us to expand the $(k_1^2 + m_W^2)$ propagator in terms of k_1^2 propagators, just as we did in (13.14) for the tree-level process. This leads to a single-scale two-loop integral belonging to the "T1" topology. The details of this topology can be found in the Appendix.

In Region 2, k_1 is hard and k_2 is soft. This means that expansions can be used to remove k_2 from the $(k_1 + k_2 + p)^2$ and $(k_2^2 + 2k_2 p)$ denominators, leaving us with k_2^2 as the only k_2-dependent propagator. In other words, the k_2-integral is scaleless and Region 2 does not contribute.

In Region 3, k_1 and k_2 are hard but $(k_1 + k_2)$ is soft. The only difference between this and Region 1 is the scale of $(k_1 + k_2)$, but this specification was not needed to transform Region 1 into a single-scale integral. This is the counterexample behind the "Proviso to Step 3" discussed in Section 7.3. We are to discard Region 3, as a failure to do so would result in a double-counting of contributions.

In Region 4, k_1 is soft and k_2 is hard. This allows us to expand k_1 out of the b quark propagators $(k_1 + p)^2$ and $(k_1 + k_2 + p)^2$ so that the k_1-integral is just a one-loop vacuum bubble at the soft scale and the k_2-integral is a one-loop self-energy diagram at the hard scale.

In Region 5, k_1 and k_2 are soft. Just as in Region 2, k_2 will be expanded out of the quark propagators $(k_1 + k_2 + p)^2$ and $(k_2^2 + 2k_2 p)$, resulting in a scaleless integral so that Region 5 does not contribute.

To summarize the list above, we have two regions to consider, both of which have hard k_2. We can allow k_1 to be either hard (Region 1) or soft (Region 4). This analysis extends to higher-order corrections to top decay. Specifically, we will always have two regions. The momentum circulating through the W and b lines may be hard or soft, but all gluon momenta must be hard.

Having established the expansion regions, we can return to the diagrams in

Figure 13.3. As mentioned above, the hard region is a straightforward calculation involving two-loop integrals from the "T1" topology. The soft region is in principle an even easier calculation because it involves the product of two one-loop integrals. Unlike the tree-level calculation, where the soft region produced no imaginary terms, there will be a non-zero contribution at $\mathcal{O}(\alpha_s)$. The leading contribution from this region is at ω^2, though. We can see this by noting that after we write the amplitude for a diagram in terms of G_F, the W propagator contribution to the loop integral is

$$\frac{(m_W^2 g_{\mu\nu} - (k_1)_\mu (k_1)_\nu)}{k_1^2 + m_W^2}. \tag{13.20}$$

Written in this form, the W propagator has no overall mass dependence and when k_1 is soft, it is $\mathcal{O}(1)$ with respect to ω. The k_1-integration element has a mass dimension of m_W^D, therefore the soft-scale vacuum bubble produces $\omega^{D/2}$ terms. With $D = 4 - 2\epsilon$, the "4" leads to ω^2 being the leading contribution from the soft region, and the "(-2ϵ)" gives rise to logarithm terms, $\ln \omega$, arising from

$$\begin{aligned} m_W^{-2\epsilon} &= m_t^{-2\epsilon} \omega^{-\epsilon} \\ &= m_t^{-2\epsilon} \left(1 - \epsilon \ln \omega + \frac{\epsilon^2}{2} \ln^2 \omega + \mathcal{O}(\epsilon^3) \right). \end{aligned} \tag{13.21}$$

Since we only have two regions, $\ln^2 \omega$ terms will be absent, lest we have $(\ln \omega)/\epsilon$ terms that cannot be canceled.

Once we calculate the contributions from the diagrams in Figure 13.3 and, referring to Chapter 8, multiply by an overall color factor of C_F, all that remains are the $\mathcal{O}(\alpha_s)$ renormalization contributions, as explained in Chapter 9. There are no gluons in the tree-level diagram, thus there is no charge renormalization to consider. The only internal quark line is massless, therefore no mass renormalization is required. This leaves the wavefunction renormalization as the only effect to consider. We need to multiply the $\mathcal{O}(\alpha_s)$ QCD wavefunction renormalization factor

$$\mathrm{WF} = -\frac{C_F \alpha_s}{4\pi} \left(\frac{3}{\epsilon} + 4 + \mathcal{O}(\epsilon) \right) \tag{13.22}$$

by the tree-level result (13.3). Since (13.22) has an $\mathcal{O}(1/\epsilon)$ term, we will need to include the the $\mathcal{O}(\epsilon)$ terms of the tree-level result.

Our final result for the $\mathcal{O}(\alpha_s)$ top decay width is

$$\Gamma_1 = \Gamma_0 C_F \left(\frac{\alpha_s}{\pi} \right) \left[\left(\frac{5}{4} - \frac{\pi^2}{3} \right) + \frac{3}{2}\omega + \omega^2 \left(\pi^2 - 6 + \frac{3}{2} \ln \omega \right) \right.$$

$$+\omega^3 \left(\frac{46}{9} - \frac{2\pi^2}{3} - \frac{2}{3} \ln\omega \right) + \omega^4 \left(-\frac{7}{4} + \frac{3}{4} \ln\omega \right)$$

$$+\omega^5 \left(-\frac{49}{300} + \frac{1}{5} \ln\omega \right) + \omega^6 \left(-\frac{1}{60} + \frac{1}{12} \ln\omega \right)$$

$$+\omega^7 \left(\frac{31}{4900} + \frac{3}{70} \ln\omega \right) + \omega^8 \left(\frac{157}{16800} + \frac{1}{40} \ln\omega \right) + \mathcal{O}\left(\omega^9 \right) , \quad (13.23)$$

in agreement with the result first obtained in [91], and cast in a notation similar to ours in [92].

13.3 $\mathcal{O}\left(\alpha_s^2\right)$ Corrections to the Decay Rate

Let us now take another step forward and address the $\mathcal{O}\left(\alpha_s^2\right)$ corrections to the decay rate. This is undeniably a difficult calculation, and as a consequence, we will be well-served to divide it into more manageable pieces:

$$X_2 = C_F \left(T_R N_L X_L + T_R N_H X_H + C_F X_A + C_A X_{NA} \right) . \quad (13.24)$$

X_2 is the $(\alpha_s/\pi)^2$ coefficient in (13.6), X_L, X_H, X_A, and X_{NA} are the contributions associated with four sets of color factors, N_L is the number of quark species that are lighter than the top, and N_H is the number of quark species whose mass is equal to that of the top. Although these factors take on specific values in the context of QCD calculations for top quark decay, the cancellation of divergences and the gauge invariance of X_2 cannot arise from coincidental cancellations between the four terms in (13.24). Instead, each of the four terms must be finite and gauge invariant in isolation.

Renormalization Contributions

We will start by describing the renormalization contributions to the $\mathcal{O}\left(\alpha_s^2\right)$ top decay width so that we can provide results for each of the four X factors within the appropriate sections. There are three ways to generate $\mathcal{O}\left(\alpha_s^2\right)$ renormalization contributions: we could apply an $\mathcal{O}\left(\alpha_s\right)$ renormalization factor to an $\mathcal{O}\left(\alpha_s\right)$ diagram, we could apply an $\mathcal{O}\left(\alpha_s^2\right)$ renormalization factor to the tree-level diagram, or we could apply an $\mathcal{O}\left(\alpha_s\right)$ renormalization factor to an $\mathcal{O}\left(\alpha_s\right)$ renormalization factor applied to the tree-level diagram. This sounds more complicated than it really is.

Assuming that we have calculated the tree-level diagram to $\mathcal{O}\left(\epsilon^2\right)$, the $\mathcal{O}\left(\alpha_s^2\right)$ onshell wavefunction renormalization factor was first calculated in [93]. It was

extended to $\mathcal{O}(\alpha_s^3)$ in [94], from which we use

$$
\begin{aligned}
\text{WF} \;=\;& 1 + a_0 C_F \left(-\frac{3}{4\epsilon} - \frac{1}{1-2\epsilon} \right) \\
& + a_0^2 C_F \left\{ T_R N_L \left[\frac{1}{8\epsilon^2} + \frac{9}{16\epsilon} + \left(\frac{\pi^2}{12} + \frac{59}{32} \right) \right] \right. \\
& + T_R N_H \left[\frac{1}{4\epsilon^2} + \frac{19}{48\epsilon} + \left(-\frac{\pi^2}{3} + \frac{1139}{288} \right) \right] \\
& + C_F \left[\frac{9}{32\epsilon^2} + \frac{51}{64\epsilon} + \left(-\frac{13\pi^2}{16} + \frac{433}{128} - \frac{3\zeta(3)}{2} + \pi^2 \ln 2 \right) \right] \\
& \left. + C_A \left[-\frac{11}{32\epsilon^2} - \frac{101}{64\epsilon} + \left(\frac{5\pi^2}{16} - \frac{803}{128} + \frac{3\zeta(3)}{4} - \frac{\pi^2}{2} \ln 2 \right) \right] \right\} ,
\end{aligned}
\tag{13.25}
$$

where

$$
a_0 = \frac{\alpha_s \Gamma(1+\epsilon) m_t^{-2\epsilon}}{\pi (4\pi)^{-\epsilon}} .
\tag{13.26}
$$

The $\overline{MS}$ charge renormalization renormalization factor is

$$
\text{PH} = 1 + a_0 \left(T_R N_L \frac{1}{3\epsilon} + T_R N_H \frac{1}{3\epsilon} - C_A \frac{11}{12\epsilon} \right) .
\tag{13.27}
$$

This follows directly from the leading term of the $\overline{MS}$ QCD β-function, as calculated to $\mathcal{O}(\alpha_s^4)$ in [95]. The observation that, for the QCD color factors of $T_R = 1/2$ and $C_A = 3$, there are not enough species of quarks in the Standard Model to make the β-function positive is the smoking gun of asymptotic freedom.

Finally, the onshell mass renormalization constant, taken from [94], is

$$
\text{MC} = i m_t a_0 C_F \left(\frac{3}{4\epsilon} + \frac{1}{1-2\epsilon} \right) .
\tag{13.28}
$$

With the renormalization factors in place, let us recapitulate the required renormalization contributions. First, we take the mass renormalization constant in (13.28) and apply it to a set of one-gluon diagrams analogous to Figure 13.3 except with one of the top quark propagators included twice. Second, we apply the charge renormalization factor in (13.27) to the complete $\mathcal{O}(\alpha_s)$ result, including terms of $\mathcal{O}(\epsilon)$, in (13.23). Remember that (13.23) includes the $\mathcal{O}(\alpha_s)$ wavefunction renormalization factor applied to the tree-level result. Finally, we apply the wavefunction renormalization factor (13.26) to both the tree-level and $\mathcal{O}(\alpha_s)$ results.

Light Quark Loop Contributions

The simplest class of $\mathcal{O}\left(\alpha_s^2\right)$ corrections to the top quark decay width involves a light virtual quark loop. The three diagrams of this type are shown in Figure 13.4. As before, diagram (a) requires a symmetry factor of 2. Provided that
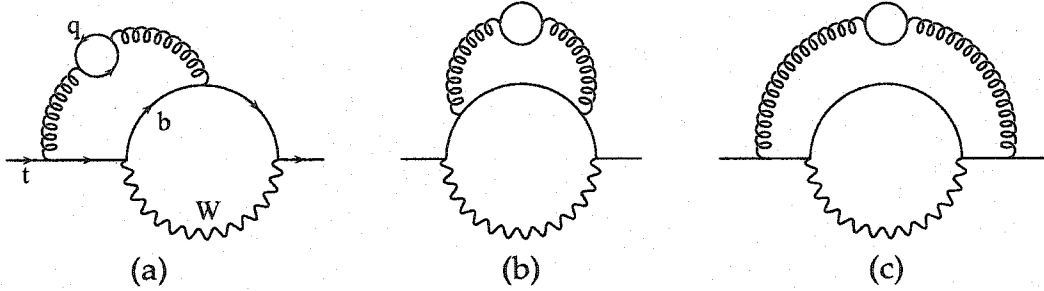
Figure 13.4: Quark loop contributions to top decay at $\mathcal{O}\left(\alpha_s^2\right)$.

we ignore the mass of the light quark altogether, the integral for the virtual quark loop can be performed immediately. The resulting topologies are identical to those of the $\mathcal{O}\left(\alpha_s\right)$ diagrams in Figure 13.3 except that the gluon propagator will now have a non-integer exponent. For the hard region, this means that we must use the "T1ep" topology instead of the "T1" topology. The recurrence relation algorithm for the "T1ep" topology was discussed in Section 4.5.

An analytic result for the light quark contribution to the top decay width at $\mathcal{O}\left(\alpha_s^2\right)$ was first obtained in [96] in the limit of $m_W = 0$. Once we calculate the three diagrams in Figure 13.4 for both the hard and soft regions, and include the relevant renormalization contributions, we reproduce this result as the leading term in an expansion in $\omega = m_W^2/m_t^2$:

$$
\begin{aligned}
X_L = {} & \left(-\frac{4}{9} + \frac{23\pi^2}{108} + \zeta(3)\right) + \omega\left(-\frac{19}{6} + \frac{2\pi^2}{9}\right) \\
& + \omega^2\left(\frac{745}{72} - \frac{31\pi^2}{36} - 3\zeta(3) - \frac{7}{4}\ln\omega\right) \\
& + \omega^3\left(-\frac{5839}{648} + \frac{7\pi^2}{27} + 2\zeta(3) + \frac{5}{3}\ln\omega\right) \\
& + \omega^4\left(\frac{4253}{8640} + \frac{\pi^2}{4} - \frac{17}{144}\ln\omega\right) \\
& + \omega^5\left(-\frac{689}{27000} + \frac{\pi^2}{15} - \frac{7}{900}\ln\omega\right) \\
& + \omega^6\left(-\frac{13187}{181440} + \frac{\pi^2}{36} + \frac{1}{48}\ln\omega\right)
\end{aligned}
$$

$$+\omega^7 \left(-\frac{2282381}{37044000} + \frac{\pi^2}{70} + \frac{2263}{88200} \ln\omega \right) + \mathcal{O}\left(\omega^8\right) . \tag{13.29}$$

Numerical results for the first three terms of this series were obtained in [92] as follows. First, they suspended the Minkowski-space onshell condition $p^2 = m_t^2$ and instead defined a parameter $z = p^2/m_t^2$. Next, they isolated the coefficient of ω^n by taking the n-th derivative of the integrand with respect to m_W^2 and then setting $m_W = 0$. With two scales remaining in the loop integrals (p^2 and m_t^2), they performed an asymptotic expansion in z to obtain single-scale integrals which, in this case, no longer contain massive lines. The resulting integrals were analytically solved using the MINCER [97] package. Having obtained an analytical result in the unphysical parameter z, their last step was to employ Padé approximations to estimate the numerical value of the series for $z = 1$. For the light quark $\mathcal{O}(\alpha_s^2)$ contribution, they obtained

$$X_L = 2.8(1) - 1.0(1)\,\omega + [-1.3(7) - 1.75\ln\omega]\,\omega^2 , \tag{13.30}$$

in agreement with the exact results of (13.29).

Heavy Quark Loop Contributions

The next class of $\mathcal{O}(\alpha_s^2)$ corrections to top quark decay that we shall consider involves a heavy quark in a loop. Once again, only the three diagrams in Figure 13.4 contribute, but now, the mass terms in the quark loop prevent us from doing an easy loop integral. These are genuine three-loop integrals that require the full force of our techniques to solve. Our final result is:

$$
\begin{aligned}
X_H &= \left(\frac{12991}{1296} - \frac{53\pi^2}{54} - \frac{\zeta(3)}{3} \right) + \omega \left(-\frac{35}{108} - \frac{4\pi^2}{9} + 4\zeta(3) \right) \\
&+ \omega^2 \left(-\frac{6377}{432} + \frac{25\pi^2}{18} + \zeta(3) \right) + \omega^3 \left(\frac{319}{27} - \frac{31\pi^2}{27} - \frac{2\zeta(3)}{3} \right) \\
&+ \omega^4 \left(\frac{76873}{8640} - \frac{8\pi^2}{9} \right) + \omega^5 \left(\frac{237107}{27000} - \frac{8\pi^2}{9} \right) + \mathcal{O}\left(\omega^6\right) .
\end{aligned}
$$

Surprisingly, this result does not contain any $\ln\omega$ factors. This follows from the spectacular total cancellation of the soft contributions from the $\mathcal{O}(\alpha_s^2)$ diagrams with the soft contributions from the $\mathcal{O}(\alpha_s)$ diagrams with $\mathcal{O}(\alpha_s)$ renormalization factors. The reason for this unexpected simplification is not known.

The numerical estimate in [92] for the heavy quark loop contributions,

$$X_H = -0.06360(1) + 0.09766(3)\,\omega + 0.15(5)\,\omega^2 , \tag{13.31}$$

agrees very well with the exact results of (13.31).

Another numerical estimate for the $\mathcal{O}(\alpha_s^2)$ corrections to top quark decay at $m_W = 0$ was presented in [98], in which the b quark was originally assumed to be quite heavy, and the calculation was extrapolated to the $m_b = 0$ limit. The resulting numerical prediction for the heavy quark loop contribution is also $-0.06360(1)$. This calculation represents one specific case of the general $Q \to q\,W$ heavy quark decay that we will discuss further in Section 13.4.

Abelian Contributions

Although we have now discussed two of the four classes of $\mathcal{O}(\alpha_s^2)$ top decay contributions, we are nowhere near halfway finished, for we still have to address diagrams with two gluon loops and there are quite a few of them. In Section 8.2, we showed that we can expect diagrams with color factors of C_F^2, $C_F(C_F - C_A/2)$, and $C_F C_A$. As a result, regardless of which two combinations of C_F and C_A that we select to be our independent color coefficients, some of the diagrams will contribute to both groups. We will use C_F^2 and $C_F C_A$ as our independent color coefficients, as expressed in (13.24). Only Abelian diagrams — diagrams with two independent gluon loops — give rise to C_F^2 factors, either directly or via $C_F(C_F - C_A/2)$. There are 19 such diagrams to consider for $\mathcal{O}(\alpha_s^2)$ top decay and these are shown in Figure 13.5. Note that 11 of these diagrams are to be multiplied by a factor of 2 in order to account for their mirror images.

Dozens of new topologies and some particularly unpleasant master integrals are required to evaluate these contributions. Many months of work culminated with the result:

$$
\begin{aligned}
X_A &= \left[5 - \frac{119\pi^2}{48} - \frac{53\zeta(3)}{8} - \frac{11\pi^4}{720} + \frac{19}{4}\pi^2 \ln 2\right] \\
&+\omega\left[-\frac{73}{8} + \frac{41\pi^2}{8} - \frac{41\pi^4}{90}\right] \\
&+\omega^2\left[-\frac{7537}{288} + \frac{523\pi^2}{96} + \frac{295\zeta(3)}{32} - \frac{191\pi^4}{720} - \frac{27}{16}\pi^2 \ln 2 \right.\\
&\qquad\qquad \left. + \left(\frac{115}{48} - \frac{5\pi^2}{16}\right)\ln\omega\right] \\
&+\omega^3\left[\frac{16499}{864} - \frac{407\pi^2}{216} - \frac{7\zeta(3)}{2} + \frac{7\pi^4}{120} - \pi^2 \ln 2 + \left(-\frac{367}{144} + \frac{5\pi^2}{9}\right)\ln\omega\right] \\
&+\omega^4\left[-\frac{1586479}{259200} + \frac{2951\pi^2}{6912} + \frac{9\zeta(3)}{2} + \left(\frac{31979}{17280} - \frac{\pi^2}{16}\right)\ln\omega\right] \\
&+\omega^5\left[-\frac{11808733}{6480000} + \frac{37\pi^2}{2400} + \frac{6\zeta(3)}{5} + \left(\frac{13589}{27000} - \frac{\pi^2}{60}\right)\ln\omega\right] + \mathcal{O}\left(\omega^6\right) .
\end{aligned}
\tag{13.32}
$$
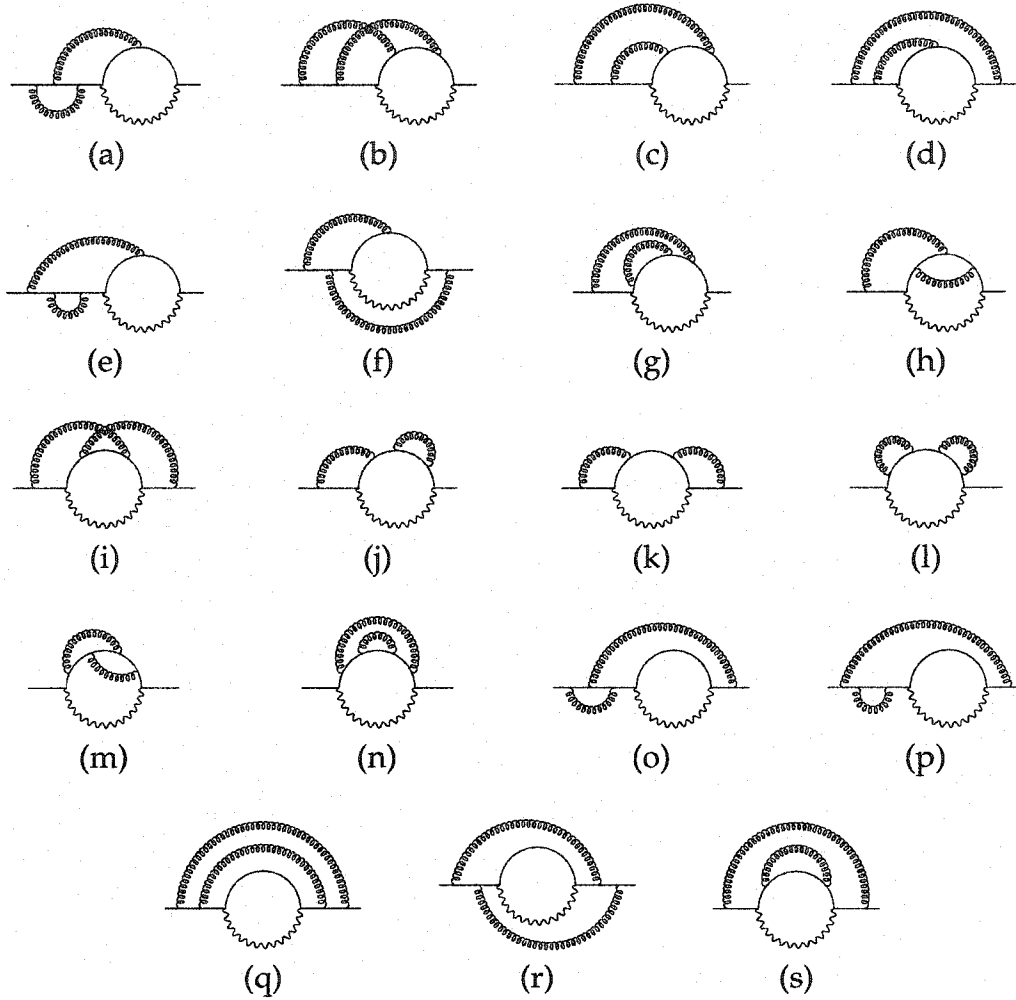
Figure 13.5: Abelian contributions to top quark decay at $\mathcal{O}\left(\alpha_s^2\right)$.

The numerical result in [92] is

$$X_A = 3.2(6) - 2.73(6)\,\omega + [4.5(2.2) - 0.7(1)\ln\omega]\,\omega^2 . \qquad (13.33)$$

While the ω^0 and $\omega^2\ln\omega$ coefficients agree with our exact results, there are discrepancies of 3 and 1.5 error bar lengths for the ω and ω^2 coefficients, respectively. We will refrain from passing judgement on the significance of these discrepancies until we see how the non-Abelian comparisons fare. The numerical prediction from the heavy b quark extrapolation in [98] for the leading term of (13.33) is 3.5(2), in agreement with our exact result.

Non-Abelian Contributions

Following the ordeal of the Abelian contributions, the non-Abelian portion of
the calculation is surprisingly manageable. There are 11 new diagrams to con-
sider, as shown in Figure 13.6, along with the $C_F C_A$ contributions from the 8
Abelian diagrams whose gluons are crossed when drawn above the quark line.
The diagrams with a gluon or ghost subloop are completely analogous to the
light quark contributions. Propitiously, the remaining non-Abelian diagrams
can easily be transformed into topologies associated with the Abelian diagrams.
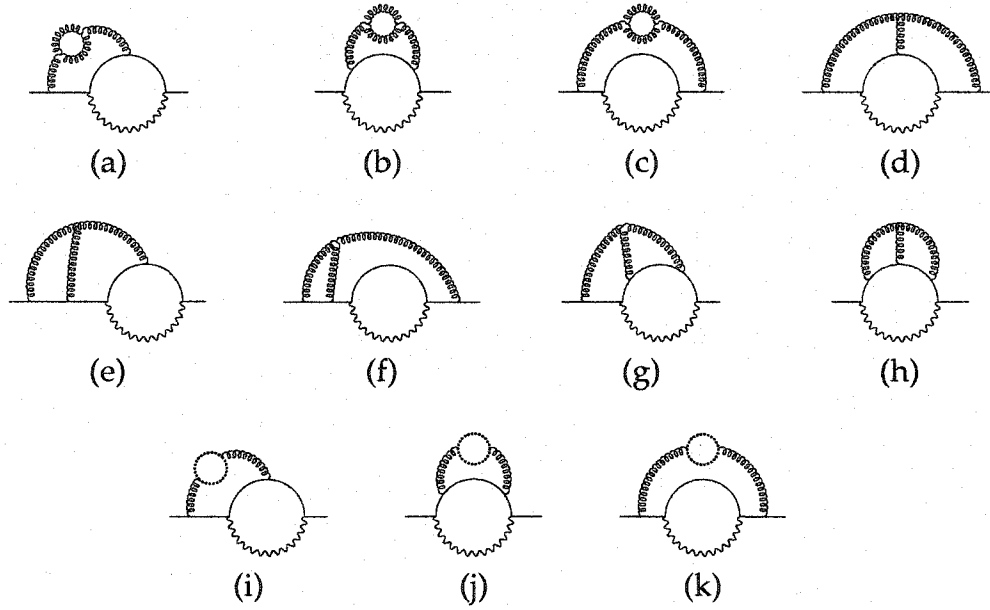
Figure 13.6: Non-Abelian contributions to top quark decay at $\mathcal{O}\left(\alpha_s^2\right)$.

Our result for the non-Abelian contribution is:

$$
\begin{aligned}
X_{NA} =\ & \left[\frac{521}{576} + \frac{505\pi^2}{864} + \frac{9\zeta(3)}{16} + \frac{11\pi^4}{1440} - \frac{19}{8}\pi^2\ln 2\right] \\
& +\omega\left[\frac{91}{48} + \frac{329\pi^2}{144} - \frac{13\pi^4}{60}\right] \\
& +\omega^2\left[-\frac{12169}{576} + \frac{2171\pi^2}{576} + \frac{377\zeta(3)}{64} - \frac{77\pi^4}{288} + \frac{27}{32}\pi^2\ln 2 \right. \\
& \left. \hspace{6cm} + \left(\frac{73}{16} - \frac{3\pi^2}{32}\right)\ln\omega\right] \\
& +\omega^3\left[\frac{13685}{864} - \frac{47\pi^2}{72} - \frac{19\zeta(3)}{4} + \frac{43\pi^4}{720} + \frac{1}{2}\pi^2\ln 2 + \left(-\frac{1121}{432} - \frac{\pi^2}{6}\right)\ln\omega\right]
\end{aligned}
$$

$$+\omega^4 \left[-\frac{420749}{103680} - \frac{3263\pi^2}{13824} - \frac{9\zeta(3)}{8} + \left(\frac{11941}{6912} - \frac{3\pi^2}{32} \right) \ln \omega \right]$$

$$+\omega^5 \left[-\frac{4868261}{12960000} - \frac{557\pi^2}{4800} - \frac{3\zeta(3)}{10} + \left(\frac{153397}{216000} - \frac{\pi^2}{40} \right) \ln \omega \right]$$

$$+\mathcal{O}\left(\omega^6\right) . \tag{13.34}$$

The numerical result in [92] is

$$X_{NA} = -8.0(3) + 3.356(3)\,\omega + [2.4(1.2) + 3.62(1) \ln \omega]\,\omega^2 . \tag{13.35}$$

The ω^0 and ω^2 coefficients agree with our exact results, but there are discrepancies of 5 and 1.5 error bar lengths in the ω and $\omega^2 \ln \omega$ coeffients, respectively. These discrepancies, along with those for the Abelian contributions, suggest that, at best, the theoretical errors have been badly underestimated. This example of yet another numerical calculation gone awry reinforces the efficacy of analytic results like (13.34). The numerical prediction from the heavy b quark extrapolation in [98] for the leading term of (13.34) is $-8.1(2)$, in agreement with our exact result.

13.4 Applications of the Result

We are now in a position to assemble the various pieces of our results in order to obtain a precise determination of the second-order QCD corrections to the top quark decay rate. Using $m_W = 80.423(39)$ GeV and $m_t = 174.3(5.1)$ GeV as the measured masses [99] of the W and t, we obtain $\omega = 0.213(12)$ as the value of the mass-square ratio at which we are to evaluate our expression for X_2. The result is $X_2 = -15.5(1)$, where the uncertainty is almost entirely due to the experimental uncertainty in m_t. The theoretical error, which originates from taking a finite number of terms in our expansion, is 20 times smaller and, if needed, could be reduced further by calculating additional terms. Using $\alpha_s(m_t) = 0.11$ in (13.6), we find that the two-loop correction decreases the tree-level decay rate by about 2%, in agreement with earlier expectations [92].

Only at the very end of our calculation have we used specific values for m_t, m_W, and α_s, which suggests that our results have a much more general interpretation as the decay of a heavy quark Q into a massless quark q and a light boson W. As the W might decay immediately into nearly massless leptons, we can regard m_W as the invariant mass of these leptons, and we describe such decays as semileptonic decays. Kinematically, the allowed range of masses for q and W spans a triangle, as shown in Figure 13.7. Semileptonic quark decays at $\mathcal{O}\left(\alpha_s^2\right)$ have been calculated in at least three other kinematic regions, all of which are as-
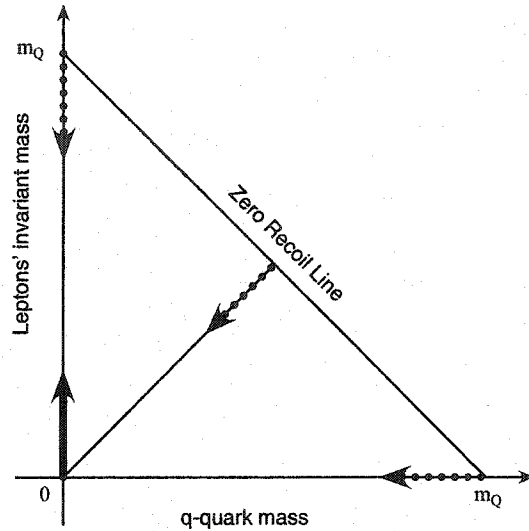
Figure 13.7: Kinematical boundaries of the semileptonic decays $Q \to q +$ leptons. The solid arrow shows the expansion presented in this chapter. Previously known expansions are indicated with dotted arrows.

sociated with the zero recoil limit. In the zero recoil limit, the quark q remains at rest with respect to the original quark Q. Our calculation in this chapter marks the first time that a complete analytic result at $\mathcal{O}(\alpha_s^2)$ has been obtained away from the zero recoil limit. The dotted arrow in the lower-right of Figure 13.7 denotes the expansion in [98] which was used to provide the numerical estimates for top quark decay at $m_W = 0$ that we used in the previous section to compare with our results. The dotted arrow in the upper left of Figure 13.7 denotes the expansion in [100]. This expansion was used to study the semileptonic b quark decay $b \to ul\nu$. It is of particular interest to us, not just because it extrapolates toward the starting point of our expansion, but because it does so along the same line. The expansion parameter in [100] is $\delta = 1 - m_W^2/m_t^2$, so that if we replace δ with $(1 - \omega)$ in these expansions and then divide them by 2 to provide the right normalization for a top quark decay interpretation, we can compare the resulting functions of ω with our results for X_L, X_H, X_A, and X_{NA}. These functions, as shown in Figure 13.8, provide a striking visual confirmation of the validity of both expansions. Although each expansion cannot cover the entire range $0 \le \omega \le 1$ reliably with only a small number of terms, a suitably chosen hybrid of the two expansions will be valid for all values of ω.

Instead of interpreting the four $\mathcal{O}(\alpha_s^2)$ $X(\omega)$ functions as contributions to the top decay width, we can instead consider them as contributions to the differential width $d\Gamma/d\omega$ of a semileptonic decay. Since ω, in this context, corresponds to the invariant mass-square of the leptons produced by the W, we will need to
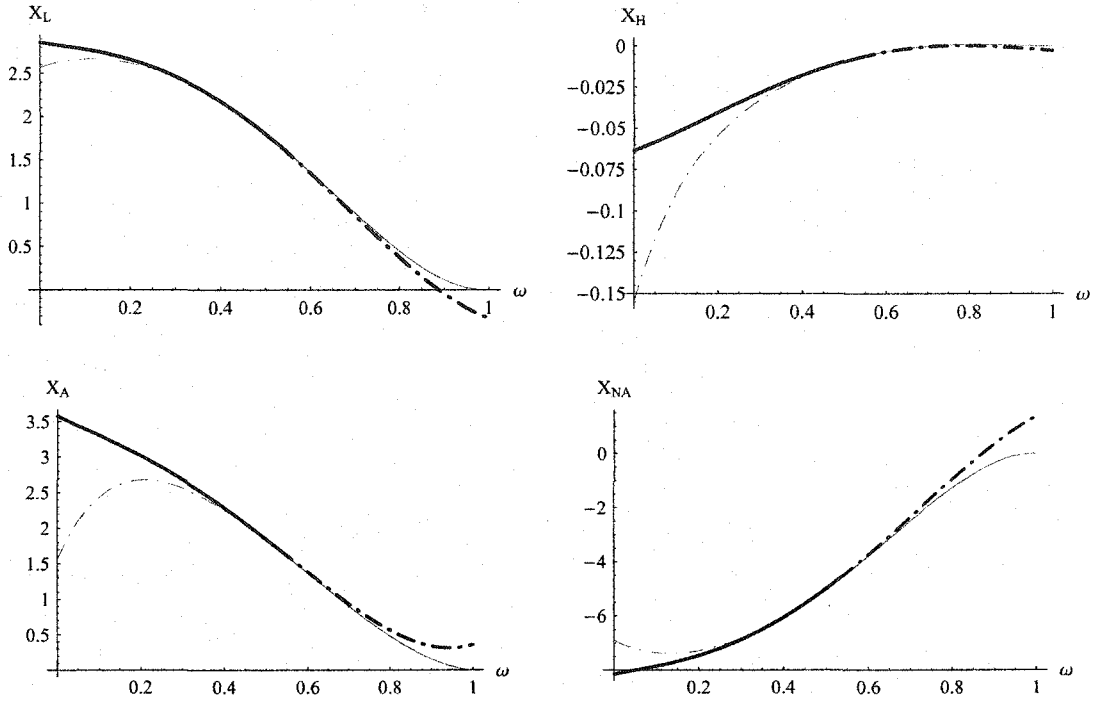
Figure 13.8: Matching of expansions around $\omega = 0$ (thick line) and $\omega = 1$ (thin line) for the four $\mathcal{O}(\alpha_s^2)$ top quark decay coefficients. The solid lines denote the resulting decay width valid in the full range of ω. Outside their regions of validity, the expansions are shown as dash-dotted lines.

integrate over all possible values of ω in order to determine the total semileptonic decay width. For the semileptonic b decay $b \to ul\nu$, when we use $N_L = 4$ and $N_H = 1$, we obtain

$$2 \int_0^1 d\omega\, X_2(\omega) = -21.288 \tag{13.36}$$

from the solid curves in Figure 13.8. This agrees almost perfectly with the -21.29553 obtained in [101]. This result is an important ingredient in the extraction of m_b and $|V_{ub}|$ from experimental measurements of b quark decays.

In a very similar fashion, we can use our results to determine the $\mathcal{O}(\alpha^2)$ QED corrections to the muon lifetime via the decay $\mu \to e\nu\bar{\nu}$. In this context, there are no non-Abelian contributions, and if we further restrict ourselves to the two-photon contributions in X_A, we find that our result,

$$2 \int_0^1 d\omega\, X_A(\omega) = 3.5594\,, \tag{13.37}$$

agrees with the 3.55887 obtained in [102, 103]. It should be mentioned that [103] was a valuable source for leading-order analytic solutions to some of the most difficult master integrals we encountered.

At this stage, there can be no doubts about the validity of the results of our calculations in this chapter. Although the most obvious application of these results is to top quark decay, we have now illustrated connections to other decays mediated by the W boson. The true significance of these results is more general still. By adding a large new class of three-loop integrals to our library, we are now in a position to consider some of the increasingly difficult physical problems that await. Of particular interest are the $\mathcal{O}\left(\alpha_s^2\right)$ perturbative calculations of mixing processes such as $B_d \leftrightarrow \overline{B}_d$ and $B_s \leftrightarrow \overline{B}_s$. These processes are currently under intense experimental scrutiny and they represent sensitive probes of New Physics.

"I could think of things I never thunk before and then I'd sit and think some more."

The Scarecrow from The Wizard of Oz (*If I Only Had a Brain*)

Chapter 14

Conclusion

In this thesis, we have shown how modern calculational techniques can be used to obtain increasingly detailed predictions from the Standard Model of particle physics. In Chapter 1 we started with the Feynman rules for the Standard Model and saw how the terms of a perturbative expansion can be constructed from Feynman diagrams with certain numbers of loops. When we integrate over all possible momenta flowing through these loops, we might obtain divergences; dimensional regularization was introduced in Chapter 2 to keep track of these divergences without discarding other features of the integrals. Loop diagrams usually contain several factors which depend on the loop momenta, and the loop momentum integrals are most easily evaluated if we first combine these factors with a parameter using one of the identities in Chapter 3. In Chapter 4 we showed how to derive the recurrence relation identities which allow us to express an arbitrary integral of a given topology in terms of a small set of master integrals or integrals from simpler topologies. Recurrence relations only apply to scalar integrals, though, and in Chapter 5 we saw how to rewrite numerator factors in a loop integral. In Chapter 6 we discussed a number of techniques that can be used to calculate the master integrals that cannot be reduced by recurrence relations. Particular attention was given to the cutting rules which allow the extraction of the imaginary parts of loop integrals. In Chapter 7 we introduced techniques which allow loop integrals with more than one external scale to be expanded as a series of single-scale integrals. The color factors that are present in perturbative QCD were explained in Chapter 8 and in Chapter 9 we showed how to incorporate renormalization effects in a perturbative calculation. Finally, in Chapter 10 we looked at why symbolic computation is such an indispensable tool for most multiloop calculations.

With these calculational techniques in place, we then applied them to solve outstanding problems in three very different areas of particle physics:

- The pion-pole light-by-light scattering contribution to the muon $g-2$, char-

acterizing the low-energy interaction of a muon with a magnetic field [45].

- The small corrections to the energy levels of QED bound states for use in atomic spectroscopy [73].

- The dynamics of the heaviest fermions in the Standard Model, and in particular, the decay of the top quark [90].

Previously, only numerical results existed for these problems, and these results were fraught with discrepancies, poor estimation of uncertainties, and calculational errors. Our approach provides a unique and definitive analytic solution to each of these three problems.

Chapter 11 deals with the anomalous magnetic moment of the muon. A troubling discrepancy between the Standard Model prediction and a recently improved measurement of the muon $g - 2$ was exacerbated by a sign error in the calculations of the light-by-light scattering contributions to the Standard Model prediction. In response to the original claims that this contribution was actually of positive sign, we evaluated the contribution analytically and confirmed the positive sign. Nevertheless, a discrepancy between theory and experiment persists, and while much effort is still being devoted to the theoretical predictions, this discrepancy could be indicative of New Physics beyond the Standard Model.

Chapter 12 addresses the energy levels of QED bound states. Beyond the basic binding effect of the long-range Coulomb interaction is a cornucopia of corrections that are suppressed by various powers of one or more small parameters of the system. Even though the bound states themselves are low-energy systems, many of the energy level corrections depend intimately on the short-distance features of QED. We showed how our calculational techniques for perturbative quantum field theory can be used to extract predictions for certain classes of higher-order effects, regardless of the masses of the bound state constituents. Incredible experimental work is being done with these low-energy systems, thus it is essential that there are corresponding improvements in the theoretical work in order to keep pace.

Chapter 13 presents the second-order QCD corrections to the decay of a top quark into a b quark and a W boson; this corresponds to a particular kinematic limit of a more general weak decay process. Our calculations are an important complement to a group of other second-order QCD corrections corresponding to different kinematic limits of heavy quark decays. Beyond top quark decay, our results are applicable to muon decay and the semileptonic decays of b quarks, and the new class of loop integrals which we solved will provide an important piece of a future study of b quark mixing in mesons.

The common feature of these calculations is the analytic formulation of the results. Every coefficient of the series expansions in small parameters like α and m/M is expressed as an exact linear combination of transcendental constants such as π, $\ln 2$, and $\zeta(3)$. Given the amount of work that goes into these calculations, it is surprising how the final results can be so compact. As Broadhurst put it [104]:

> It is as if QFT were taunting us with our ignorance of the mapping between diagrams and numbers that results from the Feynman rules. A vast quantity of data, collected by painfully inadequate methods, collapses to an amazingly simple answer. We are, physicists and mathematicians alike, stumbling on the edge of a structure that is far more refined than the clumsy methods by which we investigate it.

Nevertheless, in the absence of a better way to obtain these results, we must continue forward. The Standard Model — and its quantitative description, where possible, through pertubative quantum field theory — has been so stunningly successful thus far that we would be remiss not to push this theory to the limit of its (and our) abilities.

"Ohh, that just kept going, huh?"

Krusty the Klown (*The Simpsons*)

Bibliography

[1] M. E. Peskin and D. V. Schroeder, *An Introduction to Quantum Field Theory* (Perseus, Cambridge, MA, 1995).

[2] D. J. Griffiths, *Introduction to Elementary Particles* (Wiley, Toronto, 1987).

[3] T. Cheng and L. Li, *Gauge Theory of Elementary Particle Physics* (Oxford University Press, New York, 1984).

[4] H. Bethe, Phys. Rev. **72**, 339 (1947).

[5] J. Schwinger, Phys. Rev. **73**, 416L (1948).

[6] C. Sommerfield, Phys. Rev. **107**, 328 (1957).

[7] T. Kinoshita, B. Nizic, and Y. Okamoto, Phys. Rev. **D41**, 593 (1990).

[8] Representative works include: S. J. Brodsky and J. D. Sullivan, Phys. Rev. **156**, 1644 (1967) for the W boson contribution to the muon anomalous magnetic moment; I. B. Khriplovich, Sov. J. Nucl. Phys. **10** (1969) for the β-function of a Yang-Mills theory.

[9] D. J. Broadhurst and D. Kreimer, Phys. Lett. **B475**, 63 (2000), hep-th/9912093.

[10] G. 't Hooft and M. J. G. Veltman, Nucl. Phys. **B44**, 189 (1972).

[11] E. T. Whittaker and G. N. Watson, *A Course of Modern Analysis*, 4th ed. (Cambridge University Press, New York, 1927).

[12] *Handbook of Mathematical Functions*, edited by M. Abramowitz and I. A. Stegun (Dover, New York, 1970).

[13] I. S. Gradshteyn and I. M. Ryzhik, *Table of Integrals, Series, and Products*, 5th ed. (Academic Press, Toronto, 1994).

[14] I. M. Gel'fand and G. E. Shilov, *Generalized Functions* (Harcourt Brace, New York, 1977), Vol. 1.

[15] J. Fleischer and M. Yu. Kalmykov, Comput. Phys. Commun. **128**, 531 (2000), hep-ph/9907431.

[16] Nobel e-Museum, www.nobel.se/physics/laureates/1965/.

[17] F. V. Tkachov, Phys. Lett. **B100**, 65 (1981).

[18] K. G. Chetyrkin and F. V. Tkachov, Nucl. Phys. **B192**, 159 (1981).

[19] S. Laporta, Int. J. Mod. Phys. **A15**, 5087 (2000), hep-ph/0102033.

[20] K. Melnikov and T. van Ritbergen, Nucl. Phys. **B591**, 515 (2000), hep-ph/0005131.

[21] L. Lewin, *Polylogarithms and Associated Functions* (North Holland, New York, 1981).

[22] F. W. Byron Jr. and R. W. Fuller, *Mathematics of Classical and Quantum Physics* (Dover, New York, 1969).

[23] R. E. Cutkosky, J. Math. Phys. **1**, 429 (1960).

[24] Y. Zhou and C. Lü, hep-ph/0402103; Y. Zhou hep-ph/0403202, hep-ph/0404035.

[25] M. Yu. Kalmykov, private communication. These errors were mentioned in the footnote on p.12 of hep-ph/0212319.

[26] D. J. Broadhurst, Z. Phys. **C47**, 115 (1990).

[27] A. V. Kotikov, Phys. Lett. **B259**, 314 (1991).

[28] D. H. Bailey and D. J. Broadhurst, Math. Comput. **70**, 1719 (2001), math.NA/9905048.

[29] J. Fleischer, M. Yu. Kalmykov, and A. V. Kotikov, Phys. Lett. **B462**, 169 (1999), hep-ph/9905249.

[30] M. Beneke and V. A. Smirnov, Nucl. Phys. **B522**, 321 (1998), hep-ph/9711391.

[31] J. P. Archambault, M.Sc. thesis, University of Alberta (2003).

[32] C. M. Bender and S. A. Orszag, *Advanced Mathematical Methods For Scientists and Engineers* (McGraw-Hill, Toronto, 1978).

[33] F. J. Dyson, Phys. Rev. **85**, 631 (1952).

[34] M. A. Samuel, J. Ellis, and M. Karliner, Phys. Rev. Lett. **74**, 4380 (1995), hep-ph/9503411.

[35] V. Elias, T. G. Steele, F. Chishtie, R. Migneron, and K. Sprague, Phys. Rev. **D58**, 116007 (1998), hep-ph/9806324.

[36] H. Georgi, *Lie Algebras in Particle Physics*, 2nd ed. (Perseus, Reading, MA, 1999).

[37] P. Cvitanović, Phys. Rev. **D14**, 1536 (1976).

[38] Waterloo Maple Inc., www.maplesoft.com.

[39] Wolfram Research, Inc., www.wolfram.com.

[40] J. A. M. Vermaseren, math-ph/0010025.

[41] Denny Fliegner played a key role in the parallel implementation of FORM and was instrumental in the installation of the parallel version on the computing cluster at the Centre for Symbolic Computation at the University of Alberta. Denny used some of our code to test the performance of the parallel version on the cluster.

[42] J. K. Hwang, hep-ph/0008215, hep-ph/0011210, hep-ph/0012302.

[43] The Laporta algorithm was implemented by M. Ślusarczyk at the University of Alberta for top quark decay simultaneously with my own work with the traditional recurrence relation methods. Both methods independently obtained the correct result.

[44] J. A. M. Vermaseren, Nucl. Phys. Proc. Suppl. **116**, 343 (2003), hep-ph/0211297.

[45] I. Blokland, A. Czarnecki, and K. Melnikov, Phys. Rev. Lett. **88**, 071803 (2002), hep-ph/0112117.

[46] R. S. Van Dyck, P. B. Schwinberg, and H. G. Dehmelt, Phys. Rev. Lett. **59**, 26 (1987).

[47] G. W. Bennett *et al.*, hep-ex/0401008.

[48] A. Czarnecki and W. J. Marciano, Phys. Rev. D64, 013014 (2001), hep-ph/0102122.

[49] S. Laporta and E. Remiddi, Acta Phys. Polon. B28, 959 (1997).

[50] T. Kinoshita and M. Nio, hep-ph/0402206.

[51] S. G. Karshenboim, Phys. Atom. Nucl. 56, 857 (1993).

[52] M. Davier, S. Eidelman, A. Hocker, and Z. Zhang, Eur. Phys. J. C31, 503 (2003), hep-ph/0308213.

[53] S. Ghozzi and F. Jegerlehner, Phys. Lett. B583, 222 (2004), hep-ph/0310181.

[54] A. Czarnecki, B. Krause, and W. J. Marciano, Phys. Rev. Lett. 76, 3267 (1996), hep-ph/9512369.

[55] J. Bailey et al., Nucl. Phys. B150, 1 (1979).

[56] H. N. Brown et al., Phys. Rev. Lett. 86, 2227 (2001), hep-ex/0102017.

[57] M. Knecht and A. Nyffeler, Phys. Rev. D65, 073034 (2002), hep-ph/0111058.

[58] M. Knecht, A. Nyffeler, M. Perrottet, and E. de Rafael, Phys. Rev. Lett. 88, 071802 (2002), hep-ph/0111059.

[59] M. Hayakawa and T. Kinoshita, Phys. Rev. D57, 465 (1998), hep-ph/9708227.

[60] J. Bijnens, E. Pallante, and J. Prades, Nucl. Phys. B474, 379 (1996), hep-ph/9511388.

[61] S. L. Adler, Phys. Rev. 177, 2426 (1969).

[62] J. S. Bell and R. Jackiw, Nuovo Cim. A60, 47 (1969).

[63] J. Wess and B. Zumino, Phys. Lett. B37, 95 (1971).

[64] E. Witten, Nucl. Phys. B223, 433 (1983).

[65] M. Ramsey-Musolf and M. B. Wise, Phys. Rev. Lett. 89, 041601 (2002), hep-ph/0201297.

[66] M. Hayakawa and T. Kinoshita, Phys. Rev. D66, 0199002 (2002), hep-ph/0112102.

[67] J. Bijnens, E. Pallante, and J. Prades, Nucl. Phys. **B626**, 410 (2002), hep-ph/0112255.

[68] K. Melnikov and A. Vainshtein, hep-ph/0312226.

[69] A. Gilani, hep-ph/0404026.

[70] T. Kinoshita and M. Nio, Phys. Rev. Lett. **90**, 021803 (2003), hep-ph/0210322.

[71] R. R. Akhmetshin *et al.*, Phys. Lett. **B578**, 285 (2004), hep-ex/0308008.

[72] M. Battaglia *et al.*, Eur. Phys. J. **C33**, 273 (2004), hep-ph/0306219.

[73] I. Blokland, A. Czarnecki, and K. Melnikov, Phys. Rev. **D65**, 073015 (2002), hep-ph/0112267.

[74] E. Fermi, Z. Phys. **60**, 320 (1930).

[75] A. Czarnecki, K. Melnikov, and A. Yelkhovsky, Phys. Rev. Lett. **82**, 311 (1999), hep-ph/9809341.

[76] A. Czarnecki, K. Melnikov, and A. Yelkhovsky, Phys. Rev. **A59**, 4316 (1999), hep-ph/9901394.

[77] R. Arnowitt, Phys. Rev. **92**, 1002 (1953).

[78] M. I. Eides, H. Grotch, and V. A. Shelyuto, Phys. Rept. **342**, 63 (2001), hep-ph/0002158.

[79] K. Pachucki and S. G. Karshenboim, Phys. Rev. Lett. **80**, 2101 (1998), hep-ph/9709387.

[80] A. Czarnecki and K. Melnikov, Phys. Rev. Lett. **87**, 013001 (2001), hep-ph/0012053.

[81] G. Bhatt and H. Grotch, Phys. Rev. **A31**, 2794 (1985).

[82] G. Bhatt and H. Grotch, Ann. Phys. (NY) **178**, 1 (1987).

[83] G. Bhatt and H. Grotch, Phys. Rev. Lett. **58**, 471 (1987).

[84] K. Pachucki, Phys. Rev. **A52**, 1079 (1995).

[85] M. I. Eides, H. Grotch, and V. A. Shelyuto, Phys. Rev. **A63**, 052509 (2001), hep-ph/0012372.

[86] G. T. Bodwin, D. R. Yennie, and M. A. Gregorio, Phys. Rev. Lett. **48**, 1799 (1982).

[87] K. Pachucki, Phys. Rev. **A56**, 297 (1997).

[88] K. Pachucki and H. Grotch, Phys. Rev. **A51**, 1854 (1995).

[89] S. Willenbrock, Rev. Mod. Phys. **72**, 1141 (2000), hep-ph/0008189.

[90] I. Blokland, A. Czarnecki, M. Ślusarczyk, and F. Tkachov, hep-ph/0403221, in press in Phys. Rev. Lett.

[91] M. Jeżabek and J. H. Kühn, Nucl. Phys. **B314**, 1 (1989).

[92] K. G. Chetyrkin, R. Harlander, T. Seidensticker, and M. Steinhauser, Phys. Rev. **D60**, 114015 (1999), hep-ph/9906273.

[93] D. J. Broadhurst, N. Gray, and K. Schilcher, Z. Phys. **C52**, 111 (1991).

[94] K. Melnikov and T. van Ritbergen, Nucl. Phys. **B591**, 515 (2000), hep-ph/0005131.

[95] T. van Ritbergen, J. A. M. Vermaseren, and S. A. Larin, Phys. Lett. **B400**, 379 (1997), hep-ph/9701390.

[96] A. Czarnecki, Acta Phys. Polon. **B26**, 845 (1995), hep-ph/9503444.

[97] S. G. Gorishnii, S. A. Larin, L. R. Surguladze, and F. V. Tkachov, Comput. Phys. Commun. **55**, 381 (1989).

[98] A. Czarnecki and K. Melnikov, Nucl. Phys. **B544**, 520 (1999), hep-ph/9806244.

[99] K. Hagiwara *et al.*, Phys. Rev. **D66**, 010001+ (2002), http : //pdg.lbl.gov.

[100] A. Czarnecki and K. Melnikov, Phys. Rev. Lett. **88**, 131801 (2002), hep-ph/0112264.

[101] T. van Ritbergen, Phys. Lett. **B454**, 353 (1999), hep-ph/9903226.

[102] T. van Ritbergen and R. G. Stuart, Phys. Rev. Lett. **82**, 488 (1999), hep-ph/9808283.

[103] T. van Ritbergen and R. G. Stuart, Nucl. Phys. **B564**, 343 (2000), hep-ph/9904240.

[104] D. J. Broadhurst, hep-ph/0211194.

Appendix A

Catalog of Topologies

This appendix contains a description of all the loop integral topologies encountered in this thesis, most of which were programmed for the first time in conjunction with this work. Associated with each topology are three FORM programs: one which derives the recurrence relations, one which implements the solution algorithm, and one which performs tests on the topology in order to ensure the validity of the algorithm. This appendix is not intended to explain the inner workings of these programs. In order to provide the user with sufficient information to run the programs, we provide:

- A sketch of the topology. Massive lines are solid and massless lines are dashed.

- A numerical labeling of the lines in the topology, as used in the FORM programs.

- An indication ε for the massless lines with non-integer exponents which arise from massless subloops of a higher topology.

- An expression for the Euclidean-space loop integral which indicates the algebraic form of each propagator for a particular choice of routings of the momenta. Since these are single-scale integrals, the overall mass dimension is assumed to have been factored out already, leaving us with $p^2 = -m^2 = -1$.

- Where required, a statement about the auxiliary propagators or tensor reduction procedure used to cast arbitrary scalar products in the numerator in terms of propagators, as explained in Chapter 5.

- Where required, expressions for the master integrals of a topology. We will denote the loop factor $\Gamma(1 + \epsilon)/(4\pi)^{D/2}$ by $\mathcal{F}$.

A.1   One-Loop Topologies

gm2
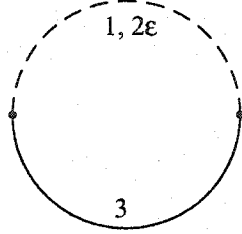
$$\int \frac{[d^D k]}{k^{2(a_1+a_2\epsilon)}(k^2+1)^{a_3}}$$

Tensor reduction is automatic
A general solution is used

M2
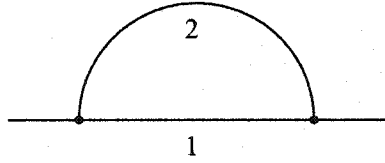
$$\int \frac{[d^D k]}{(k^2+2kp)^{a_1}(k^2+1)^{a_2}}$$

$$\frac{M2(1,1)}{\mathcal{F}} = \frac{1}{\epsilon} + \left(2-\frac{\pi}{\sqrt{3}}\right) + \left(4-\frac{2\pi}{\sqrt{3}}+\frac{\pi}{\sqrt{3}}\ln 3 - 9S_2\right)\epsilon + \mathcal{O}(\epsilon^2)$$

M3
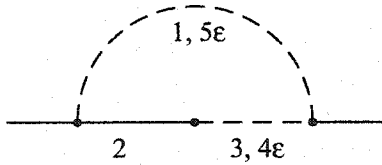
$$\int \frac{[d^D k]}{k^{2(a_1+a_5\epsilon)}(k^2+2kp)^{a_2}(k+p)^{2(a_3+a_4\epsilon)}}$$

$$\frac{M3(1,1,0,1,1)}{\mathcal{F}} = \frac{1}{3\epsilon}+\frac{4}{3}+\left(\frac{16}{3}+\frac{11\pi^2}{18}+i\pi\right)\epsilon$$
$$+\left(\frac{64}{3}+\frac{5\pi^2}{18}+7\zeta(3)+i\pi\left(7+\frac{\pi^2}{6}\right)\right)\epsilon^2+\mathcal{O}(\epsilon^3)$$

one
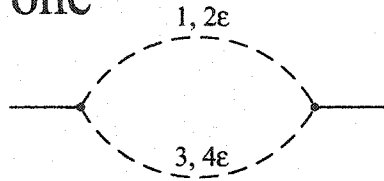
$$\int \frac{[d^D k]}{k^{2(a_1+a_2\epsilon)}(k+q)^{2(a_3+a_4\epsilon)}}$$

Tensor reduction is automatic

q can be any momentum

A general solution is used

onshell
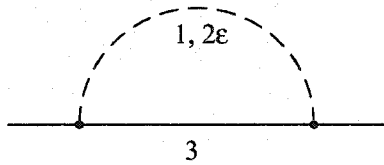
$$\int \frac{[d^D k]}{k^{2(a_1+a_2\epsilon)}(k^2 + 2kp)^{2a_3}}$$

Tensor reduction is automatic

A general solution is used

A.2 Basic Two-Loop Topologies

gm3
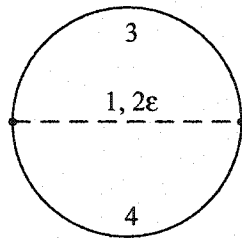
$$\int \frac{[d^D k_1][d^D k_2]}{(k_1 + k_2)^{2(a_1+a_2\epsilon)}(k_1^2 + 1)^{a_3}(k_2^2 + 1)^{a_4}}$$

Average over directions of p in numerator

A general solution is used

M5
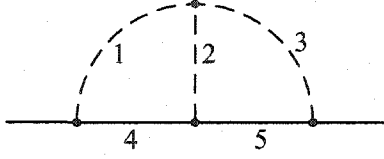
$$\int \frac{[d^D k_1][d^D k_2]}{k_1^{2a_1}(k_1 - k_2)^{2a_2} k_2^{2a_3}(k_1^2 + 2k_1 p)^{a_4}(k_2^2 + 2k_2 p)^{a_5}}$$

N5
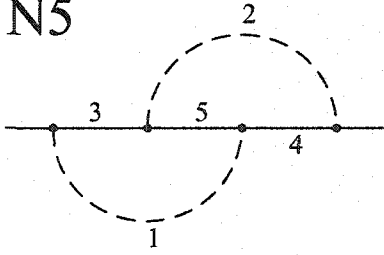
$$\frac{N5(1,1,1,1,1)}{\mathcal{F}^2} = \pi^2 \ln 2 - \frac{3\zeta(3)}{2} + \mathcal{O}(\epsilon)$$

$$\int \frac{[d^D k_1][d^D k_2]}{k_1^{2a_1} k_2^{2a_2}(k_1^2 + 2k_1 p)^{a_3}(k_2^2 + 2k_2 p)^{a_4}[(k_1 + k_2)^2 + 2(k_1 + k_2)p]^{a_5}}$$

N5a
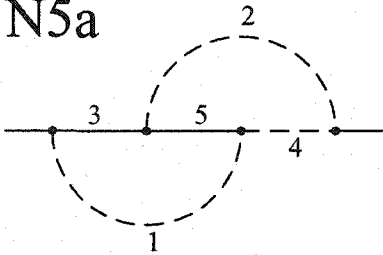
$$\frac{\mathrm{Im}\, N5a(1,1,1,1,1)}{\pi \mathcal{F}^2} = \frac{\pi^2}{6} + \left(\frac{\pi^2}{3} + 3\zeta(3)\right)\epsilon + \mathcal{O}(\epsilon^2)$$
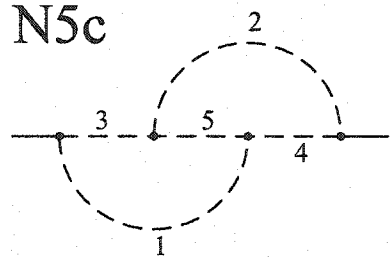
$$\int \frac{[d^D k_1][d^D k_2]}{k_1^{2a_1} k_2^{2a_2}(k_1^2 + 2k_1 p)^{a_3}(k_2 + p)^{2a_4}[(k_1 + k_2)^2 + 2(k_1 + k_2)p]^{a_5}}$$

N5b
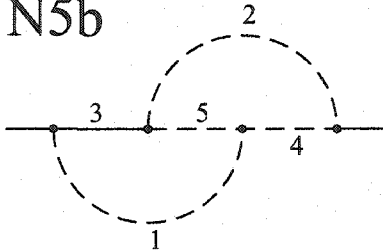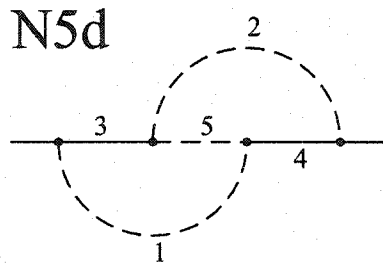
$$\int \frac{[d^D k_1][d^D k_2]}{k_1^{2a_1} k_2^{2a_2}(k_1^2 + 2k_1 p)^{a_3}(k_2 + p)^{2a_4}(k_1 + k_2 + p)^{2a_5}}$$

N5c

$$\int \frac{[d^D k_1][d^D k_2]}{k_1^{2a_1} k_2^{2a_2} (k_1 + p)^{2a_3} (k_2 + p)^{2a_4} (k_1 + k_2 + p)^{2a_5}}$$
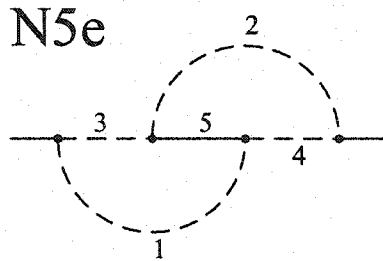
N5d

$$\frac{\text{Im } N5d(1,1,1,1,1)}{\pi \, \mathcal{F}^2} = \frac{\pi^2}{6} + \left(\frac{\pi^2}{3} + 7\zeta(3) \right) \epsilon + \mathcal{O}\left(\epsilon^2 \right)$$
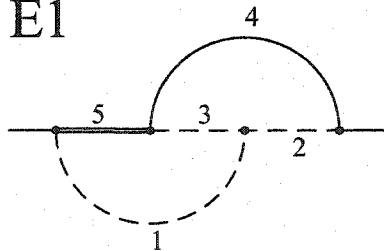
$$\int \frac{[d^D k_1][d^D k_2]}{k_1^{2a_1} k_2^{2a_2} (k_1^2 + 2k_1 p)^{a_3} (k_2^2 + 2k_2 p)^{a_4} (k_1 + k_2 + p)^{2a_5}}$$

N5e

$$\frac{\text{Im } N5e(1,1,1,1,1)}{\pi \, \mathcal{F}^2} = \frac{\pi^2}{6} + \mathcal{O}\left(\epsilon \right)$$

$$\int \frac{[d^D k_1][d^D k_2]}{k_1^{2a_1} k_2^{2a_2} (k_1 + p)^{2a_3} (k_2 + p)^{2a_4} [(k_1 + k_2)^2 + 2(k_1 + k_2)p]^{a_5}}$$

NP
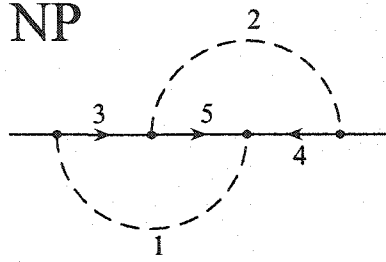
$$\int \frac{[d^D k_1][d^D k_2]}{k_1^{2a_1} k_2^{2a_2} (k_1^2 + 2k_1 p)^{a_3} (k_2^2 - 2k_2 p)^{a_4} [(k_1 + k_2)^2 + 2(k_1 + k_2)p]^{a_5}}$$

$$\frac{NP(1,1,1,1,1)}{\mathcal{F}^2} = \pi^2 \ln 2 + \frac{3\zeta(3)}{2} + \mathcal{O}(\epsilon)$$

P5
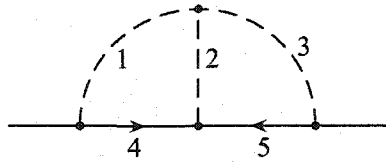
$$\int \frac{[d^D k_1][d^D k_2]}{k_1^{2a_1} (k_1 - k_2)^{2a_2} k_2^{2a_3} (k_1^2 + 2k_1 p)^{a_4} (k_2^2 - 2k_2 p)^{a_5}}$$

$$\frac{P5(0,1,0,2,2)}{\mathcal{F}^2} = \frac{\pi^2}{4} + \left(\frac{21\zeta(3)}{4} + \frac{\pi^2}{2} \ln 2 \right) \epsilon + \mathcal{O}(\epsilon^2)$$

T1
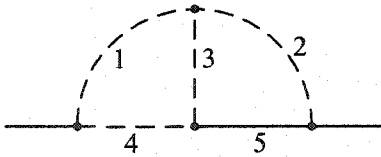
$$\int \frac{[d^D k_1][d^D k_2]}{k_1^{2a_1} k_2^{2a_2} (k_1 - k_2)^{2a_3} (k_1 + p)^{2a_4} (k_2^2 + 2k_2 p)^{a_5}}$$

T2
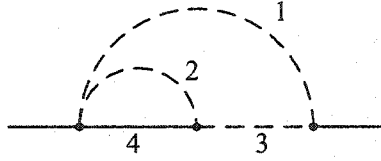
$$\int \frac{[d^D k_1][d^D k_2]}{k_1^{2a_1} k_2^{2a_2} (k_1 + p)^{2a_3} [(k_1 + k_2 + p)^2 + 1]^{a_4}}$$

Tensor reduction: $k_2 \perp (k_1 + p)$

T4b
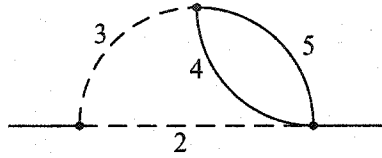
$$\int \frac{[d^D k_1][d^D k_2]}{(k_2 + p)^{2a_2} k_2^{2a_3} [k_1^2 + 1]^{a_4} [(k_1 + k_2)^2 + 1]^{a_5}}$$

Tensor reduction: $k_1 \perp k_2$

$$\frac{\operatorname{Im} T4b(1,1,1,1)}{\pi \, \mathcal{F}^2} = \frac{1}{\epsilon} + 2 + \left(4 - \frac{\pi^2}{3}\right) \epsilon + \mathcal{O}\left(\epsilon^2\right)$$

A.3 Two-Loop Topologies With an ϵ-Propagator

T1ep
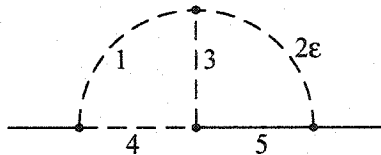
$$\int \frac{[d^D k_1][d^D k_2]}{k_1^{2a_1} k_2^{2(a_2+\epsilon)} (k_1 - k_2)^{2a_3} (k_1 + p)^{2a_4} (k_2^2 + 2k_2 p)^{a_5}}$$

Y1
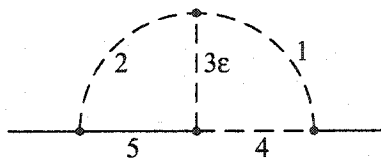
$$\int \frac{[d^D k_1][d^D k_2]}{k_1^{2a_1} k_2^{2a_2} (k_1 - k_2)^{2(a_3+\epsilon)} (k_1 + p)^{2a_4} (k_2^2 + 2k_2 p)^{a_5}}$$

Y1a
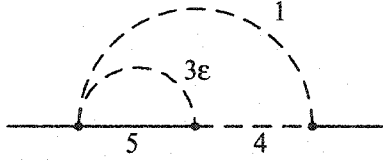
$$\int \frac{[d^D k_1][d^D k_2]}{k_1^{2a_1} k_2^{2(a_3+\epsilon)}(k_1+p)^{2a_4}[(k_1+k_2+p)^2+1]^{a_5}}$$

Tensor reduction: $k_2 \perp (k_1+p)$

$$\frac{\operatorname{Im} Y1a(1,1,1,1)}{\pi \, \mathcal{F}^2} = -\frac{1}{2\epsilon} - \frac{3}{2} + \left(-\frac{7}{2} - \frac{\pi^2}{12}\right)\epsilon + \mathcal{O}\left(\epsilon^2\right)$$

Y2
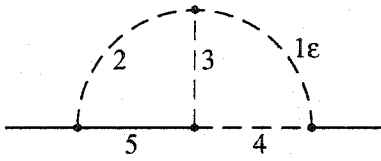
$$\int \frac{[d^D k_1][d^D k_2]}{k_1^{2(a_1+\epsilon)} k_2^{2a_2}(k_1-k_2)^{2a_3}(k_1+p)^{2a_4}(k_2^2+2k_2p)^{a_5}}$$

Y2a
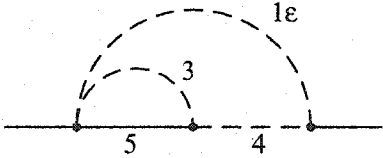
$$\int \frac{[d^D k_1][d^D k_2]}{k_1^{2(a_1+\epsilon)} k_2^{2a_3}(k_1+p)^{2a_4}[(k_1+k_2+p)^2+1]^{a_5}}$$

Tensor reduction: $k_2 \perp (k_1+p)$

$$\frac{\operatorname{Im} Y2a(1,1,1,1)}{\pi \, \mathcal{F}^2} = \frac{1}{2} + \frac{11}{4}\epsilon + \left(\frac{85}{8} - \frac{5\pi^2}{12}\right)\epsilon^2 + \mathcal{O}\left(\epsilon^3\right)$$

Y2b
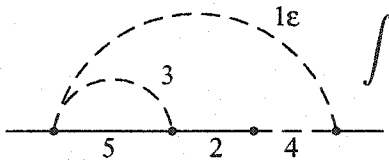
$$\int \frac{[d^D k_1][d^D k_2]}{k_1^{2(a_1+\epsilon)}(k_1^2+2k_1p)^{a_2} k_2^{2a_3}(k_1+p)^{2a_4}[(k_1+k_2+p)^2+1]^{a_5}}$$

Tensor reduction: $k_2 \perp (k_1+p)$

Y3
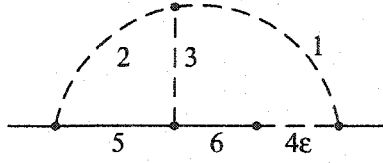
$$\int \frac{[d^D k_1][d^D k_2]}{k_1^{2a_1} k_2^{2a_2} (k_1 - k_2)^{2a_3} (k_1 + p)^{2(a_4+\epsilon)} (k_2^2 + 2k_2 p)^{a_5} (k_1^2 + 2k_1 p)^{a_6}}$$

Y4
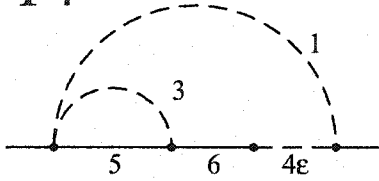
Tensor reduction: $k_2 \perp (k_1 + p)$

$$\int \frac{[d^D k_1][d^D k_2]}{k_1^{2a_1} k_2^{2a_3} (k_1 + p)^{2(a_4+\epsilon)} [(k_1 + k_2 + p)^2 + 1]^{a_5} (k_1^2 + 2k_1 p)^{a_6}}$$

$$\frac{\mathrm{Im}\, Y4(1,1,0,1,0)}{\pi\, \mathcal{F}^2} = \frac{1}{2} + \left(\frac{9}{2} - \frac{\pi^2}{6} \right) \epsilon + \left(\frac{55}{2} - \frac{13\pi^2}{12} - 8\zeta(3) \right) \epsilon^2$$
$$+ \left(\frac{285}{2} - \frac{23\pi^2}{4} - 36\zeta(3) - \frac{59\pi^4}{180} \right) \epsilon^3 + \mathcal{O}\left(\epsilon^4\right)$$

Y5
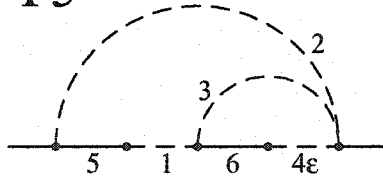
Tensor reduction: $k_1 \perp (k_2 + p)$

$$\int \frac{[d^D k_1][d^D k_2]}{(k_2 + p)^{2a_1} k_2^{2a_2} k_1^{2a_3} (k_1 + k_2 + p)^{2(a_4+\epsilon)} (k_2^2 + 2k_2 p)^{a_5} [(k_1 + k_2 + p)^2 + 1]^{a_6}}$$

Y6
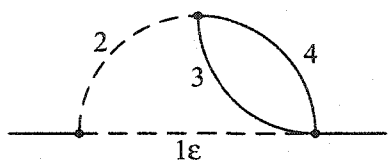
$$\int \frac{[d^D k_1][d^D k_2]}{(k_1 + p)^{2(a_1+\epsilon)} k_1^{2a_2} (k_2^2 + 1)^{a_3} [(k_1 + k_2 + p)^2 + 1]^{a_4}}$$

Tensor reduction: $k_2 \perp k_1$

Y6a
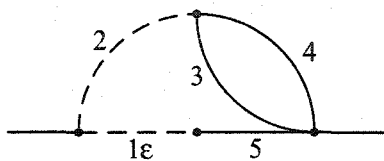
Tensor reduction: $k_2 \perp k_1$

$$\int \frac{[d^D k_1][d^D k_2]}{(k_1 + p)^{2(a_1+\epsilon)} k_1^{2a_2} (k_2^2 + 1)^{a_3} [(k_1 + k_2 + p)^2 + 1]^{a_4} (k_1^2 + 2k_1 p)^{a_5}}$$

Y7
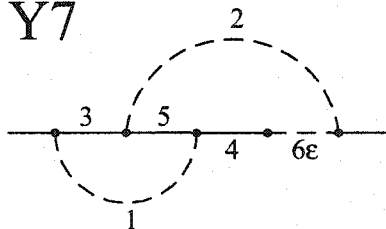
$$\int \frac{[d^D k_1][d^D k_2]}{k_1^{2a_1} k_2^{2a_2} (k_1^2 + 2k_1 p)^{a_3} (k_2^2 + 2k_2 p)^{a_4} [(k_1 + k_2 + p)^2 + 1]^{a_5} (k_2 + p)^{2(a_6+\epsilon)}}$$

$$\frac{\operatorname{Im} Y7(1,1,1,0,1,0)}{\pi \mathcal{F}^2} = \epsilon + (12 - 4\zeta(3))\,\epsilon^2 + \left(91 - \frac{5\pi^2}{6} - 20\zeta(3) - \frac{\pi^4}{3}\right)\epsilon^3 + \mathcal{O}\left(\epsilon^4\right)$$

Y8

$$\int \frac{[d^D k_1][d^D k_2]}{k_1^{2a_1} k_2^{2(a_2+\epsilon)} (k_1 - k_2)^{2a_3} (k_1 + p)^{2a_4} (k_2^2 + 2k_2 p)^{a_5}}$$

Y9
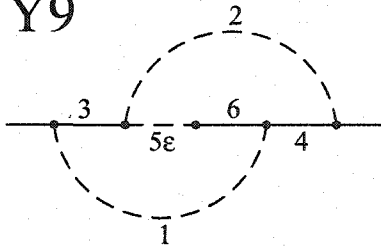
$$\int \frac{[d^D k_1][d^D k_2]}{k_1^{2a_1} k_2^{2a_2} (k_1^2 + 2k_1 p)^{a_3} (k_2^2 + 2k_2 p)^{a_4} (k_1 + k_2 + p)^{2(a_5+\epsilon)} [(k_1 + k_2 + p)^2 + 1]^{a_6}}$$

$$\frac{\operatorname{Im} Y9(1,1,1,1,0,0)}{\pi \, \mathcal{F}^2} = \left(-1 + \frac{\pi^2}{6}\right) \epsilon + \left(-12 + \frac{5\pi^2}{6} + 9\zeta(3)\right) \epsilon^2$$
$$+ \left(-91 + 5\pi^2 + 45\zeta(3) + \frac{23\pi^4}{90}\right) \epsilon^3 + \mathcal{O}\left(\epsilon^4\right)$$

A.4   Two-Loop Topologies With an Eikonal Propagator

E1

$$\int \frac{[d^D k_1][d^D k_2]}{k_1^{2a_1} k_2^{2a_2} (k_1 - k_2)^{2a_3} (k_2^2 + 2k_2 p)^{a_4} (2k_1 p)^{a_5}}$$

A general solution is used

Pole term for $(2k_1 p)$ is $+$ or $-$ in Minkowski space

E2
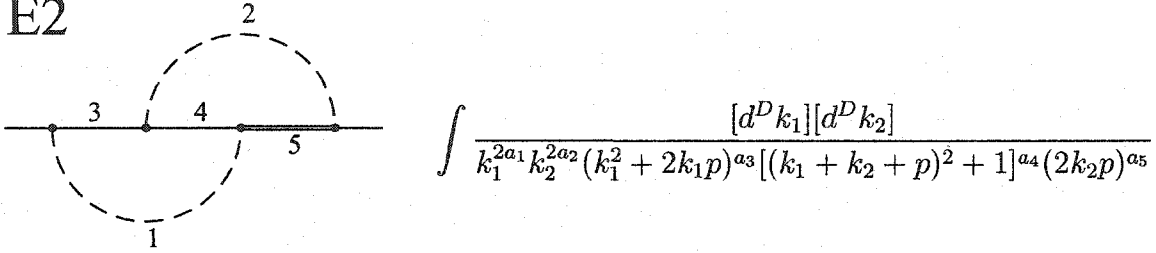
$$\int \frac{[d^D k_1][d^D k_2]}{k_1^{2a_1} k_2^{2a_2} (k_1^2 + 2k_1 p)^{a_3} [(k_1 + k_2 + p)^2 + 1]^{a_4} (2k_2 p)^{a_5}}$$

$$E2(1,0,0,1,1) \equiv J_1 \qquad\qquad E2(0,0,1,1,1) \equiv J_2$$

The $J_1^{\pm}$ and $J_2^{\pm}$ master integrals are listed in (6.37) and (6.38)

Pole term for $(2k_2 p)$ is $+$ or $-$ in Minkowski space

E3
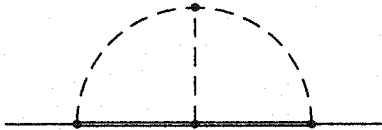
Scaleless integrals $\Rightarrow$ Zero

A.5   Three-Loop Topologies

T3
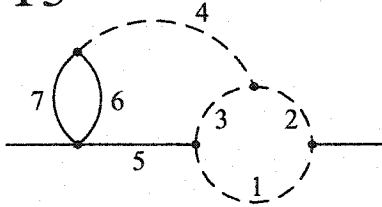
Tensor reduction: $k_3 \perp k_2$

$$\int \frac{[d^D k_1][d^D k_2][d^D k_3]}{k_1^{2a_1} (k_1 + p)^{2a_2} (k_1 + k_2 + p)^{2a_3} k_2^{2a_4} (k_2^2 + 2k_2 p)^{a_5} [(k_2 + k_3)^2 + 1]^{a_6} [k_3^2 + 1]^{a_7}}$$

$$\frac{\text{Im } T3(1,1,1,0,1,1,1)}{\pi \, \mathcal{F}^3} = \frac{1}{2\epsilon^2} + \frac{5}{2\epsilon} + \left(\frac{15}{2} - \frac{\pi^2}{6} - 2\zeta(3) \right)$$
$$+ \left(\frac{29}{2} - \frac{\pi^2}{6} - 9\zeta(3) + \frac{\pi^4}{60} \right) \epsilon + \mathcal{O}\left(\epsilon^2 \right)$$

T3a
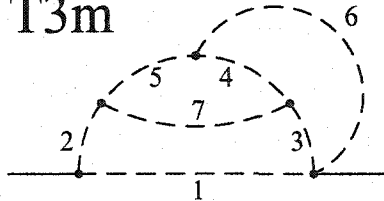

Auxiliary propagator: $[9] = (2k_1k_3)$
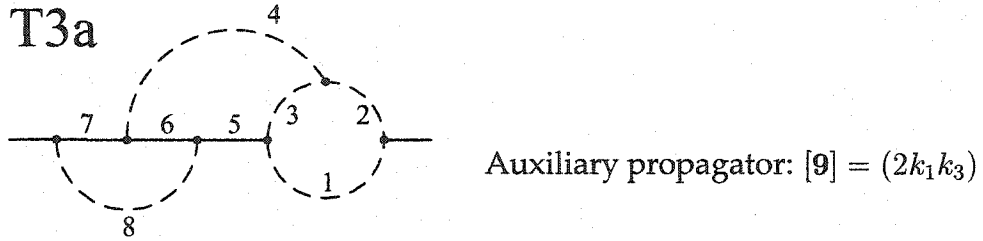
$$\int \frac{[d^D k_1][d^D k_2][d^D k_3]}{k_1^{2a_1}(k_1+p)^{2a_2}(k_1+k_2+p)^{2a_3}k_2^{2a_4}(k_2^2+2k_2p)^{a_5}[(k_2+k_3+p)^2+1]^{a_6}}$$
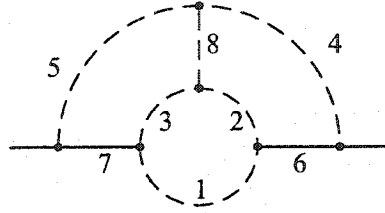$$\times \frac{1}{(k_3^2+2k_3p)^{a_7}k_3^{2a_8}(2k_1k_3)^{2a_9}}$$
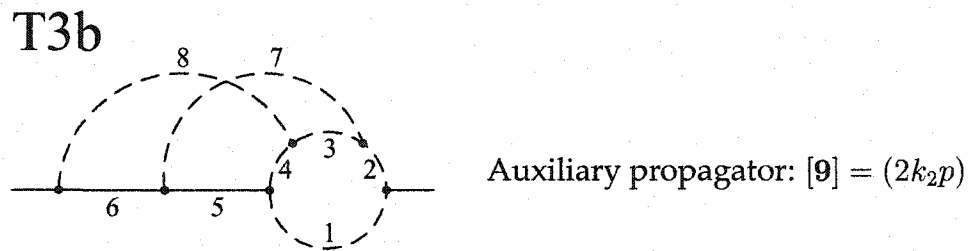
T3b

Auxiliary propagator: $[9] = (2k_2p)$

$$\int \frac{[d^D k_1][d^D k_2][d^D k_3]}{k_1^{2a_1}(k_1+p)^{2a_2}(k_1+k_2+p)^{2a_3}(k_1+k_2+k_3+p)^{2a_4}[(k_2+k_3+p)^2+1]^{a_5}}$$
$$\times \frac{1}{(k_3^2+2k_3p)^{a_6}k_2^{2a_7}k_3^{2a_8}(2k_2p)^{2a_9}}$$

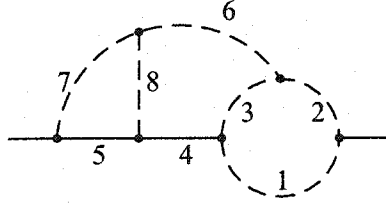$$\frac{\text{Im}\,T3b(1,1,1,1,1,1,1,1,0)}{\pi\,\mathcal{F}^3} = \frac{3\pi^4}{40} + \mathcal{O}(\epsilon)$$

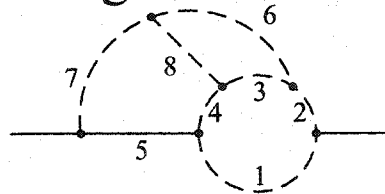## T3c

Auxiliary propagator: $[9] = (2k_2p)$
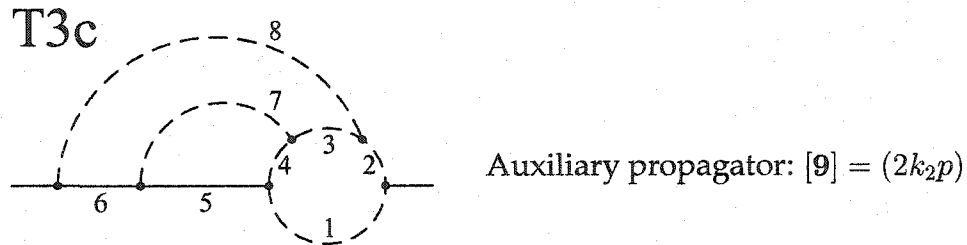
$$\int \frac{[d^D k_1][d^D k_2][d^D k_3]}{k_1^{2a_1}(k_1 + p)^{2a_2}(k_1 + k_3 + p)^{2a_3}(k_1 + k_2 + k_3 + p)^{2a_4}[(k_2 + k_3 + p)^2 + 1]^{a_5}}$$
$$\times \frac{1}{(k_3^2 + 2k_3 p)^{a_6} k_2^{2a_7} k_3^{2a_8} (2k_2 p)^{2a_9}}$$

T3d
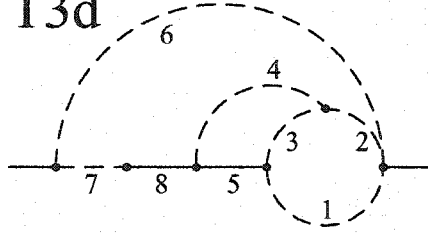
Tensor reduction: $k_3 \perp (k_3 + p)$

$$\int \frac{[d^D k_1][d^D k_2][d^D k_3]}{k_1^{2a_1}(k_1 + k_3 + p)^{2a_2}(k_1 + k_2 + k_3 + p)^{2a_3} k_2^{2a_4}[(k_2 + k_3 + p)^2 + 1]^{a_5}}$$
$$\times \frac{1}{k_3^{2a_6}(k_3 + p)^{2a_7}(k_3^2 + 2k_3 p)^{a_8}}$$

T3e
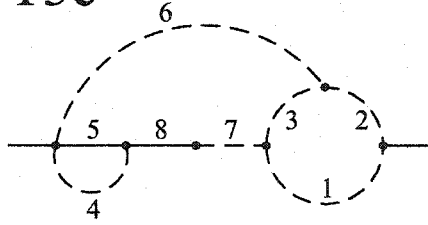
Tensor reduction: $k_3 \perp (k_2 + p)$

$$\int \frac{[d^D k_1][d^D k_2][d^D k_3]}{k_1^{2a_1}(k_1 + p)^{2a_2}(k_1 + k_2 + p)^{2a_3} k_3^{2a_4}[(k_2 + k_3 + p)^2 + 1]^{a_5}}$$
$$\times \frac{1}{k_2^{2a_6}(k_2 + p)^{2a_7}(k_2^2 + 2k_2 p)^{a_8}}$$

T3f
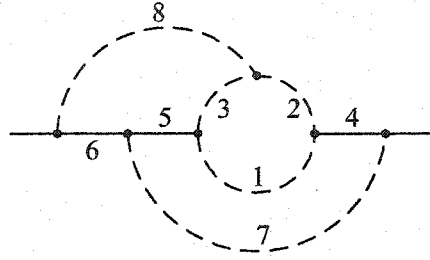
Auxiliary propagator: $[9] = (2k_1 p)$

$$\int \frac{[d^D k_1][d^D k_2][d^D k_3]}{k_1^{2a_1}(k_1 + k_2 + p)^{2a_2}(k_1 + k_2 + k_3 + p)^{2a_3}(k_2^2 + 2k_2 p)^{a_4}[(k_2 + k_3 + p)^2 + 1]^{a_5}}$$
$$\times \frac{1}{(k_3^2 + 2k_3 p)^{a_6} k_2^{2a_7} k_3^{2a_8}(2k_1 p)^{a_9}}$$

T3h
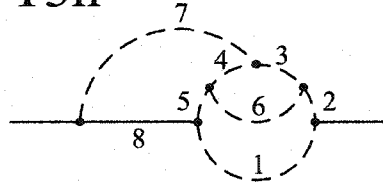
Auxiliary propagator: $[9] = (2k_2 p)$

$$\int \frac{[d^D k_1][d^D k_2][d^D k_3]}{k_1^{2a_1}(k_1 + p)^{2a_2}(k_1 + k_2 + p)^{2a_3}(k_1 + k_2 + k_3 + p)^{2a_4}(k_1 + k_3 + p)^{2a_5}}$$
$$\times \frac{1}{k_2^{2a_6} k_3^{2a_7}(k_3^2 + 2k_3 p)^{a_8}(2k_2 p)^{a_9}}$$

T3i
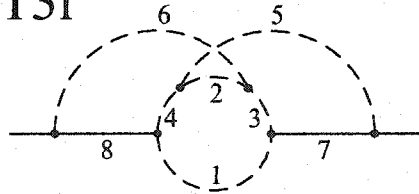
Auxiliary propagator: $[9] = (2k_1 p)$

$$\int \frac{[d^D k_1][d^D k_2][d^D k_3]}{k_1^{2a_1}(k_1 + k_2 + k_3 + p)^{2a_2}(k_1 + k_2 + p)^{2a_3}(k_1 + k_3 + p)^{2a_4} k_2^{2a_5}}$$
$$\times \frac{1}{k_3^{2a_6}(k_2^2 + 2k_2 p)^{a_7}(k_3^2 + 2k_3 p)^{a_8}(2k_1 p)^{2a_9}}$$

$$\frac{\operatorname{Im} T3i(1,1,1,1,1,1,1,1,0)}{\pi \, \mathcal{F}^3} = \frac{49\pi^4}{180} - 2T_2 + \mathcal{O}\left(\epsilon\right)$$

T_2 is a finite combination of transcendentals whose analytic value is not needed for our results. More specifically, it is the (leading) $\mathcal{O}\left(\epsilon\right)$ term of a similar integral which can be used as a master integral.

T3k
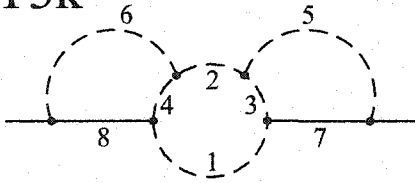
Auxiliary propagator: $[\mathbf{9}] = (2k_2 k_3)$

$$\int \frac{[d^D k_1][d^D k_2][d^D k_3]}{k_1^{2a_1}(k_1 + p)^{2a_2}(k_1 + k_2 + p)^{2a_3}(k_1 + k_3 + p)^{2a_4} k_2^{2a_5}}$$
$$\times \frac{1}{k_3^{2a_6}(k_2^2 + 2k_2 p)^{a_7}(k_3^2 + 2k_3 p)^{a_8}(2k_2 k_3)^{2a_9}}$$

$$\frac{\operatorname{Im} T3k(1,0,1,1,1,1,1,1,0)}{\pi \, \mathcal{F}^3} = \frac{\pi^4}{15} + \mathcal{O}\left(\epsilon\right)$$

T3m
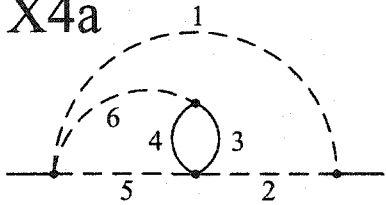

Tensor reduction: $k_1 \perp (k_1 + p)$

$$\int \frac{[d^D k_1][d^D k_2][d^D k_3]}{k_1^{2a_1}(k_1 + p)^{2a_2}(k_1 + k_2 + p)^{2a_3}(k_1 + k_2 + k_3 + p)^{2a_4}(k_1 + k_3 + p)^{2a_5} k_2^{2a_6} k_3^{2a_7}}$$

T3nd

Auxiliary propagator: $[9] = (2k_1 p)$

$$\int \frac{[d^D k_1][d^D k_2][d^D k_3]}{k_1^{2a_1}(k_1 + k_2 + p)^{2a_2}(k_1 + k_3 + p)^{2a_3} k_2^{2a_4} k_3^{2a_5}(k_2^2 + 2k_2 p)^{a_6}}$$
$$\times \frac{1}{(k_3^2 + 2k_3 p)^{a_7}(k_2 - k_3)^{2a_8}(2k_1 p)^{a_9}}$$

T3ne

Auxiliary propagator: $[9] = (2k_1 k_3)$

$$\int \frac{[d^D k_1][d^D k_2][d^D k_3]}{k_1^{2a_1}(k_1 + p)^{2a_2}(k_1 + k_2 + p)^{2a_3}(k_2^2 + 2k_2 p)^{a_4}(k_3^2 + 2k_3 p)^{a_5}}$$
$$\times \frac{1}{k_2^{2a_6} k_3^{2a_7}(k_2 - k_3)^{2a_8}(2k_1 k_3)^{a_9}}$$

T3ng

Auxiliary propagator: $[9] = (2k_2 p)$

$$\int \frac{[d^D k_1][d^D k_2][d^D k_3]}{k_1^{2a_1}(k_1 + p)^{2a_2}(k_1 + k_2 + p)^{2a_3}(k_1 + k_3 + p)^{2a_4}(k_3^2 + 2k_3 p)^{a_5}}$$
$$\times \frac{1}{k_2^{2a_6} k_3^{2a_7}(k_2 - k_3)^{2a_8}(2k_2 p)^{a_9}}$$

X1
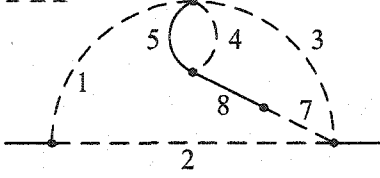
Tensor reduction: $k_2 \perp k_3$ then $k_3 \perp k_1$

$$\int \frac{[d^D k_1][d^D k_2][d^D k_3]}{k_1^{2a_1}(k_1 + p)^{2a_2}(k_1 + k_3)^{2a_3} k_2^{2a_4}[(k_2 + k_3)^2 + 1]^{a_5} k_3^{2a_7}(k_3^2 + 1)^{a_8}}$$

X2
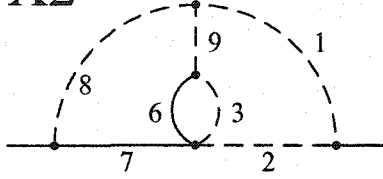
Tensor reduction: $k_2 \perp (k_1 - k_3)$

$$\int \frac{[d^D k_1][d^D k_2][d^D k_3]}{k_1^{2a_1}(k_1 + p)^{2a_2} k_2^{2a_3}[(k_1 + k_2 - k_3)^2 + 1]^{a_6}(k_3^2 + 2k_3 p)^{a_7} k_3^{2a_8}(k_1 - k_3)^{2a_9}}$$

$$\frac{\operatorname{Im} X2(1,1,1,1,1,1,0)}{\pi\,\mathcal{F}^3} = \frac{1}{2\epsilon^2} + \frac{7}{2\epsilon} + \left(\frac{33}{2} - \frac{\pi^2}{3} - 2\zeta(3)\right)$$
$$+ \left(\frac{131}{2} - \frac{7\pi^2}{3} - 10\zeta(3) - \frac{7\pi^4}{180}\right)\epsilon + \mathcal{O}\left(\epsilon^2\right)$$

X3
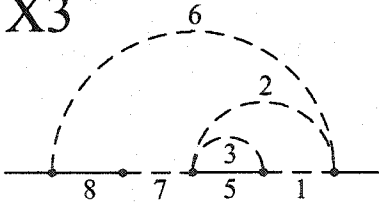
Tensor reduction: $k_2 \perp k_1$ then $k_1 \perp (k_3 + p)$

$$\int \frac{[d^D k_1][d^D k_2][d^D k_3]}{k_1^{2a_1}(k_1 + k_3 + p)^{2a_2}(k_1 + k_2)^{2a_3}(k_2 + 1)^{a_5} k_3^{2a_6}(k_3 + p)^{2a_7}(k_3^2 + 2k_3 p)^{a_8}}$$

X4
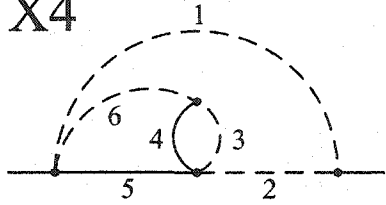
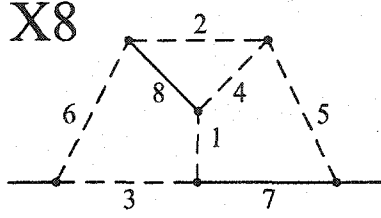
Tensor reduction: $k_2 \perp k_1$ then $k_1 \perp (k_3 + p)$

$$\int \frac{[d^D k_1][d^D k_2][d^D k_3]}{k_3^{2a_1}(k_3 + p)^{2a_2}(k_1 + k_2)^{2a_3}(k_2 + 1)^{a_4}[(k_1 + k_3 + p)^2 + 1]^{a_5} k_1^{2a_6}}$$

X4a

Tensor reduction: $k_2 \perp k_1$ then $k_1 \perp (k_3 + p)$

$$\int \frac{[d^D k_1][d^D k_2][d^D k_3]}{k_3^{2a_1}(k_3 + p)^{2a_2}[(k_1 + k_2)^2 + 1]^{a_3}(k_2 + 1)^{a_4}(k_1 + k_3 + p)^{2a_5} k_1^{2a_6}}$$

X5
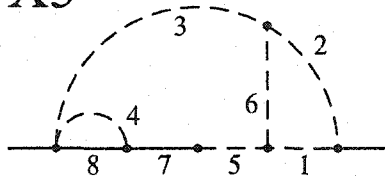
Tensor reduction: $k_3 \perp (k_2 + p)$

$$\int \frac{[d^D k_1][d^D k_2][d^D k_3]}{(k_1 + p)^{2a_1} k_1^{2a_2} k_2^{2a_3} k_3^{2a_4}(k_2 + p)^{2a_5}(k_1 - k_2)^{2a_6}(k_2^2 + 2k_2 p)^{a_7}[(k_2 + k_3 + p)^2 + 1]^{a_8}}$$

X5a
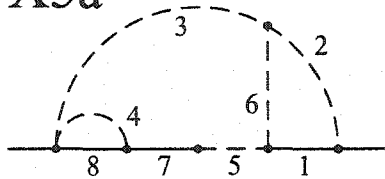
Tensor reduction: $k_3 \perp (k_2 + p)$

$$\int \frac{[d^D k_1][d^D k_2][d^D k_3]}{(k_1^2 + 2k_1 p)^{a_1} k_1^{2a_2} k_2^{2a_3} k_3^{2a_4} (k_2 + p)^{2a_5} (k_1 - k_2)^{2a_6} (k_2^2 + 2k_2 p)^{a_7} [(k_2 + k_3 + p)^2 + 1]^{a_8}}$$
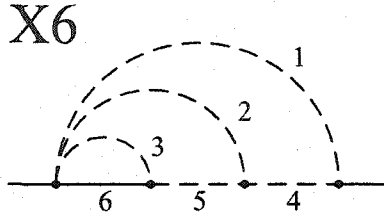
X6

Tensor reduction: $k_3 \perp (k_1 + k_2 + p)$ then $k_2 \perp (k_1 + p)$

$$\int \frac{[d^D k_1][d^D k_2][d^D k_3]}{k_1^{2a_1} k_2^{2a_2} k_3^{2a_3} (k_1 + p)^{2a_4} (k_1 + k_2 + p)^{2a_5} [(k_1 + k_2 + k_3 + p)^2 + 1]^{a_6}}$$
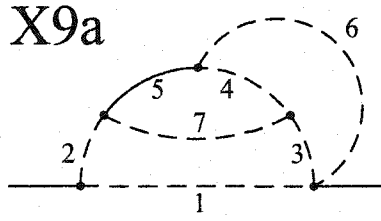
X6a
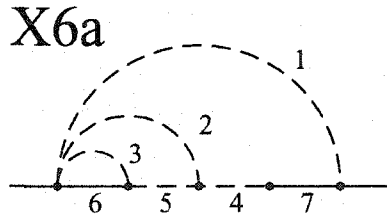
Tensor reduction: $k_3 \perp (k_1 + k_2 + p)$ then $k_2 \perp (k_1 + p)$

$$\int \frac{[d^D k_1][d^D k_2][d^D k_3]}{k_1^{2a_1} k_2^{2a_2} k_3^{2a_3} (k_1 + p)^{2a_4} (k_1 + k_2 + p)^{2a_5} [(k_1 + k_2 + k_3 + p)^2 + 1]^{a_6} (k_1^2 + 2k_1 p)^{a_7}}$$

X7
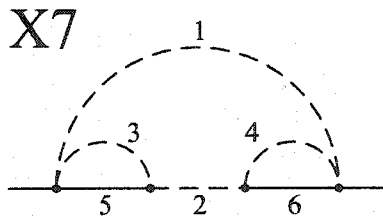
Tensor reduction: $k_2, \ k_3 \perp (k_1 + p)$

$$\int \frac{[d^D k_1][d^D k_2][d^D k_3]}{k_1^{2a_1} (k_1 + p)^{2a_2} k_2^{2a_3} k_3^{2a_4} [(k_1 + k_2 + p)^2 + 1]^{a_5} [(k_1 + k_3 + p)^2 + 1]^{a_6}}$$

X8

Auxiliary propagator: $[9] = (2k_3 p)$

$$\int \frac{[d^D k_1][d^D k_2][d^D k_3]}{(k_1 - k_2)^{2a_1} k_3^{2a_2} (k_1 + p)^{2a_3} (k_2 + k_3)^{2a_4} k_2^{2a_5} k_1^{2a_6}}$$
$$\times \frac{1}{(k_2^2 + 2k_2 p)^{a_7} [(k_1 + k_3)^2 + 1]^{a_8} (2k_3 p)^{a_9}}$$
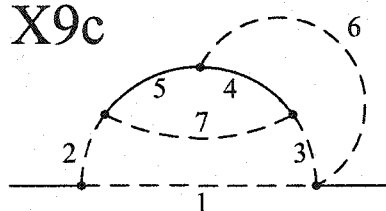
X9a

Tensor reduction: $k_1 \perp (k_1 + p)$

$$\int \frac{[d^D k_1][d^D k_2][d^D k_3]}{k_1^{2a_1} (k_1 + p)^{2a_2} (k_1 + k_2 + p)^{2a_3} (k_1 + k_2 + k_3 + p)^{2a_4} [(k_1 + k_3 + p)^2 + 1]^{a_5} k_2^{2a_6} k_3^{2a_7}}$$
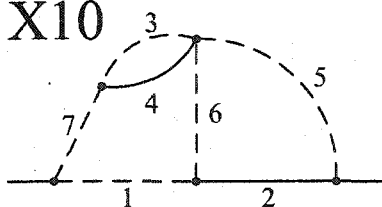
X9b
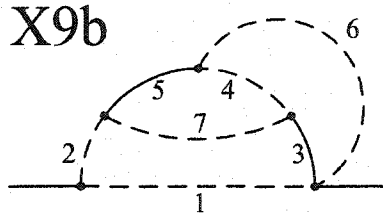
Tensor reduction: $k_1 \perp (k_1 + p)$

$$\int \frac{[d^D k_1][d^D k_2][d^D k_3]}{k_1^{2a_1} (k_1 + p)^{2a_2} [(k_1 + k_2 + p)^2 + 1]^{a_3} (k_1 + k_2 + k_3 + p)^{2a_4}}$$
$$\times \frac{1}{[(k_1 + k_3 + p)^2 + 1]^{a_5} k_2^{2a_6} k_3^{2a_7}}$$

$$\frac{\text{Im } X9b(1, 0, 1, 1, 1, 1, 1)}{\pi \, \mathcal{F}^3} = \left(-2 + \frac{\pi^2}{6} + \frac{13\zeta(3)}{4} - \frac{\pi^2}{2} \ln 2 \right)$$

$$+ \left(-\frac{203}{2} + \frac{83\pi^2}{12} + 7\zeta(3) - \frac{59\pi^4}{360} + \pi^2 \ln 2 + T_2 - C_2 \right) \epsilon + \mathcal{O}\left(\epsilon^2 \right)$$

$$\frac{\text{Im } X9b(1,0,1,2,1,1,1)}{\pi \, \mathcal{F}^3} = -\frac{1}{2\epsilon} + \left(-\frac{7}{2} - \frac{\pi^2}{12} \right)$$

$$+ \left(-\frac{35}{2} + \frac{3\pi^2}{4} - \frac{31\zeta(3)}{4} + \frac{\pi^2}{2} \ln 2 \right) \epsilon + C_2 \epsilon^2 + \mathcal{O}\left(\epsilon^3 \right)$$

T_2 and C_2 are finite combinations of transcendentals whose analytic values are not needed for our results.

X9c

Tensor reduction: $k_1 \perp (k_1 + p)$

$$\int \frac{[d^D k_1][d^D k_2][d^D k_3]}{k_1^{2a_1} (k_1 + p)^{2a_2} (k_1 + k_2 + p)^{2a_3} [(k_1 + k_2 + k_3 + p)^2 + 1]^{a_4}}$$
$$\times \frac{1}{[(k_1 + k_3 + p)^2 + 1]^{a_5} k_2^{2a_6} k_3^{2a_7}}$$

$$\frac{\text{Im } X9c(1,0,1,1,1,1,1)}{\pi \, \mathcal{F}^3} = \left(1 - \frac{\pi^2}{6} + \zeta(3) \right)$$

$$+ \left(14 - \frac{7\pi^2}{6} - 3\zeta(3) + \frac{\pi^4}{18} \right) \epsilon + \mathcal{O}\left(\epsilon^2 \right)$$
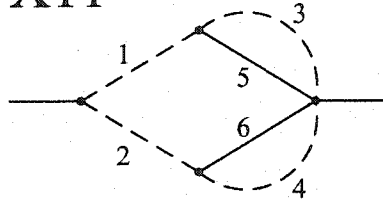
X10

Tensor reduction: $k_2 \perp k_1$

$$\int \frac{[d^D k_1][d^D k_2][d^D k_3]}{(k_1 + p)^{2a_1} (k_3^2 + 2k_3 p)^{2a_2} (k_1 + k_2)^{2a_3} (k_2^2 + 1)^{a_4} k_3^{2a_5} (k_1 - k_3)^{2a_6} k_1^{2a_7}}$$

$$\frac{\text{Im } X10(1,1,1,1,1,1,0)}{\pi \, \mathcal{F}^3} = \frac{1}{\epsilon} + \left(11 - \frac{\pi^2}{6} - \zeta(3)\right)$$
$$+ \left(77 - \frac{13\pi^2}{6} - 13\zeta(3) - \frac{7\pi^4}{90}\right)\epsilon + \mathcal{O}\left(\epsilon^2\right)$$
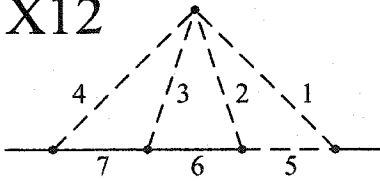
X11

Tensor reduction: $k_2 \perp k_1$ and $k_3 \perp (k_1 + p)$

$$\int \frac{[d^D k_1][d^D k_2][d^D k_3]}{k_1^{2a_1}(k_1 + p)^{2a_2} k_2^{2a_3} k_3^{2a_4}[(k_1 + k_2)^2 + 1]^{a_5}[(k_1 + k_3 + p)^2 + 1]^{a_6}}$$
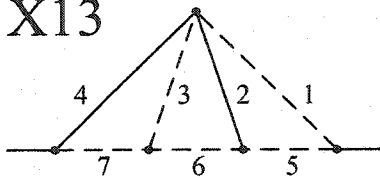
X12

Auxiliary propagators: $[8] = (k_2^2)$ and $[9] = (2k_1 k_3)$

$$\int \frac{[d^D k_1][d^D k_2][d^D k_3]}{k_1^{2a_1}(k_1 - k_2)^{2a_2}(k_2 - k_3)^{2a_3} k_3^{2a_4}(k_1 + p)^{2a_5}[(k_2 + p)^2 + 1]^{a_6}}$$
$$\times \frac{1}{[(k_3 + p)^2 + 1]^{a_7} k_2^{2a_8}(2k_1 k_3)^{a_9}}$$

$$\frac{\text{Im } X12(1,1,1,1,1,1,1,0,0)}{\pi \, \mathcal{F}^3} = \frac{\pi^4}{18} + \mathcal{O}(\epsilon)$$
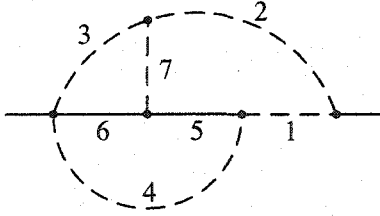
X13

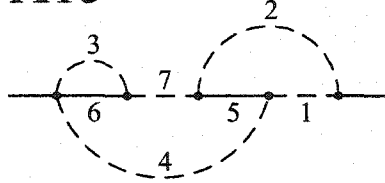
Auxiliary propagators: $[8] = (k_2^2)$ and $[9] = (2k_1 k_3)$

$$\int \frac{[d^D k_1][d^D k_2][d^D k_3]}{k_1^{2a_1}[(k_1 - k_2)^2 + 1]^{a_2}(k_2 - k_3)^{2a_3}(k_3^2 + 1)^{a_4}(k_1 + p)^{2a_5}(k_2 + p)^{2a_6}}$$
$$\times \frac{1}{(k_3 + p)^{2a_7} k_2^{2a_8}(2k_1 k_3)^{a_9}}$$

X14

Auxiliary propagators: $[8] = (2k_1 p)$ and $[9] = (2k_3 p)$

$$\int \frac{[d^D k_1][d^D k_2][d^D k_3]}{(k_2 + p)^{2a_1} k_2^{2a_2} k_1^{2a_3} k_3^{2a_4}[(k_2 + k_3 + p)^2 + 1]^{a_5}[(k_1 + k_3 + p)^2 + 1]^{a_6}}$$
$$\times \frac{1}{(k_1 - k_2)^{2a_7}(2k_1 p)^{a_8}(2k_3 p)^{a_9}}$$

X15

Tensor reduction: $k_1 \perp (k_3 + p)$

$$\int \frac{[d^D k_1][d^D k_2][d^D k_3]}{(k_2 + p)^{2a_1} k_2^{2a_2} k_1^{2a_3} k_3^{2a_4}[(k_2 + k_3 + p)^2 + 1]^{a_5}}$$
$$\times \frac{1}{[(k_1 + k_3 + p)^2 + 1]^{a_6}(k_3 + p)^{2a_7}}$$

$$\frac{\mathrm{Im}\, X15(1,1,1,1,1,1,0)}{\pi \mathcal{F}^3} = \frac{1}{2\epsilon^2} + \frac{5}{2\epsilon} + \left(\frac{15}{2} + \frac{5\zeta(3)}{4} - \frac{\pi^2}{2}\ln 2\right)$$
$$+ \left(\frac{29}{2} - \frac{\pi^2}{6} + \frac{9\zeta(3)}{2} - \frac{11\pi^4}{240} - \pi^2 \ln 2\right)$$

$$-\frac{\pi^2}{3}\ln^2 2 + \frac{1}{3}\ln^4 2 + 8\text{Li}_4(1/2)\Bigg)\,\epsilon$$

$$+\left(\frac{7}{2} - \frac{3\pi^2}{2} + 4\zeta(3) + \frac{79\pi^4}{360} + 2\pi^2\ln 2 - C_6\right)\epsilon^2$$

$$+\mathcal{O}\left(\epsilon^3\right)$$

$$\frac{\text{Im }X15(1,1,1,1,1,1,1)}{\pi\,\mathcal{F}^3} = \frac{\pi^2}{6\epsilon} + \left(\frac{\pi^2}{4} + \frac{5\zeta(3)}{4} - \frac{\pi^2}{2}\ln 2 + N\right)$$

$$+\left(\frac{7\pi^2}{12} + \zeta(3) - \frac{11\pi^4}{240} - \pi^2\ln 2\right.$$

$$\left. -\frac{\pi^2}{3}\ln^2 2 + \frac{1}{3}\ln^4 2 + 8\text{Li}_4(1/2) + N\right)\epsilon$$

$$+\left(\frac{19\pi^2}{12} - 10\zeta(3) - \frac{\pi^4}{48} + \pi^2\ln 2 - C_6 + N\right)\epsilon^2$$

$$+\mathcal{O}\left(\epsilon^3\right)$$

C_6 and N are finite combinations of transcendentals whose analytic values are not needed for our results. Since $\text{Li}_4(1/2)$, $\ln^2 2$, and $\ln^4 2$ do not appear in our final results, there must exist a simpler basis set of master integrals.